Kingston University London

APPLICATION OF MODAL TESTING METHODS IN ROTATING MACHINERY

by

HISHAM AHMAD HUMADI AL-KHAZALI

Supervisor

Dr. Mohamad R. Askari

A thesis submitted to the

Kingston University London

In partial fulfilment of the requirements

For the degree of

Doctor of Philosophy

Submitted to

Faculty of Science, Engineering and Computing (SEC),
School of Mechanical and Automotive Engineering,
Kingston University,
London, SW15 3DW, UK

K0903888@kingston.ac.uk

November 2012

Abstract

The experimental and analytical modal analysis is used to establish a system modelling methodology in rotating structures, which subsequently can help in design and development of rotating machinery.

The purpose of the study is to develop and use modal testing and vibration analysis which would involve obtaining the mathematical model of the system from the test data and subsequently obtaining the unbalanced parameters. The research work includes the application of modal testing method in rotor rig to investigate different modal parameters and detect the behaviour and performance of rotating machinery. This method would be capable of solving many of the related rotating machine problems, such as in turbine and compressor.

Unbalance is one of the problems which exist in rotating machinery. Balancing is usually an expensive and laborious procedure and a balancing system would be beneficial for rotor dynamic systems and power generation applications.

Excess vibration can cause noise, cyclic stress and wear in machinery. It is important to identify all the critical speeds within the range of operation and analyse the damping effect, mass unbalance and other phenomena in rotating machinery and their effects in their safe operation. These will be investigated in this study.

There are several phenomena associated with rotating machinery such as centrifugal and gyroscopic forces which would create complexity in the mathematical procedures in modal analysis that they need to be addressed and interpreted appropriately before they could be used in modal testing of rotating machinery.

The experimental technique used in this thesis to obtain the modal and dynamic response properties of structures. This technique has been applied to rotating structures, however the full implementation of modal testing in rotating structures and the implications are not fully understood and are therefore in need of further investigations.

In this study the Frequency Response Function (FRF) data obtained from the specific experimental results are curve-fitted by theoretical data regenerated from overall statistical analysis of measured data.

Different excitation methods are used in experiment (hammer and shaker). For hammer test, transient signal is produced. While for shaker test, different vibration signals are produced (Sine, Random and Burst Random).
In shaker test, a special frame was designed and used around a plain bearing and the accelerometers were attached to the outer surface of the bearing to measure the response of the lateral motion on several points of the shaft. The excitation force with help of push rod was generated and applied to the shaft. This method can help to solve the problem in the attachment of shaker and force transducers to the rotor system.

The analysis of vibration suppression with different locations and configurations of the unbalanced masses and effect of the adding of balance masses to suppress the vibration amplitude has been studied properly.

The experimental results were used for verification of Finite Element (FE) models, since it has good capability for eigen analysis and also good graphical facility. 3-D models result in large number of nodes and elements. This project demonstrates how to extract a plane 2-D model from the 3-D model that can be used with fewer nodes and elements with no loss in accuracy of the results.
Transient orbit analysis in the literature indicates that the bearing stiffness and damping affects the vibration amplitude. In this project the study of the effects on the bearing reaction forces and cyclic bending stress will be investigated.

It is envisaged that the approach is not limited to the condition diagnosis and predictive failure but could help the designers to have better understanding of rotor performance at the system design stage.

The experimental data are used to characterise the dynamic behaviour of the system and introduce to the correction unbalance to suppress the excess vibration.
The experimental data are also used to generate the FE models and subsequently calculate the dynamic reaction forces in the bearings and the cyclic bending stress.

***Keywords**: Modal testing; Modal parameters; Balancing effect; Rotor-dynamic system; Vibration; gyroscopic effect; FRF data; FE models.*

To my Parents God have mercy on, brothers, sisters and my wife with all my love

Acknowledgements

I would like to thank my supervisors, Dr. Mohamad R Askari (DOS), Prof. Tao Zhang and Mr. Denis R Marchant, for the guidance and support they provided throughout this research project. I would also like to thank the members of the Dynamics Section at Kingston University with whom; I had the pleasure of working during my research work.

Special thank to all the technical staff; Mr. MacBeen who assisted me in setting up the equipment and Mr. Anilal, for his advice in using the lab facility. A word of appreciation to the administrative officer for research and short courses Ms. Jackie Deacon, for keeping me informed of all the rules and regulations and facilitating the submission of my reports and thesis.

I feel in debt to my colleagues Mr. Fatih Dogan and Mr. Zhibin Chen for their useful advice personal or research related, which helped me to get through the difficult stages of my study.

Many thanks also to my friend and colleague Dr. Opukuro David West who made many helpful suggestions in using the computational techniques.

I would like to express my sincere gratitude to all library staff of the university for all facilities they provided during my search.

Finally, the author is deeply appreciative for the support provided by the Iraqi Ministry of Higher Education and Iraqi cultural attaché in London for their financial support and sponsorship. I would like to thank all other friends I have not named here who made my college life especially enjoyable. Finally, I would like to thank all my family for their ceaseless support and understanding.

Hisham AL-Khazali, London, UK, November 2012.

Contents

List of Figures

List of Tables

PUBLICATIONS

Journals

1-**H. A. H. Al-Khazali,** M. R. Askari, *"Experimental technique to investigate vibration monitoring in revolving structures using oscilloscopic/modal testing"*, in 'International Journal of Engineering Science and Technology', vol. 3, no. 10, pp. 7799-7814, ISSN 0975-5462, 2011.

2-**H. A. H. Al-Khazali,** M. R. Askari, *"Modal analysis design for exposure of gyroscopic effect in rotating machinery using experimental and analytical computational techniques"*, in 'International Journal of Engineering Science and Technology', vol. 3, no. 9, pp. 7234-7243, ISSN 0975-5462, 2011.

3-**H. A. H. Al-Khazali,** M. R. Askari, *"Accurate identification of performance for rotor-bearing systems using the modified modelling under gyroscopic effect"*, in 'International Journal of Modern Engineering Research (IJMER)', vol. 1, no. 2, pp. 527-537, ISSN 2249-6645, 2011.

4-**H. A. H. Al-Khazali,** M. R. Askari, *"Computer simulation to investigate system identification and vibration monitoring in rotor dynamic analysis"*, in 'International Journal of Advances in Science and Technology', vol. 3, no. 4, pp. 1-15, ISSN 2229-5216, 2011.

5-**H. A. H. Al-Khazali,** M. R. Askari, *"Calculations of frequency response functions (FRF) using computer smart office software and Nyquist plot under gyroscopic effect rotation"*, in 'International Journal of Computer Science, Information Technology and Security (IJCSITS)', vol. 1, no. 2, pp. 90-97, ISSN 2249-9555 and 2250-1355, 2011.

6-**H. A. H. Al-Khazali,** M. R. Askari, *"The experimental analysis of vibration monitoring in system rotor dynamic and validation of results using simulation data"*, in 'International Scholarly Research Network (ISRN Mechanical Engineering)', Volume 2012 (2012), January, pp. 1-17. DOI 10.5402/2012/981010, ISSN: 2090-5130, 2012.

7-**H. A. H. Al-Khazali,** M. R. Askari, *"Thermal effects for shaft–pre-stress on rotor dynamic system"*, in 'International Journal of Research and Reviews in Applied Sciences (IJRRAS)', vol. 11, no. 2, pp. 285-290, ISSN: 2076-734X and EISSN: 2076-7366, 2012.

8-**H. A. H. Al-Khazali,** M. R. Askari, *"Improvement in modal testing for dynamics of revolving structures to investigate the gyroscope effect and performance"*, in 'The International Journal of Science and Technology (IJST)', vol. 1, no. 3, pp. 151-163, ISSN: 2049-7318, 2012.

9-**H. A. H. Al-Khazali,** M. R. Askari, *"Analyzing data for rotating machines with high speeds using the spectral map wizard"*, in 'International Journal of Scientific and Engineering Research (IJSER)', vol. 3, no. 6, pp. 1-11, ISSN: 2229-5518, 2012.

10-**H. A. H. Al-Khazali,** M. R. Askari, *"Defect diagnosis in rotor systems by vibrations data collectors using trending software"*, in 'International Journal of Advanced Computer Science and Applications (IJACSA)', vol. 3, no. 5, pp. 33-43, ISSN: 2156-5570 and ISSN: 2158-107X, 2012.

11-**H. A. H. Al-Khazali,** M. R. Askari, *"Geometrical and graphical representations analysis of Lissajous figures in rotor dynamic system"*, in 'IOSR Journal of Engineering (IOSRJEN)', vol. 2, no. 5, pp. 971-978, ISSN: 2250-3021, 2012.

12-**H. A. H. Al-Khazali,** M. R. Askari, *"Investigational analysis using Lissajous figures in rotating machinery"*, in 'International Journal of Mechanical Engineering and Materials Science ', vol. 5, no. 2 pp. 77-82, ISSN: 0974-584X, 2012.

13-**H. A. H. Al-Khazali,** M. R. Askari, *"Dynamic investigation using the spectral chart wizard and modal testing data in rotors systems"*, in 'International Review of Modelling and Simulations (IREMOS)', vol. 5, no. 3, pp. 1360-1367, Print ISSN: 1974-9821, E-Journal ISSN:1974-983X, 2012.

14-**H. A. H. Al-Khazali,** M. R. Askari, *"Significance of fault diagnosis and reduced shock module in rotating machinery by data collectors using trending software and modal analysis"*, in 'International Review of Modelling and Simulations (IREMOS)', vol. 5, no. 4, pp. 1867-1875, Print ISSN: 1974-9821 and E-Journal ISSN:1974-983X, 2012.

15-**H. A. H. Al-Khazali,** M. R. Askari, *"Investigation of balancing in rotating structures using modal testing and analysis for structural health monitoring purpose and design"*, in ' International Review of Modelling and Simulations (IREMOS)', vol. 5, no. 5, pp. 2104-2118, Print ISSN: 1974-9821, E-Journal ISSN:1974-983X, 2012.

Chapter in Book

1-**H. A. H. Al-Khazali,** M. R. Askari, "System identification in rotating structures using vibration and modal analysis", in 'Topics in Modal Analysis I, Volume 5', Springer BWF, Edited by Allemang, R.; De Clerck, J.; Niezrecki, C.; Blough, J. R., pp. 481-497. DOI 10.1007/978-1-4614-2425-3_46, ISBN-10: 1461424240, ISBN-13: 978-1-4614-2424-6, Springer-Verlag New York, 2012.

Conferences

1-**H. A. H. Al-Khazali,** M. R. Askari, *"System identification in rotating structures using vibration and modal analysis"*, IMAC XXX conference and exposition on Structural Dynamics, 30 years of Modal Analysis, from laboratory to real world. Proceedings of the 30 SEM IMAC XXX Conference, FL USA ©2011 Society for Experimental Mechanics Inc., January 30 - February 2, pp. 507-518, Jacksonville, Florida, USA, 2012.

2-**H. A. H. Al-Khazali,** M. R. Askari, *"Identification of gyroscopic effect in rotating structures using experimental modal analysis and finite element data"*, Conference of Engineering Sciences, Iraqi Cultural Attaché-London, October 1-2, University College London (UCL), UK, 2011.

3-**H. A. H. Al-Khazali,** M. R. Askari, *"Establishing a system identification methodology in modal testing using the analytical/computational techniques in rotating machinery"*, ANSYS, Engineering the system, 2011 Regional conferences, ANSYS UK Conference, November 9, Heritage Motor Centre, Banbury Road, Gaydon, United Kingdom, UK, 2011.

4-**H. A. H. Al-Khazali,** M. R. Askari, *"Detection of gyroscopic effect in rotating machinery from the modal data"*, recent advancements in rotor dynamics", Proceedings of the Second National Symposium on Rotor Dynamics, (NSRD-2011), 19th-21 December, Chennai–600036, Tamil Nadu, India IIT, pp. 76-86, ISBN 978-935-059-056-0, Madras, India, 2011.

5-**H. A. H. Al-Khazali,** M. R. Askari, *"Condition monitoring and fault diagnosis in rotating machinery using modal testing and finite element analysis"*, 4th International conference on Computational Mechanics and Virtual Engineering-COMEC2011, Transilvania University, 20-22 October, vol. I, pp. 269-277, ISBN 978-973-131-122-7, Brasov, Romania, 2011.

6-**H. A. H. Al-Khazali,** M. R. Askari, *"Validation of modal data in rotating machinery using finite element analysis"*, ICAST 2011, 22nd International conference on adaptive structures and technologies, University of Patras, Greece, 10-12 October, Corfu, Greece, 2011.

7-**H. A. H. Al-Khazali,** M. R. Askari, *"Application of modal testing and finite element modelling in rotating structures"*, 2nd International Conference on Modelling and Simulations (ICOMOS), University of Naples, Italy, July 11-25, vol. 1, no. 1, pp. 41-55, ISSN 2038-3975, Naples, Italy, 2011.

8-**H. A. H. Al-Khazali,** M. R. Askari, *"Determination and simulation of modal parameter on revolving machines using vibration analysis"*, in 'SMART STRUCTURES', Proceedings of the 5th European Conference on Structural Control – EACS 2012, Edited by: Endrea E. DEL GROSSO and Paolo BASSO, 18-20 June, pp. 1-10, ISBN 978-88-95023-13-7, Genoa, Italy 2012.

9-**H. A. H. Al-Khazali,** M. R. Askari, *"Significance of fault diagnosis and reduced shock module in rotating machinery by data collectors using trending software and modal analysis"*, 3rd International Conference on Modelling and Simulations (ICOMOS) 2012, VIRTUAL FORUM, University of Naples, Italy, July 16-30, vol. 1, no. 1, pp. 1-9, ISSN 2038-3975, Naples, Italy, 2012.

10-**H. A. H. Al-Khazali,** M. R. Askari, *"Importance of using vibration signal characteristics for the diagnosis of rotor vibrations"*, ICAST 2012, 23rd International Conference on Adaptive Structures and Technologies, (NUAA) Nanjing University of Aeronautics and Astronautics, College of Aerospace Engineering, 11-13 October, Nanjing, China. 2012.

11-**H. A. H. Al-Khazali,** M. R. Askari, *"Detection of resonance in rotor machines for improvement in safety in the design problems"*, 7th International IET System Safety Conference, Incorporating the Cyber Security Conference 2012, Institution of Engineering and Technology (IET), 15-18 October 2012, Edinburgh, UK, 2012.

Presentation (Seminar)

1-**H. A. H. Al-Khazali,** *"Balancing in rotating machinery using system identification/modal analysis"*, Faculty of Science, Engineering and Computing – Research Seminar, July 25, Kingston University London, Roehampton Vale, UK, 2012.

About the Author

Mr. Hisham A. H. Al-Khazali, He is a PhD Student in Kingston University London, UK and member in Society for Experimental Mechanics (SEM), Inc., in USA. Furthermore, a member of The Science and Information Organization (SAI) in USA. He was born in 28 August 1973 Baghdad/ Iraq. He received his BSc (Eng.) in Mechanical Engineering 1996, University of Technology, Baghdad. MSc in Applied Mechanics, University of Technology, Baghdad 2000.

NAME: **HISHAM AHMAD HUMADI AL-KHAZALI**
E-MAIL: k0903888@kingston.ac.uk
INSTITUTION: Kingston University London.
DEP./STR.: Faculty of Science, Engineering and Computing (SEC),
School of Mechanical and Automotive Engineering, Kingston University London, UK.
CITY/ZIP: UNITED KINGDOM, LONDON, ROEHAMPTON VALE CAMPUS,
SW15 3DW.

Nomenclature

1. Latin and Arabic Symbols

$\boldsymbol{M}, \boldsymbol{C}, \boldsymbol{K}$	Mass, damping, and stiffness matrices
$\boldsymbol{x}, \boldsymbol{f}$	Displacement, external force vectors
N	Total number of components
$\eta_r, \boldsymbol{v}_r$	Components of the modal coordinate and the mode shape vector at the rth mode
$\boldsymbol{U}$	Mode shape matrix
$\boldsymbol{M}$, $\boldsymbol{C}$ and $\boldsymbol{K}$	Diagonal mass, damping, and stiffness matrices
ϕ_{jr}	The jth component of the rth mode shape vector
$\boldsymbol{x} = \hat{\boldsymbol{x}}$	Displacement vector of the spatial model
$\boldsymbol{f}_j = \hat{\boldsymbol{f}}_j$	Exciting force vector
ω	Excitation frequency rad /s, Hz
ω_r	Natural frequency of the rth mode (modal parameters)
ζ_r	Damping ratio of the rth mode (modal parameters)
FRF	Frequency response functions
$\boldsymbol{H}_{ij}$	Ratio of the ith displacement component $\hat{\boldsymbol{x}}_i$ to the jth exciting force component $\hat{f}_j$
FFT	Fast Fourier transform
$DOFs$	Degree of freedom systems
ODS	Operating deflection shape
$\hat{\boldsymbol{f}}_j$	Exciting force component
$\boldsymbol{H}_{ij,r}$	Peak value of FRF at the rth mode
Y, Z	Directions at each of the bearing supports
i	Unit imaginary
$[A], [B]$	Matrices
$\bar{\boldsymbol{f}}$	Force vector

$\{f(t)\}$	Time-domain force vector
$\{F(\omega)\}$	Vector of force amplitudes in the frequency domian
$[C]$	Damping matrix
H_{jk}	Accelerance frequency response function corresponding to a response measured at DOF_j and an excitation force applied at DOF_k
$[K]$	Stiffness matrix
k_1, k_2	Spring stiffness coefficients
x_1x_2	coordinate system
$[D]$	Dynamic matrix in state space form
$[G]$	Gyroscopic matrix
$[I]$	Identity matrix
$[F]$	Field matrix
m	Mass
m_u	Unbalance mass
$[M]$	Mass matrix
n	Integer number
N	System order
t	Time
$[T]$	Coordinate transformation matrix
T	Kinetic energy
U	Strain
δW	Virtual work
$\{y\}$	Vector of unknowns in a linear system of equations
q_i	Generalized forces
Fq_i	Generalized forces, and denotes differentiation with respect to time t.
xyz	Coordinate system is related to the XYZ coordinate system
ψ ,θ and ϕ	Angles to distinguish orientation of one first rotates it by an amount ψ around the z axis; then by an amount θ around the new x axis

$\{\phi_L\},\{\phi_R\}$	Left and right eigenvector
u, w	Designate the coordinates of O in R_0
M_D	Mass of the disc
T_D	Kinetic energy of disc
T_s	Kinetic energy of the shaft
$I_{Dy}\,\Omega\,\dot{\psi}\,\theta$	Gyroscopic (Coriolis) effect.
ρ	Mass per unit volume
S	Cross-sectional area of the beam
I	Area moment of inertia of the beam cross -section about the neutral axis
$u^*,\ w^*$	Displacements of the geometric centre with respect to the x, z axis
ε	Strain
ε_l	Linear terms
ε_{nl}	Nonlinear terms
σ	Stress
F_u, F_w	Components of the generalized force
L	Length of shaft
l_1	Situation of a symmetric disc with a mass unbalance
l_2	Situation of a bearing
ω_i	Frequency
T or TR	Transmissibility or Transmission ratio
s, F	Subscript for scaled-rotor, full-rotor respectively
{F},{f}	Force vector
R, T	Rotation, Translation (subscript)
λ	Scaling factor for (subscripted)
d	For disc element (superscript)
b	For bearing element (superscript)
s	For shaft element (superscript)
r	Radius

2. Greek Symbols

$\alpha_{jk}(\omega)$, α_{jk}	Element of the receptance matrix for the jth response measurement and k^{th} excitation locations / simplified Notation
β , θ	Angle between two coordinate axes
$[\Phi_G]$	Transposed matrix of rows of the normalised left eigenvector matrix
$\{\Phi_G\}_{k_o}$	k_o^{th} Column of matrix $[\Phi_G]$
$[\Phi_L]$, $[\Phi_R]$	Normalised left and right eigenvector matrices
$[\Phi_{L1}]$, $[\Phi_{L2}]$	'Displacement' components of the space-state left eigenvector matrix
$(\Phi_L)_{kr}$, $(\Phi_R)_{kr}$	k^{th} elements of the left and right eigenvectors of the rth mode
$[\Phi_{R1}]$, $[\Phi_{R2}]$	'Displacement' components of the space-state right eigenvector matrix
η_r	Hysteretic damping loss factor
$[\lambda_1]$, $[\lambda_2]$	$N \times N$ state-space eigenvalue sub-matrices
$[\lambda]$, $[\tilde{\lambda}]$	Eigenvalue matrix and its state space representation
λ_r	Eigenvalue of the rth mode
ω	Eigenvalue of the rth mode
ω_r , $\overline{\omega}_r$	Undamped and damped natural frequencies of the rth Mode
Ω	Speed of rotation
$[\Psi_L]$, $[\Psi_R]$	Matrix of non-normalised left and right eigenvectors
$\{\Psi_L\}_r$, $\{\Psi_R\}_r$	Non-normalised left and right eigenvectors of the rth Mode
δ , ∞	Displacement vector, Aspect ratio
ζ_r	Critical viscous damping ratio of the rth mode
$\{q\}$, $\{\eta\}$	Displacement vector
$(\alpha d, \beta d)$	Disc centre of mass in y, z direction respectively
Re([ ])	Real part of a complex matrix
Im([ ])	Imaginary part of a complex matrix

CHAPTER 1

Introduction

1.1 Resonant vibration

The amplitude of forced vibration can become very large when a frequency component of the excitation source approaches the natural frequency of the system. Such a condition is referred to as resonance and phenomena, this is potential causing failure in both machine and structure, so for this reason it is very important for designer to have a methodology of determining the natural frequency of the structure [1-3].

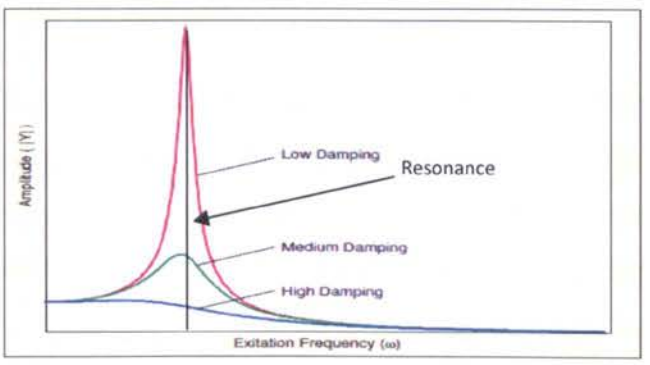

Figure 1.1 The resonance [4].

Resonance is the tendency of a system usually a linear system to oscillate at large frequencies. These are known as the system's resonant frequencies (or resonance frequencies), see Figure 1.1. Resonance effect occur when $\omega = \omega_n$, where ω = circular natural frequency rad/sec, at these frequencies even small periodic driving forces can produce large amplitude oscillations [1, 5].

Resonances occur when a system is able to store and easily transfer energy between two or more different storage modes such as kinetic energy and potential energy in the case of a pendulum. However, there are some losses from cycle to cycle, called damping. When damping is small, the resonant frequency is approximately equal to a natural frequency of the system. Some systems have multiple, distinct resonant frequencies. Machine and structural system vibrate freely about the static equilibrium position when displaced from those positions and released. The frequency they vibrate, known as their natural frequencies depend on mass and elasticity (stiffness) of the system [6].

1.1.1 Type of vibration

All vibration types are a combination of both forced and resonant vibration [1]. Forced vibration can be due to:

(i) Internally generated forces.
(ii) Unbalances.
(iii) External loads.
(iv) External excitation.

Resonant vibration occurs when one or more of the resonances or natural modes of vibration of a machine or structure is excited. Resonant vibration typically amplifies the vibration response far beyond the level deflection, stress, and strain caused by static loading.

1.1.2 Effect of damping on motion

There are many sources of excitation that cause machines and structures to vibrate; they include unbalanced rotating devices, vortex shedding, moving vehicles and surfaces. When excitation frequency equal to the natural frequency of the structure this matter caused damage (named resonance), which can cause large displacement and accompanying stresses in machines and structures. These large alternating tensile and compressive stresses can lead to fatigue failures. Vibration isolation analysis is concerned with reducing the magnitude of force transmitted [7, 8]. Isolation such as rubber or neoprene, damping tends to reduce the efficiency of an isolation system. Some damping must be present to minimize the resonance peak response when the system passes through resonance during start up/ shut down.

Some of crucial factors to the quality and performance of the rotor system such as vibration amplitude are resulted from bearing wear, damping effects, mass unbalances and passing the system resonances critical speed. Damping effect will cause the vibration oscillation to vanish gradually, so after working speed the system through the resonance point, the vibration amplitude decreased to nearly a constant value [9, 10].

Damping ratio is either one of the following:

$\zeta > 1$ system non-oscillatory, over damping.

$\zeta = 1$ critical damping.

$\zeta < 1$ under damped, very important in analyzing vibration system.

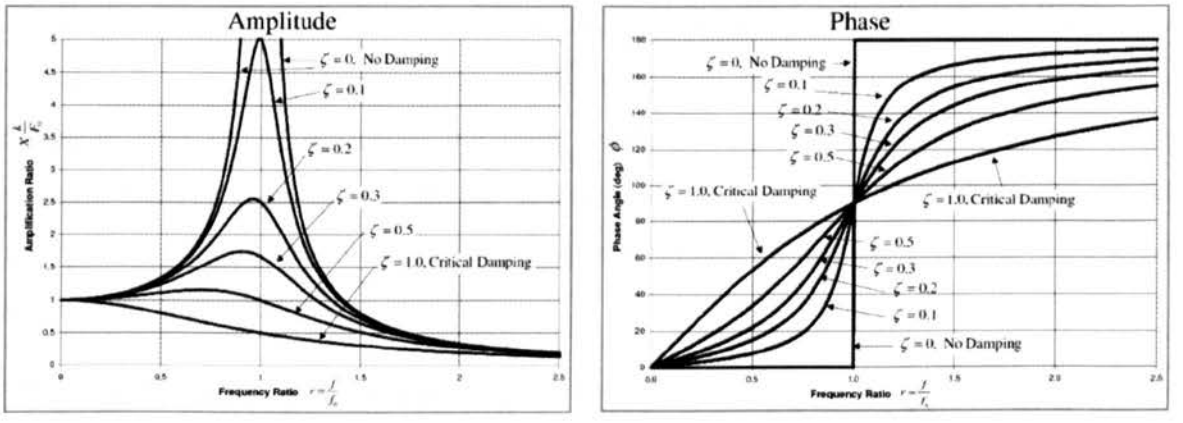

Figure 1.2 Variations of amplitude and phase angle with frequency ratio [1].

1.2 Modal testing

Modal testing is the process involved in testing components or structures with the objective of obtaining the mathematical model to describe the vibration properties of a structure based on test data rather than conventional theoretical analysis [11, 12]. As such, it has application throughout the entire field of engineering. However; a relatively high level of theoretical competence is expected in order to understand properly the implications and limitations of the different types of measurement methods, random and transient excitations.

1.2.1 Introduction of modal testing

Experimental observation has been made for the two major objectives.

1) Determining the nature and extent of vibration response levels.

2) Verifying theoretical models and predictions.

Today, structural vibration problems present major hazard and design limitation for very wide range of engineering products. First, there are a number of structures, from turbine blades to suspension bridges, for which structural integrity is of paramount concern, and second the precise knowledge of dynamics characteristics is essential [11, 13].

The two vibration measurement objectives indicated above represent two corresponding types of test. The first is one where vibrations force or more usually, responses are measured during operation of the machine or structure under study, while the second is a test where structure or component is vibrated with known excitation, often out of its normal service environment. Second type is generally made under much more closely–controlled conditions than the former and consequently yield more accurate, and detailed information. The type of test

including both the data acquisition and its subsequent analysis is nowadays called "Modal Testing". It is used here to encompass the processes involved in testing components or structures with the objective of obtaining mathematical description of their dynamic or vibration behaviour [14, 15]. Modal testing has evolved through various phases when descriptions such as resonance testing and mechanical impedance methods were used to describe the general activity.

1.2.2 Application of modal testing

There are many applications to which the results from a modal test can be applied and several of these are in fact quite powerful. The major application areas in rotating machinery diagnostics and analysis of noise and vibration problems related to rotational forces, e.g. in automotive and aircraft engines, transmissions, gearboxes, pumps, turbines, compressors and electric motor.

In all cases a modal test can be undertaken in order to obtain a mathematical model of structure but it is in subsequent use of the model analysis that differences arise.

Perhaps the most commonly used application is the measurement of vibration modes in order to compare these with corresponding data produced by finite element or theoretical models [16, 17]. For the specific application all that we require from the test are:

A- Accurate estimates of natural frequencies.

B- Description of the mode shape using just sufficient detail and accuracy to permit their identification and correlation with the theoretical model [18]. The next application area to be reviewed is that of using a modal test in order to produce a mathematical model of a component which may then be used to incorporate that component into structural assembly.

C- The generation of a model which may be used for predicting the effects of modification to the original structure, as tested.

D- Another application for model produced by a modal test is for force determination. The modal testing can be described by; 1) Data measurement. 2) Analysis of the measured data. 3) Derivation of a mathematical model of the structure. 4) Reducing the vast amount of actual measurements to small and efficient data set as usually referred to as the modal model [15, 19].

1.2.3 Modal testing analysis

It is a procedure whereby the measured parameters are analysed in such a way as to find theoretical model which most closely resembles the behaviour of the actual test piece. The process itself falls into two stages: first, to identify the appropriate type of model, second, to determine the appropriate parameters of the chosen model.

The great majority of the modal analysis effort involves the matching or curve–fitting expression [20, 21].

There are various parameters which can be measured:

Mobility:- is defined as the ratio of velocity response to force input. However, when considering sinusoidal vibration we have a simple relationship between displacement and velocity (and thus between receptance and mobility).

Modal Model:- This model is defined as a set of natural frequencies with corresponding vibration mode shapes and modal damping factors.

Inertance or Accelerance:- is relation of acceleration to force these represent the main formats of FRF although there exist yet more possibilities by defining the functions in an inverse way, namely as:

1- Dynamics Stiffness = forces/displacement.

2- Mechanical Impedance = forces/velocity.

3- Apparent Mass = force/acceleration.

1.2.3.1 Response parameter

Table 1.1 gives definitions of FRF parameters and of the names and symbols variously used for them.

Table 1.1
Definitions of Frequency Response Functions (FRFs) [11].

Response Parameter R	Standard R/F	Inverse F/R
Displacement	Receptance Admittance Dynamics Compliance Dynamics Flexibility	Dynamic Stiffness
Velocity	Mobility	Mechanical Impedance
Acceleration	Accelerance Inertance	Apparent Mass

Many types of parameters to be measured by using excitation devices such as hammer and shaker will be explained in detail in chapter 2.
The modal parameters which would result from the modal analysis would be distorted in order to compensate for the influence the out of range modes in the measured data.

1.2.3.2 Mathematical models

The subject is sufficiently broad that no single model is suitable for all cases and so the particular combination of measurement and analysis steps will vary according to the application. Thus we arrive at a most important aspect of the modelling process, the need to decide exactly which type of model we should seek before setting out on the acquisition and processing of experimental data [11, 16 and 22]. The three main categories of system model were identified, these being: 1) The spatial model of mass, stiffness, and damping properties, for theoretical response analysis and conversely response model–spatial for an experimental study. 2) The Modal Model comprising the natural frequencies and mode shapes, albeit an incomplete one can be constructed using just one single mode and including only a hard full of coordinates, even through the structure has many modes and coordinates. 3) Responses Model (in our case consisting of a set of frequency response functions), the response type of model in the form of a FRF matrix such as the mobility matrix, also need only included information concerning a limited number of points of interest–not all the coordinates must be considered [14, 23].

1.2.4 Display modal model; static display and dynamic display

One of the attractions of modal model is the possibility of obtaining a graphic display of its form by plotting the mode shape.

1.2.4.1 Response model

Regeneration and synthesis of FRF curves: There are two main requirements in the form of response model. The first being that of regenerating "theoretical" curves for the frequency response function actually measured and analysed and the second being that of synthesising the other functions which were not measured. In general, the form of response model with which we are concerned is FRF matrix whose order is dictated by the number of coordinates

included in the test. Note that this is not necessarily equal to the number of modes studied. FRF matrix from a modal model can be obtained using [14, 16]:

$$[H]_{n\times n} = [\Phi]_{n\times m}\left[(\lambda_r^2 - \omega^2)\right]^{-1}_{m\times m}[\Phi]^T_{m\times n} \quad \text{.....} \; 1.1$$

At the very least, the natural frequencies and damping factors of the individual mode should be rationalised throughout the model but even that is insufficient to ensure satisfactory model.

1.2.4.2 Spatial models

It is clear that a pair of pseudo matrices can be computed using the properties of just single mode.

Because the rank of each pseudo matrix is less than its order, it cannot be inverted and so we are unable to construct stiffness or mass matrices from this approach [6, 11].

1.2.4.3 Mobility skeletons and system models

Skeletons idea in greater detail presents a useful additional tool to the modal analysis.

Dramatic advances are being made in measurement and analysis techniques which will reduce the limitations and enhance both the viability and quality of good data, thus enabling the modal analyst to make even more precise and confident assessments of structural dynamic behaviour [24, 25].

1.2.5 Comparison of experiment and prediction

There are different methods of comparison between predictions for the dynamic behaviour of structure and these actually observed in practice. Sometimes this process is referred to as "validating" a theoretical model although to do this effectively, several steps must be taken; (i) The first of these is to take a direct and objective comparison of specific dynamic properties measured versus predicted data. (ii) To quantify the extent of the differences or similarities between the two sets of data [12, 26]. If all of them are achieved, theoretical model can be said have been validated and used for further analysis [14, 27].

1.2.5.1 Comparison of response properties

There are fewer uncertainties introduced in the process of computing the frequency response properties from the basis of spatial model than arise in the alternative process of deriving spatial model of the structure from test data [11, 13].

In Figure 1.3 comparisons between direct measurement and prediction of point FRF for simple beam like structure is shown. The plot clearly shows systematic discrepancy between the two sets of data. Resulting in steady frequency shift between the two curves while the same time indicating high degree correlation in amplitude [28].

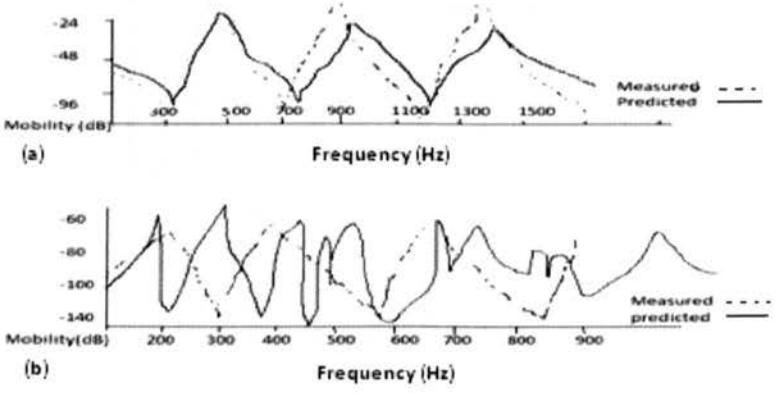

Figure 1.3 Comparison between measured and predicted mobility data [11]: (a)- Point mobility for beam structure. (b)- Transfer mobility for plate structure.

1.2.5.2 Comparison of modal properties

Although the response data are the most directly available from test for comparison purposes, some theoretical analysis packages are less than convenient when it comes to predicting FRF plots.

1.2.5.3 Comparisons of natural frequencies

This is often done by a simple tabulation of the two sets of results but a more useful format is by plotting the experimental value against the predicated one for each of the modes included in the comparison as shown in Figure 1.4. In this way it is possible to see not only the degree of correlation between the two sets of results, but also the nature (and possible case) of any discrepancies which do exist. The points plotted should lie on or close to straight line of slope = 1. If they lie close to a line of different slope then almost certainly the cause of the discrepancy is an erroneous material property used in the predictions. If the points lie scattered widely about a straight line then there is a serious failure of the model to represent the test structure and fundamental re-evolution is called for. If the scatter is small and randomly distributed about 45° line then this may be expected from normal modelling and measurement process. However, a case of particular interest is where the points deviate slightly from the ideal line but in a systematic rather than a random fashion as this situation

suggests that there is a specific characteristic responsible for the deviation and that this cannot simply be attributed to experimental errors [12, 29 and 30].

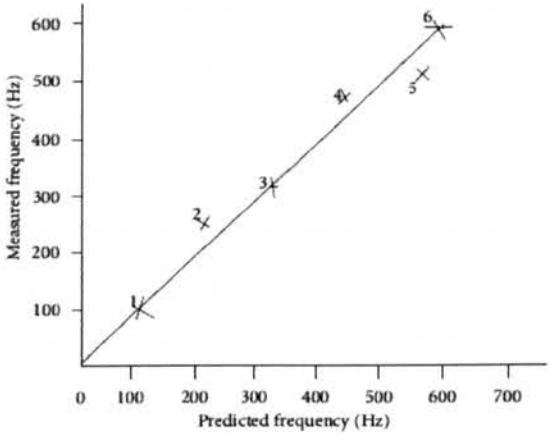

Figure 1.4 Comparison of measured and predicted natural frequencies [11].

1.3 Subject of the research work

The use of modal testing approach to the study of rotating machinery dynamics allows us to model their dynamic behaviour based exclusively on their response to controlled excitation forces, without focusing on the interactions between their components. Thus, by taking the effects of rotation into account, modal analysis and testing methods that were originally designed for conventional, non-rotating structures can be adapted for their use with rotating machinery. The research work reported in this thesis deals with the adaptation of conventional modal analysis and testing methods to the study of rotating machinery dynamics. The systems treated here will be referred to as rotating machinery structures, to highlight the fact that their study was undertaken using a structural dynamics approach. Attention is focused on the methods used for the derivation of the models of these systems, a process that will be referred to as modal characterisation.

1.4 Definition of problem

There is a growing tendency today to extract information about the prognostic parameters based on system analysis through various diagnostic techniques to assess the health of the plant or equipment. Vibration monitoring helps in reducing the machine down time and to

provide valuable information for the diagnosis of symptoms that helps in maintenance planning.

A vibration signature measured at the external surface of machine or at any other suitable place contains a good amount of information to reveal the running condition of the machine. Thus, it provides very useful information regarding symptoms of rotating machinery failure and prevents costly breakdowns. Considering the importance of vibration analysis in the rotating machinery, this approach has been applied in this research for studying the dynamic characteristics of the rotor system as well as obtaining the parameters for correcting the unbalance in the system by modal testing technique.

Balancing is usually a difficult procedure and a balancing system would be beneficial for all rotating machinery systems and application. Vibration caused by mass imbalance is a common problem in rotating machinery such as steam turbines and compressors. In this research, the unbalance parameters that exist in rotating machinery have been identified and modal testing technique of rotating dynamics system was developed to create a mathematical model of the system from the test data and subsequently obtaining the unbalanced parameters. The research work included the development of relevant theoretical ground work originated from principles of rotor dynamics. We present here a generalise procedure for investigating many of related rotating machine problems. The experimental analysis used is called modal testing. This technique has been applied to rotating structures, however, the full implementation of modal testing in rotating structures and the implications are not fully understood and are, therefore, in need of much further and more in-depth investigations. We find the system identification methodology using the analytical/computational techniques and update the model using experimental techniques already established for stationary structures to rotating structures.

As the rotating machine wears, foundations settle, and parts deform, subtle changes in the dynamic properties of the machine begin to occur. Shafts become misaligned, parts begin to wear, rotors become unbalanced, and clearances increase. All of these factors are reflected in an increase in vibration energy, which as it is dissipated throughout the machine, excites resonances and puts considerable extra dynamic loads on bearings. Increased complexities of rotating machinery and demands for higher speeds and greater power have created more complicated vibration problems. Engineering judgments based on understanding of physical phenomena are needed to provide the diagnosis methods for correcting the rotating machinery faults. Mode shapes are used as a simple and efficient means of characterizing

resonant vibration. The majority of structures can be made to resonate. That is, under the proper conditions, a structure can be made to vibrate with excessive, sustained, oscillatory motion. Resonant vibration is often the cause of, or at least a contributing factor to many of the vibration related problems that occur in structures and operating machinery. To better understand any structural vibration problem, the resonances of a structure need to be identified and quantified. A common way of doing this is to define the structure's modal parameters.

In this research, effects of modal parameters such as natural frequency, mode shapes, and damping have been studied. Comprehensive experimentation is carried out for analysis of vibrations for a rotor supported by plain bearings at higher speeds, the inertia effects of the rotating parts must be represented in order to predict the rotor behaviour.

Excess vibration can cause noise and wear in machinery and bearing, it is important to identify all the critical speeds within the range of operation and analyse the damping effects, mass unbalance and other phenomena in rotating machinery and their effects in the safe operation of rotating machinery, which would be the subject of study in this research work.

1.5 Objectives of research work

The main objective of the research work presented here is to develop and use modal testing and vibration analysis results for purpose of the modal characterisation of rotating structures in order to detect the dynamic parameters of the rotor system. It is envisaged that the approach could help designers to have better understanding of rotor performance at the system design stage.

Modal testing involves extraction of modal parameters and their validation using data obtained from FE models.

It is important to obtain mathematical formulations for FRF in stationary and rotating structures in order to understand the gyroscopic effect which is an inherent dynamic property of rotating structures, and to identify the unbalanced parameters that exist in rotating machinery.

It is intended that this study will provide a state of the art technical basis for better and more qualitative design of rotor systems with minimal amplitude and noise arising from vibration.

Furthermore, investigating of the modal testing results using vibration analysis software in experiment; which is an essential tool for analyzing and evaluating the mechanical vibration that occur in rotating machine.

1.6 Overview of the thesis

This thesis presents a method for the dynamic characterisation of rotating machinery structures using modal analysis techniques and FE simulation.
The material presented here covers the underlying theory used for the formulation of the method, its mathematical derivation and its application to the rotor dynamic systems. The thesis is organised in the following way:

Chapter 2 starts with a description of the modal analysis theory in rotor-dynamic systems that used in this thesis with some of its applications and theoretical background for the measurement of the Frequency Response Function (FRF) which is very important in reducing vibration and noise occurring in all rotating machines. Reviews of the relevant literature on existing techniques in rotor system for the balancing, auto balancing and modelling are presented in this chapter.

In chapter 3, a brief description of the basic elements of any rotor system including disc, shaft, bearings and seals with the determination of the model, mass unbalance and forces (synchronous and asynchronous). The fundamental equations of motions together with the gyroscopic effect and its association with the rotating machinery are presented. The mathematical model of FRF for stationary and rotating structures are formulated and described.

In chapter 4 the material properties for a rotor-dynamic analysis have been defined and the device set up in experimental techniques used in this thesis has been discussed.
The modal parameters of a rotor system with one, two and overhung discs rotor were investigated in different applications for correcting the unbalance in the system before and after added mass. The study of operational deflection shapes in Jeffcott rotor system was performed.

Shaker test was used for interpretation of the results obtained from experimental measurement of dynamic behaviour by hammer test.

Chapter 5 presents finite element modelling methodology and the performance of a rotor-dynamic system with different disc configurations and geometry definition, to detect dynamic behaviour of the system which gives more results that support the thesis.
The reaction forces in the bearings with different rotation speeds and the cyclic bending stress have been obtained.

Validation of the modal testing data using FE simulation was mentioned in chapter six.
Gyroscopic phenomena was described, and its relation with increasing rotational speeds were studied experimentally and computationally (Campbell diagram). The theoretical calculations have been used to validate the results.

Finally, chapter 7 presents the conclusions obtained from this research work and presents some possible research activities that could be carried out as a continuation of the work presented here.

CHAPTER 2

Background and Literature Review

2.1 Introduction

Modal analysis has been used in many engineering disciplines and technology fields to solve increasingly demanding structural dynamic problems. Modal analysis has become a major technology in the quest for determining, improving and optimization of dynamic characteristics of engineering structure and has also discovered profound application for civil and building structure, biomechanical problems, space structures, acoustical instrument, transportation and nuclear plants. Contemporary design of complex mechanical, aeronautical or civil structure requires them to become increasingly lighter, more flexible and yet strong.

For instance resources have been devoted by car manufactures to achieve reductions of product body weight [11, 27]. Aerospace structures such as satellite antennas do deserve weight reduction of every possible gram in order to minimize their mass. These stringent demands on contemporary structure often made them more susceptible to unwanted vibrations.

Modal analysis is process of determining the inherent dynamic characteristics of system in form of natural frequencies, damping factor and mode shapes and using them to formulate a mathematical model for its dynamic performance. The formulated mathematical model is referred to as the modal model of the system and information for the characteristics is known as its modal data [21, 31].

Modal analysis is based upon the fact that the vibration response of linear time invariant dynamics system can be expressed as the linear combination of set of simple harmonic motion called the natural mode of vibration. The natural modes of vibration are inherent to a dynamic system and are determined completely by its physical properties (mass, stiffness and damping) and their spatial distributions [11, 25].

Modal analysis embraces both theoretical and experimental techniques. The theoretical modal analysis anchors on physical model of dynamics system comprising its mass, stiffness and damping properties, it may be given in form of partial differential equations.

2.2 Modal analysis theory of a SDOF dynamic system

2.2.1 Amplitude–phase plot

Amplitude–phase plot consist of two parts: The magnitude of the FRF versus frequency and the phase versus frequency [27, 32].

It is customary in modal analysis to plot FRF data using logarithmic scales. This can be done in different way; 1) Logarithmic scale for modulus axis only linear-log plot, 2) Logarithmic scales for both modulus and frequency axes (log–log plot). In both cases, the magnitude of the FRF is converted into its decibel scale defined as:

$FRF_{dB} = 20 \log_{10}$ linear magnitude/unit FRF

Figure 2.1 show the linear–log plot of an FRF in receptance, mobility and accelerance forms.

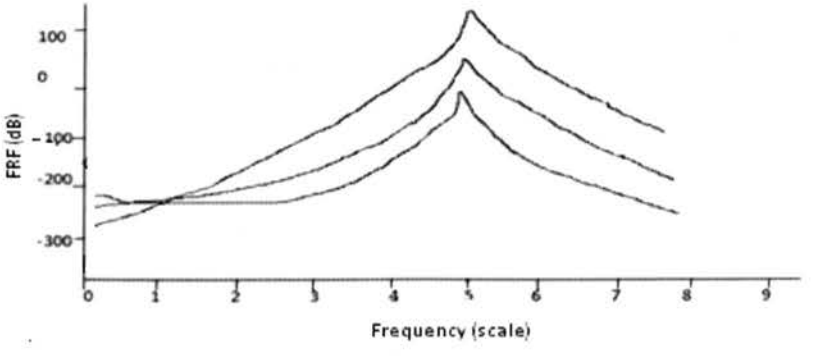

Figure 2.1 Linear-log plot of a FRF in receptance, mobility and accelerance forms [16].

Since the analytical expression of a FRF is determined by system parameters (mass, stiffness and damping) as well as the variable ω, it is reasonable to expect that these parameters can be derived from the FRF plot easily [11, 33]. When damping cause significant complexity to FRF, it becomes unreliable to derive the asymptote properties. Figure 2.2 shows log-log plot of first point FRF of the 4DOF system in receptance, mobility and accelerance forms.

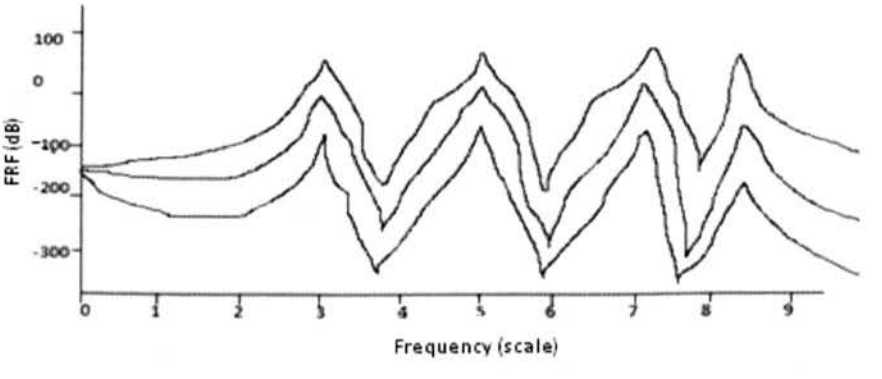

Figure 2.2 Log-log plot of the first point FRF of the 4DOF system in receptance, mobility and accelerance forms [16].

2.2.2 Real and imaginary plots

Real and imaginary plots consist of two parts: the real part of FRF versus frequency and the imaginary part of the FRF versus frequency. Using the structural damping model, the real and imaginary parts of the FRF are [14, 31]:

$$Re(\alpha(\omega)) = (k - \omega^2 m)/((k - \omega^2 m)^2 + h^2) \quad \text{.....} 2.1$$

$$Im(\alpha(\omega)) = (-h) / ((k - \omega^2 m)^2 + h^2) \quad \text{.....} 2.2$$

Figure 2.3 show these two functions. Obviously the resonance frequency occurs when the real part become zero.

Likewise, the real and imaginary parts of the FRF with viscous damping are derived as:

$$Re(\alpha(\omega)) = (k - \omega^2 m)/((k - \omega^2 m)^2 + (\omega c)^2) \quad \text{.....} 2.3$$

$$Im(\alpha(\omega)) = (-\omega c) / ((k - \omega^2 m)^2 + \omega c)^2 \quad \text{.....} 2.4$$

These functions are shown in Figure 2.4.

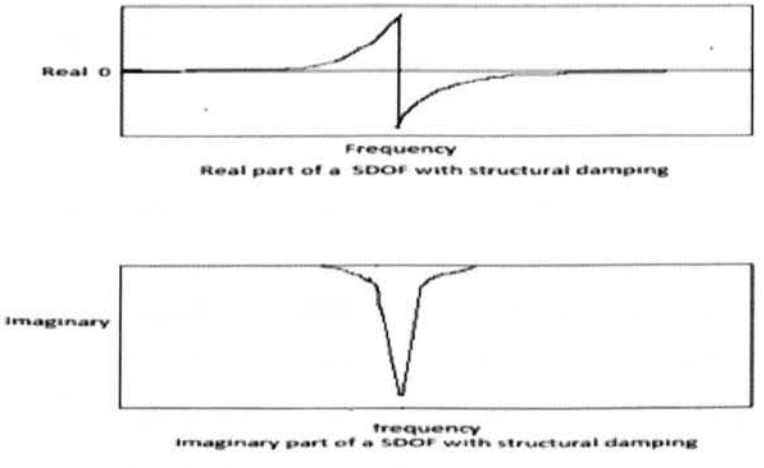

Figure 2.3 Real and Imaginary part of SDOF with structural damping [16].

2.2.3 Nyquist plot

A Nyquist plot shows on the complex plane the real part of a FRF against its imaginary part with frequency as an implicit variable. It was a parametric plot of a transfer function used in automatic control and signal processing. The most common use of Nyquist plots is for

assessing the stability of a system with feedback in Cartesian coordinates. The real part of the transfer function is plotted on the x axis while the imaginary part is plotted on the y axis. The frequency is swept as a parameter. Alternatively, in polar coordinates, the gain of the transfer function is plotted as the radial coordinate, while the phase of the transfer function is plotted as the angular coordinate. The Nyquist plot is named after Harry Nyquist, a former engineer at bell laboratories.

The benefit of using Nyquist plot comes from the circularity of a FRF on the complex plane. For a SDOF system with structural damping, we can draw Nyquist plot for its receptance, mobility and accelerance FRFs as shown in Figure 2.5. These three plots are not drawn to scale.

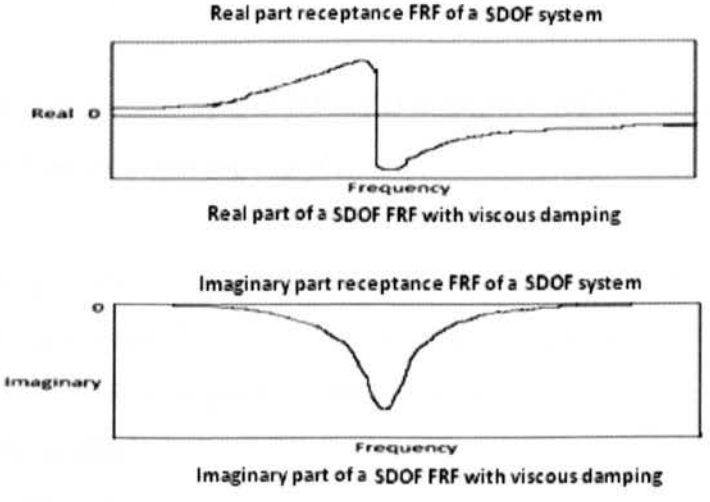

Figure 2.4 Real and Imaginary part of SDOF FRF with viscous damping [12, 16].

Although all three plots in Figure 2.5 appear to be circles, only the receptance FRF is a real one. From Equations 2.1 and 2.2 we can see that the receptance FRF begins from point $\{(k/(k^2+h^2)),((-h/(k^2+h^2))\}$ while both mobility and accelerance FRFs begin from origin. All three end at the origin. For measured FRF data, only a finite frequency range is covered and a limited number of data points are available so that we always have a fraction of complete Nyquist plot [14, 34].

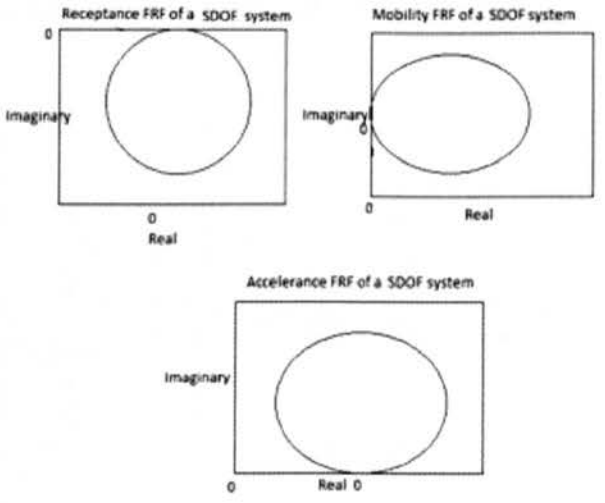

Figure 2.5 Nyquist plot of three FRFs with structural damping [12].

2.2.4 Display and properties of a FRF of a damped MDOF system

2.2.4.1 Amplitude –phase plot and log-log plot

The amplitude–phase plot of the FRF for a damped MDOF system consists of the plot of its magnitude versus frequency and that of its phase versus frequency [14].

There are many methods used to measure in MDOF, such as:

1- Extension of SDOF method.

2- General curve fit approach.

3- Lightly-damped structures.

2.2.4.2 Plots of real and imaginary parts of complex amplitudes

The real and imaginary plots consist of two parts: the real part of the FRF versus frequency and its imaginary part versus frequency. Real and imaginary plots are retracted to be its first part without damping. For MDOF system with structural damping, the real and imaginary parts can be derived analytically as [16, 35]:

$$Re\ (\alpha_{jk}(\omega))=Real(\sum_{r=1}^{n} \{(\phi_{jr}\ \ \phi_{kr})/(\lambda^2_r-\omega^2)\}) \qquad 2.5$$

$$Im\ (\alpha_{jk}(\omega))=Imag(\sum_{r=1}^{n} \{(\phi_{jr}\ \ \phi_{kr})/(\lambda^2_r-\omega^2)\}) \qquad 2.6$$

Figure 2.6 show the real and imaginary plots of a FRF for the 4DOF system.

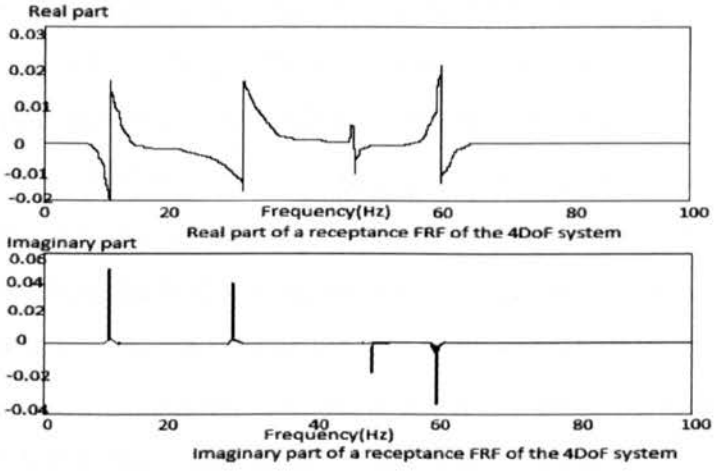

Figure 2.6 Real and Imaginary parts of FRF of the 4DOF system [13].

2.2.4.3 Nyquist plot

The main benefit of using the Nyquist plot for an SDOF FRF comes from its circularity property in the complex plane. This is still valid for a damped MDOF system. The circularity property does not exactly apply here since any vibration mode will be influenced by other modes of the system, thus compromising the simplicity form of a SDOF of FRF. Thus, the Nyquist plot is still one of the most useful plots for a damped MDOF of FRF. Figure 2.7 shows the Nyquist plot of a FRF of the 4DOF system [16, 36]. The data points do not connect full circles because of frequency resolution.

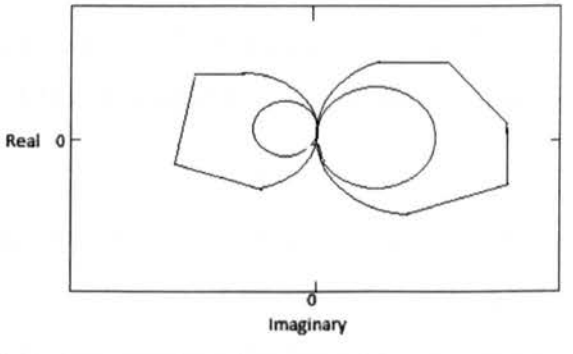

Figure 2.7 Nyquist plot of a FRF of the 4DOF system [33, 37].

2.3 Frequency Response Function (FRF)

The FRF describes the input-output relationship between two points on a structure as a function of frequency. Therefore, a FRF is actually defined between a single input DOF (point and direction), and a single output DOF. Although the FRF was previously defined as a ratio of the Fourier transforms of an output and input signal, it is actually computed differently in all modern FFT analyzers. This is done to remove random noise and non linearity's (distortion) from the FRF estimates. FRF is a measure of how much displacement, velocity, or acceleration response a structure has at an output DOF, per unit of excitation force at an input DOF. For some time–domain analysis it is to obtain either the free decaying impulse response or the response due to ambient excitations. As a result, we obtain the data for group of FRFs that can be used later for modal analysis to derive the model of structure [12, 38].

Theoretically, the type of force does not matter as the FRF is defined as the ratio between the responses and force. Whenever practical using force that has sufficient energy and frequency components to excite all vibration modes of interest and allow minimum error in signal processing, leading to the formation of accurate FRF data [39].

The FRF measurement cannot succeed if the dynamic properties of structure vary during the measurement. For this reason the structure should be time–invariant. This condition is usually met in FRF measurements. With multiple force inputs it becomes possible to make the structure vibration with reasonably uniform amplitudes rather than having great disparity of amplitudes across it under single input. This type of measurement in used property can result in more accurate FRF data and subsequently modal data. FRF data are not the only type of data acquired for modal analysis. As for a special category of modal analysis that utilizes the responses in time history, either free vibration response or impulse response function data are needed [40, 41].

However, if the excitations are not harmonic, it is usually necessary to use some numerical method such as the fourth order Range Kutta method to obtain the total responses of system. The modal analysis (modal superposition) method involves solving a number of uncoupled differential equations (equal to the degree of freedom). Uncoupled equations are expressed in terms of systems principle coordinates, modal damping factors and natural circular frequency i.e. eigenvalues.

Many special–purpose programs are available for simultaneous integration of n coupled differential equation. One widely used program is CSMP (Continuous System Modelling Program) [1, 30 and 42].

The modal analysis approach works equally well in obtaining the forced vibration responses of multiple–degree of freedom system using uncoupled equation of motion expressed in terms of the systems natural circular frequency and modal damping factors.

2.3.1 Measuring Frequency Response Functions

The Frequency Response Function (FRF) is a function of the characteristics of the system, and is independent of the input force. We assume linearity, time invariance; observability and reciprocity when calculating FRFs, measurement is made between a reference transducer and response transducer. The operating conditions have to be steady state since we average the data to get FRFs. Normally measuring FRFs using the H1 estimator. We do not have to use the H1 estimator, but it is available with most data acquisition system, alternatively H2 estimator can be used [43, 44], we will explain in detail later. The FRF magnitudes have peaks at the resonances and dips at the anti-resonances. The FRF could be categorised into the three types:

1) Bode plot is a graph of the transfer function of a linear, time-invariant system versus frequency, plotted with a log-frequency axis, to show the system's frequency response. It is usually a combination of a magnitude plot, expressing the magnitude of the frequency response gain, and a phase plot, expressing the frequency response phase shift. Phase drops 180° degrees through a resonance and rise 180° degrees through anti-resonance see Figure 2.8.

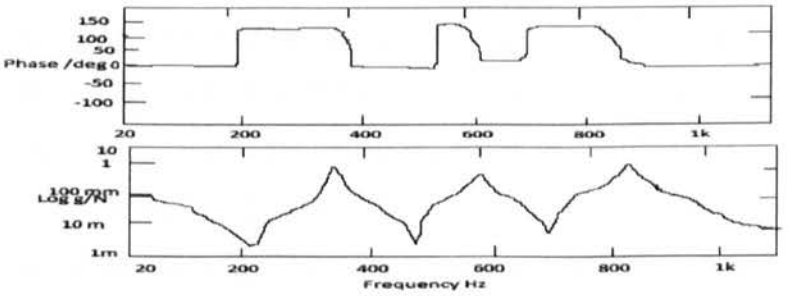

Figure 2.8 FRF magnitude and phase, Bode plot [45].

2) Real and imaginary versus frequency is a measurement where the input location and direction is the same as the output location and direction. Furthermore you can measure real

and imaginary between any two points. The imaginary part of a drive point FRF should be completely positive or completely negative, depending on the positive or negative orientation of the input and output signals. The peaks or dips of the imaginary part of a drive point FRF correspond to the system resonances, Figure 2.9 [44, 46].

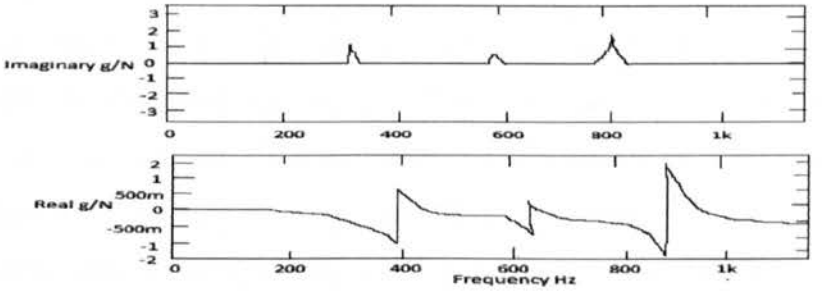

Figure 2.9 Real and Imaginary parts of drive points [44].

3) The last type was Nyquist plots which was explained previously in details.

2.3.2 General measurement setup

A typical measurement set-up in a laboratory environment should have three constituents.
First part is responsible for generating the excitation force to the test structure.
Second part is for measuring and acquiring the response data. Third part provides signal processing capacity to derive FRF data from the measured force and response data [40].

2.3.3 Measurement devices

In general the measurement devices categorised into the following categories:-

2.3.3.1 Excitation devices

The first part of measurement set-up is an excitation mechanism; excitation is achieved either by connecting vibration generator or shaker, or by using some form of transient input such as hammer that applies a force of sufficient amplitude and frequency contents to the structure. The two most common devices used are explained below [41, 46]:

1) Impact test (a hammer) Figure 2.10; is that produces an excitation force pulse to the test structure. It consists of: hammer tip, force transducer (another type of sensor used in modal testing, the accuracy effects are similar to that for an accelerometer), balancing mass and handle. Impact testing was developed during the late1970's, and has become the most popular modal testing method used today. Impact testing is a fast, convenient, and low cost way of finding the modes of machines and structures. It is simply means of exciting the

structure into vibration. Basically magnitude of the impact is determined by the masses of hammer head and the velocity of moving when it hits the structure [16, 47].

Two parameters are available to reduce the impact time for a given structure: tip stiffness and hammer mass. There are two types of tip stiffness; one is harder tip with short time duration and broader frequency range, and another type is soft tip with long time duration and smaller frequency range. The main consideration in selecting a force transducer is to understand how it interacts with the excitation device to which it connects. For example, when a force transducer is used on an impact hammer, variation of hammer tip and mass of the hammer handle can cause a different force transducer calibration. When the force transducer is used with an excitation shaker, the presence of its mass may cause significant distortion to the force signal measured at structural resonance. The extent of distortion is dependent on the mass difference between the transducer and the structure. The two near zero frequency spectrums can be avoided by making the impact duration T smaller so that first zero frequency is pushed outside the frequency and zero's operating range see Figure 2.11.

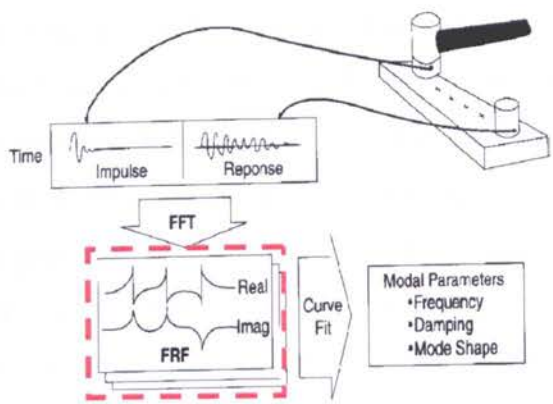

Figure 2.10 Impact test [48].

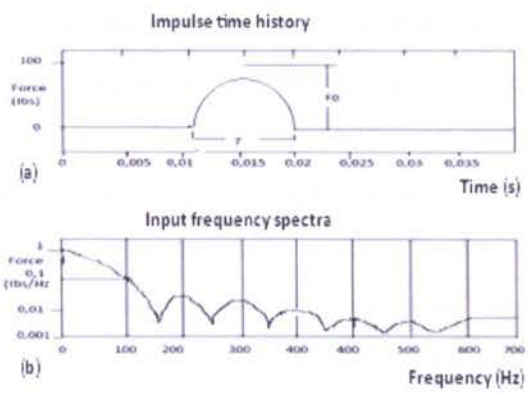

Figure 2.11 Ideal half–sine impulse function [32]: (a)- Time history showing peak value F and duration T.(b)- Corresponding frequency spectrum.

Generally we conclude if the window width is closer to the pulse duration these two curves are even closer, that advantageous to use transient window to reduce uncertainty in the input due to instrument noise [49].

2) A shaker Figure 2.12 also known as an electromagnetic (or electro-dynamic) shaker consists of: a magnet, moving block and a coil in the magnet.

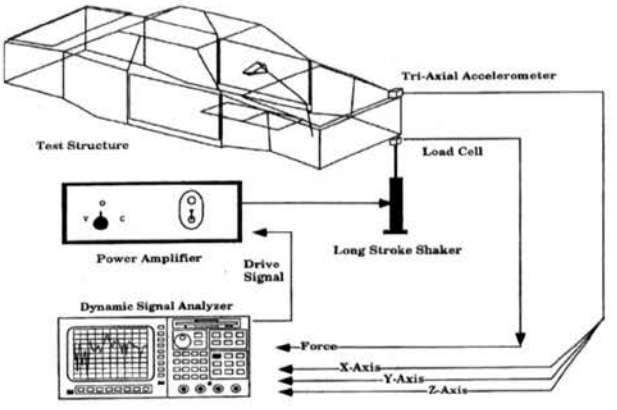

Figure 2.12 Shaker test setup [41].

The most common type of exciter is the electromagnetic (or electro-dynamic) shaker, in which supplied input is converted to an alternating magnetic field in which is placed a coil, which is attached to the drive part of the device, and to the structure. In this case the frequency and amplitude of excitation are controlled independently of each other.

It givens more operational flexibility–especially useful as it is generally found that it is better to vary the level of excitation as responses are passed through [12]. Another type of exciter to be considered is the hydraulic (or electro hydraulic). In this device the power amplification to generate substantial force is achieved through the use of hydraulic and although more costly and complex than their electromagnetic counter parts, these exciters do have potentially significant advantage, that is their ability to apply simultaneously a static load as well as dynamic vibratory. There are several important considerations that must be taken into account in order to obtain accurate results. They include pre trigger delay, force and exponential windowing and accept/reject capability [11, 41].

2.3.3.2 Response devices

1) Accelerometer:- is the most common sensor for modal testing used for vibration measurement transducer due to its small size, wide range of sensitivities and large usable frequency range. It measures acceleration of a test structure and output the signal in the form of voltage. The accelerometer response to sinusoidal and transient motion has been investigated.

Piezoelectric transducers are commonly used in accelerometer and forces transducer because: small size, large stiffness, low damping, and high sensitivity, accelerometers and force transducers often uses piezoelectric sensing elements to achieve certain design natural

frequency [40, 50]. Three types of piezoelectric transducer are available for mobility measurements-force gauges, accelerometers and impedance heads. However piezoelectric sensors are charge generators that require special amplifiers called charge amplifier. The improper amplifier use can significantly affect the measurements, but in this work, accelerometer with built in amplifier has been used.

Transducer manufacturers provide calibration information concerning their instruments voltage sensitivities. It is designed to measure force or acceleration under a wide variety conditions. There are some environmental factors that can alter or change transducer's performance such as: a) base strain (structure can have significant bending strain) when there is no motion to record but a lot of bending strain or surfaces curvature is transmitted to the piezoelectric sensing element through transducer's base, can cause output signals when there is no motion to reduce this element motion. Compression design has the most bending sensitivity while shear design usually have minimum sensitivity to bending strain, b) cable noise, c) humidity and dirt, d) monitoring the transducer, e) nuclear radiation, f) temperature, g) transducer mass, h) transverse sensitivity [51, 52].

2) Proximity sensor:- beside the accelerometers, one of the other devices which could be used to obtain the response of a system is proximity probe which is able to detect the presence of nearby objects without any physical contact. It often emits an electromagnetic or electrostatic field, or a beam of electromagnetic radiation (infrared, for instance), and looks for changes in the field or return signal. The object being sensed is often referred to as the proximity sensors target. Different proximity sensor targets demand different sensors. For example, a capacitive or photoelectric sensor might be suitable for a plastic target; an inductive proximity sensor requires a metal target. The maximum distance that this sensor can detect is defined as "nominal range". Some sensors have adjustments of the nominal range or means to report a graduated detection distance. Proximity sensors can have a high reliability and functional life because of the absence of mechanical parts and lack of physical contact between sensor and the sensed object [53-55].

2.3.4 Selection of excitation forces

1- Sinusoidal excitation (exciting the structure with high vibration level).
2- Random excitation.
3- Pseudo-Random excitation.

4- Impact excitation is relatively simple excitation technique compared with the shaker excitation, because of no physical connection between the excitation and the structure. Impact test avoids the problem of interaction between them but the main disadvantages of impact excitation are as notable its advantages, it is difficult to control either the force level or the frequency range of the impact [32, 48].

2.3.5 Selection of excitation function (source type)

In general the excitation function is the mathematical signal transfers as an input and the excitation system is the physical mechanism which delivers the signal. The selection of the excitation function will lead to selection of the excitation system. For instance a choice of a random function will require a shaker system and an impulsive type of excitation function will require the choice of hammer.

The main excitation function could be categorised into the following categories;

1- Steady – state functions.
2- Random functions.
3- Burst Random.
4- Sine Sweep.
5- Chirp.
6- Periodic Random functions.
7- Transient functions.

Where, **Random** source type generates a random signal. The main disadvantage of a true random signal is that it is always non-periodic in the sampling window. Therefore, a special time domain window (a hanning window or one like it), must always be used with true random testing to minimize leakage [12, 56].

Burst random excitation has the combined advantages of both pure random and pseudo random testing. That is, its signals are leakage free and when using with spectrum averaging, will remove non-linearity from the FRFs. In burst random testing, either a true random or time varying pseudo random signal can be used, but it is turned off prior to the end of the sampling window time period. This is done in order to allow the structural response to decay within the sampling window. This ensures that both the excitation and response signals are completely contained within the sampling window. Hence, they are periodic in the window and leakage free.

The **Periodic Random** source type is a short sequence random signal composed of phase randomized sine components on FFT analysis line. This can be used for fast structural measurements that require a minimum of averaging.

The **Sine** source type generates a sine wave at a single specified frequency.

The **Sine sweep** source type can be used with sine reduction for complete resonance of each test system or for general structural (modal) analysis.

The **Chirp and Burst Chirp** source type is a fast sine sweep within one FFT analysis bloc. It can be used for structural testing to reduce measurement time. A burst chirp signal is the same as a chirp, except that it is turned off prior to the end of the sampling window, just like burst random. The advantage of burst chirp over chirp is that the structure has returned to rest before the next average of data is taken.

To sum up, in order to choose the most suitable excitation function for a structure, it is best to take into account several factors such as the availability of the signal processing equipment, the natural characteristics of the dynamic structure, the purpose of the measurements, and the feasibility of excitation system.
In practice the amount of damping and the density of the modal dynamics of the structure will be one of the first factors of choosing a particular excitation function [20, 49].
For instance, in the case which the structural modes are closely together and /or the structure is under damped (ζ is less than 1); a leakage free excitation function (burst random "shaker") will be the best choice.
All of excitation systems are generally classified into four groups which are: shakers, impactors, step relaxations and self operating mechanisms.

2.3.6 Special characteristics of a FRF

From the theory of modal analysis we can derive some characteristics of a FRF and use them to assess the FRF data measured in modal testing [49, 57].

1- First characteristic is that for point FRF measurement we expect to see anti-resonance between two adjacent resonances. If this characteristic is on a point measurement, it is likely that the force and response transducers are not actually at the same coordinate,

as they should be. Any minor offset of the two could degenerate some of anti-resonances.

2- For grounded structure, at very low frequency range the predominant characteristic of the structure is its static stiffness. Therefore at the beginning of the FRF we should see stiffness line before the first resonance appears. On other hand, for a freely supported structure, the prevailing characteristic at very low frequency is the mass and inertia, this mean we should see mass line at the beginning of the FRF Figure 2.13.

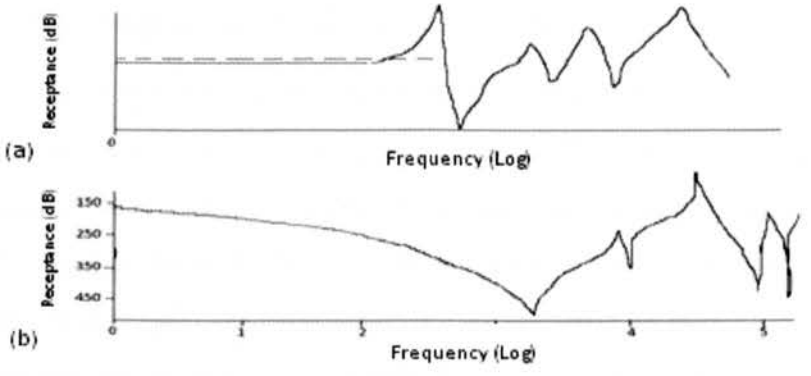

Figure 2.13 A point FRF of a free structure with the dotted mass line [16]: (a)- A point FRF of a grounded structure with the dotted stiffness line. (b)-A point FRF of a free structure with the dotted mass line.

2.4 Reducing noise in the measurements

We can eliminate or reduce zero-mean noise that is non–coherent with respect to the measured input signal by averaging the FRFs with respect to the input signal. Example of non–coherent noise sources are electrical noise on the transducer signal, and noise due to any unmeasured excitation sources that are non–coherent with respect to the measured input signal. Averaging reduces the variance of the estimated FRFs [58].

The signal processing of the measurements may cause errors in the FRFs, common example of signal processing errors are aliasing and leakage. Aliasing occurs when there is problem associated with digital spectral analysis, these results from the originally continuous time history with this process, the existence of very high frequencies in the original signal may well be misinterpreted if the sampling rate is too slow. So, it occurs when the frequency components larger than ½ the sampling frequency wrap around into the frequency range less than ½ the sampling frequency [46]. We eliminate aliasing error by using analogy anti-alias filters, although some aliasing effects may occur in the frequency range where the anti-filters have roll-off.

Leakage occurs when the Fourier transformed signal is not periodic or perfectly observed transient in the time block. The FFT assumes that the signal to be transforming is periodic in the transform window. The transform window is the samples of data used by the FFT. To be periodic in the transform window, the wave form must have no discontinuities at its beginning or end, if it were repeated outside the window. Signals that are always periodic in the transform window are:

1) Signals that are completely contained within the transform window.
2) Cyclic signals that complete an integer number of cycles within the transform window.

If a time signal is not periodic in the transform window, when it is transformed to the frequency domain, a smearing of its spectrum will occur, this is called leakage. It distorts the spectrum and makes it inaccurate. Therefore, if the response signal in an impact test decays to zero (or near zero) before the end of the sampling window, there will be no leakage, and no special windowing is required. We reduce leakage by selecting an appropriate excitation type and applying time domain window to the signals before the Fourier transform. Increasing the frequency resolution also reduces leakage effects [58]. Once we have leakage in the data with randomized inputs; we can reduce it but not eliminate it. We can essentially eliminate leakage with impact testing, as long as the signals are zero at the start of the data acquisition time block and we apply appropriate force /exponential windows so that the signals are completely observed transients. Leakage and aliasing cannot be reduced by averaging [44].

Nonlinear noise is due to nonlinearities in the system. When we measure FRFs, we assume the system is linear. A nonlinear system results in distorted FRF measurements. We reduce nonlinear noise by linearising the system as much as possible, and by randomizing the input signals to the system.

There are two possible signal processing problems related with impact testing. Firstly, long time recording can cause noise to be present in either response or force signal. Secondly, in short time recording, leakage can be present in the response signal. A windowing technique can be applied to compensate for the problems. Usually the force pulse is shorter in comparison to the length of the time record. The noise which occurs after the pulse is a portion of the signal which can be eliminated without causing any disruptions to the pulse. To accomplish this, a window design has been applied known as force window as shown in the Figure 2.14. Towards the end of the pulse, a small amount of oscillation occurs which is part of the pulse, this must not be truncated as it is a result of signal processing [11, 12].

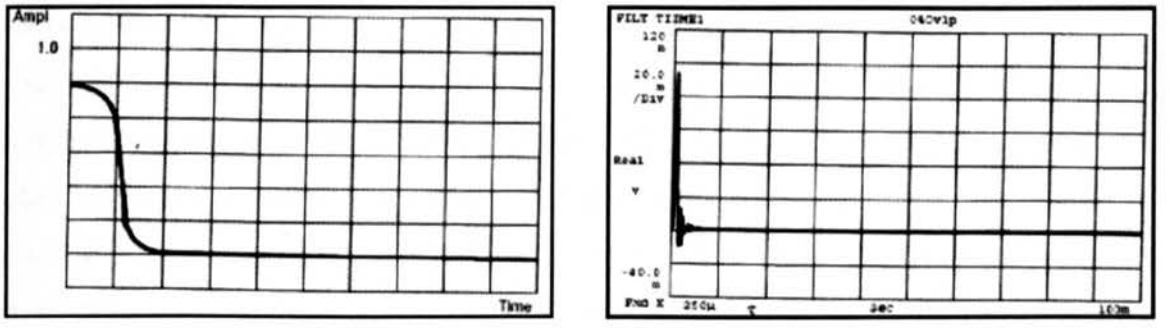

Figure 2.14 Reducing noise in measurement (force pulse with force window) [59].

The response signal is an exponential decaying function and may decay out before or after the end of the measurement [60].

The response possibly will decay out sooner than the end of the time record if the structure is heavily damped. The remaining noise in the time record can be eliminated by using the response window. The response may continue further than the end of the time record if the structure is lightly damped. In this case, to minimize leakage it must be artificially forced to decay out. To achieve any of the two above results, a window designed known as exponential window must be used as shown in Figure 2.15.

The rule of thumb for setting the time constant, (the time required for the amplitude to be reduced by a factor of 1/e), is about one-fourth the time record length. The result of this is shown in Figure 2.15.

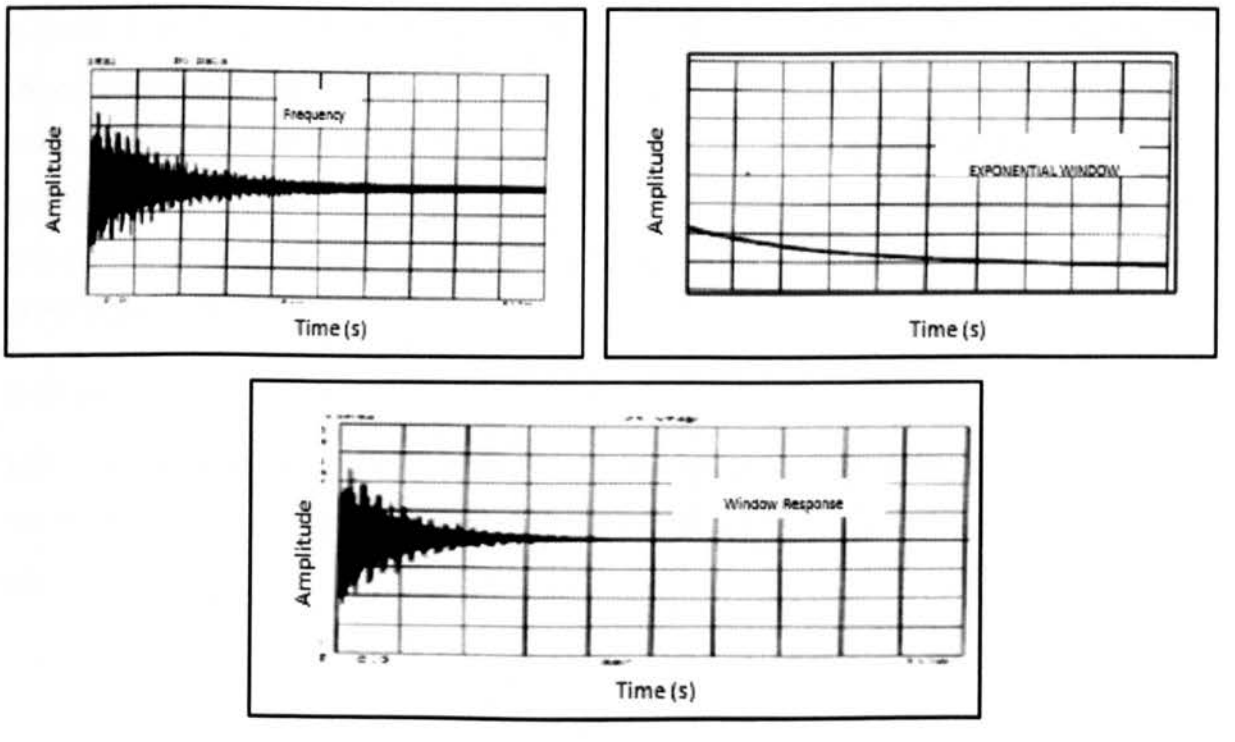

Figure 2.15 Decaying response with exponential window applied [59, 60].

The frequency response can be altered when using the exponential window unlike the force window. This is due to the effect of adding artificial damping to the system. After signal processing the added damping coefficient can usually be backed out of the measurement. For lightly damped structures, this can cause numerical problems. This can occur when the true damping in the structure is less than the added damping from the exponential window. To obtain more accurate measurements is to zoom, which records for a longer time ensuring the whole response is captured on the exponential window [14, 29 and 59].

2.4.1 Coherence function and its relationship to H_1 and H_2

A- Noise on the output H_1

This FRF estimate assumes that random noise and distortion are summing into the output, but not the input of the structure and measurement system. In this case, the FRF is calculated as:

$$H_1 = \frac{XPS}{Input\ \ APS} \quad \text{.....} \quad 2.7$$

Where XPS denotes Cross Power Spectrum estimate between the input and output signals, and input APS denotes the Auto Power Spectrum of the input signal. The measurement capability of all multi – channel FFT analyzer is built around a tri-spectrum averaging loop. This loop assumes that two or more time domain signals are simultaneously sampled. Three spectral estimates, APS for each channel, and the XPS between the two channels, are calculated in the tri-spectrum averaging loop. After the loop has completed, a variety of other cross channel measurements (including the FRF), are calculated from these three basic spectral estimates. It can be shown that H_1 is a least squared error estimate of the FRF when extraneous noise and randomly excited nonlinearity's are modelled as Gaussian noise added to the output [30, 61].

B-Noise on the input H_2

This FRF estimator assumes that random noise and distortion are summing into the input, but not the output of the structure and measurement system. For this model, the FRF is calculated as:

$$H_2 = \frac{Output\ \ APS}{XPS} \quad \text{.....} \quad 2.8$$

Likewise, it can be shown that H_2 is a least squared error estimate for the FRF when extraneous noise and randomly excited non-linearity are modelled as Gaussian noise added to the input.

C-Noise on the input and output

This FRF estimator assumes that random noise and distortion are summing into both the input and the output of the system, because we have used different quantities for these two estimates, we must be prepared for eventuality that they are not identical as, according to theory, they should be and to this end we shall introduce a quantity γ^2, which is usually called the "Coherence" and which is defined as [11]:

$$\gamma^2 = \frac{H_1}{H_2} \quad \text{.....} \quad 2.9$$

The coherence can be shown to be always less than or equal to 1.0. Clearly, if all is well with measurement, the coherence should be unity and we shall be looking for this condition in our test to reassure us that the measurements have been well made.

2.4.2 The effects of signal noise on FRF measurements

$$\gamma^2(\omega) = H_1(\omega) / H_2(\omega) = 1 / \{1 + G_{nn}(\omega) / G_{ff}(\omega)\} \quad \text{.....} \quad 2.10$$

The coherence function is sensitive to the input signal's noise relative to the actual signal at each frequency (ω). The decrease in coherence is dependent on the noise to signal ratio [33, 52].

$$IS/N(\omega) = \{G_{ff}(\omega)/G_{ff}(\omega)\} = \{\gamma^2(\omega) / (1 - \gamma^2(\omega))\} \quad \text{.....} \quad 2.11$$

Good input signal to noise ratio results when the coherence is close to unity.

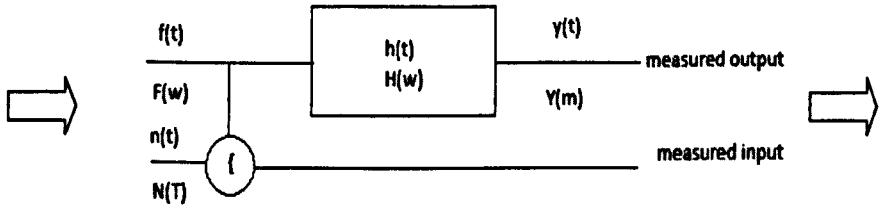

Figure 2.16 Linear models with noise n (t) in input signal [26, 52].

The higher coherence, the closer together are two estimates, however remember that low coherences is an indication of measurement problems and high coherences is usually an indication of good quality measurements, there are situations where coherent noise in both measurements will give high coherences and poor measurements. Coherence is measured on a scale of 0.0 to 1.0, where 1.0 indicates perfect coherence is near the natural frequency of the system because the signals are large and are less influenced by the noise. Coherence values less than unity are caused by poor resolution, system nonlinearities, extraneous noise and uncorrelated input signals. Because coherence is normalized, it is independent of the shape of frequency response function [62, 63].

2.4.3 Type of window using to reduce the noise

1- Uniform, see Figure 2.17.
2- Exponential
3- Force /Exponential
4- Flattop
5- Hanning
6- Hamming [56].

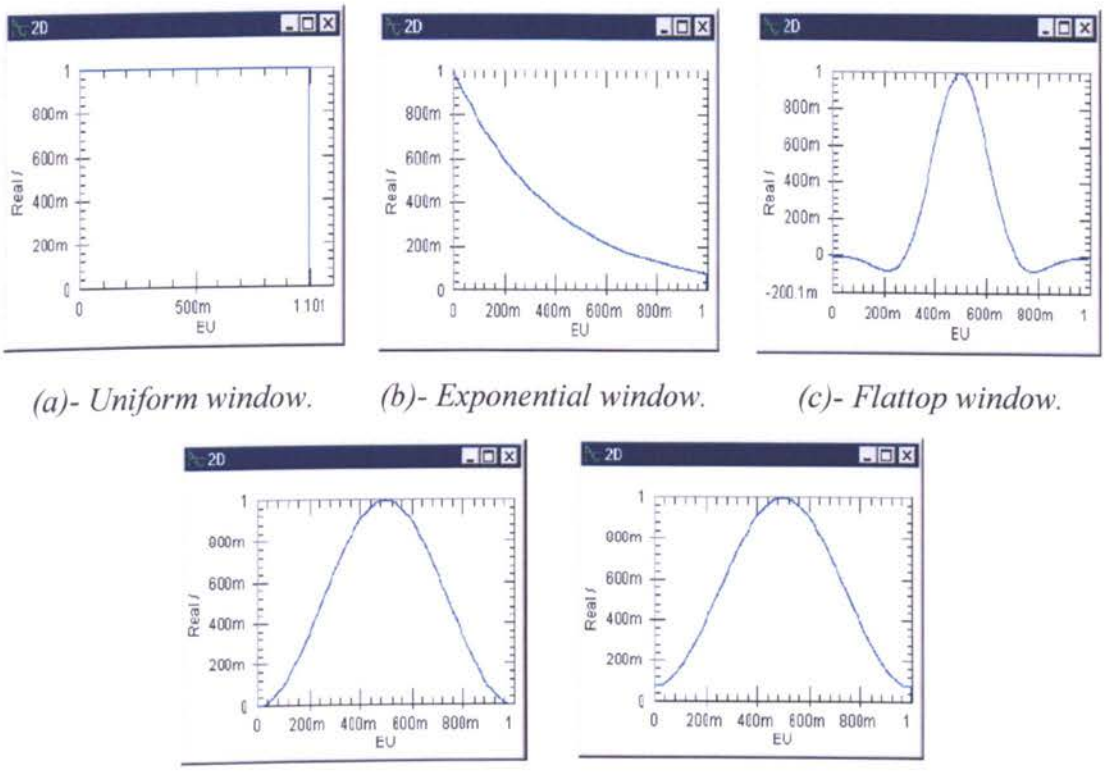

(a)- Uniform window. *(b)- Exponential window.* *(c)- Flattop window.*

(d)- Hanning window. *(e)- Hamming window.*

Figure 2.17 Available time domain windows [56].

Using (exponential or force/exponential) a transient signal in impact testing provides the same leakage free measurements, but with more controllability over the test.

Probably the most popular excitation signal used for shaker testing with an FFT analyzer is the true random signal with a hanning window. Ideally, the entire shaker signals that are leakage free (periodic in the window) should yield the same results.

2.4.4 What is the mode shape

A vibrating structure by nature deforms into certain patterns at the natural frequencies of the structure. The deformation patterns and their natural frequencies depend only on the characteristics of the structure, and not on the input force. These deformation patterns are the mode shapes of the structure, see Figure 2.18.

Modes are inherent properties of a structure. They are determined by the material properties (mass, stiffness and damping properties), and boundary conditions of the structure. Each mode is defined by a **natural frequency** and a **mode shape** [45, 58].

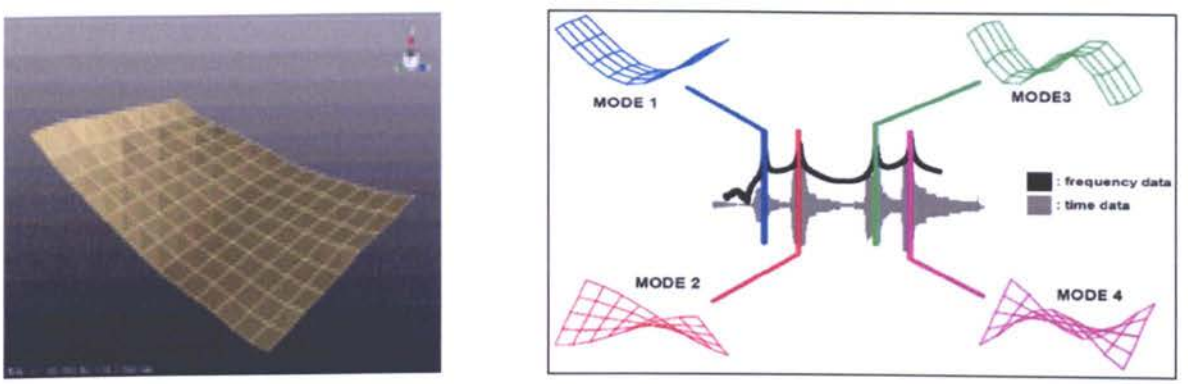

Figure 2.18 Mode shape [15, 56].

2.4.5 Modal frequencies

The modal frequencies are the roots of the characteristic equation of the system and contain damping and natural frequencies of the modes. Also refer to modal frequencies as roots, characteristic values, eigenvalues or poles. A modal frequency can be a complex value. The real part of modal frequency is related to rate of decay or damping coefficient of the mode and imaginary part is the damped natural model frequency or pole, as

$$\lambda_i = \sigma_r + j\omega_r \qquad 2.12$$

For the under damped system, the modal frequencies occur in complex conjugate pairs. Unless there is active damping mechanisms, most structure are typically under damped, with modal damping ratios normally less than 10% [15, 24].

If two or more modes have the same modal frequency, the system has repeated roots. Repeated roots are common in symmetric structures, but can occur in non-symmetric structures as well. Closely spaced or pseudo-repeated roots occur in the frequency range where there is high modal density. In theory; there is a difference between frequencies of the mode. For the rth mode, we express the corresponding repeated and pseudo–repeated roots, but in practice, they are the same.

2.5 Existing techniques in rotor dynamics

2.5.1 For balancing

Vibration caused by mass imbalance is a common problem in rotating machinery [64, 65].

Qu, L. S. and Qiu, H. Xu. [28] carried out the Rotor Balancing Based Holospectrum Analysis Method, it is developed by Qu and can fully describe the vibration information and plays an important role in improving the precision of the balancing, but this method is employed to solve minimum unbalancing problem.

Daniel et al [65] carried out the Sequential Quadratic Problem Method (SQPM) which is based on the minimum solution; these methods are efficient in reducing the maximal vibration. They have some limitation; they are convenient in dealing with constraints.

For example; balancing examples of test rotor of 300 MW steam turbine motor in Figure 2.19 show that SQPM algorithms can solve the balancing weight optimization problem effectively; moreover, SQPM algorithms are convenient in dealing with the constraints [64-66].

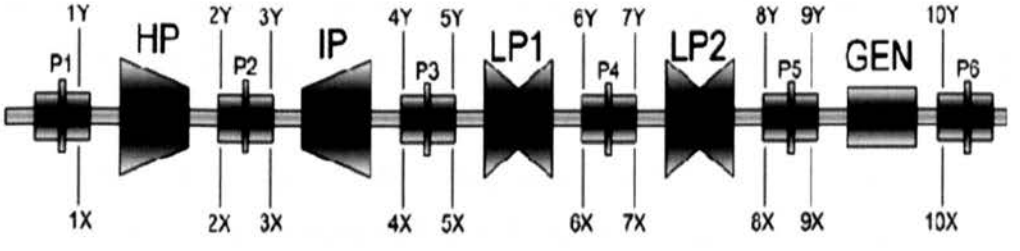

Figure 2.19 300 MW steam turbine system [28].

There is another method by Qu, L. S. and Qiu H. Xu. [28] called Influence Coefficient Method (ICM), the flexible motor balancing problem based on the influence coefficient method and holospectrum technique is formulated as a mini-max optimization problem, this is an experimental method originally proposed by Goodman [67].

This method was good because this formulation can solve mini-max high speed rotating balancing problem under particular balancing constrains effectively while ensuring the balancing machinery run up safely.

ICM is the first practical balancing method, but in field balancing, the correction weight in a correction mass plane is always constrained, for example the maximal weight can be added is constrained by the available space, this problem can be solved by adding the practical correction weight as constraint.

Another problem to be solved by ICM is balancing rotating machinery at its running speed. It is possible the correction weight calculated at the high speed makes the low speed vibration during run up in some balancing planes unacceptable, causing the results obtained by the method to be not accurate compared by other method.

In ICM, it also need large number of trial runs to obtain the vibration responses of trial weight in different correcting planes and vibration measurement always depends on a signal sensor in one measuring section.

Keyu et al [31] and Jimin et al [16] carried out Modal Balancing Method (MBM). This method used with ICM method for solving flexible rotor balancing problem. It can be added in ICM low speed, vibration can be used as constraint in calculating the balance weight of running speed to ensure the machinery run-up and down safely. However, this method has limitations: it needs large number of trial runs to obtain the vibration responses of trial weight in different correcting plane.

Shi [68] and Liangsheng et al [69-71] carried out the Holospectrum and Genetic Algorithm; a large amount of statistical data indicates that the mass unbalance of rotors is usually the major cause of excessive vibration of large capacity turbine. The method is based on assumption that a rotor bearing has an equal rigidity in different directions. Holospectral technique based on conventional FFT spectra and information fusion is applied in the field balancing of flexible rotor system. This is helpful to simplify the balancing procedure and enhance the balancing accuracy and efficiency. It is a good method because it successfully applies the holospectral principle in traditional balancing method of flexible rotor systems

and decreases the number of tests with increase in precision and efficiency of field balancing. This method track a completed field balancing process of given rotor set and utilize the holospectral techniques before further balancing. It measure original vibration of each bearing section in no load trial running and reduce errors in balancing calculation due to limited utilization of the information. However, this method has two limitations. Firstly the analysis errors would occur when the bearing rigidity is different, and secondly, in hole-balancing method, angle compensation is used to correct the error due to different rigidities.

The Genetic Algorithm Method (GAM), has been used by Cooley et al [22] and Goldberg [72]. This method will be used to optimize the correction masses for a better vibration distribution on the entire rotor system and utilize transfer matrices to get correction masses and angles on each balancing plane but the angle of balancing weights still stand. It applies appropriate correction masses to realize optimization.

Tseng et al [73], Lund and Tonneson [74] carried out the Dynamics Balancing Scheme for Motor Armature Method (DBSMAM). This technique applied to dynamic balancing of armature in an automobile starting motor, because of major source of vibration in an electric motor is unbalance in the armature. This method was developed by using adaptive parameter estimation method. The results obtained show that balancing system achieves a better balancing performance than a system based on the conventional influence coefficient method. Basic principal of the method: is to develop two-plane balancing technique for dynamic balancing of a rigid rotor using two- planes and develop dynamic balancing system comprising unbalance measurement machine and milling machine for the balancing of automobile starting motor armature.
These experiments are performed to verify the proposed approach and to evaluate its performance compared to balancing scheme based on the conventional influences coefficient method.

Using Finite Element Method to Solve Balancing Problem by Ewins et al [29], Dobson [37], Edney et al [75], Wang et al [76] and Dyka et al [77]. The study developed a multipurpose finite element solution model with the theoretical ground work development of finite element solution for analysis of the dynamics behaviour and balancing effects of an induction motor system. This model is capable of solving many of related rotating machine problems such as

high speed gas bearing spindles and electric machines. Finite Element Analysis (FEA) becomes an effective numerical approach to solve the rotor dynamic problems; because structure of industrial rotor–bearing systems such as the above–mentioned induction motor is always complex and finding the exact solution is hardly feasible.

Animesh [5] and Rieger [78] carried out Method of Dynamic Balancing in NMR Double Rotor System. This method gives exact solution problem of dynamic balancing in NMR double rotor system. This will enable one to perform high speed spinning about two intersecting axes. NMR method provided information about chemical bonding and imbalance due to symmetric distribution of weight about rotation axes.

Other researchers such as; Gyunghyun [79], Matanachai, Yano [80] and Gokcen et al [81] used the Method of Mixed–Model Line Balancing. They adopted the goal programming approach and designed an appropriate algorithm process. The model may be very useful for operation managers to make decisions on their job scheduling efforts. The limitation of this method is that the mixed model assembly line must be re-balanced as needed due to the season change on the products life cycle as well as the line must be stable enough to the daily change on the seasonal changes when the model change.

2.5.2 Auto balancing

Michal et al [82], Kyung, Sundar [83] and Mahfoud et al [84] carried out auto balancing by Using Robotics and Mechatronics:- Using method of design of fault detection isolation and restoration systems for rotating machineries. This study present theoretical background, results of experimental research into Fault Detection, Isolation and Restoration (FDIR) system for rotating machineries. FDIR presented system solution concerning the problem of automatic balancing of rotating systems while in operation. Simulations and experimental results proved that application of presented solution leads to reduction in vibration caused by imbalance without hindering service.

Lum et al [85] and Fuller et al [86] applied the Direct Active Vibration Control (DAVC) method. This technique applied a control force directly to the rotor. Typical example of DAVC with magnetic bearing; the force generated can be changed rapidly. Rapid changes in

the forces can be used not only for suppressing synchronous (imbalance) vibration but also for non- synchronous (imbalance).
The main disadvantage is force limitation–for high rotational speed the force that can be generated by the imbalance can easily exceed the maximum force that can be generated by DAVC devices.

Method of PI Observer Detect Abnormal by Tsai, Mi-Ching et al [87]. Information in an Auto–Balancing Two Wheeled Cart (ABTWC); caused by actuator faults and steering load torque. A fault diagnostic scheme which contains the strategies of both fault – detection and fault – evaluations is proposed. This method has disadvantage in that most critical situation; apparently the uncertainty model describes possible actuator faults mathematically because ABTWC system becomes unstable when the actuator is off.

Another technique has been used is Development and Adoptive Imbalance Vibration Control of Magnetic Suspension System called Active–Magnetic-Bearing (AMB) by Tang et al [88] and Tiwari et al [89]. In this method model is developed to describe the translational and rotational motion of an active magnetic bearing – suspended rigid rotor in a single gimbals' control moment gyro on board a rigid satellite. This model strictly reflects the motion characteristics of the rotor by considering the dynamics and static imbalance as well as the coupling between the gimbals' and rotor's motion on satellite platform. Electromagnetic balancing with AMB proves to be pattering way, especially in high–precision control using high speed actuators.
AMB suspension, different from the mechanical bearing, is of a soft support type, and its rotor cannot always be kept at the AMB centre.

2.5.3 Modelling of rotating structures

The modal model (natural frequencies, mode shapes and modal damping) of a machine based on the in-situ experimental modal tests is one possible modelling approach.
Most of the research investigations are performed based on vibration characteristics of rotor bearing system. Nelson and Mcvaugh [90] first used the finite element method and derived various property matrices. They gave the detailed information about critical speed and unbalance response. Instability due to internal damping and hysteretic damping is given by

Nelson and Mcvaugh [90], Zorzi and Nelson [91]. Lin and Lin [92] have investigated the optimal weight design of rotor-bearing system. Aleyaasin et al [93] have used the dynamic stiffness matrix method to perform the lateral vibration analysis of rotor-bearing system. Firoozian and Zhu [94] have used transfer matrix method to study lateral vibration of rotor-bearing system. Wu and Yang [95] used transfer matrix method, finite element method and Lagrangian dynamics method to study coupled torsional lateral vibration analysis of rotor-bearing system. Most of literature contains research carried out on actual full-size rotor bearing system. Wu [96] and Thompson et al [97] developed a methodology to study vibration characteristics of full sized rotor system based on scaled models: Scaled Rotor. He gave a systematic approach to the methodology of scaling laws and dimensional analysis applied to a rotor bearing system. The theory and predicted values agree with each other in case of eigen frequencies and steady state response.

Irretier [98] gave an overview of different experimental modal analysis techniques. Such an experimental model is expected to avoid all uncertainties in the mathematical modelling approach, often FE model. The dynamics of the fluid bearings during machine operation and the rotation of the shaft itself influence the dynamic behaviour of the complete machine, which imposes certain limitations on the modal testing for rotating machines. Bucher and Ewins [99] have discussed these issues in detail. Irretier [100] gave the mathematical background to extract the modal model for rotating structures which are characterised by non-symmetric and time-variant matrices, unlike the assumptions for the experimental modal analysis of stationary structures, namely a linear, time-invariant system where reciprocity holds. Another alternative is the use of a modal model of the foundation alone together with the FE model of the rotor and the mathematical model for the bearings, Pennacchi et al [101].

There has been a long-standing interest in rotor dynamic modelling that has evolved since the first and incorrect rotor dynamic analysis by Rankin in 1869. The models contain more intricate geometric complexities, bearings, seals, and attached components such as discs, blades, fans, and couplings. Some models involve relatively simple beam representations of the rotor on bearings that are represented as stiffness and damping. The standard analysis of rotor systems includes critical speeds, stability, and unbalanced response [102].

Considering the difficulties and limitations in the modelling and/ or the modal testing for rotating machines, the most promising avenue is to identify a model of the foundation directly from measured vibration data, and use this with a good FE model for the rotor and a fairly accurate model for the plain bearings. The research work in this direction was initiated

by Lees [103] in 1988, and since then a number of approaches have been proposed by researchers across the world.

2.6 Summary

Modal analysis theory for single and multi degree of freedom systems is presented in this chapter.

FRFs characteristics and measurement are outlined, which is the most important modal parameter in reducing the vibration and noise in the rotating machinery.

General measurement set up used in this thesis is described for both hammer and shaker tests, with an overview about different excitation signals used with shaker test. The effect of signal noise on the FRF measurement is described and different types of window can be used to reduce the noise production. The effect of coherence on H1 and H2 is outlined, which will be performed in chapter 4.

Furthermore, a description of existing technique in rotating machinery is provided.

CHAPTER 3

Theory of Rotor Dynamics Prediction

3.1 Introduction

In the design of rotating machinery it is necessary to predict the dynamic behaviour of the rotors in bending and torsion deformations, these predictions are as follows [36];

1- The static and dynamic behaviour in torsion deformations is performed. The natural frequencies which give the critical speeds must be determined. In addition, when electric motors or generators are present, the dynamic behaviour during start-up or under short-circuit must be predicted.

2- The dynamic behaviour in bending is performed last. The natural frequencies as a function of the speed of rotation, which give the critical speeds, and possible instabilities must be determined. Then, the effect of forces of excitation is calculated, mass unbalance being the most important of these.

The basic elements of a rotor are the disc, the shaft, the bearings and the seals [104, 105]. The mass unbalances which cannot be completely avoided must also be considered. Kinetic energy expressions are necessary to characterize the disc, shaft and mass unbalances. The forces due to bearing or seals are used to calculate their virtual work, and then the corresponding forces acting on the shaft are obtained. The general rotor equations are provided by mean of the following steps:-

1- The kinetic energy T, the strain U and the virtual work δW of external forces are calculated for the elements of the system.

2- A numerical method is chosen: The Rayleigh–Ritz method for a very small number of degrees of freedom, and the finite element method for engineering applications.

3- Lagrange's equations are applied in the following form:

$$\frac{d}{dt}\left(\frac{\partial T}{\partial \dot{q}}\right) - \frac{\partial T}{\partial q_i} + \frac{\partial U}{\partial q_i} = F q_i \quad \text{.....} \quad 3.1$$

Where N $(1 \leq i \leq N)$ is the number of degrees of freedom, q_i are generalized independent coordinates, Fq_i are generalized forces, and denotes differentiation with respect to time t.

3.1.1 The Disc

The disc is assumed to be rigid and is then characterized solely by its kinetic energy. R_0 *(XYZ)* is an inertial frame and *R(x, y, z)* is fixed to the disc Figure 3.1. The *xyz* coordinate system is related to the *XYZ* coordinate system through a set of three angles ψ, θ and ϕ . To achieve the orientation of the disc one first rotates it by an amount ψ around the Z axis; then by an amount θ around the new *x* axis, denoted by x_1 ; and lastly by an amount ϕ around the final *y* axis. The instantaneous angular velocity vector of the *xyz* frame is [66, 106]

$$\omega_{R/R_0} = \dot{\psi}\ Z + \dot{\theta}\ x_1 + \dot{\phi}\ y \quad \text{.....3.2}$$

Where *Z*, x_1 and *y* are unit vector along the axes *Z*, x_1 and *y*, the kinetic energy of the disc about its centre of mass O is calculated using the frame *R*. In this system the angular velocity vector becomes

$$\omega^{R}_{R/R_0} = \begin{bmatrix} \omega_x \\ \omega_y \\ \omega_z \end{bmatrix} = \begin{bmatrix} -\dot{\psi}\cos\theta\sin\phi + \dot{\theta}\cos\phi \\ \dot{\phi} + \dot{\psi}\sin\theta \\ \dot{\psi}\cos\theta\cos\phi + \dot{\theta}\sin\phi \end{bmatrix} \quad \text{..... 3.3}$$

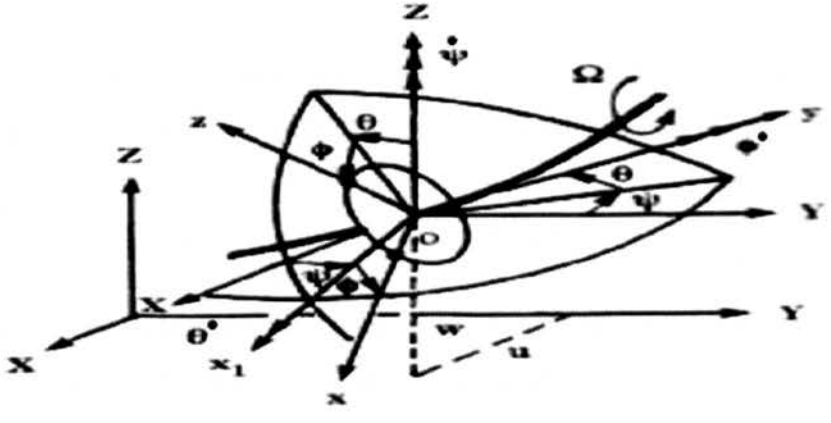

Figure 3.1 Reference frame for a disc on a rotating flexible shaft [107].

Let *u* and *w* designate the coordinates of O in R_0, the coordinate along *Y* being constant. In addition, the mass of the disc is M_D and its tensor of inertia in O as *xyz* are principle direction of inertia is

$$I_{/0} = \begin{bmatrix} I_{Dx} & 0 & 0 \\ 0 & I_{Dy} & 0 \\ 0 & 0 & I_{Dz} \end{bmatrix} \quad \text{.....} 3.4$$

The expression for the kinetic energy of disc is

$$T_D = 1/2\, M_D(\dot{u}^2 + \dot{w}^2) + 1/2\,(I_{Dx}\,\omega_x^2 + I_{Dy}\,\omega_y^2 + I_{Dz}\,\omega_z^2) \text{ ..... } 3.5$$

Which can be simplified here as the disc is symmetric ($I_{Dx}=I_{Dz}$), the angles θ and ψ are small, and the angular velocity is constant; that is, $\dot{\phi} = \Omega$. Equation 3.5 above becomes

$$T_D = 1/2\, M_D(\dot{u}^2 + \dot{w}^2) + 1/2\, I_{Dx}(\dot{\theta}^2 + \dot{\phi}^2) + I_{Dy}(\Omega^2 + 2\,\Omega\dot{\psi}\,\theta) \text{..... } 3.6$$

Where the term ½ $I_{Dy}\,\Omega^2$, which is a constant, has no influence in the equations and represents the energy of the disc rotating at Ω, all the other displacements being zero. The last term, $I_{Dy}\,\Omega\,\dot{\psi}\,\theta$, represents the gyroscopic (Coriolis) effect.

3.1.2 The Shaft

The shaft is represented as a beam with a circular cross-section, and is characterized by strain and kinetic energies [108, 109].

3.1.2.1 Kinetic energy

The general formulation of the kinetic energy of the shaft comes from an extension of the disc Equation 3.6. For an element of length L, the expression for the kinetic energy is:

$$T_s = \rho\, S/2\int_0^L(\dot{u}^2 + \dot{w}^2)\,dy + \rho I/2\int_0^L(\dot{\psi}^2 + \dot{\theta}^2)\,dy + \rho IL\,\Omega^2 + 2\,\rho IL\,\Omega\int_0^L(\dot{\psi}\,\theta\,dy) \text{..} 3.7$$

Where ρ is the mass per unit volume, S is the cross-sectional area of the beam, supposed to be constant, and I is the area moment of inertia of the beam cross–section about the neutral axis, also supposed to be constant. The first integral of Equation 3.7 is the classical expression for the kinetic energy of a beam in bending; the second integral is the secondary effect of rotatory inertia; the term $\rho IL\Omega^2$ is a constant and has no influence on the equations; and the last integral represents the gyroscopic effect.

3.1.2.2 Strain energy

The following notation is used refer to Figure 3.2: C is the geometric centre of the beam, B *(x, z)* is a typical point on the cross-section, E is the Young's modulus of material, ε and σ are normal strains and stresses, and u^* and w^* are displacements of the geometric centre with respect to the x, z axis [110].

If second–order terms are included, the longitudinal strain of point B can be shown to be:

$$\varepsilon = -x\frac{\partial^2 u^*}{\partial y^2} - z\frac{\partial^2 w^*}{\partial y^2} \quad \text{.....} \quad 3.8$$

$$\varepsilon = \varepsilon_l + \varepsilon_{nl} \quad \text{.....} \quad 3.9$$

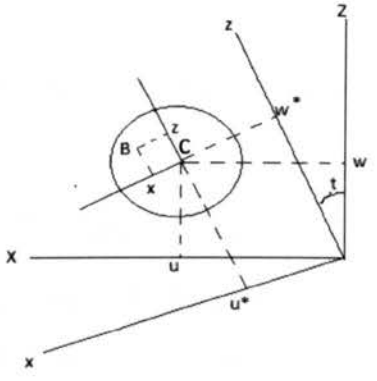

Figure 3.2 Coordinates of the geometric centre C and an arbitrary point B on the shaft [36].

Where ε_l contains the linear terms and ε_{nl} the nonlinear terms. The strain energy is

$$U_l = \int_0^{\mathcal{T}} \varepsilon^T \sigma \quad \text{.....} \quad 3.10$$

Where, T is the matrix transposition symbol. The relationship between stresses and strains is

$$\sigma = E\,\varepsilon \quad \text{.....} \quad 3.11$$

Then

$$U_l = E/2 \int_0^{\mathcal{T}} (\varepsilon_l^2 + 2\,\varepsilon_l\,\varepsilon_{nl} + \varepsilon_{nl}^2)\, d\mathcal{T} \quad \text{.....} \quad 3.12$$

The symmetry of the beam cross –section with respect to x and z results in

$$\int_0^{\mathcal{T}} \varepsilon_{nl}\,\varepsilon_l\, d\mathcal{T} = 0 \quad \text{.....} \quad 3.13$$

And the third term under the integral in Equation 3.12 is a second–order term and is neglected. The strain energy is

$$U_1 = \frac{E}{2}\int_0^L \int_S \left(-x\frac{\partial^2 u^*}{\partial y^2} - z\frac{\partial^2 w^*}{\partial y^2} \right)^2 dS\ dy \quad \text{..... } 3.14$$

$$U_1 = \frac{E}{2}\int_0^L \int_S \left[x^2\left(\frac{\partial^2 u^*}{\partial y^2}\right)^2 + z^2\left(\frac{\partial^2 w^*}{\partial y^2}\right)^2 + 2xz\frac{\partial^2 u^*}{\partial y^2}\frac{\partial^2 w^*}{\partial y^2} \right] dS\ dy \quad \text{..... } 3.15$$

Because of symmetry, the integral which corresponds to the third term in Equation 3.15 is nil.

3.1.3 Bearings and seals

The stiffness and viscous damping terms are assumed to be known, and the bending influence can in general be neglected Figure 3.3. The virtual work δW of the forces acting on the shaft can be written as [90, 111]:

$$\delta W = -k_{xx}\, u\, \delta u - k_{xz}\, w\, \delta u - k_{zz}\, w\, \delta w - k_{zx}\, u\, \delta w - c_{xx}\, \dot{u}\, \delta u - c_{xz}\, \dot{w}\, \delta u - c_{zz}\, \dot{w}\, \delta w - c_{zx}\, \dot{u}\, \delta w \quad .3.16$$

or

$$\delta W = F_u\, \delta_u + F_w\, \delta_w \text{.....} \quad 3.17$$

where F_u and F_w are the components of the generalized force. In matrix form the two Equations 3.16 and 3.17 can be written in matrixes form;

$$\begin{bmatrix} F_u \\ F_w \end{bmatrix} = -\begin{bmatrix} k_{xx} & k_{xz} \\ k_{zx} & k_{zz} \end{bmatrix}\begin{bmatrix} u \\ w \end{bmatrix} - \begin{bmatrix} c_{xx} & c_{xz} \\ c_{zx} & c_{zz} \end{bmatrix}\begin{bmatrix} \dot{u} \\ \dot{w} \end{bmatrix} \text{.....} 3.18$$

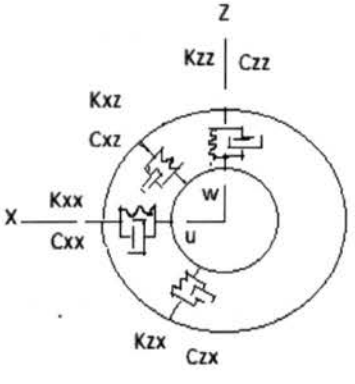

Figure 3.3 Bearing stiffness and damping [36, 54].

Frequently $k_{xx} \neq k_{zz}$ and $c_{xx} \neq c_{zz}$, and in addition it is very common that $k_{xz} \neq k_{zx}$ and $c_{xz} \neq c_{zx}$. Let us now consider the case when the equations are expressed using the displacement components in R, and supposing that only k_{xx} and k_{zz} are non–zero.

The expression for the virtual work is then [112]:

$\delta W = - k_{xx}\ (u^* \cos \Omega t + w^* \sin \Omega t)\ (\delta u^* \cos \Omega t + \delta w^* \sin \Omega t) - k_{zz}\ (-u^* \sin \Omega t + w^* \cos \Omega t)\ (-\delta u^* \sin \Omega t + \delta w^* \cos \Omega t)$ 3.19

or

$\delta W = -[\ (k_{xx} \cos^2 \Omega t + k_{zz} \sin^2 \Omega t)\ u^* + \sin 2\Omega t / 2\ (k_{xx} - k_{zz})\ w^*\ ]\ \delta u^* - [(k_{xx} \sin^2 \Omega t + k_{zz} \cos^2 \Omega t)\ w^* + \sin 2\Omega t / 2\ (k_{xx} - k_{zz})\ u^*\ ]\ \delta w^*$ 3.20

Equation 3.20 shows that, if $k_{xx} \neq k_{zz}$, terms coming from the bearing will contain explicitly the time in the rotating frame R. This leads to extreme difficulties in solving the equations. Then the rotor equations have to be written in the inertial reference frame R_0 [113].

3.2 Mass Unbalance

The unbalance is defined by a mass m_u situated at a distance d from the geometric centre of the shaft; its kinetic energy T_u has to be calculated.

The mass remains in a plane perpendicular to the y axis and its coordinate along the y axis is a constant Figure 3.4 [36, 105].

In R_0 the coordinates of the mass are

$$\boldsymbol{OD} = \begin{pmatrix} u + d \sin \Omega t \\ constant \\ w + d \cos \Omega t \end{pmatrix} \quad \text{.....} \ 3.21$$

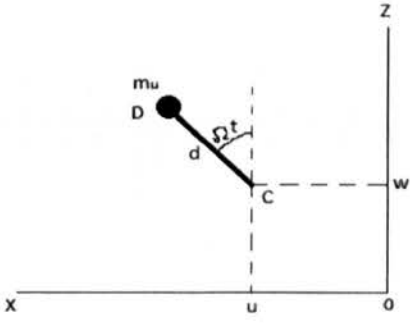

Figure 3.4 Mass unbalance [36, 113].

Then

$$V = d\boldsymbol{OD}/dt = \begin{pmatrix} \dot{u} + d\Omega \cos \Omega t \\ 0 \\ \dot{w} - d\Omega \sin \Omega t \end{pmatrix} \quad \text{.....} \ 3.22$$

And the kinetic energy of the mass is

$$T_u = m_u / 2\,(\dot{u}^2 + \dot{w}^2 + \Omega^2 d^2 + 2\,\Omega\, d\, \dot{u} \cos \Omega t - 2\,\Omega\, \dot{w}\, d \sin \Omega t) \quad \text{.....3.23}$$

The term $m_u \Omega^2 d^2/2$ is a constant and has no influence on the equations [66].

The mass m_u is much smaller than the mass of the rotor, so the kinetic energy can be written as

$$T_u \cong m_u \Omega\, d\, \dot{u}\,(\cos \Omega t - \dot{w} \sin \Omega t) \quad \text{.....3.24}$$

Application of Lagrange's equations will give the so-called centrifugal force vector.

3.3 Determination of the model

$R_0\,(XYZ)$ is the inertial frame, the rotor axis is along the Y axis, and the speed of rotation Ω is constant Figure 3.5. In order to make hand calculations, only one degree of freedom is used for the displacements in the X and Z directions. The rotor is then supposed to be simply supported at both ends. It consists of [113]:

- a symmetric shaft of length L;
- a symmetric disc with a mass unbalance, both situated at $y = l_1$;
- a bearing situated at $y = l_2$.

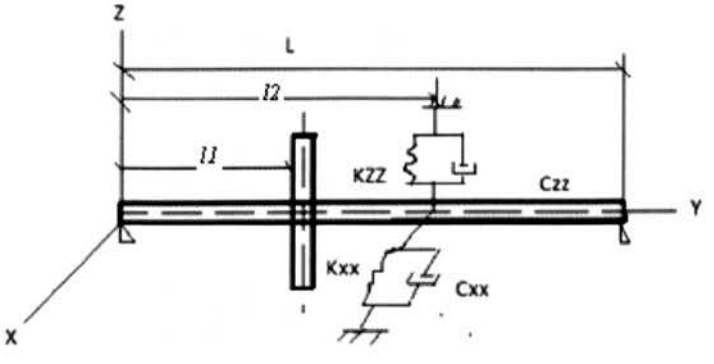

Figure 3.5 Model of the rotor [36, 114].

Depending on the characteristics of rotor properties used, the rotor will be symmetric or asymmetric. In addition, forces are supported to exist at $y = l_3$. The expressions for kinetic energy, strain energy and virtual work are used for each element of the rotor, and constant term appearing in the expression for the kinetic energy is systematically cancelled as its contribution to the equations is nil. The expressions for the displacements in the x and z directions are respectively [115, 116].

$$u(y, t) = f(y)\, q_1(t) = f(y)\, q_1 \quad \text{.....} 3.25$$

$$w(y, t) = f(y)\, q_2(t) = f(y)\, q_2 \quad \text{.....} 3.26$$

Where q_1 and q_2 are generalized independent coordinates. As the angular displacements ψ and θ Figure 3.6, are small, they are approximated by

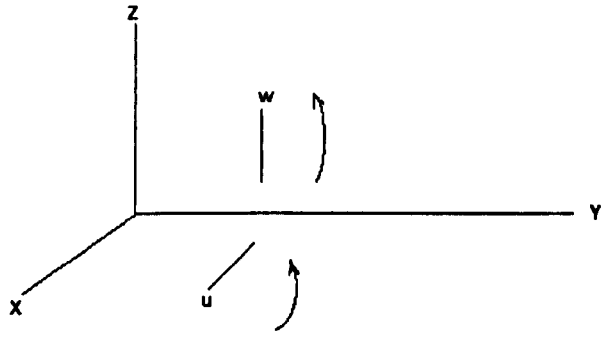

Figure 3.6 Coordinates [105].

$$\theta = \frac{\partial w}{\partial y} = \frac{df(y)}{dy}\, q_2 = g(y)\, q_2 \quad \text{.....} 3.27$$

$$\psi = -\frac{\partial u}{\partial y} = -\frac{df(y)}{dy}\, q_1 = -\, g(y)\, q_1 \quad \text{.....} 3.28$$

The second–order derivatives of u and w are necessary to express the strain energy; their expressions are

$$\frac{\partial^2 u}{\partial y^2} = \frac{d^2 f(y)}{dy^2}\, q_1 = h(y)\, q_1 \quad \text{.....} 3.29$$

$$\frac{\partial^2 w}{\partial y^2} = \frac{d^2 f(y)}{dy^2}\, q_2 = h(y)\, q_2 \quad \text{.....} 3.30$$

3.3.1 The disc

The kinetic energy T_D of the disc comes from Equation 3.6 and Equations 3.25 – 3.28, so [58, 106].

$$T_D = \tfrac{1}{2} M_D f^2(l_l)\,(\dot{q}_1^2 + \dot{q}_2^2) + 1/2\, I_{Dx}\, g^2(l_l)\,(\dot{q}_1^2 + \dot{q}_2^2) - I_{Dy}\, \Omega\, g^2(l_l)\, \dot{q}_1 q_2 \quad \text{.....} 3.31$$

This can be written as

$$T_D = \tfrac{1}{2}\,[M_D f^2(l_l) + I_{Dx}\, g^2(l_l)]\,(\dot{q}_1^2 + \dot{q}_2^2) - I_{Dy}\, \Omega\, g^2(l_l)\, \dot{q}_1 q_2 \quad \text{.....} 3.32$$

3.3.2 The shaft

The kinetic energy T_s of the shaft comes from the Equations 3.25-3.28 and Equation 3.7 [110].

$$T_s=\rho S/2 \int_0^L f^2(y)\,dy\,(\dot{q}_1^2+\dot{q}_2^2) + \rho I/2 \int_0^L g^2(y)\,dy\,(\dot{q}_1^2+\dot{q}_2^2) - 2\rho I\Omega \int_0^L g^2(y)\,dy\,\dot{q}_1 q_2 \quad \text{.....3.33}$$

$$T_s = 1/2\,(\dot{q}_1^2+\dot{q}_2^2)\,[\rho S \int_0^L f^2(y)\,dy + \rho I \int_0^L g^2(y)\,dy] - 2\rho I\,\Omega\,\dot{q}_1 q_2 \int_0^L g^2(y)dy \quad \text{.....3.34}$$

Hence the kinetic energy T of the disc–shaft assembly is:

$$T = T_D + T_S \quad \text{..... 3.35}$$

that is

$$T = 1/2\,[M_D f^2(l_1) + I_{Dx} g^2(l_1) + \rho S \int_0^L f^2(y)\,dy + \rho I \int_0^L g^2(y)\,dy]\,(\dot{q}_1^2+\dot{q}_2^2) - \Omega[I_{Dy} g^2(l_1) + 2\rho I \int_0^L g^2(y)\,dy]\,\dot{q}_1 q_2 \quad \text{.....3.36}$$

Equation 3.36 can be written in a more compact form as

$$T = 1/2\,m\,(\dot{q}_1^2+\dot{q}_2^2) - \Omega\,a\,\dot{q}_1 q_2 \quad \text{.....3.37}$$

The strain energy of the shaft U_s, comes from Equations 3.29 and 3.30. Then, if the axial force is nil [115],

$$U_s = EI/2 \int_0^L h^2(y)\,dy \quad (q_1^2+q_2^2) \quad \text{..... 3.38}$$

Equation 3.38 can be written in a more compact form as

$$U_s = 1/2\,k\,(q_1^2+q_2^2) \quad \text{..... 3.39}$$

3.3.3 The bearing

The virtual work done by the force due to bearing acting on the shaft is given by [90, 113].

$$\delta W = -k_{xx}u(l_2)\delta u(l_2) - k_{xz}w(l_2)\delta u(l_2) - k_{zz}w(l_2)\delta w(l_2) - k_{zx}u(l_2)\delta w(l_2) - c_{xx}\dot{u}(l_2)\delta u(l_2) - c_{xz}\dot{w}(l_2)\delta u(l_2) - c_{zz}\dot{w}(l_2)\delta w(l_2) - c_{zx}\dot{u}(l_2)\delta w(l_2) \quad \text{.....3.40}$$

Using Equations 3.25 and 3.26 in 3.40 becomes

$$\delta W = -k_{xx} f^2(l_2)\, q_1\, \delta q_1 - k_{xz} f^2(l_2)\, q_2\, \delta q_1 - k_{zz} f^2(l_2)\, q_2\, \delta q_2 - k_{zx} f^2(l_2)\, q_1\, \delta q_2 - c_{xx} f^2(l_2)\, \dot{q}_1\, \delta q_1 - c_{xz} f^2(l_2)\, \dot{q}_2\, \delta q_1 - c_{zz} f^2(l_2)\, \dot{q}_2\, \delta q_2 - c_{zx} f^2(l_2)\, \dot{q}_1\, \delta q_2 \quad \text{3.41}$$

As

$$\delta W = F q_1\, \delta q_1 + F q_2\, \delta q_2 \quad \text{3.42}$$

A simple identification of the expressions Equations 3.41 and 3.42 gives the two components Fq_1 and Fq_2 of generalized force acting on the shaft [76, 89].

3.3.4 Mass unbalance

The kinetic energy of the mass unbalance is [78]:

$$T_u = m_u\, \Omega\, d f(l_1)\, (\dot{q}_1 \cos\Omega t - \dot{q}_2 \sin\Omega t) \quad \text{3.43}$$

3.3.5 Forces

The two components of the forces are supposed to be

$$F_u = F_1(t) \quad \text{3.44}$$

$$F_w = F_2(t) \quad \text{3.45}$$

And, as their action is supposed to act at $y = l_3$

$$\delta W = F_1(t)\, u(l_3) + F_2(t)\, \delta w(l_3) \quad \text{3.46}$$

This can be written as

$$\delta W = F_1(t) f(l_3)\, q_1 + F_2(t) f(l_3)\, q_2 \quad \text{3.47}$$

A simple identification of expression of Equation 3.47 with 3.42 shows that the two components of the force are [106, 116]:

$$F q_1 = F_1(t) f(l_3) \quad \text{3.48}$$

$$F q_2 = F_2(t) f(l_3) \quad \text{3.49}$$

3.4 Equations of motion for rotor systems

3.4.1 Equations of motion for stationary rotor

The FRF data of any structure can be obtained through experimental modal testing or by means of the FE simulation method [44, 117]. For the vibration equation of a system, the mathematical model can be expressed as follows [11]:

$$M\ddot{x} + C\dot{x} + Kx = f(t) \quad \text{.....} \quad 3.50$$

Where M, C, and K are the mass, damping, and stiffness matrices of the system, respectively. Moreover, x and f are the displacement and external force vectors, respectively. In Equation 3.50, the displacement vector of the system can be represented in the modal coordinate with the following mode shape matrix.

$$x_{N\times 1} = \sum_{r=1}^{N} \eta_r v_r = U_{N\times N}\eta_{N\times 1} \quad \text{.....} \quad 3.51$$

Where N is the total number of components in the modal coordinate; η_r and v_r are the components of the modal coordinate and the mode shape vector at the rth mode, respectively; $U=v_1, v_2, \ldots, v_N$ denotes the mode shape matrix; and $\eta=\eta_1,\eta_2,\ldots,\eta_N{}^T$ refers to the modal coordinate vector. Substituting Equation 3.51 into Equation 3.50, the equation of spatial motions transformed into the equation of decoupled motion:

$$MU\ddot{\eta} + CU\dot{\eta} + KU\eta = f \quad \text{.....} \quad 3.52$$

Multiplying the matrix U^T at both sides of Equation 3.52 produces the following:

$$\mathbb{M}\ddot{\eta} + \mathbb{C}\dot{\eta} + \mathbb{K}\eta = U^T f = \mu \quad \text{.....} \quad 3.53$$

Where $\mathbb{M}$, $\mathbb{C}$ and $\mathbb{K}$ are the diagonal mass, damping, and stiffness matrices, respectively; and μ is the modal force vector. The equation of motion at the rth mode is represented as follows:

$$m_r\ddot{\eta}_r + c_r\dot{\eta}_r + k_r\eta_r = \mu_r \quad \text{.....} \quad 3.54$$

Where $\mu_r = v_r{}^T f = \sum_{J=1}^{N} \phi_{jr} f_j$ and ϕ_{jr} (the jth components of the rth mode shape vector). By considering the harmonic excitation acting on the system, the component of the modal

coordinate and the modal force at the rth mode can be designated as $\eta_r = \hat{\eta}\ e^{i\omega t}$ and $\mu_r = \hat{\mu}_r\ e^{i\omega t}$ respectively. Equation 3.51 becomes the summation of a series consisting of the exciting force, components of the mode shape, and the modal parameters:

$$\hat{x}_{N\times 1} = \sum_{r=1}^{N} \hat{\eta}_r\, v_r = \sum_{r=1}^{N}\sum_{j=1}^{N} \frac{\phi_{jr}\,\hat{f}_j}{m_r\left[\omega_r^2 - \omega^2 + 2i\omega\xi_r\omega_r\right]}\, v_r \quad \text{.....} \quad 3.55$$

Where $x = \hat{x}\ e^{i\omega t}$ is the displacement vector of the spatial model, and $f_j = \hat{f}_j\ e^{i\omega t}$ is the exciting force. In addition, ω_r and ζ_r stand for the rth natural frequency and damping ratio (called modal parameters) respectively. Considering just a single component $\hat{f}_j$ of the exciting force, the ith component of the displacement vector can be rewritten as:

$$\hat{x}_i = \sum_{r=1}^{N}\sum_{j=1}^{N} \frac{\phi_{ir}\,\phi_{jr}\,\hat{f}_j}{m_r\left[\omega_r^2 - \omega^2 + 2i\omega\xi_r\omega_r\right]} \quad \text{.....} \quad 3.56$$

The FRF H_{ij} is defined as the ratio of the ith displacement component $\hat{x}_i$ to the jth exciting force component $\hat{f}_j$ it can also be shown as follows:

$$\boxed{\frac{\hat{x}_i}{\hat{f}_j} = H_{ij} = \sum_{r=1}^{N} H_{ij,r} = \sum_{r=1}^{N} \frac{\phi_{ir}\,\phi_{jr}}{m_r\left[\omega_r^2 - \omega^2 + 2i\omega\xi_r\omega_r\right]}} \quad \text{.....} \quad 3.57$$

Where $H_{ij,r}$ is the peak value of FRF at the rth mode. Equation 3.57 represents the relationship between the single exciting force and displacement. However, the situation of multiple excitations is not considered in the following theory.

3.4.2 Equations of motion for rotating structures

3.4.2.1 General system matrices (symmetric or asymmetric)

Linear structures for the purpose of vibration analysis may be modelled either as a continuous system or a discrete one. In the case of the latter method, the mass of the system is lumped into a finite number of masses connected by springs and dampers representing the stiffness and damping in the system respectively. The system is then said to possess a finite number of degrees of freedom. Damping mechanism comes in different forms such as viscous,

structural, hysteretic and Coloumb. The viscous damping is being the most common form. The equations of motion of the discrete model consists of a finite number of second order ordinary differential equations coupled together, in which case they have to be solved simultaneously. The process becomes progressively more difficult as the number of degrees of freedom increases.

There is a way of de-coupling the equations of motion using the orthogonality properties of the natural modes. In this method, the system is transformed from generalised coordinates to a new set of coordinates called principal coordinates, in which case the equations are solved independently and inverse transformed into the generalised coordinates.

In modal analysis applied to stationary structures (non-rotating) it is described that the system matrices are symmetric, which simplifies the transformation. While the symmetric description of system matrices is valid for stationary structures, it is not suitable for structures containing rotating elements. If the theory of modal analysis for stationary structures is applied to rotating structures the full de-coupling is not achieved. However, it is possible to use a different technique to achieve full de-coupling of the differential equations of motion. In the new transformation the system matrices are description to be asymmetric and consequently they are not identical to their transpose. It follows that there are two sets of eigenvectors in this case, one set for the original matrix and one set for the transpose of the matrix, the former set is called the right hand eigenvector and the latter is left hand eigenvectors. And both sets are needed to de-couple the equations of motion [6, 36].

The general equations of motion for a multi-degree of freedom vibratory system may be written as [11, 118 and 119]:

$$[M]\{\ddot{q}(t)\}+[C(\Omega)]\{\dot{q}(t)\}+[K(\Omega)]\{q(t)\}=\{F(t)\} \qquad \text{.....3.58}$$

In the Equation 3.58 the mass, damping and stiffness matrices are not symmetric and are speed dependent. The damping matrix also includes the gyroscopic effect of the rotating system.

3.4.2.2 Free vibration analysis

The Equation 3.58 is first needed to be solved in its homogenous form in order to calculate the natural properties of the system such as the natural frequencies, modal damping ratios and the mode shapes embedded in the eigenvalues and eigenvectors of the system. In the case of asymmetric system matrices, the equation with the transpose of system matrices must also be solved. The free vibration solution is obtained by:

$$[M]\{\ddot{q}(t)\}+[C(\Omega)]\{\dot{q}(t)\}+[K(\Omega)]\{q(t)\}=\{0\} \quad \text{.....} \; 3.59$$

A trial solution for the above equation is:

$$\begin{aligned}\{q(t)\} &= \{\bar{q}\}e^{st}\\ \{\dot{q}(t)\} &= s\{\bar{q}\}e^{st} = s\{q(t)\}\\ \{\ddot{q}(t)\} &= s^2\{\bar{q}\}e^{st} = s^2\{q(t)\}\end{aligned} \quad \text{.....} \; 3.60$$

Substituting the set of Equations 3.60 into 3.59:

$$\begin{cases} s^2[M]+s[C]+[K]\{\bar{q}\}e^{st}=0 & (a)\\ s^2[M]^T+s[C]^T+[K]^T\{\bar{q}\}e^{st}=0 & (b)\end{cases} \quad \text{.....} \; 3.61$$

$$\det\left[s^2[M]+s[C]+[K]\right]=0 \quad \text{.....} \; 3.62$$

The determinant of the Equations 3.61a and b, are identical, which means that the eigenvalues for both the system and its transpose are identical. However there are two sets of eigenvectors called the right eigenvectors and the left eigenvectors.

$$\begin{cases} s_r^2[M]+s_r[C]+[K]\{\psi_R\}_r=\{0\}\\ s_r^2[M]^T+s_r[C]^T+[K]^T\{\psi_L\}_r=\{0\}\end{cases} \quad \text{.....} \; 3.63$$

$\{\psi_R\}_r$ is the right eigenvector and $\{\psi_L\}_r$ is the left eigenvector.

The free vibration response of the system is

$$\begin{aligned}&\{q(t)\}=c_1\{\psi_R\}_1e^{s_1t}+c_2\{\psi_R\}_2e^{s_2t}+\text{.....}+c_{2n}\{\psi_R\}_{2n}e^{s_{2n}t}\\ &\equiv\{q(t)\}=\sum_{r=1}^{2n}c_r\{\psi_R\}_re^{s_rt}\\ &\{q(t)\}=\sum_{r=1}^{2n}d_r\{\psi_L\}_re^{s_rt}\end{aligned} \quad \text{.....} \; 3.64$$

c_r and d_r are constants which may be found by knowing the initial conditions.

3.4.2.3 Transformation from vector space to state space

The equations of motion are a set of n second order differential equations and therefore are in vector space. These equations are de-coupled more simply in their state space form. It is therefore essential to carry out the transformation from vector space to state space. As a result

of the transformation the number of equations is doubled into 2n first order differential equations.

The procedure for the transformation is as follows:

$$[M]\{\ddot{q}(t)\}+[C(\Omega)]\{\dot{q}(t)\}+[K(\Omega)]\{q(t)\}=\{F(t)\} \qquad \text{..... } 3.65$$

A new coordinate system containing the generalised coordinate system is introduced:

$$\{u(t)\}=\begin{Bmatrix}\{q(t)\}\\ \{\dot{q}(t)\}\end{Bmatrix} \qquad \text{..... } 3.66$$

Equation 3.58 now may be re-written in terms of the new coordinates:

$$\begin{bmatrix}[C] & [M]\\ [M] & [0]\end{bmatrix}\{\dot{u}(t)\}+\begin{bmatrix}[K] & [0]\\ [0] & -[M]\end{bmatrix}\{u(t)\}=\begin{Bmatrix}\{F(t)\}\\ \{0\}\end{Bmatrix} \qquad \text{..... } 3.67$$

or:

$$[A]\{\dot{u}(t)\}+[B]\{u(t)\}=\begin{Bmatrix}\{F(t)\}\\ \{0\}\end{Bmatrix} \qquad \text{..... } 3.68$$

The eigen solution of the above equations is obtained by considering the free vibration form i.e.:

$$[A]\{\dot{u}(t)\}+[B]\{u(t)\}=\begin{Bmatrix}\{0\}\\ \{0\}\end{Bmatrix}=\{0\} \qquad \text{..... } 3.69$$

Using a trial solution similar to the one used in the vector space form of the equations of motion i.e.:

$$\begin{aligned}\{q(t)\} &= \{\bar{q}\}e^{st}\\ \{\dot{q}(t)\} &= s\{\bar{q}\}e^{st} = s\{q(t)\}\\ \{\ddot{q}(t)\} &= s^2\{\bar{q}\}e^{st} = s^2\{q(t)\}\end{aligned} \qquad \text{..... } 3.70$$

Results in the following set for the state space form:

$$\begin{aligned}\{u(t)\} &= \begin{Bmatrix}\{\bar{q}\}\\ s\{\bar{q}\}\end{Bmatrix}e^{st} = \{\bar{u}\}e^{st}\\ \{\dot{u}(t)\} &= \begin{Bmatrix}s\{\bar{q}\}\\ s^2\{\bar{q}\}\end{Bmatrix}e^{st} = s\{\bar{u}\}e^{st}\end{aligned} \qquad \text{..... } 3.71$$

Combining Equations sets 3.68, 3.69 and 3.71:

$$[s[A]+[B]]\{\bar{u}\}e^{st} = \{0\} \qquad \text{..... } 3.72$$

The eigen problem applied to the Equation 3.72:

$$\begin{aligned} &[s_r[A]+[B]]\{R\}_r = \{0\} && (a) \\ &\left[s_r[A]^T + [B]^T\right]\{L\}_r = \{0\} && (b) \end{aligned} \qquad \text{..... } 3.73$$

Where $\{R\}_r$ and $\{L\}_r$ are the arbitrary normalised right and left eigenvectors in the state space form respectively and s_r is the eigenvalues of the system. The eigenvalues are identical to the ones in the vector space form. The relationships between the eigenvalues and eigenvectors in the vector space and state space are as follows in Table 3.1.

Table 3.1

Comparison between the eigenvalues and eigenvectors in the vector space and state space.

	Vector Space	State Space
Eigenvalues	s_r	s_r
Right eigenvector	$\{\psi_R\}_r$	$\{R\}_r = \begin{Bmatrix} \{\psi_R\}_r \\ \{\psi_R\}_r s_r \end{Bmatrix}_r$
Left eigenvector	$\{\psi_L\}_r$	$\{L\}_r = \begin{Bmatrix} \{\psi_L\}_r \\ \{\psi_L\}_r s_r \end{Bmatrix}_r$

3.4.2.4 De-coupling the equations of motion using Bi-Orthogonality relationships

Pre-multiplying the Equation 3.73a, by transpose of the qth left eigenvectors:

$$\{L\}_q^T[s_r[A]+[B]]\{R\}_r = 0 \qquad \text{..... } 3.74$$

Equation 3.73b may be re-written for mode q and post-multiplied by the right eigenvector for mode r :

$$\{L\}_q^T[s_q[A]+[B]]\{R\}_r = 0 \qquad \text{..... } 3.75$$

Subtracting Equation 3.75 from 3.74 gives:

$$\{L\}_q^T[A]\{R\}_r(s_r - s_q)=0 \qquad \text{..... } 3.76$$

Since q and r are generally two different modes $s_r \neq s_q \quad or \quad s_r - s_q \neq 0$

Therefore:

$$\{L\}_q^T [A]\{R\}_r = 0 \qquad \text{.....3.77}$$

Similar relationship may be obtained for matrix [B] by multiplying Equations 3.74 and 3.75 by q^{th} and r^{th} eigenvalues respectively as follows:

$$\begin{aligned} &\{L\}_q^T [s_r s_q [A] + s_q [B]]\{R\}_r = 0 \quad (a) \\ &\{L\}_q^T [s_r s_q [A] + s_r [B]]\{R\}_r = 0 \quad (b) \end{aligned} \qquad \text{..... 3.78}$$

Subtracting Equation 3.78a from 3.78b gives:

$$\{L\}_q^T [B]\{R\}_r (s_r - s_q) = 0 \qquad \text{..... 3.79}$$

Again the two modes r and q are separate modes therefore $s_r - s_q \neq 0$ and:

$$\{L\}_q^T [B]\{R\}_r = 0 \qquad \text{.....3.80}$$

Equations 3.77 and 3.80 represent Bi-Orthogonality relationships between system matrices, left and right eigenvectors for non-repeated eigenvalues.

As can be seen in the Bi-Orthogonity equations the left and right eigenvectors to satisfy the relationship belongs to two distinct modes i.e.: Non diagonal parts of the matrices. It is important to find out what happens when the left and right eigenvectors belong to the same modes i.e.: $r = q$. i.e.:

$$\{L\}_r^T [s_r [A] + [B]]\{R\}_r = 0 \qquad \text{..... 3.81}$$

or:

$$s_r \{L\}_r^T [A]\{R\}_r + \{L\}_r^T [B]\{R\}_r = 0 \qquad \text{..... 3.82}$$

Since generally $[A] \neq 0$ $[B] \neq 0$ therefore:

$$\begin{aligned} &\{L\}_r^T [A]\{R\}_r \neq 0 \\ &\{L\}_r^T [B]\{R\}_r \neq 0 \end{aligned} \qquad \text{..... 3.83}$$

Therefore:

Substituting the above relationships in Equation 3.82 gives:

$$\{L\}_r^T [A]\{R\}_r = a_r$$
$$\{L\}_r^T [B]\{R\}_r = b_r \qquad \text{.....} 3.84$$

$$s_r a_r + b_r = 0 \qquad \text{.....} 3.85$$

In Equation 3.85, a_r and b_r do not have unique values and can be arbitrarily scaled in isolation from each other. However the ratio of (b_r/a_r) is unique and is equal to the rth eigenvalue. The terms a_r and b_r are equivalent to the terms m_r (modal mass) and k_r (modal stiffness) in the dynamic system with symmetric mass and stiffness matrices. In this case as in the case with symmetric system matrices, the matrices are diagonalised using Bi-Orthogonality relationships, i.e.:

$$[L]^T [A][R] = diag\,[a_r]$$
$$[L]^T [B][R] = diag\,[b_r] \qquad \text{.....} 3.86$$

3.4.2.5 Normalisation of eigenvectors

Eigenvectors of a matrix are not unique and can be arbitrarily scaled. In modal analysis the eigenvectors are scaled or normalised in such a way that one matrix is an identity matrix and the other diagonal matrix contains all the eigenvalues of the system. This procedure gives orthonormalised or mass-normalised set of eigenvectors since the eigenvectors are scaled such that the mass matrix becomes an identity matrix. In the systems with symmetric system matrices there is only one set of eigenvectors (right eigenvector) and those eigenvectors are normalised. In the case of systems with general matrices there are two sets of eigenvectors (right and left eigenvectors) and the uniqueness in the scaling process would affect both sets of the eigenvectors as both sets are involved in the normalisation process, in this case could also be done for systems with general matrices [120, 121 and 122].

3.4.2.6 Mass-normalisation in symmetric matrices

In this case the eigenvectors are scaled such a way that the mass matrix becomes identity and the stiffness matrix becomes a diagonal matrix containing all the eigenvalues of the system. The transformation is as follows:

Using the arbitrarily scaled eigenvectors $[\psi]$ to obtain the modal mass matrix:

$$[\psi]^T[M][\psi] = diag[m_r] \qquad \text{.....} \; 3.87$$

In mass-normalisation the uniquely scaled eigenvectors $[\phi]$ must satisfy the following relationship:

$$[\phi]^T[M][\phi] = [I] \qquad \text{.....} \; 3.88$$

3.4.2.7 A-normalisation in symmetric system matrices

In this case the mass $[M]$ and stiffness $[K]$ system matrices in vector space are converted and replaced by system matrices in the state space form matrices $[A]$ and $[B]$ respectively. In this case there is only one set of eigenvectors (right eigenvector).

$$[R]^T[A][R] = diag[a_r] \text{.....} 3.89$$

The uniquely scaled set must satisfy the following relationship:

$$[R_N]^T[A][R_N] = [I] \text{.....} \; 3.90$$

And

$$[R_N]^T[B][R_N] = diag[-s_r] \text{.....} \; 3.91$$

Therefore:

$$\{R_N\}_r = \frac{1}{\sqrt{a_r}}\{R\}_r \text{.....} \; 3.92$$

3.4.2.8 A-normalisation in asymmetric system matrices

The procedure explained before for symmetric matrices system could be used for asymmetric matrices as follows:

$$\begin{aligned} [L]^T[A][R] &= diag\ [a_r] \\ [L]^T[B][R] &= diag\ [b_r] \end{aligned} \qquad \text{.....} \; 3.93$$

Pre and post-multiplying the above Bi-Orthogonality relationships by $diag\left[\frac{1}{\sqrt{a_r}}\right]$ gives:

$$\left[\frac{1}{\sqrt{a_r}}\right][L]^T[A][R]\left[\frac{1}{\sqrt{a_r}}\right] = \left[\frac{1}{\sqrt{a_r}}\right][a_r]\left[\frac{1}{\sqrt{a_r}}\right] = [I]$$

$$\left[\frac{1}{\sqrt{a_r}}\right][L]^T[B][R]\left[\frac{1}{\sqrt{a_r}}\right] = \left[\frac{1}{\sqrt{a_r}}\right][b_r]\left[\frac{1}{\sqrt{a_r}}\right] = diag\ [-s_r] \quad \text{.....} 3.94$$

The a-normalised right and left eigenvectors are obtained from

$$\{R_N\}_r = \frac{1}{\sqrt{a_r}}\{R\}_r \quad or \quad [R_N] = [R]\left[\frac{1}{\sqrt{a_r}}\right] \quad \text{.....} 3.95$$

And similarly:

$$\{L_N\}_r = \frac{1}{\sqrt{a_r}}\{L\}_r \quad or \quad [L_N]^T = \left[\frac{1}{\sqrt{a_r}}\right][L]^T \quad \text{.....} 3.96$$

The main difference between a-normalisation for symmetric matrix system and asymmetric matrix system is that in the symmetric case there is one set of eigenvector and therefore is scaled individually, whereas in the asymmetric case the pair of eigenvectors are scaled within which the values of each can be arbitrarily scaled. For example if left eigenvector is multiplied by a number and the right eigenvector by inverse of that number the value of a_r remains the same. One possible way of scaling is to split the scaling factor equally between the right and left eigenvectors.

3.4.2.9 Forced response analysis in state space

The general equations motion for an n-degree of freedom system in vector space is as follows:

$$[M]\{\ddot{q}(t)\} + [C]\{\dot{q}(t)\} + [K]\{q(t)\} = \{F(t)\} \quad \text{.....} 3.97$$

The above equations may be expressed in 2n equation in state space system [30]:

$$[A]\{\dot{u}(t)\} + [B]\{u(t)\} = \begin{Bmatrix} F(t) \\ 0 \end{Bmatrix} \quad \text{.....} 3.98$$

Where $$\{u(t)\} = \begin{Bmatrix} q(t) \\ \dot{q}(t) \end{Bmatrix} \quad \text{.....} 3.99$$

The Bi-Orthogonality relationships derived in the previous section are used to de-couple the equations of motion for the forced response in the state space.

The system's response vector $\{u(t)\}$ can be expressed as a linear combination of the right and left eigenvectors. i.e.:

$$\{u(t)\} = \sum_{r=1}^{2n} \{R\}_r p_r(t) = [R]\{p(t)\} \quad \text{.....} \quad 3.100$$

Where $$\{p(t)\} = \{p_1(t)\ p_2(t)\ p_3(t) \text{.....} p_{2n}(t)\}^T \quad \text{.....} \quad 3.101$$

$p_r(t)$ a modal coordinates, in which the matrices are de-coupled. Transformation from the generalised coordinates to modal coordinates takes place as follows:

In the Equation 3.98 substituting for $\{u(t)\} = [R]\{p(t)\}$

$$[A][R]\{\dot{p}(t)\} + [B][R]\{p(t)\} = \begin{Bmatrix} \{F(t)\} \\ \{0\} \end{Bmatrix} \quad \text{.....} \quad 3.102$$

Pre-multiplying Equation 3.102 by the transpose of left eigenvector gives:

$$[L]^T[A][R]\{\dot{p}(t)\} + [L]^T[B][R]\{p(t)\} = [L]^T \begin{Bmatrix} \{F(t)\} \\ \{0\} \end{Bmatrix} \quad \text{.....} \quad 3.103$$

Using the Bi-Orthogonality relationships: Equations 3.93 give:

$$[a_r]\{\dot{p}(t)\} + [b_r]\{p(t)\} = [L]^T \begin{Bmatrix} \{F(t)\} \\ \{0\} \end{Bmatrix} \quad \text{.....} \quad 3.104$$

Equation 3.104 represents 2n de-coupled equations. For the rth mode the equation of motion is:

$$a_r \dot{p}_r(t) + b_r p_r(t) = \{L\}_r^T \begin{Bmatrix} \{F(t)\} \\ \{0\} \end{Bmatrix} \quad \text{.....} \quad 3.105$$

Or:

$$\dot{p}_r(t) - s_r p_r(t) = \frac{\left(\{L\}_r^T \begin{Bmatrix} \{F(t)\} \\ \{0\} \end{Bmatrix} \right)}{a_r} \quad \text{.....} \quad 3.106$$

$\{F(t)\}$ is a general forcing function used for excitation of the system.

3.4.2.10 Determination of frequency response function to harmonic excitation

It is a common practise to determine the frequency response functions of systems to varying sinusoidal forces with the same frequency and altering amplitude and phase values. While the

other forms of excitations such as random and transient is not considered in this analysis, but in practise complex excitation waveforms may be represented by sum of many harmonic components of varying frequency. The final expression gives the frequency response function resulted from response at coordinate j to a single force at point k.

Residue and zero method

The system is assumed to be linear

The excitation force is harmonic and therefore has the form: $\{F(t)\} = \{\overline{F}\}e^{i\omega t}$ and the general response is of harmonic type of the same frequency.

$$\{q(t)\} = \{\overline{q}\}e^{i\omega t} \quad \Rightarrow \quad \{\dot{q}(t)\} = i\omega\{q(t)\} \quad \Rightarrow \quad \{\ddot{q}(t)\} = -\omega^2\{q(t)\} \qquad 3.107$$

Substituting the above set of trail solutions in the equations of motion, Equation 3.58

$$\left[-\omega^2[M] + i\omega[C] + [K]\right]\{\overline{q}\}e^{i\omega t} = \{\overline{F}\}e^{i\omega t} \qquad 3.108$$

and

$$\{\overline{q}\} = \left[-\omega^2[M] + i\omega[C] + [K]\right]^{-1}\{\overline{f}\} \qquad 3.109$$

The receptance matrix of the system is

$$[H(\omega)] = \left[-\omega^2[M] + i\omega[C] + [K]\right]^{-1} \qquad 3.110$$

The receptance matrix in the state space may be calculated as follows:

$$\begin{aligned} \{u(t)\} &= \begin{Bmatrix} \{q\} \\ \{\dot{q}\} \end{Bmatrix} = \begin{Bmatrix} \{\overline{q}\} \\ \{\overline{q}\}i\omega \end{Bmatrix} e^{i\omega t} = \{\overline{u}\}e^{i\omega t} \\ \{\dot{u}(t)\} &= \begin{Bmatrix} \{\dot{q}\} \\ \{\ddot{q}\} \end{Bmatrix} = \begin{Bmatrix} \{\overline{q}\}i\omega \\ -\{\overline{q}\}\omega^2 \end{Bmatrix} e^{i\omega t} = i\omega\{u(t)\} = i\omega\{\overline{u}\}e^{i\omega t} \end{aligned} \qquad 3.111$$

Substituting the above set of equations in the equations of motion in the state space Equation 3.68 gives:

$$[i\omega[A] + [B]]\{\overline{u}\}e^{i\omega t} = \begin{Bmatrix} \{f\} \\ \{0\} \end{Bmatrix} e^{i\omega t} \qquad 3.112$$

And

$$\{\overline{u}\} = [i\omega[A] + [B]]^{-1}\begin{Bmatrix} \{f\} \\ \{0\} \end{Bmatrix} \qquad 3.113$$

The new receptance matrix (Augmented Receptance Matrix) is:

$$[A(\omega)] = [i\omega[A] + [B]]^{-1}$$

or

$$[A(\omega)]^{-1} = [i\omega[A] + [B]] \quad \text{.....} \quad 3.114$$

Pre and post-multiplying the above Equation 3.114 by the transpose of the normalised (augmented) left eigenvector matrix and right eigenvector matrix respectively:

$$[L_N]^T [A(\omega)]^{-1} [R_N] = [L\ ]^T [i\omega[A] + [B]][R_N] \quad \text{.....} \quad 3.115$$

Applying the Bi-Orthogonality relationships to the right hand side of Equation 3.115 gives:

$$[L_N]^T [A(\omega)]^{-1} [R_N] = [i\omega[I] - diag[s_r]] = diag[\ \ (i\omega - s_r)\ \ ]$$

$$or: \quad \text{.....} \quad 3.116$$

$$[R_N]^{-1} [A(\omega)][L_N]^{-T} = diag\left[\ \ \frac{1}{(i\omega - s_r)}\ \ \right]$$

Pre and post-multiplying by $[R_N]$ and $[L_N]^T$ respectively gives:

$$[A(\omega)] = [R_N]\left[\ \ \frac{1}{i\omega - s_r}\ \ \right][L_N]^T \quad \text{.....} \quad 3.117$$

Expanding the above equation for all the modes:

$$[A(\omega)] = [\{R_N\}_1\ \{R_N\}_2\ \{R_N\}_3 \text{.....} \{R_N\}_{2n}]\left[\ \ \frac{1}{i\omega - s_r}\ \ \right]\begin{bmatrix} \{L_N\}_1^T \\ \{L_N\}_2^T \\ \vdots \\ \vdots \\ \{L_N\}_{2n}^T \end{bmatrix} \quad \text{.....} \quad 3.118$$

$$[A(\omega)] = \left[\frac{\{R_N\}_1}{(i\omega - s_1)}\ \ \frac{\{R_N\}_2}{(i\omega - s_2)} \text{.....} \frac{\{R_N\}_{2n}}{(i\omega - s_{2n})}\right]\begin{bmatrix} \{L_N\}_1^T \\ \{L_N\}_2^T \\ \vdots \\ \vdots \\ \{L_N\}_{2n}^T \end{bmatrix} \quad \text{.....} \quad 3.119$$

$$[A(\omega)] = \frac{\{R_N\}_1\{L_N\}_1^T}{(i\omega - s_1)} + \frac{\{R_N\}_2\{L_N\}_2^T}{(i\omega - s_2)} + \text{.....} + \frac{\{R_N\}_{2n}\{L_N\}_{2n}^T}{(i\omega - s_{2n})} \quad \text{.....} \quad 3.120$$

$$[A(\omega)] = \sum_{r=1}^{2n} \frac{\{R_N\}_r \{L_N\}_r^T}{(i\omega - s_r)} \quad \text{.....} \quad 3.121$$

$$[A(\omega)] = \sum_{r=1}^{2n} \frac{\begin{Bmatrix} \{\phi_R\}_r \\ s_r\{\phi_R\}_r \end{Bmatrix} \begin{Bmatrix} \{\phi_L\}_r \\ s_r\{\phi_L\}_r \end{Bmatrix}^T}{(i\omega - s_r)} \quad \text{.....} \quad 3.122$$

Expanding the above equations:

$$[A(\omega)] = \begin{bmatrix} \sum_{r=1}^{2n} \frac{\{\phi_R\}_r \{\phi_L\}_r^T}{(i\omega - s_r)} & \sum_{r=1}^{2n} \frac{s_r \{\phi_R\}_r \{\phi_L\}_r^T}{(i\omega - s_r)} \\ \sum_{r=1}^{2n} \frac{s_r \{\phi_R\}_r \{\phi_L\}_r^T}{(i\omega - s_r)} & \sum_{r=1}^{2n} \frac{s_r^2 \{\phi_R\}_r \{\phi_L\}_r^T}{(i\omega - s_r)} \end{bmatrix} \quad \text{.....} \quad 3.123$$

The above receptance matrix is in state space form which has elements which are multiples of one element. The upper left matrix is sufficient to define the receptance matrix for the vector space form. i.e.:

$$[H(\omega)] = \sum_{r=1}^{2n} \frac{\{\phi_R\}_r \{\phi_L\}_r^T}{(i\omega - s_r)} \quad \text{.....} \quad 3.124$$

The receptance for one measurement between two coordinates j and k is given by:

$$H_{jk} = \sum_{r=1}^{2n} \frac{{}_r\phi_{Rj} \; {}_r\phi_{Lk}}{(i\omega - s_r)} \quad \text{.....} \quad 3.125$$

The above expression is useful for theoretical modal analysis study of such systems as long as the values of 2n eigenvalues and the corresponding relatively scaled right and left eigenvectors are known. However, in experimental modal analysis the above expression is not readily suitable, one major problem being the fact that a summation of 2n modes is required but in an n degree of freedom system there could only be n modes and subsequently n eigenvalues and vectors. However, in a viscously damped n degrees of freedom system the resulting n second-order ordinary differential equations of motion have 2n roots which are the eigenvalues of the system these roots occur in pairs, one pair for every degree of freedom. During the transformation from vector space to state space forms which was used to convert the n second order differential equations to 2n first order differential equations the original

relationship between the pairs were lost. A methodology is needed to re-group the pairs and find out the relationships in the new state.

In the following section it is assumed that the eigenvalues and vectors occur in complex conjugate pairs. This is true provided all the modes represent oscillatory motion. Equation 3.125 may then be re-written as:

$$H_{jk}(\omega) = \sum_{r=1}^{n} \left(\frac{{}_r\phi_{Rj}\ {}_r\phi_{Lk}}{(i\omega - s_r)} + \frac{{}_r\phi_{Rj}^{*}\ {}_r\phi_{Lk}^{*}}{(i\omega - s_r^{*})} \right) \quad \text{.....} \quad 3.126$$

For simplification the following terms are introduced:

$${}_rG_{jk} = {}_r\phi_{Rj}\ {}_r\phi_{Lk} \quad \text{and} \quad {}_rG_{jk}^{*} = {}_r\phi_{Rj}^{*}\ {}_r\phi_{Lk}^{*}$$

Equation 3.126 becomes:

$$H_{jk}(\omega) = \sum_{r=1}^{n} \left(\frac{{}_rG_{jk}}{(i\omega - s_r)} + \frac{{}_rG_{jk}^{*}}{(i\omega - s_r^{*})} \right) \quad \text{.....} \quad 3.127$$

Or:

$$H_{jk}(\omega) = \sum_{r=1}^{n} \left(\frac{{}_rG_{jk}(i\omega - s_r^{*}) + {}_rG_{jk}^{*}(i\omega - s_r)}{(i\omega - s_r^{*})(i\omega - s_r)} \right) \quad \text{.....} \quad 3.128$$

However the complex eigenvalues have the following forms:

$$s_r, s_r^{*} = -\omega_r\zeta_r \pm i\omega_r\sqrt{1-\zeta_r^{2}} \quad \text{.....} \quad 3.129$$

Substituting Equation 3.129 into 3.128 and simplifying gives:

$$\boxed{H_{jk}(\omega) = \sum_{r=1}^{n} \left(\frac{2\omega_r\left(\zeta_r \operatorname{Re}({}_rG_{jk}) - \sqrt{1-\zeta_r^{2}}\left(\operatorname{Im}({}_rG_{jk})\right)\right) + i\left(2\omega \operatorname{Re}({}_rG_{jk})\right)}{(\omega_r^{2} - \omega^{2} + 2i\omega\omega_r\zeta_r)} \right)} \quad \text{.....} \quad 3.130$$

Equation 3.130 used to show the behaviour of rotor with strong gyroscopic effect and represents the receptance between two coordinates j and k for a system with n degree of freedom. The denominator is identical to the denominator of the receptance expression for an n degree of freedom system with symmetric system matrices (stationary structure) see Equation 3.57, but the numerator is very different due to the behaviour of rotor with strong gyroscopic effect in rotating structure.

3.5 Summary

Theory of rotor dynamics prediction is described. The basic elements of all rotating machinery are disc, shaft, bearings and seals, which are discussed in this chapter. Mass unbalance and the forces due to the bearings or seals are considered to determine the rotor dynamic properties.

The equation of motion for rotating structures is formulated and then compareed with the equation of motion for stationary structures.

The comparison of Equation 3.57 and Equation 3.130 show that the denominator of equations is identical for stationary and rotating structures, while the numerator is difference due to gyroscopic effect which will be discussed in details in chapter 4.

CHAPTER 4

Experimental Measurements and Methodology

4.1 Introduction

The experimental technique (modal testing) is used to obtain the modal and dynamic response properties of structures. The majority of structures can be made to resonate, that is, under the proper conditions; a structure can be made to vibrate with high-level, sustained, oscillatory motion. Modes are used as a simple and efficient means of characterizing resonant vibration, and are inherent properties of a structure. Natural modes are determined by the material properties (mass, stiffness, and damping properties), and boundary conditions of the structure. Each mode is defined by a natural frequency, modal damping, and a mode shape. If either the material properties or the boundary conditions of a structure change, its modes will change. At or near the natural frequency of a mode, the overall vibration shape (Operating Deflection Shape) of a machine or structure will be dominated by associating the mode shape [62, 118 and 123].

In this chapter different techniques and configurations are presented to interpret the results obtained from experimental measurement of dynamic performance of machinery.

In modal testing, FRF measurements are usually made under controlled conditions, where the test structure is artificially excited by using either an impact hammer, or one or more shakers. A multi-channel FFT analyzer is then used to make FRF measurements between input and output DOF pairs on the test structure [88, 124]. Modal testing requires that FRFs be measured from at least one row or column of the FRF matrix. Modal frequency and damping are global properties of a structure, and can be estimated from any or all of the FRFs in a row or column of the FRF matrix. On the other hand, each mode shape is obtained by assembling together FRF numerator terms (called residues) from at least one row or column of the FRF matrix. Not all structures can be impact tested, for instance, structure with delicate surfaces cannot be impact tested or because of its limited frequency range or low energy density over a wide spectrum, the impacting force is not sufficient to adequately excite the modes of interest. When impact testing cannot be used, FRF measurements must be made by providing artificial excitation with one or more shakers, attached to the structure [125, 126]. Each method has a different application depending on the objective of the test and the time

available. For example, impact testing with a hammer, which is quick and easy, is ideal for studying a car's exhaust system's vibration problems.

Rotating machines such as steam or gas turbines, turbo-generators, internal combustion engines, motors, and disc drives can develop inertia effects that can be analyzed to improve the design and decrease the possibility of failure. Current trends in rotating equipment design focus on increased speeds, which increase operational problems caused by vibration. At higher rotational speeds, the inertia effects of rotating parts must be consistently represented to accurately predict rotor behaviour. Inertia effects in rotating structures are usually caused by gyroscopic moment introduced by the precession of the vibrating rotor as it spins. As spin velocity increases, the gyroscopic moment acting on the rotor becomes critical. It is also important to consider bearing stiffness, support structure flexibility, and damping characteristics to understand the stability of a vibrating rotor. The best method for measurement of dynamic performance of machine is to obtain the frequency response functions at appropriate points [127, 128].

4.2 Methodology in experimental technique

4.2.1 The Rig

RK4 Rotor Kit made by Bently Nevada, was used to extract the necessary information for diagnostic of rotating machinery, such as turbines and compressor. The rig consist of motor, shaft, bearings, and bearings block, rotor mass wheel (disc), speed and keyphasor probes, safety cover, and base with adjustable base support as shown in Figure 4.1. Various type of bearing could be used with this rig such as rigid and fluid film bearing [113, 129].

4.2.1.1 General description

The Bently Nevada Rotor Kit is a versatile and compact model of a rotating machine that simulates several categories of lateral shaft vibration by duplicating vibration-producing phenomena found in large rotating machinery. Various vibration characteristics may be observed by changing [53, 54]:

- Rotor speed
- Shaft bow
- Rotor stiffness
- Amount and angle of unbalance
- Shaft rub or hitting condition
- Rotor-bearing relationship

The rotor kit used to measure these phenomena (vibration phenomena) with proximity transducers. The signals from the transducers have been observed by using an oscilloscope or other monitoring equipment.

Figure 4.1 shows the main components of the rotor kit. The following sections describe rotor kit options for simulating additional vibration phenomena like oil whirl and whip and loose rotating parts, in addition to machinery behaviour, the rotor kit can be used to teach the fundamentals of proximity probe placement, gapping and troubleshooting. It can also be used to teach how to read and interpret proximity probe signals by an oscilloscope.

A measurement and diagnostic tool, such as an oscilloscope and other diagnostic instruments connected with rotor kit model RK4 in order to observe the machine behaviour.

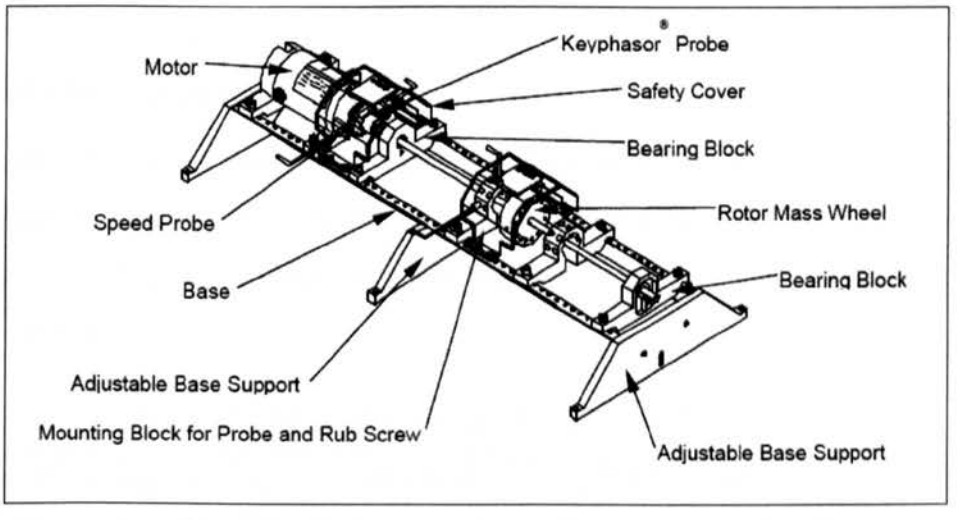

Figure 4.1 The main components of rotor kit [53].

4.2.1.2 Performance and features

The RK4 Rotor kit has a V-frame design that has been developed to provide better control of the housing dynamic stiffness properties. The mechanical tolerances have also been tightened, resulting in more accurate machine behaviour modelling.

The RK4 Rotor Kit motor can closely hold the desired speed with changes in loading conditions. This has been accomplished by incorporating a direct current motor and high performance control circuitry.

The motor can run in either a clockwise or counter-clockwise direction and has adjustable slow roll speed capability. It can be controlled remotely by using a ± 5 volt control input, such as a signal generator or DC power supply, to drive the motor speed control device [129]. Rotor speed is displayed on a digital tachometer with a large LCD readout.

4.2.1.3 Rotor kit specifications

A) Electrical

Power input	95 to 125 Vac, 45 to 65 Hz, 3 Amp, single phase; or 190 to 250 Vac, 45 to 65 Hz, 3 Amp, single phase.
Proximator	
Power output	-18.0 Vdc ± 0.8 Vdc at 140 mA max.
Maximum speed	10,000 rpm, typical.
Ramp rate control	15,000 rpm/min typical [130].

B) Mechanical

RPM range to	10,000 rpm.

4.2.1.4 Shaft specifications

The rig consist of a shaft of length 610 mm supported on bearings, effective rotor length 480 mm (the effective rotor length is the distance between the bearing blocks) [53].

The mechanical properties for shaft and disc are shown in Table 4.1, which have been used later in FE simulation.

Table 4.1 Mechanical properties for shaft and disc [109, 131].

Mechanical properties	***SI unite***	***Shaft (Iron)***	***Disc (Steel)***
Young's modulus	(GPa)	147	225
Poisson's ratio		0.287	0.28
Density	(kg/m^3)	7870	7800
Shear modulus	(GPa)	82	87.89

The vibrations of the rotor were measured by four inductance displacement probes or accelerometer, an additional inductance displacement probe was presented to measure the key phase, and the key phase signal was used to get the phase angle information of vibration or can be used two accelerometers.

4.2.2 Measurement of the dynamic characteristic

Measurement of the dynamic characteristic of the system performs by calculating the output response behaviour to a measurable input excitation into the system. For the experimental

part, the input signal was applied using both the transient and others excitation techniques using hammer and shaker as explained in details in chapter 2.

For hammer techniques (modal hammer) there is a force transducer inside the hammer head which is to measure the input excitation signals. The accelerometer or proximity probes are used to measure output signal, two sets of the signals are sent to the computer through an acquisition channel IDAQ. The acquisition channel will then transfers the data (signals) received from the input and output sensor to the smart office analyzer software through a USB2 port which is connected to the computer, and hence the frequency response function of the system can be worked out, this setup shown in Figure 4.2.

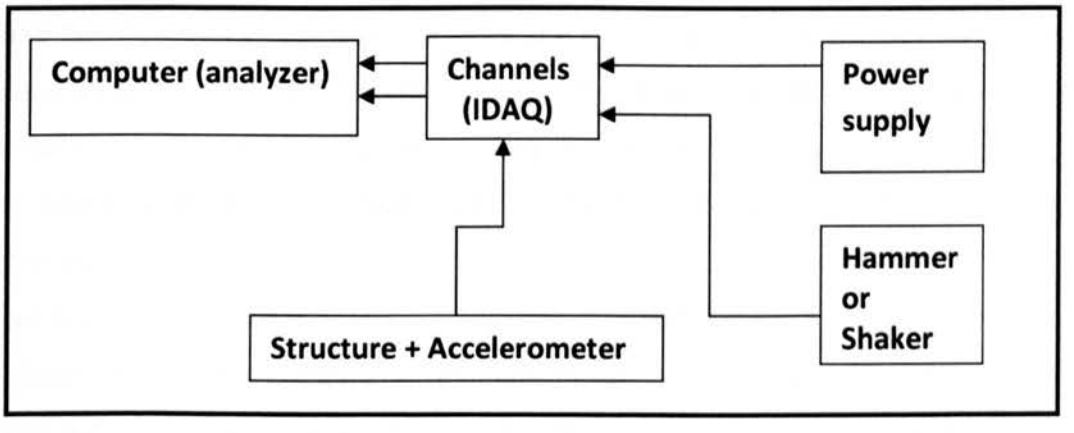

Figure 4.2 Scheme of devices setup.

4.2.3 Computer simulation of experimental data

A computer simulation or a computer model is a computer program that attempts to simulate an abstract model of a particular system. Simulations have become a useful part of mathematical modelling of many natural systems in physics, chemistry, and biology, human systems in economics, psychology, and social science and in the process of engineering new technology, to gain insight into the operation of those systems [132]. Traditionally, the formal modelling of systems has been via a mathematical model, which attempts to find analytical solutions to problems which enable the prediction of the behaviour of the system from a set of parameters and initial conditions. Computer simulations build on, and are a useful adjunct to purely mathematical models in science, technology and entertainment. The reliability and the trust people put in computer simulations depends on the validity of the simulation model. Computer simulations vary from computer programs that run a few minutes, to network-based groups of computers running for hours, to ongoing simulations that run for days. The

scale of events being simulated by computer simulations has far exceeded anything possible (or perhaps even imaginable) using traditional paper-and-pencil mathematical modelling [8]. There are many type of computational simulation such us:-

4.2.3.1 Smart Office Analyzer software

The smart office analyzer is the software which is used in this project [56]; The Smart Office analyzer is suitable for accurate and efficient noise and vibration measurements, third-party data import/export, data analysis and reporting of the results. The SO analyzer supports a wide range of measurement which enables the applications from 2 to 100 of input channels.
As the smart office software is used to calculate the Frequency Response Functions (FRFs) and mode simulations of each setup, to measure the dynamic characteristic of a system or structure, a measure of the output response behaviour to measurable input excitation into the system has to be calculated, as it can be seen from the Figure 4.3, by dividing the output response signals to the input excitation signal, it is possible to determine the transfer function of the system.
The input signal changes as it travels through any dynamic system. Therefore, the ratio of the output signal to the input contains information on the inherent properties of the system. In modal testing the function measured is the frequency response function. On the other hand, the same function, in most electronic and control is known as transfer function.

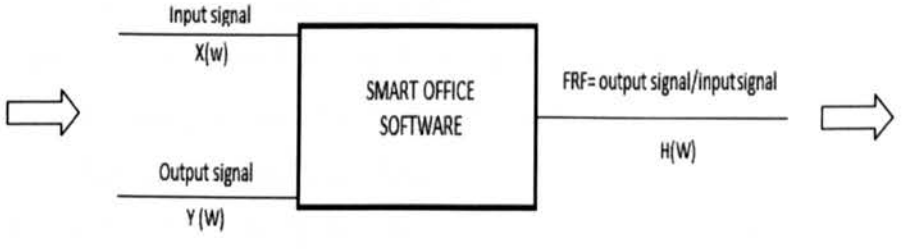

Transfer Function (FRF) = Response/Input

Figure 4.3 Scheme of signal processing.

4.2.3.2 Use of the smart office software in experiments (description of the software)

A step by step description of how to use the software in experiments is shown in the Figure 4.4a.

At first by Getting started icon in the manger tree box and choosing the Add Work Space, a workspace will be made.

Next choosing the Geometry Wizard from the analysis toolbar, the wizard will help to create the Geometry of the system which the measurements are going to be based on.

The FRF measurements setup has to be created. This can be done; either by choosing FRF impact wizard from the application toolbar or manually choosing the setups from the setup area.

The next step of the wizard is to set the transducer information of the devices attached to the channels. It is important to make sure that the excitation and the response channels are set correctly. The first line of the table corresponds to the first acquisition channel which in our case, is connected to the impact hammer device.

The resistibility of the excitation and response devices has to be set at this stage of the wizard. This enable the program to calibrate the signals according to the values entered in this stage.

The next step is to set the range and pre-loading configurations of the transducers which are built inside the devices and are attached to the acquisition channel.

For accelerometer and impact hammer devices, AC coupling has to be chosen, whereas case of using the proximity probe, as for the type of the device, DC coupling is preferred.

Also in this stage excitation and response channels should be named.

There is an option to select a Roving hammer or Roving transducers. In an impact test, it is possible to both fix the transducer location and rove the hammer, or to have fixed hammer location and rove the transducer along the nodes.

In this step of the impact wizard function, by selecting one of the roving options, it is possible to verify the impact testing method which is going to be used.

By selecting the hammer, the program will assume that for each impact at any nodes, the response transducer will be fixed at same point and only the hammer is to be moved. Whereas by selecting the transducer, the program will assume that the response transducer is to be moved while impacting at one place.

Also in this stage, the numbers and directions and the points that measurement is going to be taken has to be selected from the node list box, see Figure 4.4b.

Then, the acquisition parameters have to be chosen. And all the sampling parameters such as sample rate, useful band width, block-size, triggering and auto-ranging margin can be adjusted.

By changing the bandwidth, the program will automatically recalculate the required sample rate. The recalculated sample rate value will be discretionary and can be changed.

The impact testing wizard triggering, triggers on the excitation channel. When the excitation channel exits, the signal will be read according to the set mode.

The trigger level is the minimum voltage input level that the impact testing wizard accepts for triggering. The default trigger voltage level is set at 0.5 Volt.

Next is to select the window parameters. There are two types of windows, uniform and force /exponential. The force/exponential window is applied to both excitation and response channels.

Then, by selecting the measurement functions from the list provided, it is possible to save the selected measurements to the workspace of the hard disk of the computer.

Also in this step the delay time before the automatic save in the acquisition window and the name of the mode setup can be chosen.

The best way to display the mode-shape and FRFs of every mode at a single workspace, the operating deflection shape wizard function can be utilised from the analysis tool bar. The operating deflection shape wizard will guide through the operational deflection analysis and animations.

By selecting the type of the measurement saved and choosing the measurement directions and clicking next, another window will appear showing the list of the measurements saved.

Next by clicking on the next button the analysis window will appear showing all the nodes and measurements. This window is for information only and does not require any changes, this window is divided into two sections; the FRF graphical area (this is bode plot) and the geometry simulation area.

The frequency response function of the nodes for any geometry can be added together or subtracted away from one another. The software has a very strong calculator function, which could be used to add or subtract any similar-category measurements. This function can be used to add the FRFs of each node in the geometry in order to produce one FRF for the whole system.

The end step is curve fitting by selecting the advanced MDOF wizard. Then, curve fit of the points selected will be displayed on a graph and the mode shape at the selected frequency is displayed on the right hand side of the screen along with a frequency value and damping ratio.

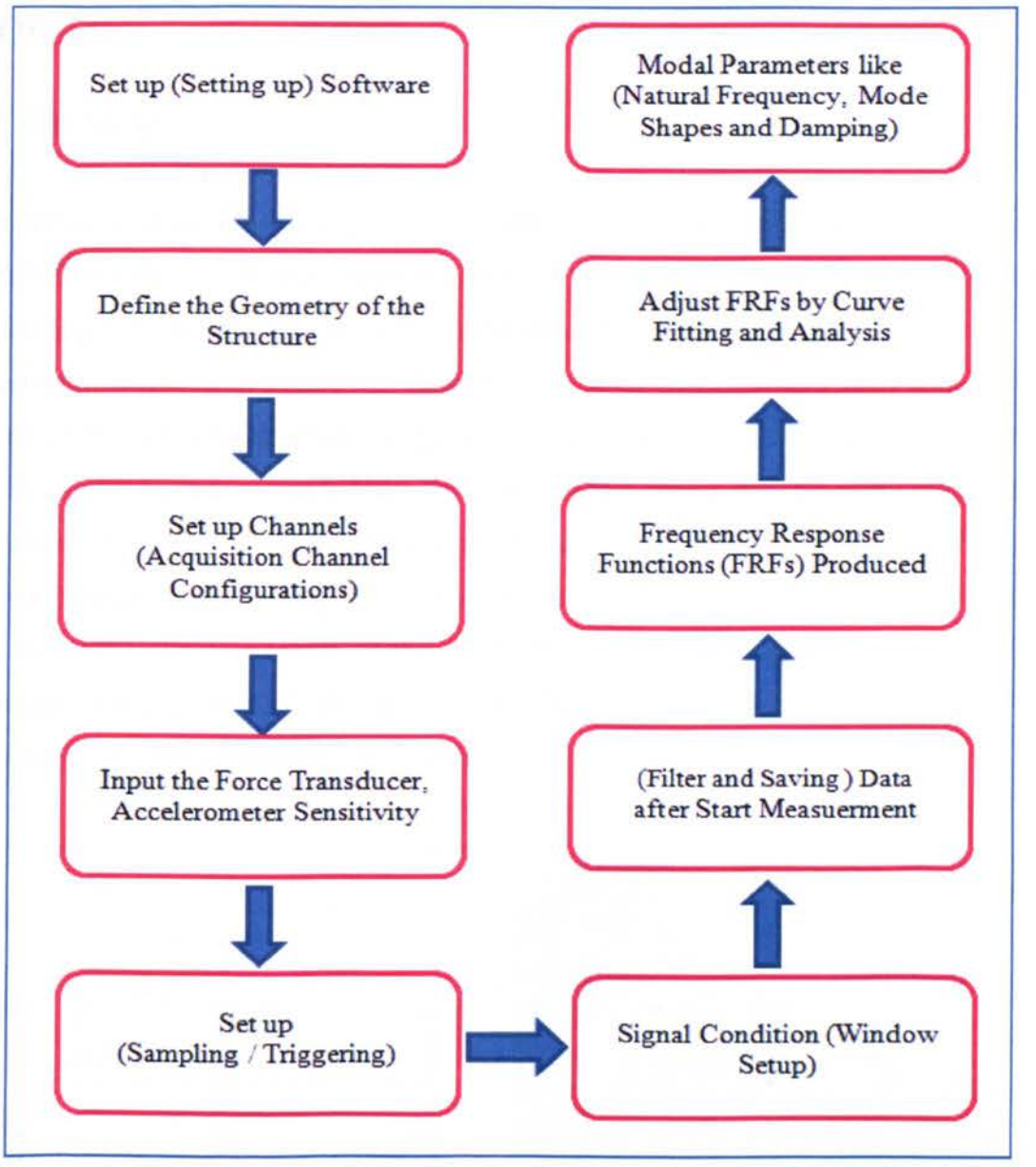

(a)- Scheme shows how to use the software in experiments.

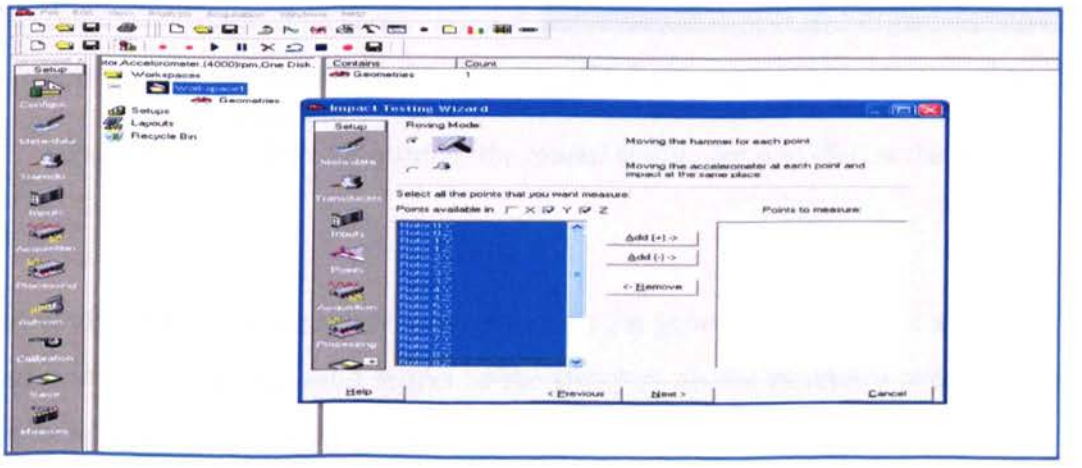

(b)- Show roving mode.

Figure 4.4 Use of the smart office software in experiments.

4.3 One disc configuration

4.3.1 Test setup

The analysis software used in experiment is part of (M + P) International Ltd. It is designed for analyzing noise or vibration problems related to the speed characteristics of rotating or reciprocating components of a machine in operation [43, 56 and 133].

The test rotor is shown in Figure 4.5. Basically, the rotor consisted of a shaft with a nominal diameter of 10 mm, with an overall length of 610 mm and two plain bearings. RK4 Rotor Kit made by Bently Nevada is used. Then, the experimental modal analysis using the impact test was carried out, installing two accelerometer (model 333B32, sensitivity 97.2 and 98.6 mV/g) in Y and Z direction and roving the hammer (model 4.799.375, S.N24492) on each point (12 points along the effective length of the shaft) for the purpose of generating strength of the movement for the vibration body and then the signal transfer through the acquisition to the computer Smart Office software. Finally the results obtained from the computer.

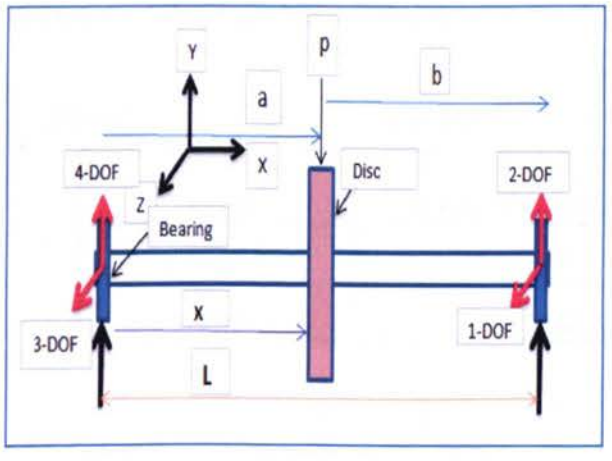

(a)-Schematic of a rotor one disc setup parameter.

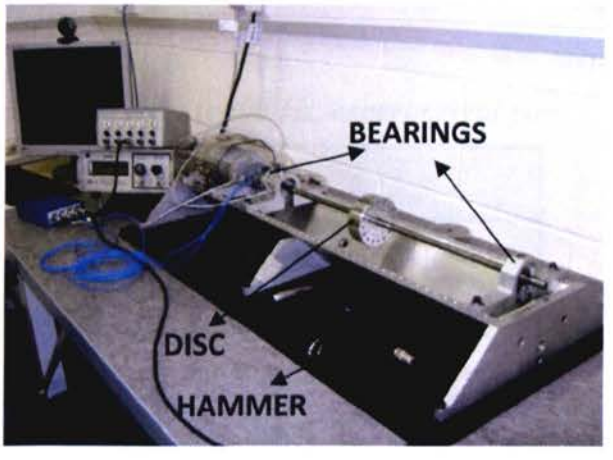

(b)-Rotor rig with one disc configuration.

Figure 4.5 Experimental setup of the modal testing for one disc in the middle.

The test configuration on the rotary machines with the geometry design are shown in Figure 4.6a and b, it represents the solid model of the structure on the geometry area, (a) at start of rotation and (b) at rotation 1000 rpm for one disc rotor system.

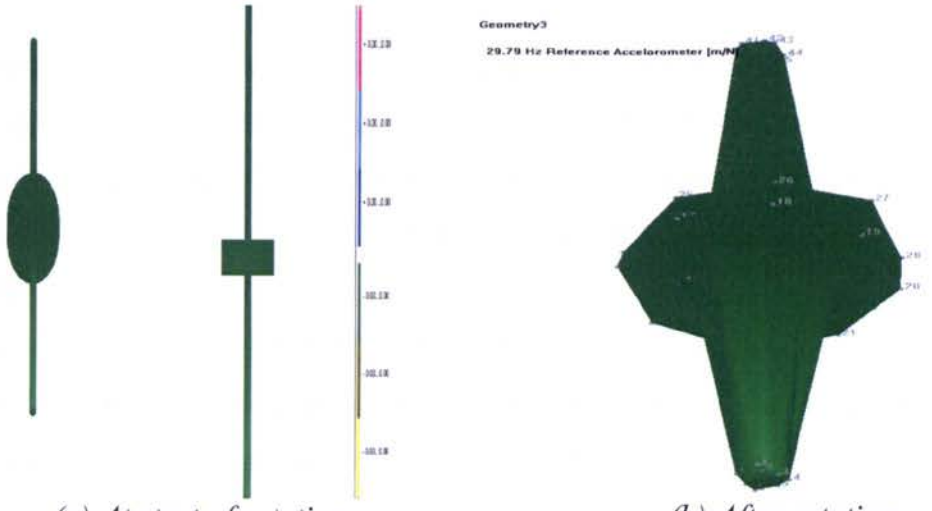

(a)-At start of rotation. *(b)-After rotation.*

Figure 4.6 Geometry design for model with one disc in the middle, experimental test using smart office.

4.3.2 Detection of natural frequency and damping ratio from modal analysis

We find the natural frequency and damping ratio ζ for different mode shapes by curve fitting [134, 135] to the experimental data in Smart Office software which explained previously in the methodology, Table 4.2 and see Figure 4.7.

Table 4.2
Natural frequency and damping ratio ζ for one disc range 0-500 Hz, experimental part.

Name	Natural Frequency (Hz)	Damping Ratio (ζ) %
Mode 1	29.79	18.701
Mode 2	242.74	7.561

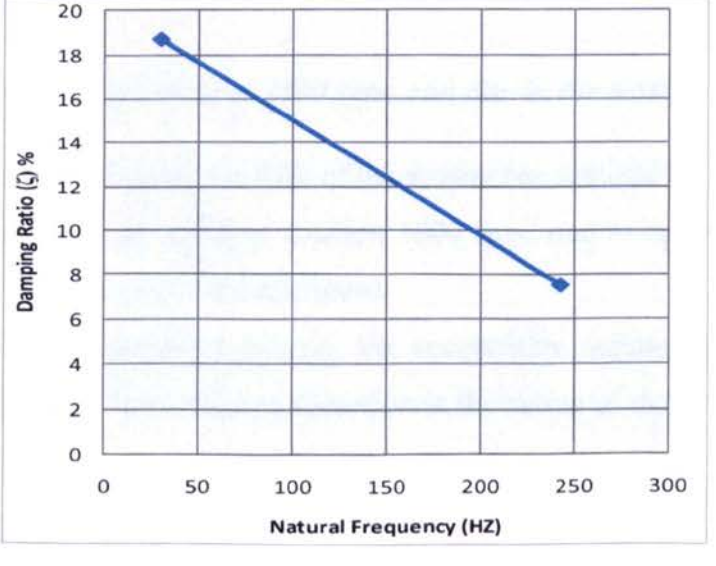

Figure 4.7 Damping ratio (ζ) versus natural frequency(Hz), one disc.

4.3.3 Unbalance with added mass

In this experiment, trial weight 8 gram of excessive load is added to the loading of the system, the excessive loading is away from the centre of the shaft by 30 mm. The locations of the additional balance masses to suppress the vibration amplitudes was found to be at angles of $\varnothing$=135° and $\varnothing$=315° respectively. The Figure 4.8 below shows the unbalance loading of the setup of the rig.

In the following experimental study, unbalance loading is applied to the system. ANSYS simulation of the set is done after the experiments. Both the theoretical simulations and experiments showed that the natural frequency of the system should reduce slightly, due to the additional load of the unbalance, Figures 4.9, 4.10 and 4.11 for different speeds of rotation show this fact.

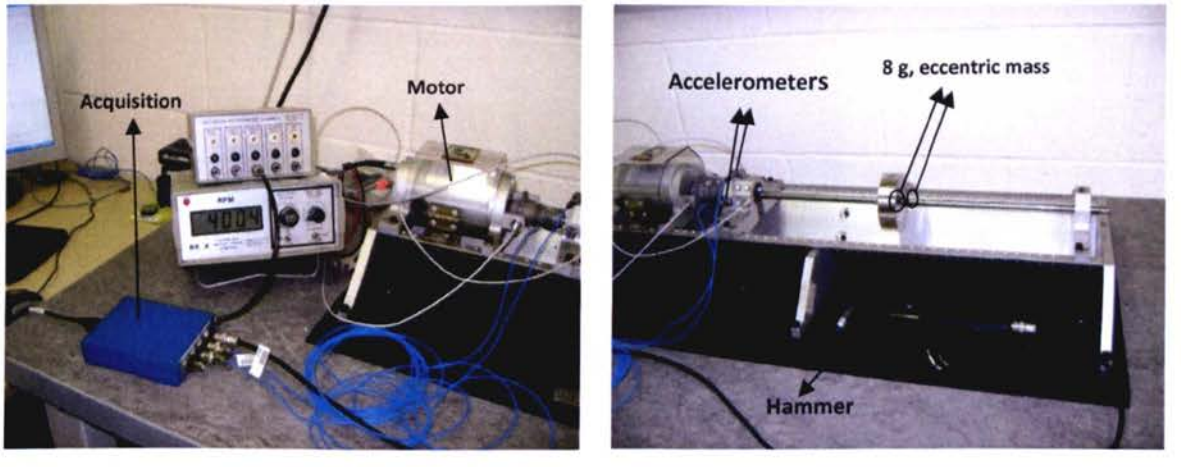

(a)-Acquisition channel. *(b)-Unbalance loading setup of the rig.*

Figure 4.8 Experimental setup of the rig, one disc.

4.3.3.1 Unbalance with added mass at 1000 rpm, one disc in the middle

As it can be seen from the figures, the FRF of the system has reduced by 10 db for first mode and 5 db for second mode at speed of rotation 1000 rpm, due to applying an excessive 8 grams of loading to the system at the same speed.

By adding the correcting balanced masses, the eccentricity reduces and resulting in the reduction of the centrifugal force causing reduction in the radius of shaft orbit.

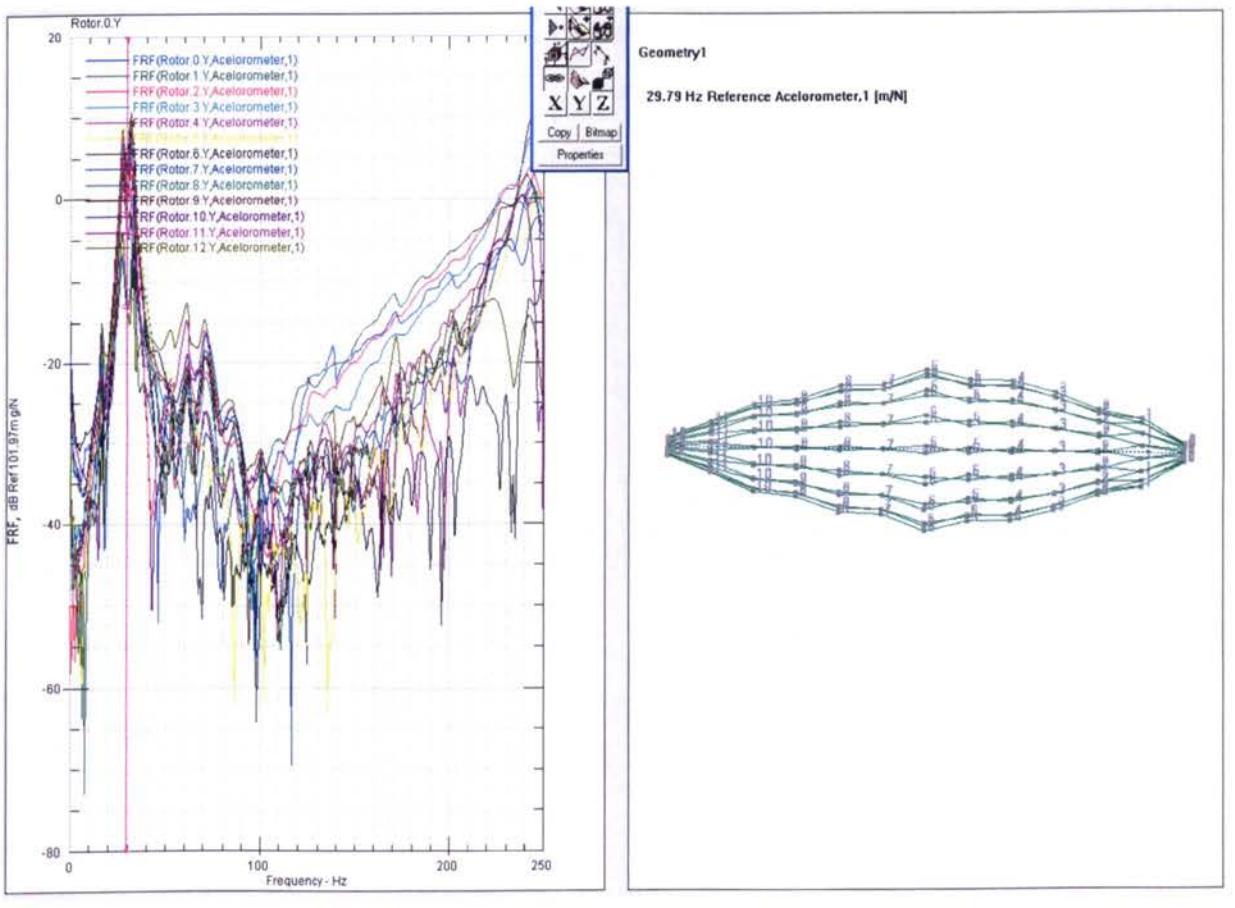

(a)-Before added mass.

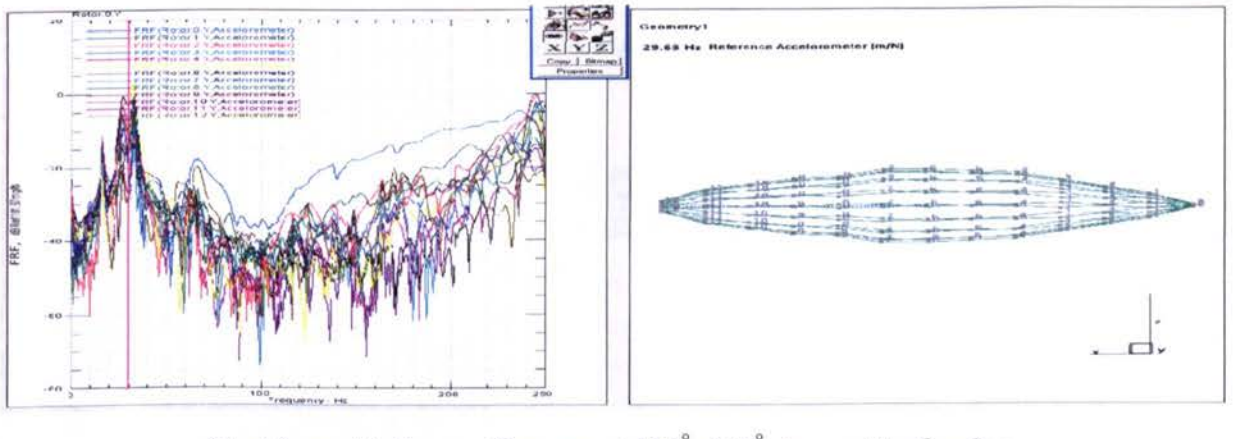

(b)-After added mass (8 gram at 135°, 315° degree) in the disc.

Figure 4.9 FRF versus frequency (Hz), speed of rotation 1000 rpm, one disc, first mode shape.

The left hand side plots in Figure 4.9a and b show the FRF graphical area, in which the vertical axis represents the FRF versus the frequency in horizontal axis, this is a bode plot, while the mode shape with frequency value are shown on the right hand side of the figure. The rotor 0 to 12 represents the name and number of each node along the effective length of the shaft which experimental testing has been performed.

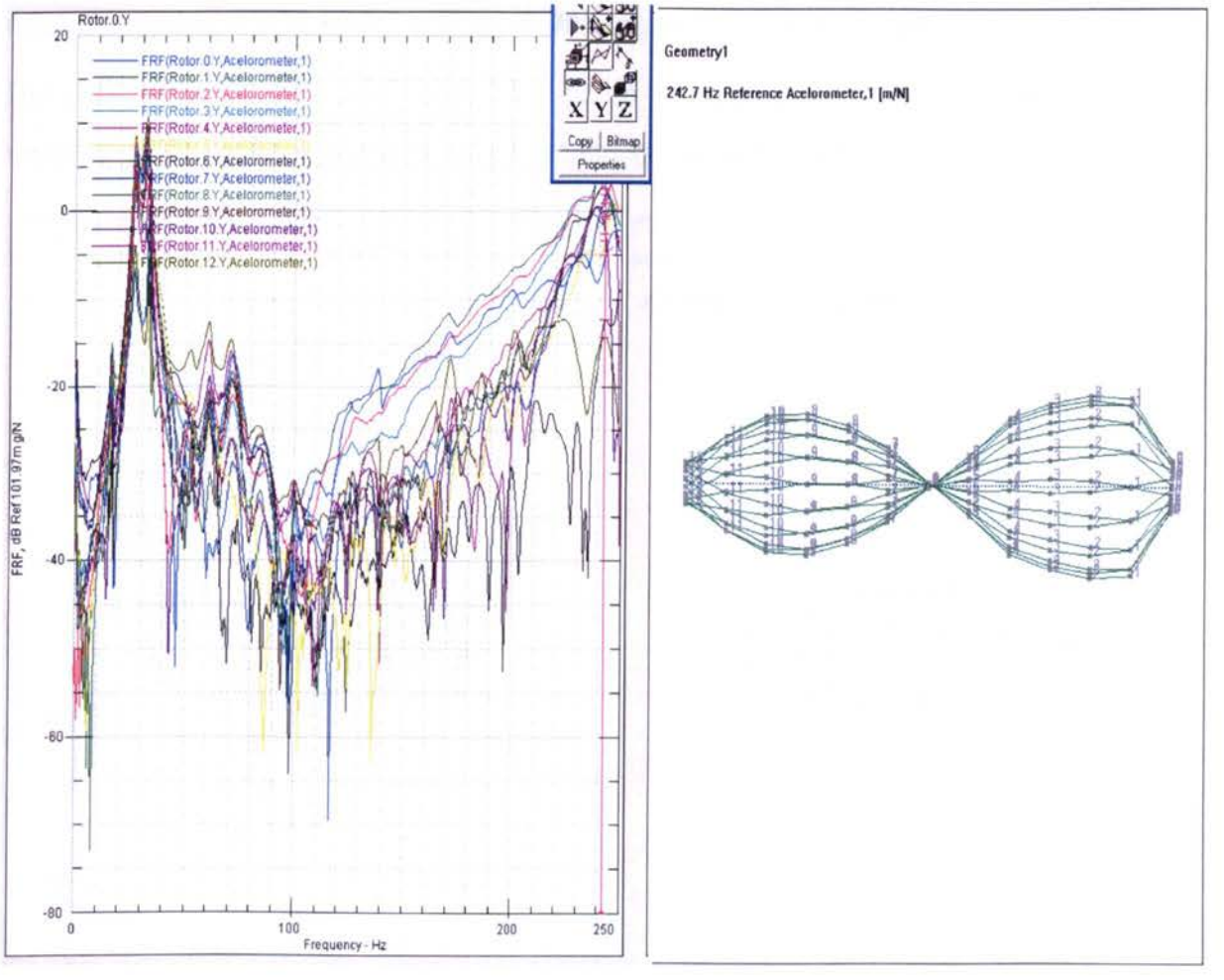

(a)- Before added mass, second mode shape.

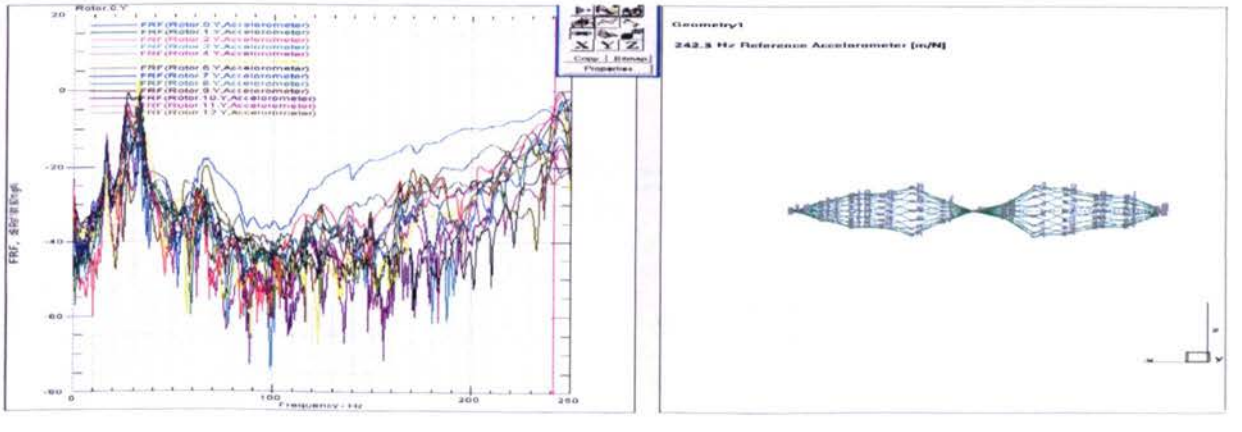

(b)- After added mass (8 gram at 135°, 315° degree) in the disc.

Figure 4.10 FRF versus frequency (Hz), speed 1000 rpm, one disc, second mode shape.

4.3.3.2 Unbalance with added mass at 4000 rpm, one disc in the middle.

The FRF of the system has reduced by 12 db for first mode at speed 4000 rpm due to applying an excessive 8 grams of loading to the system at the same speed.

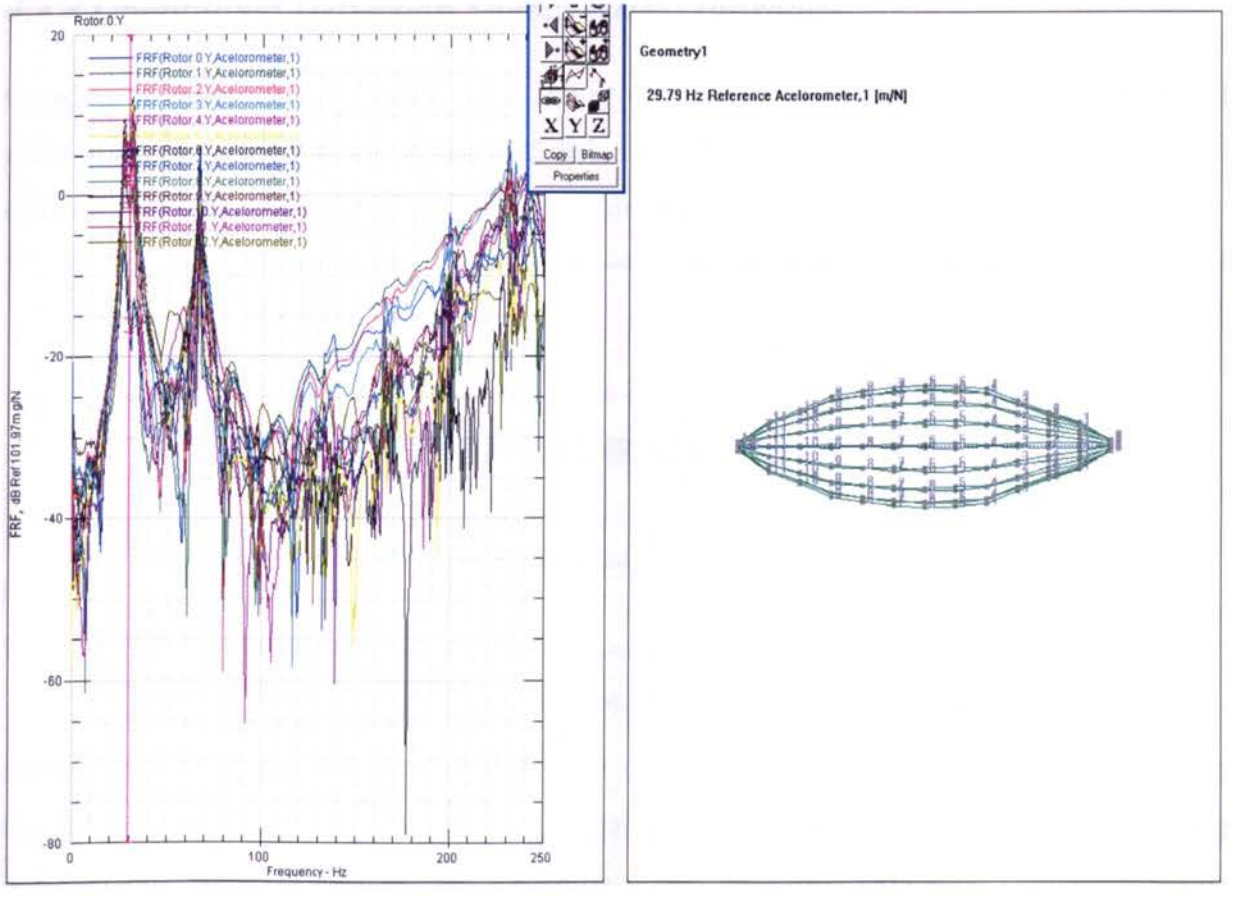

(a)- Before added mass, first mode shape.

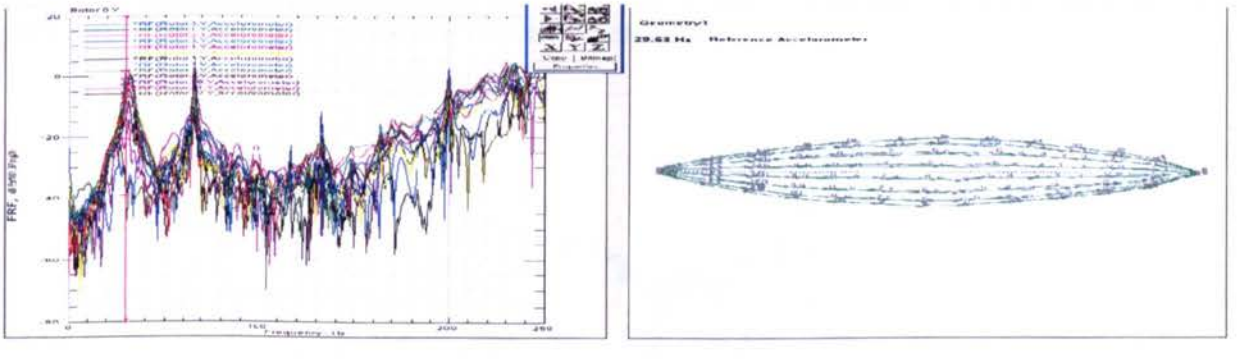

(b)- After added mass (8 gram at 135°, 315° degree) in the disc.

Figure 4.11 FRF versus frequency (Hz), speed 4000 rpm, one disc, first mode shape.

It can be seen from the Figures 4.9, 4.10 and 4.11, the experiment shows that by applying a small additional loading to the system, the value of the natural frequency does not change significantly.

4.3.4 Operational Deflection Shapes (ODS) for rotors

Consider a Jeffcott rotor (named after Henry Homan Jeffcott, also known as the de Laval rotor in Europe), that has an unbalanced disc, i.e. a disc with an offset (e) between its centre of mass (point G) and its centre of rotation (point S) as in Figure 4.12.

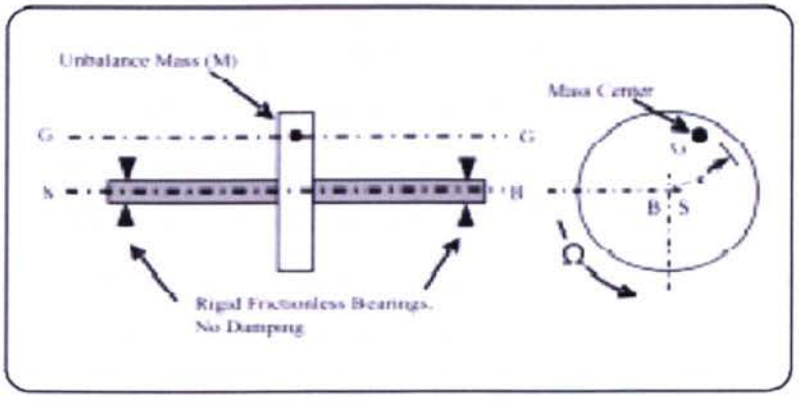

Figure 4.12 Jeffcott rotor configuration for low spin speed, courtesy of [122].

As the rotor spins, speed increases. The offset will cause point S to move outward relative to the bearing centreline (axis B) there by producing a forced whirling motion. Forced whirling is a dynamic response motion with a definite shape, called the Operating Deflection Shape (ODS). It is important that the natural whirling modes not be confused with the ODS. Although different in concept, they are related. For each spin speed a set of weighting factors can be found such that the weighted sum of the normalized natural whirling modes is equal to the ODS. This is known as the rotor-dynamic expansion theorem.

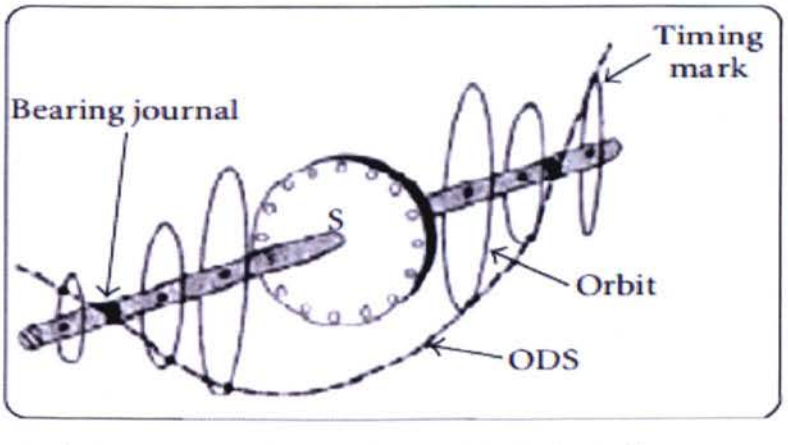

Figure 4.13 A typical Operating Deflection Shape (ODS) for Jeffcott rotor, courtesy of [122].

In this review we shall be concerned mainly with an ODS for which the whirling rate is equal to the spin speed, a condition known as synchronous whirling. Synchronous whirling is caused by unbalance (imbalance) and plots as a straight line of positive slope in ω, Ω coordinates. It is also referred to as the one-times spin speed line and labelled 1X, has good agreement with Figure 4.13 [122].

4.3.5 Coherence graph using experimental Smart Office software

As mentioned before in chapter 2, the force window is applied to the excitation, and for response the exponential window has been applied in the impact test. This type of window can be selected from the pull-down list of the windows section in Smart Office software.

A force window has a flat portion of value 1, wide enough to capture the force input signal, and a cosine taper after the flat portion that decays rapidly to zero to remove the noise after the impact. Applying force window improves the signal-to-noise ratio of the excitation block. We can see two different figures. Firstly, Figure 4.14a and b before using window and another Figure 4.15a-c after using filtering (force/exponential window). We know coherence is measured on a scale of (0.0 to 1.0), where 1.0 indicates perfect coherence is near the natural frequency of the system because the signals are large and less influenced by the noise. We get good input signal to noise ratio results when the coherence is close to unity. Coherence values less than unity are caused by poor resolution, system nonlinearities, extraneous noise and uncorrelated input signals.

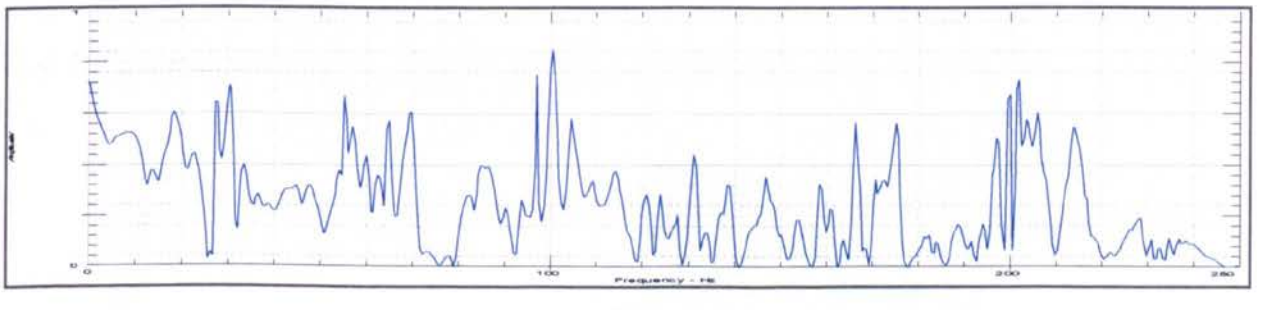

(a)

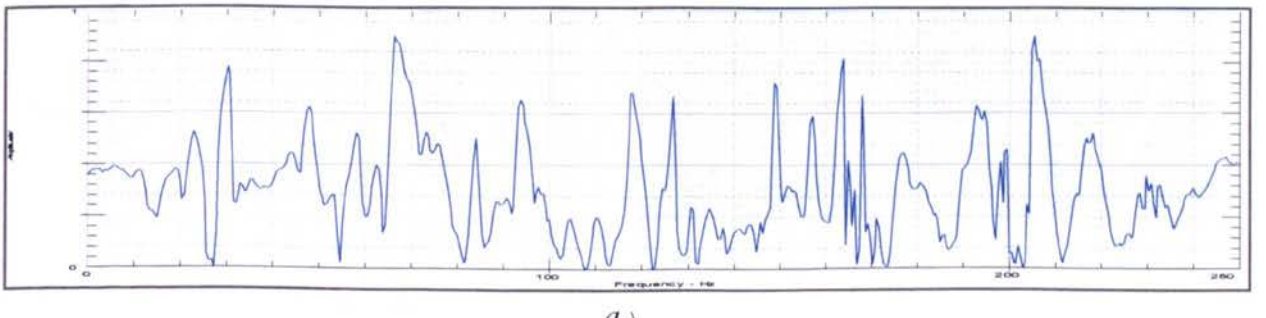

(b)

Figure 4.14 Coherence graph before filtering.

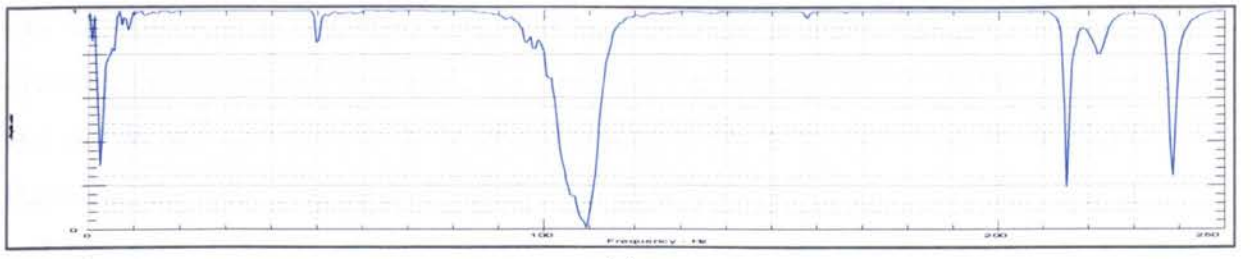

(a)

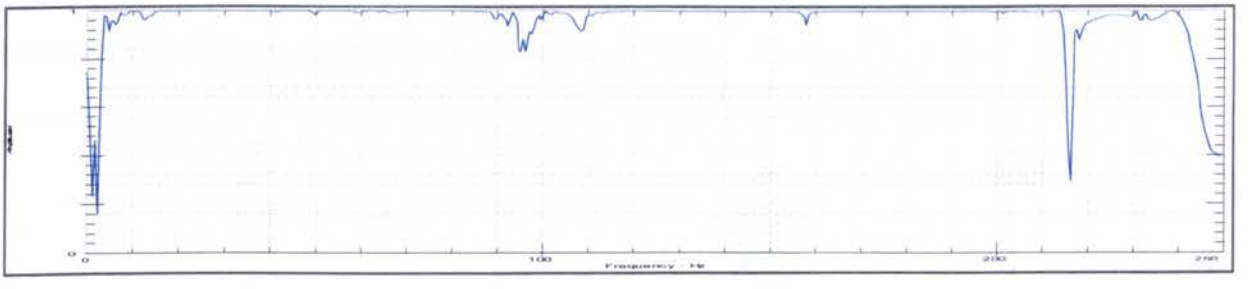

(b)

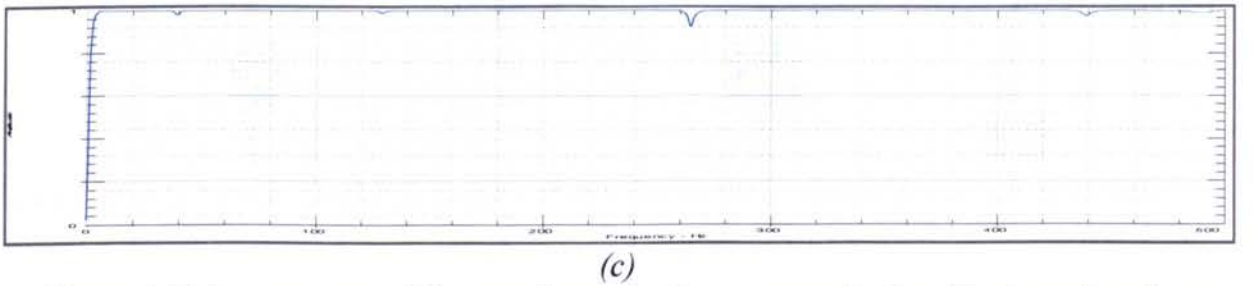

(c)

Figure 4.15 Improvement of the experimental coherence graph after filtering using (force /exponential) window in impact test.

4.4 Two discs configuration

4.4.1 Test setup

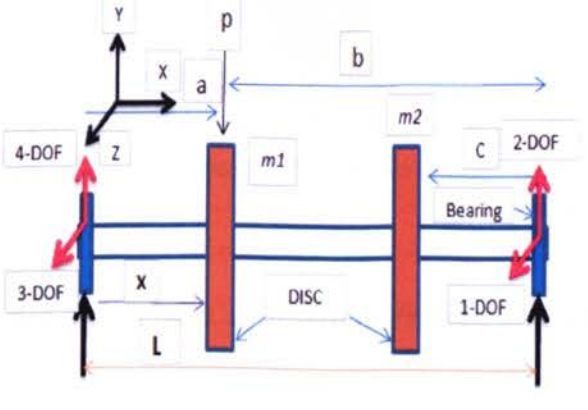

(a)-Schematic of a rotor with two discs setup parameter.

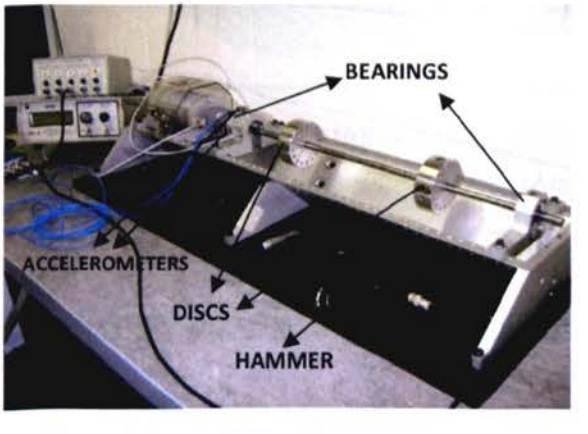

(b)-Rotor rig with two discs configuration.

Figure 4.16 Experimental setup of the modal testing for two discs configuration.

The experimental setup here is described as in one disc configuration, but two discs with a diameter of 75 mm are considered. The first disc was installed at 25% of the effective length and the second one at 75% of the effective length. The test rotor is shown in Figure 4.16. Basically, the rotor consisted of a shaft with same dimensions as in one disc configuration, and two plain bearings. It is tested to extract the necessary information for diagnostic of rotating machinery. The model for the experimental testing at start off rotation and after rotation with different speeds is shown in Figure 4.17.

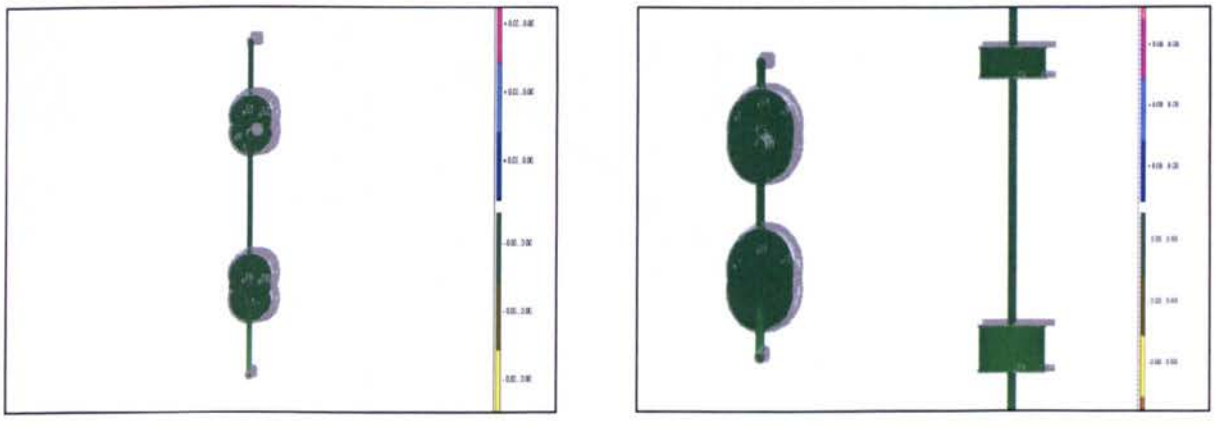

(a)-At set off rotating.

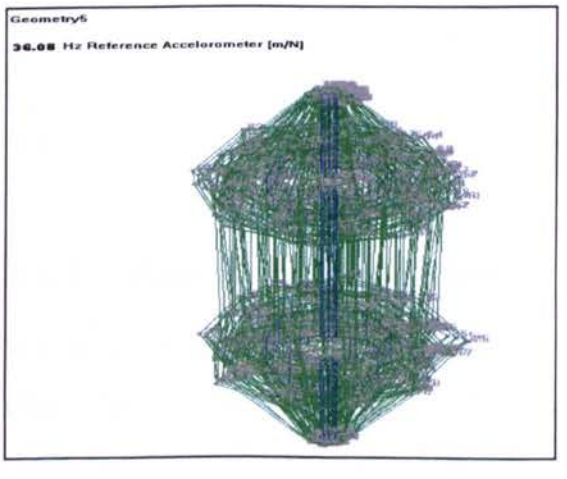

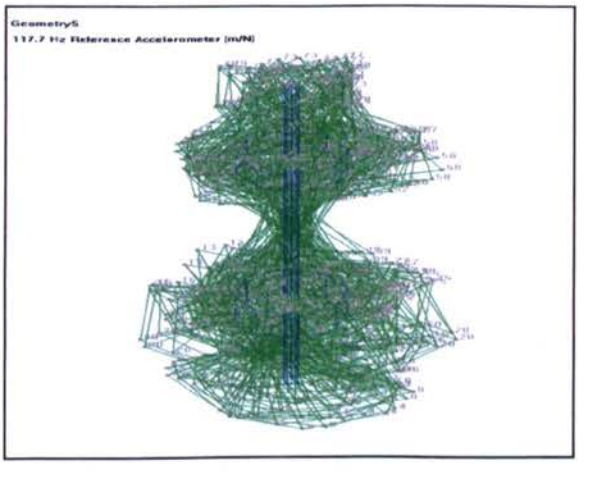

(b)-After rotation. *(c)-After rotation.*

Figure 4.17 Geometry design for model with two discs configuration, experimental test using smart office.

4.4.2 Detection of natural frequency and damping ratio from modal analysis

Detection of natural frequency and damping ratio ζ for different mode shapes by curve fitting multi degree of freedom system in experimental part with two disc, Table 4.3, and see Figure 4.18.

Table 4.3
Natural frequency and damping ratio ζ for two discs range 0-500 Hz, experimental part.

Name	Natural frequency (Hz)	Damping ratio (ζ)%
Mode 1	36.08	19.715
Mode 2	117.74	12.095
Mode 3	181.6	3.337

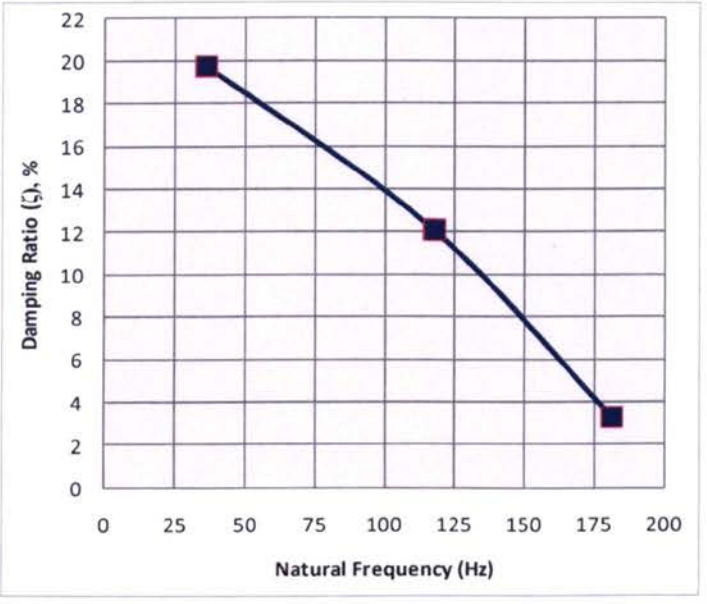

Figure 4.18 Damping ratio (ζ) versus natural frequency, two discs.

4.4.3 Unbalance with added mass

Vibration caused by mass imbalance is a common problem in rotating machinery such as steam turbines and compressors. For the analysis of vibration suppression with different eccentricities of the unbalanced masses, it is noticed that the adding of balance masses will normally suppress the vibration amplitude effectively until the point where an optimum amount that causes the minimum balanced vibration amplitudes is observed and vibration can be used as constraint in calculating the balance weight of running speed to ensure the machinery run-up and down safely. The Figure 4.19 shows the unbalance loading of the setup of the rig with two discs in effective length. In this experiment, unbalance loading is applied to the system. The natural frequency of the system should reduce slightly, due to the additional load of the unbalance, Figures 4.20, 4.21 and 4.22 at speed of rotations 1000 rpm show this fact. In this experiment, trial weight of 16 gram (8 gram per each disc) is added to

the loading of the system for two discs configuration, the extra loading is away from the centre of the shaft by 30 mm.

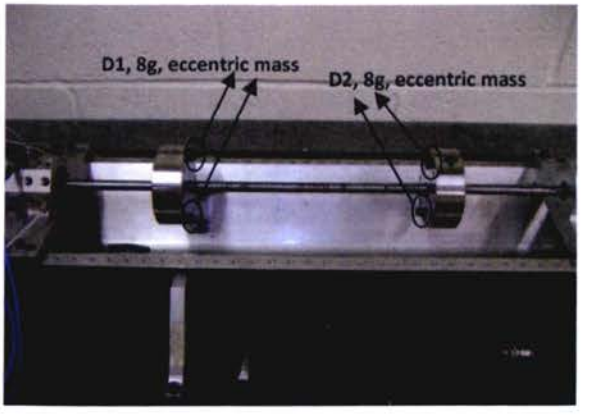

(a)- Rotor kit motor speed control. *(b)- Unbalance loading setup of the rig.*

Figure 4.19 Experimental setup of the rig with two discs.

From the Figures 4.20, 4.21 and 4.22 the experiment shows that by applying added mass to the system the value of the natural frequency does not change significantly.

These figures also show the FRF of balanced rotor setup (a), versus achieved unbalanced frequency response function of the setup (b), as it can be seen from the figures, the FRF of the system has reduced by 19 db for first mode, 6 db for second mode and 5 db for third mode, due to applying an excessive 16 grams of loading to the system (8gram per each disc) at the same speed. That mean the amplitude is reducing in the shaft after added mass in the disc 1 with angle $\varnothing = (45^{\circ}, 225^{\circ})$ and in disc 2 with angle $\varnothing = (180^{\circ}, 0^{\circ})$, the noise is reducing as well due to reduce excess vibration.

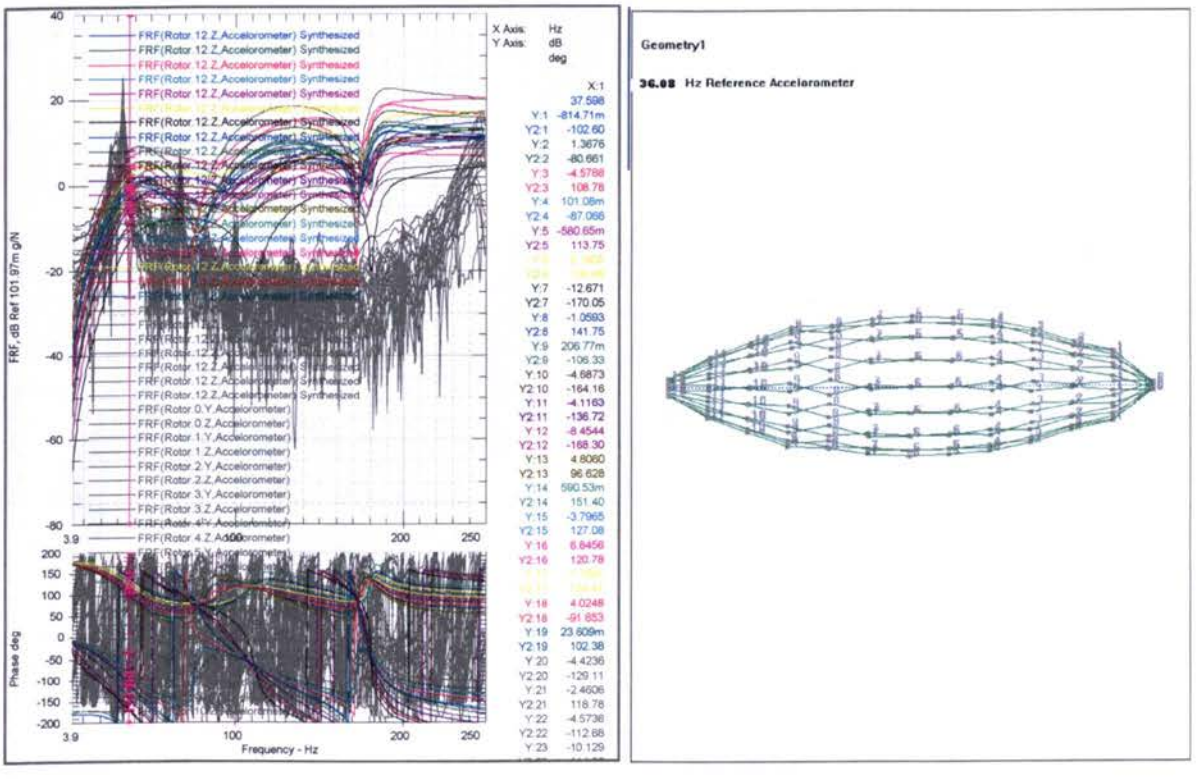

(a)-Before added mass, first mode shape.

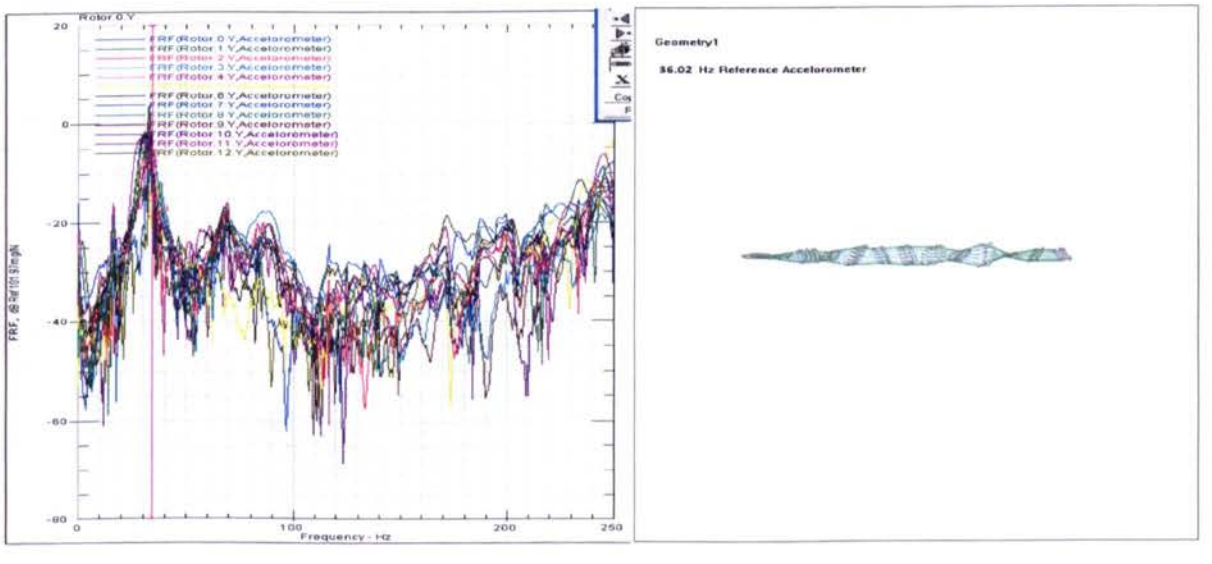

(b)-After added mass (8 gram at disc 1, (45°, 225°) and 8 gram at disc 2, (180°, 0°)).

Figure 4.20 Mode shape of the rotating system with two discs shows FRF versus frequency (Hz), first mode shape, speed of rotation 1000 rpm.

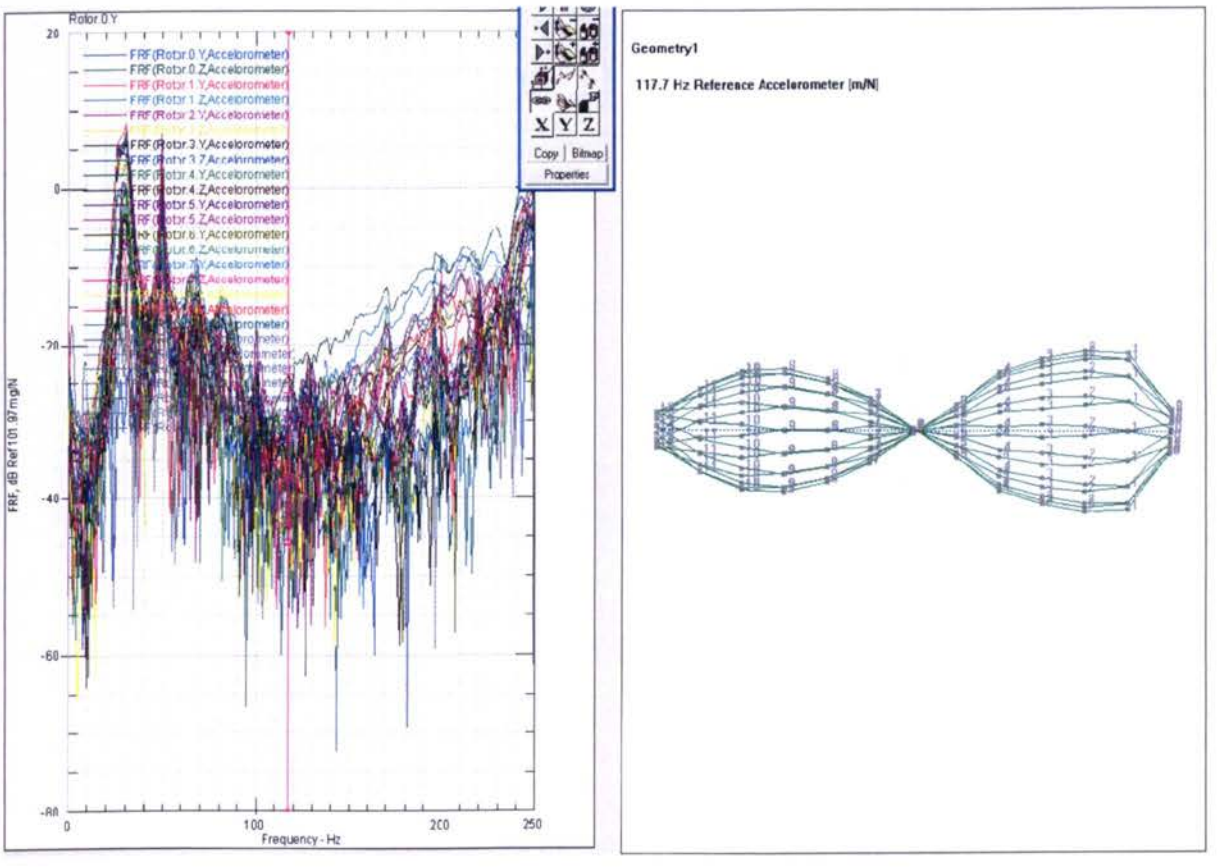

(a)- Before added mass, second mode shape.

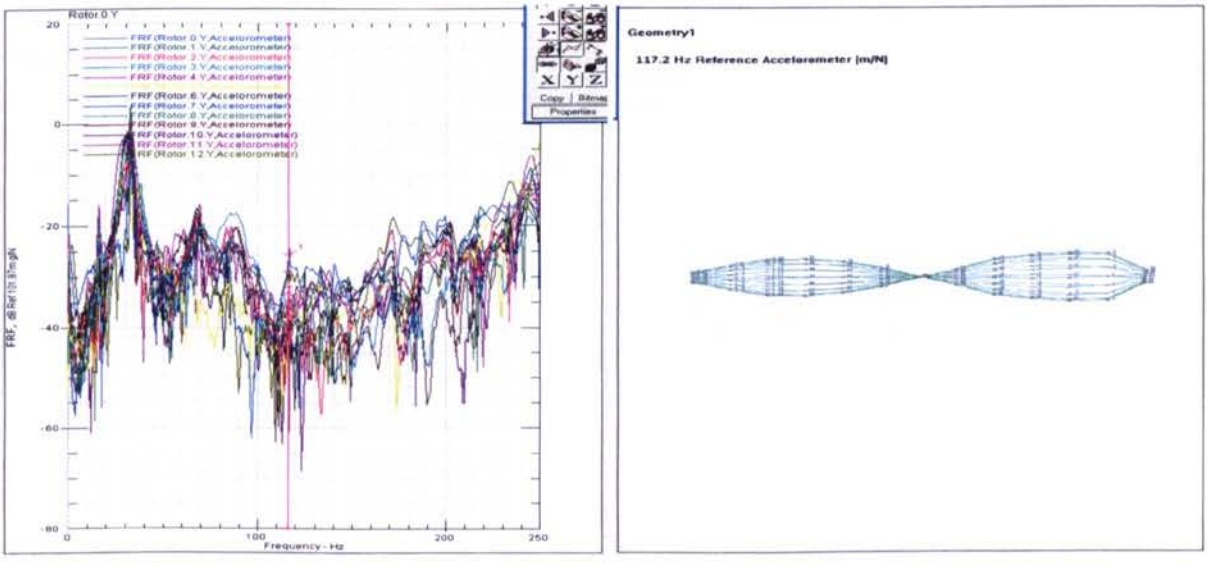

(b)- After added mass (8 gram at disc 1, (45°, 225°) and 8 gram at disc 2, (180°, 0°)).

Figure 4.21 Mode shape of the rotating system with two discs shows FRF versus frequency (Hz), second mode shape, speed of rotation 1000 rpm.

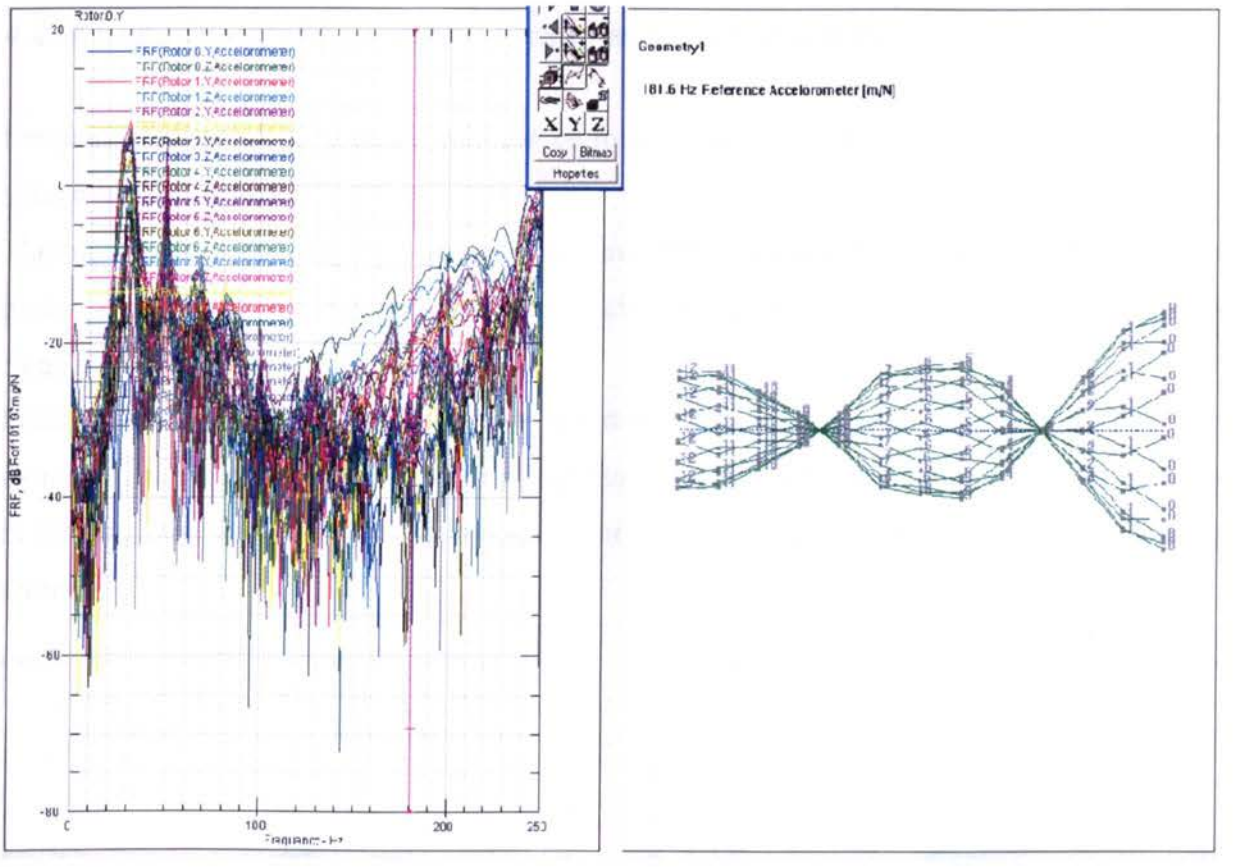

(a)- Before added mass, third mode shape.

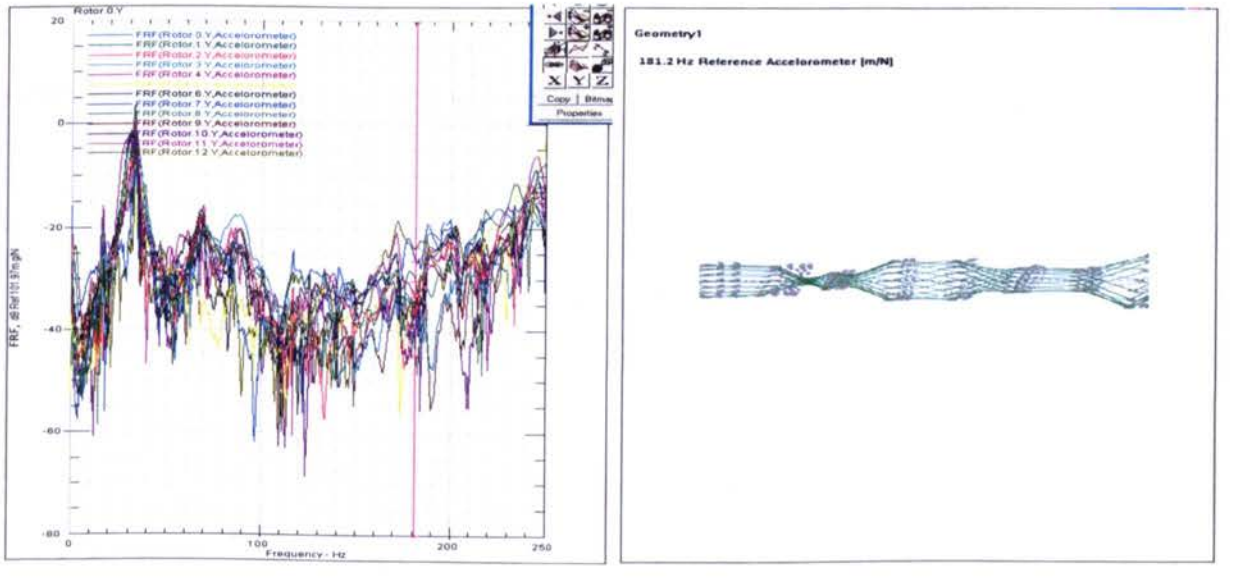

(b)- After added mass (8 gram at disc 1, (45°,225°) and 8 gram at disc 2, (180°, 0°)).

Figure 4.22 Mode shape of the rotating system with two discs shows FRF versus frequency (Hz), third mode shape, speed of rotation 1000 rpm.

4.4.4 Experimental Nyquist plot using modal testing software

Frequency Response Function (FRF) can be found experimentally using Nyquist plot and are shown in Figure 4.23.

The main benefit of using the Nyquist plot comes from its circularity property in the complex plane. The data point does not connect full circles because of frequency resolution that is clear in Figure 4.23i.

From Figure 4.23, multi circles at low speed for multidisc configuration are shown; with increasing the speed slowly the circles begin to rotate by 180° due to gyroscopic phenomena in rotating machinery. Study of this phenomenon will be discussed in details in the following sections.

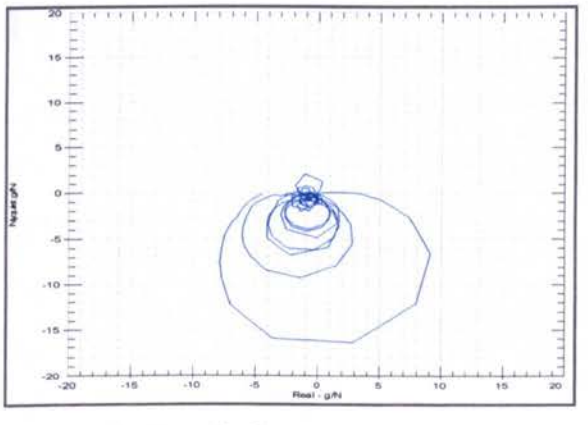

(a)-Speed of rotation 250 rpm.

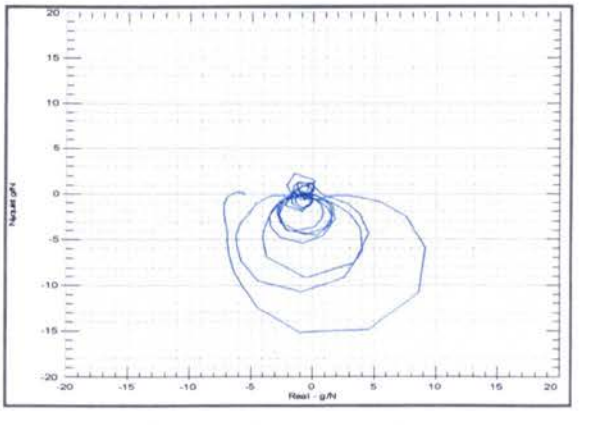

(b)-Speed of rotation 500 rpm.

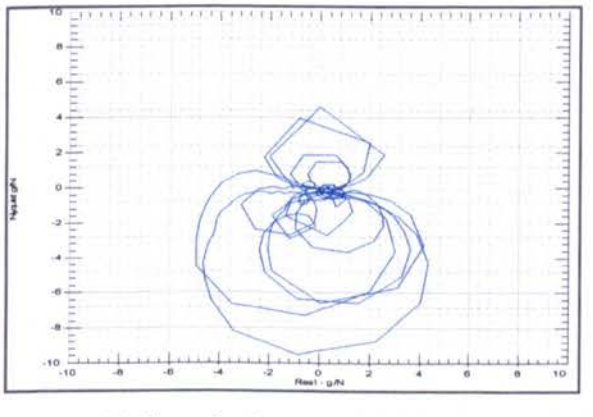

(c)-Speed of rotation 1000 rpm.

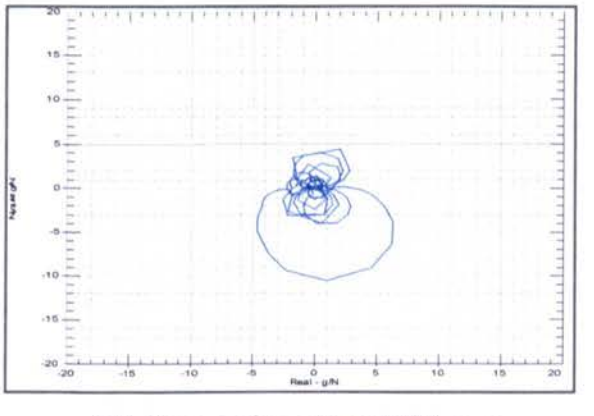

(d)-Speed of rotation 2000 rpm.

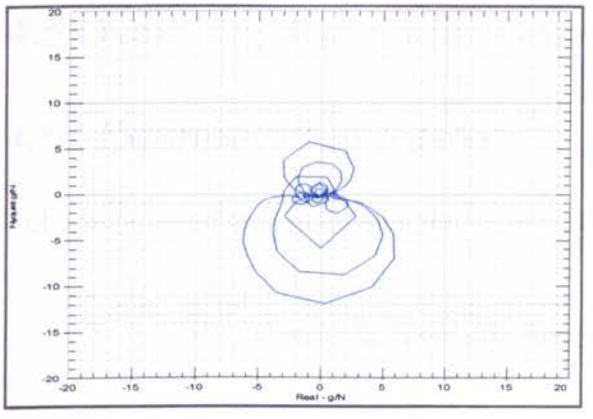

(e)-Speed of rotation 3000 rpm.

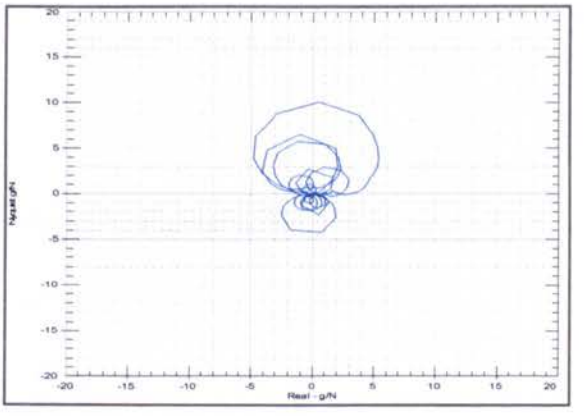

(f)-Speed of rotation 4000 rpm.

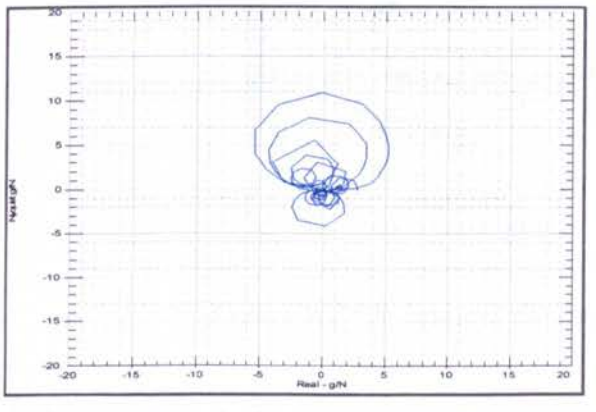

(g)-Speed of rotation 5000 rpm.

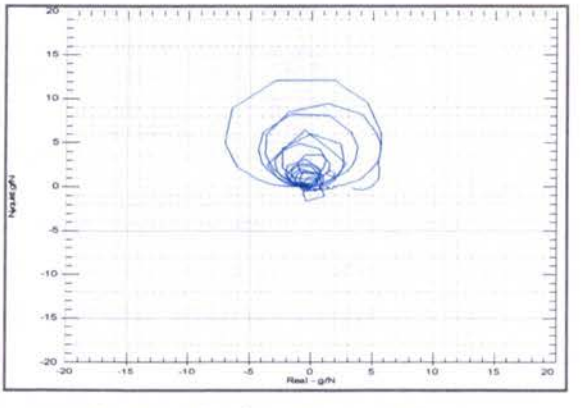

(h)-Speed of rotation 6000 rpm.

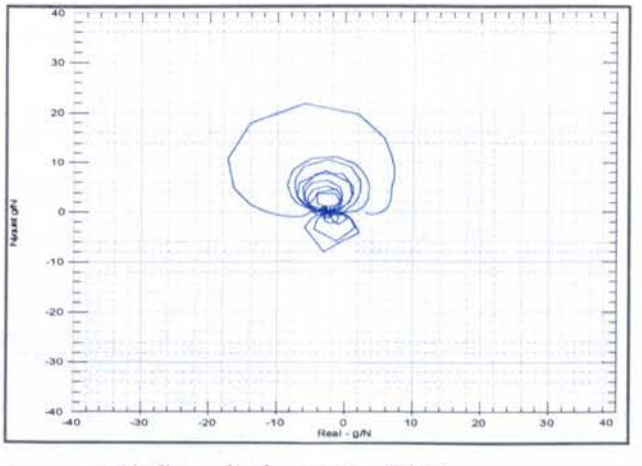

(i)-Speed of rotation 7000 rpm.

Figure 4.23 Experimental results show Nyquist plot (frequency response function curve), imaginary versus real for different speeds of rotation, two discs configuration.

4.5 Overhung disc configuration

4.5.1 Experimental procedures

Schematic overhung rotor disc setup parameter is shown in Figure 4.24.

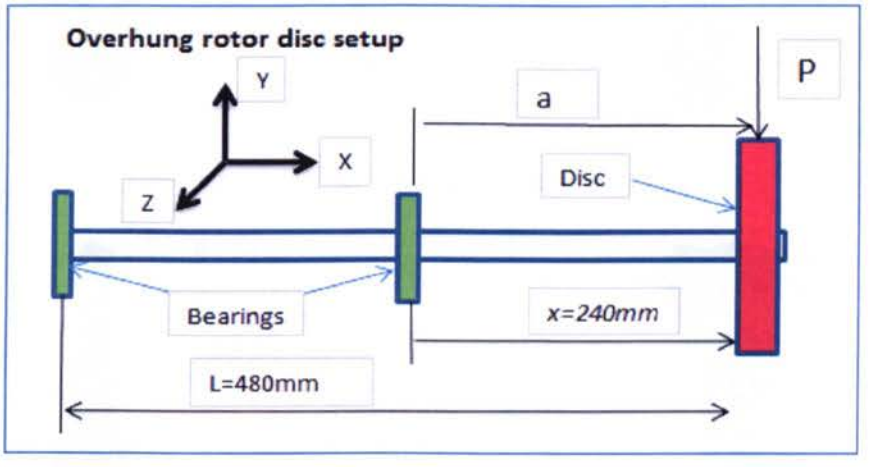

Figure 4.24 Schematic for overhung rotor disc setup parameter.

The procedure of the experiment is the same as of the previous sections with the difference in the position of the disc which is placed at one end of the shaft and the two bearings are placed one in the middle while the other one at the other end of the shaft.

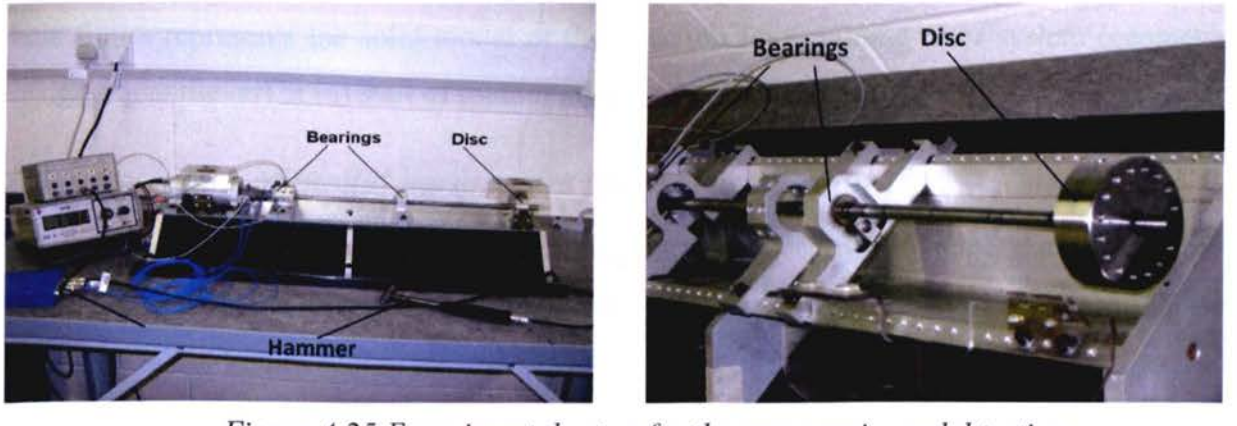

Figure 4.25 Experimental setup for the gyroscopic modal testing.

The experimental setup shown in Figure 4.25 was used to carry out the experimental technique utilizing the impact test with two accelerometers fixed (same specification discussed in the previous sections) in Y and Z direction and roving the hammer on several points mutually perpendicular to the shaft longitudinal axis. Measured data in rotating frame and results at different speeds of rotation are shown in Figure 4.26a-c.

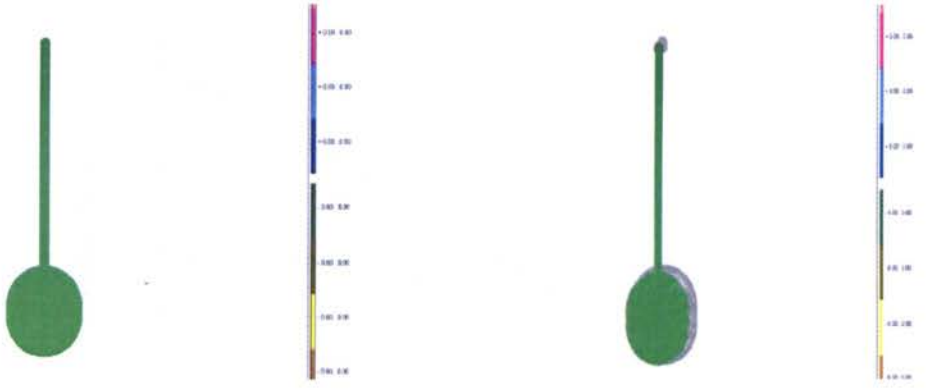

(a)- At start of rotation.

(b)-After rotation. Natural frequency 15.137Hz. *(c)- Natural frequency 216.51Hz.*

Figure 4.26 Geometry design model for overhung disc configuration, experimental test using smart office.

This figure represents the solid model of the structure for overhung rotor system (geometry design of cantilever) at (a) start of rotation, (b) at rotation 1000 rpm, and (c) at 2000 rpm.

4.5.2 Detection of modal parameters for overhung rotor rig

We detect the natural frequency and damping ratio ζ for different mode shapes by curve fitting the data obtained from experimental part for multi degree of freedom system, as shown in Table 4.4 and Figure 4.27.

Table 4.4
Natural frequency and damping ratio ζ for overhung rotor disc range 0-500 Hz, experimental part.

Name	Natural frequency (Hz)	Damping ratio (ζ) %
Mode 1	15.137	19.773
Mode 2	216.51	6.637

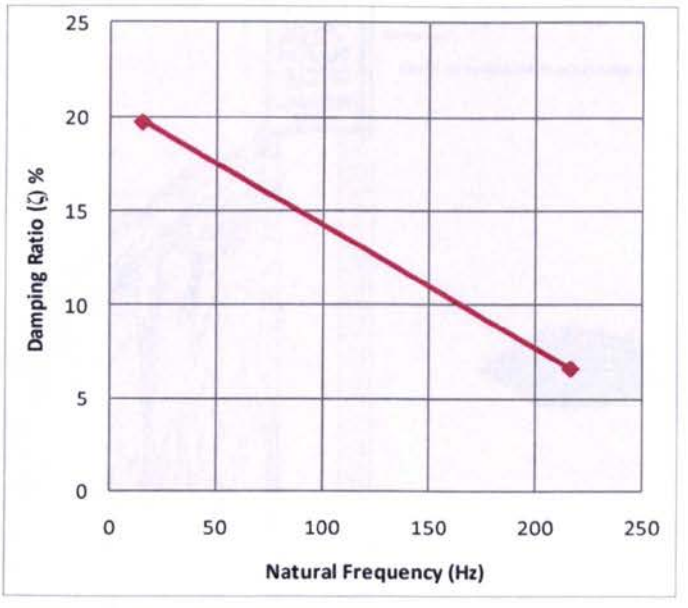

Figure 4.27 Damping ratio (ζ) versus natural frequency 0-500 Hz, overhung rotor disc.

Different mode shapes and FRF at speed 30 rpm for overhung rotor system are shown in the following figures:

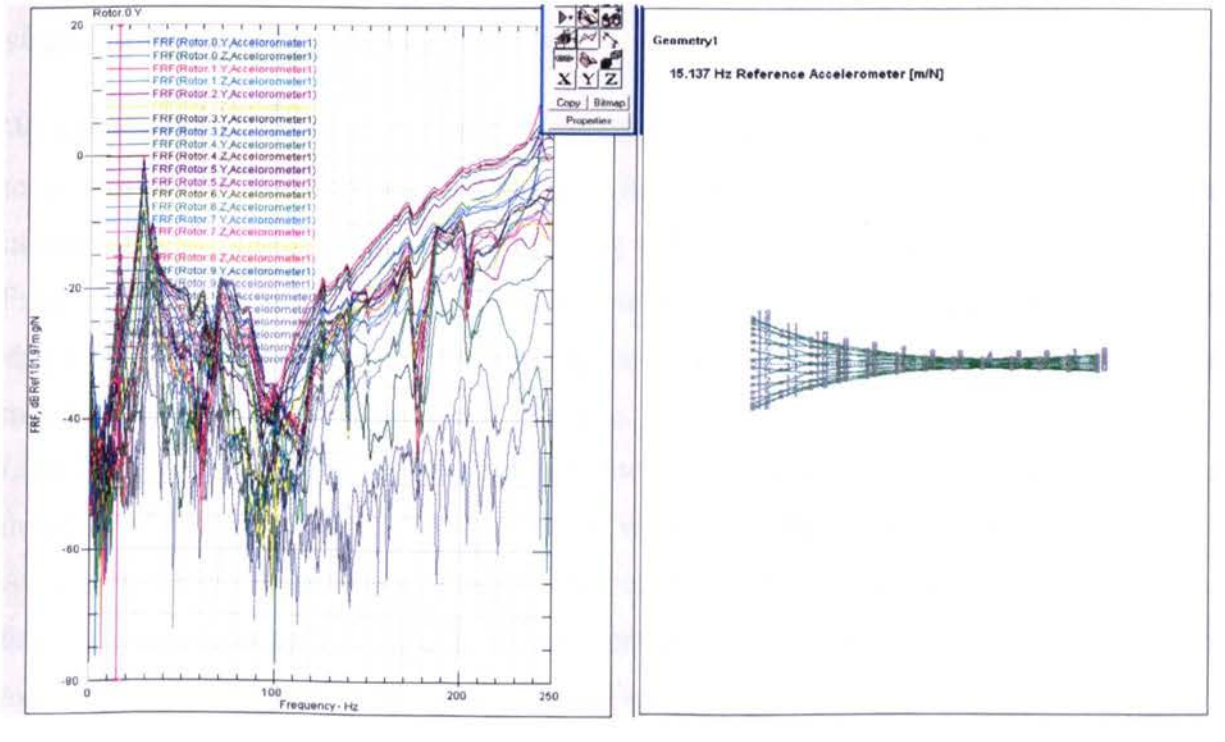

Figure 4.28 Mode shape of the overhung rotor system with one disc at the end. FRF versus frequency (Hz), first mode shape. Natural frequency 15.137Hz.

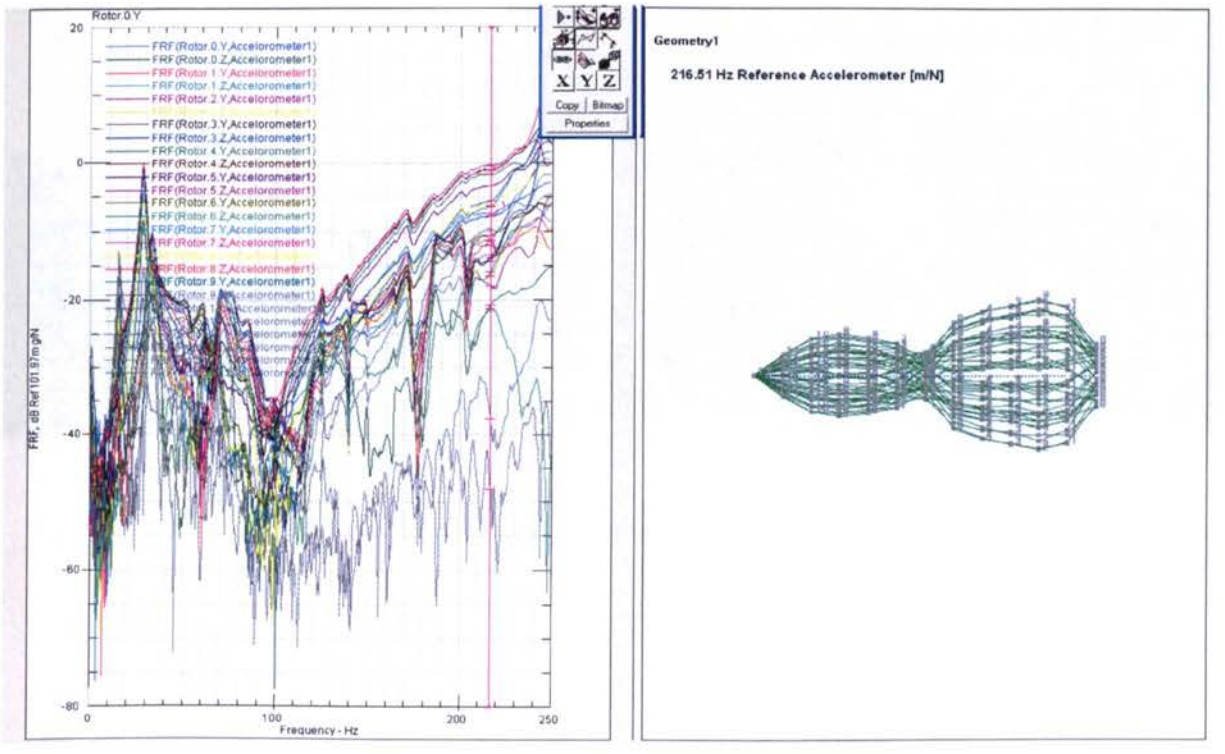

Figure 4.29 Mode shape of the overhung rotor system with one disc at the end. FRF versus frequency (Hz), second mode shape. Natural frequency 216.51Hz.

4.5.3 Experimental results of the overhung rotor system for the first mode shape at different speeds of rotation

We can use the Stroboscope (model ST1, supply 1, volts 230, 50Hz) as shown in Figure 4.30 to recognize the Forward Whirl (FW) and Backward Whirl (BW) components, causing increase and decrease in frequency respectively with increased rotor speed.

From experimental test Figures 4.31 and 4.32 to find natural frequency and extract the mode shape, the natural frequency of the rotor splits up as the speed of rotation increases. That means the gap widens up as the speed increases.

Like it was discussed, this phenomenon is known as gyroscopic effect and occurs because of the BW and FW of the rotor. The eigenvectors would show these phenomena.

All figures in the experiment obtained FRF of the geometry by overlaying the response functions are shown in Figure 4.31, for different speeds of rotation, and we can see the first mode shape for different speeds of rotation in Figure 4.32.

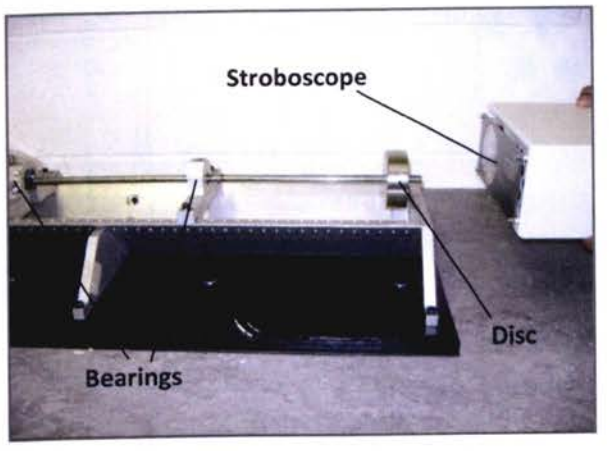

(a)- FW and BW detection.

(b)- Stroboscope body.

Figure 4.30 Experimental setup for detection of the gyroscopic FW and BW.

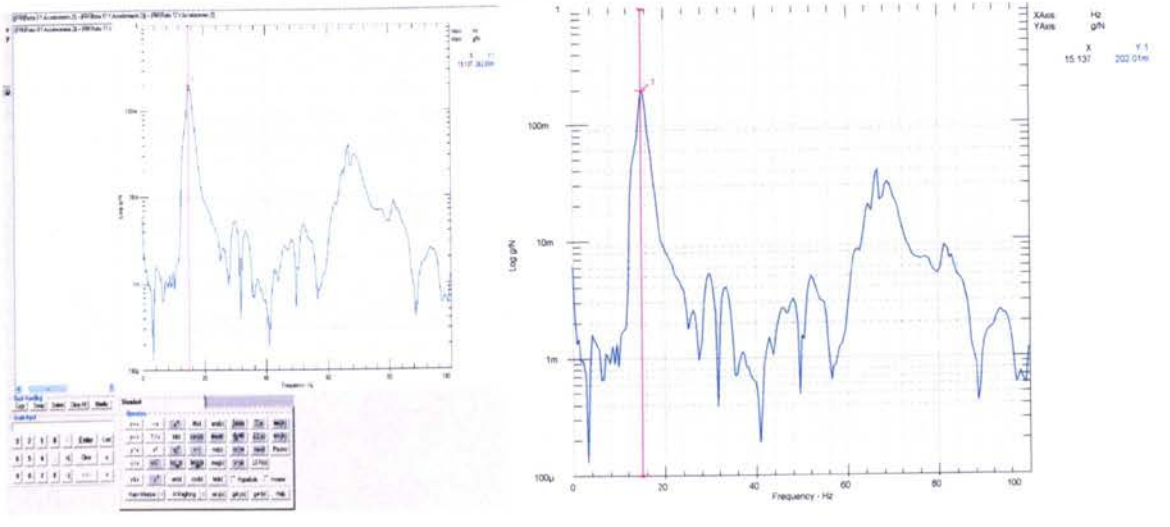

(a)- Speed of rotation 30 rpm.

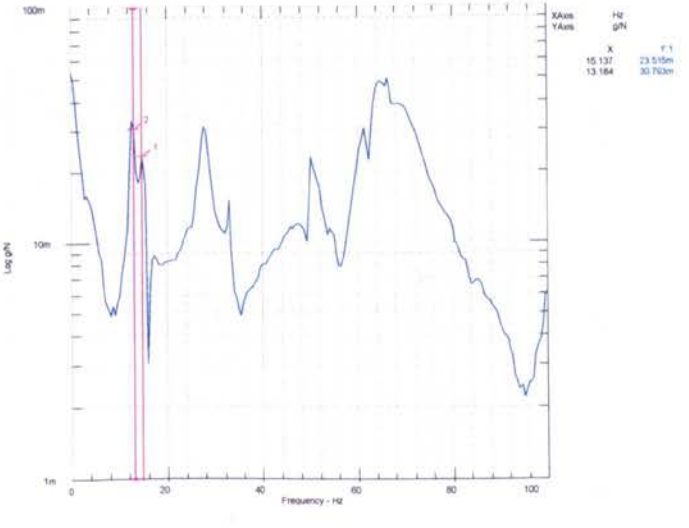

(b)- Speed 2000 rpm.

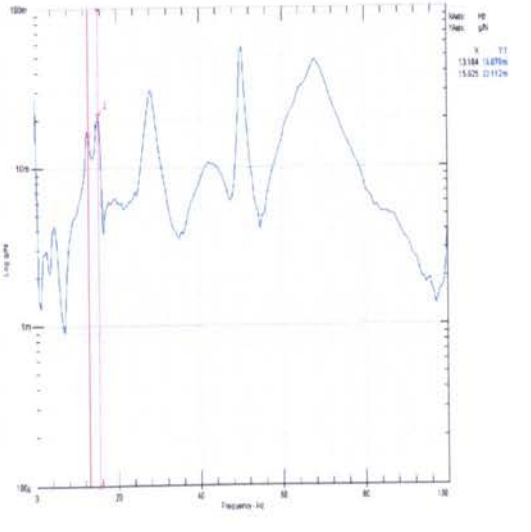

(c)- Speed 3000 rpm.

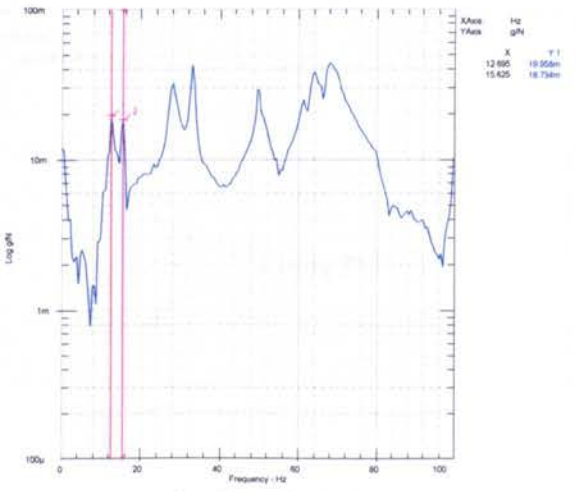

(d)- Speed 4000 rpm.

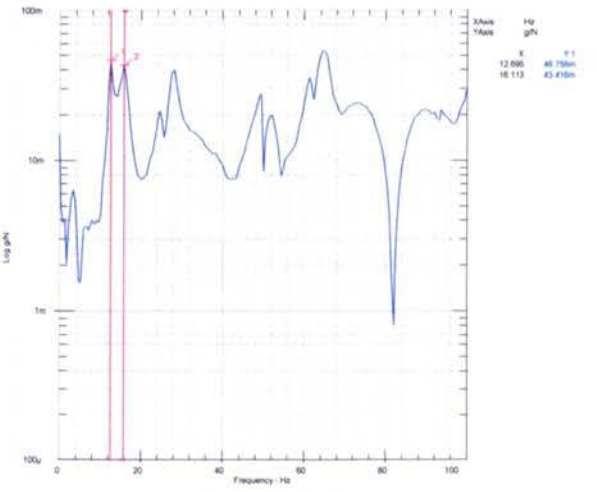

(e)- Speed 6000 rpm.

Figure 4.31 Experimental result show frequency response function curve, FRF versus natural frequency (Hz) for different speeds of rotation, first natural frequency.

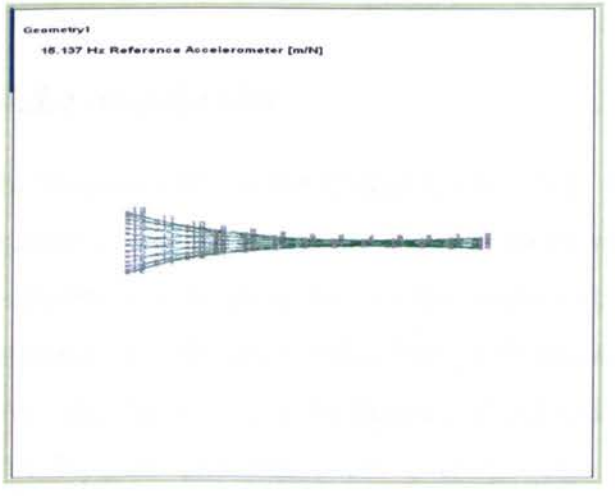

(a)- 15.137 Hz, at speed 30, 2000 rpm (FW).

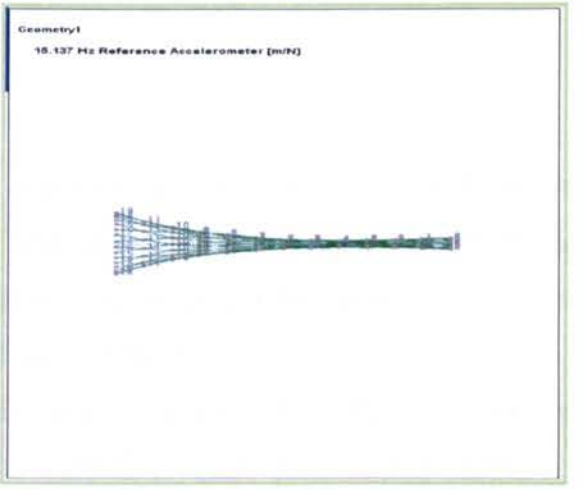

(b)- 15.137 Hz, at speed 30 rpm (BW).

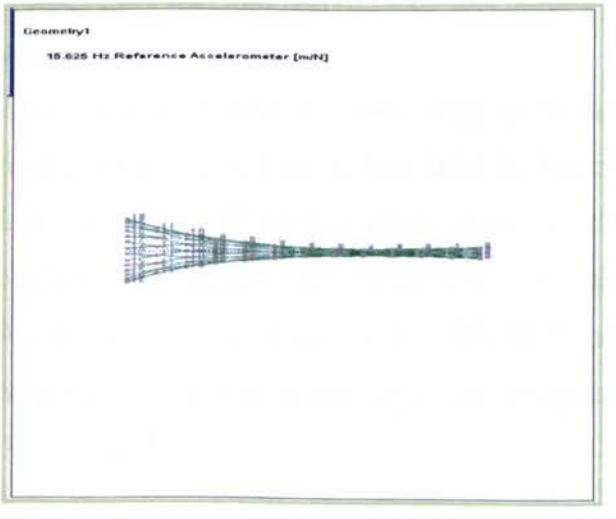

(c)- 15.625 Hz, at speed 3000,4000 rpm (FW).

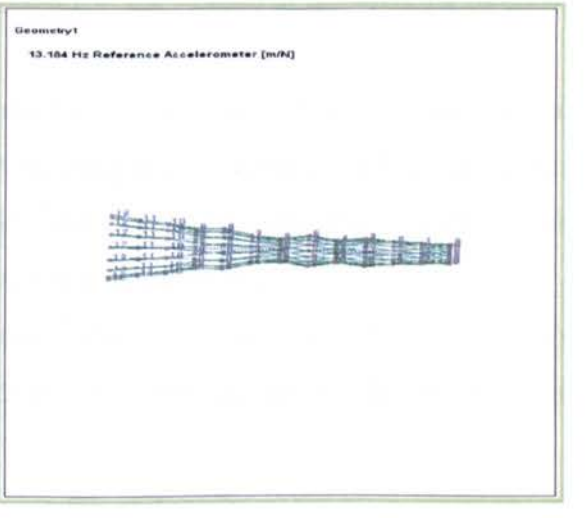

(d)- 13.184 Hz, at speed 2000, 3000 rpm (BW).

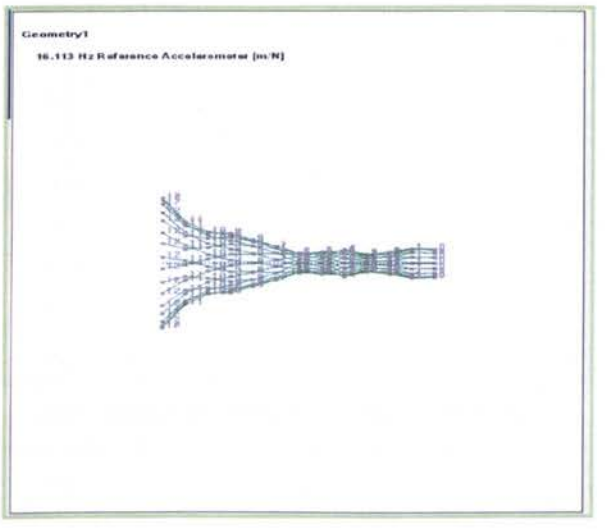

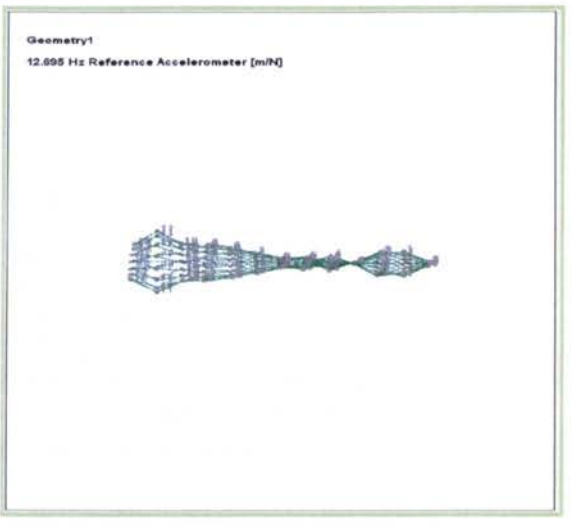

(e)- 16.113Hz, at speed 6000 rpm (FW). *(f)- 12.695 Hz at speed 4000, 6000 rpm (BW).*

Figure 4.32 Experimental results show first mode shape for different speeds of rotation (overhung rotor).

4.5.4 Nyquist plot

In Nyquist plot, as mentioned in chapter 2, the imaginary part reaches a maximum at the resonant frequency and is 90° out of phase with respect to the input. Figure 4.33 show the experimental Nyguist plot of the system (Imaginary versus Real) for different speed of rotation at 0, 30, 1000, 2000, 3000, 4000 and 6000 rpm respectively.

As it can be seen from the Figure 4.33a-d, and as it was expected at 0, 30, 1000 and 2000 rpm the Nyquist plot traces out a circle. This is a normal Nyquist plot display which is experimentally expected for any system. Having only one circular display in the Nyquist plot is due to the fact that there is only one natural frequency in the system at the selected range of speed.

As mentioned before for this setup (overhung rotor), as the speed increases, the natural frequency split into two; forward and backward whirl component frequencies, because of this fact, the circular display of the Nyquist plot divides into two, so that the intersection of each circle to the imaginary axis present one natural frequency of the system.

As the rotor speed increases, the difference between forward and backward whirl frequency expands. As a result, at 6000 rpm, the Nyquist plot of the system rotates by 180° as shown in the Figure 4.33g.

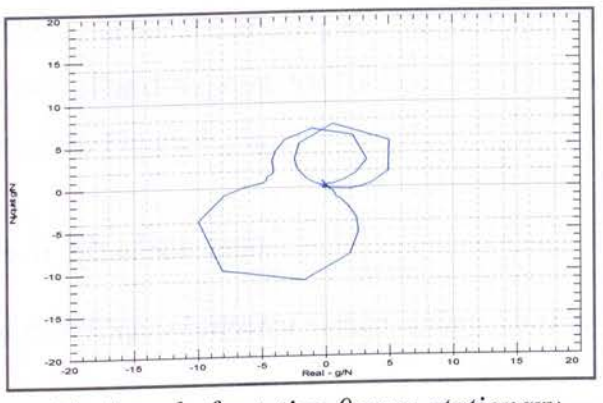

(a)- Speed of rotation 0 rpm, stationary.

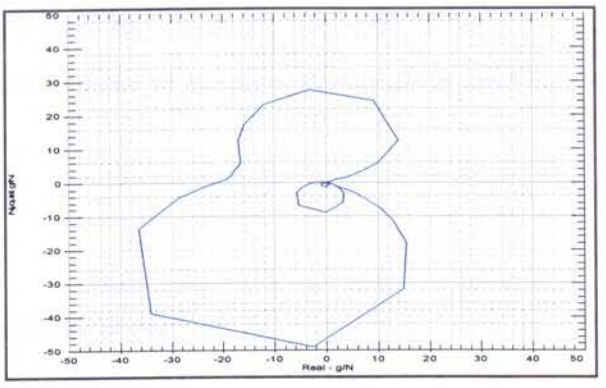

(b)- Speed of rotation 30 rpm.

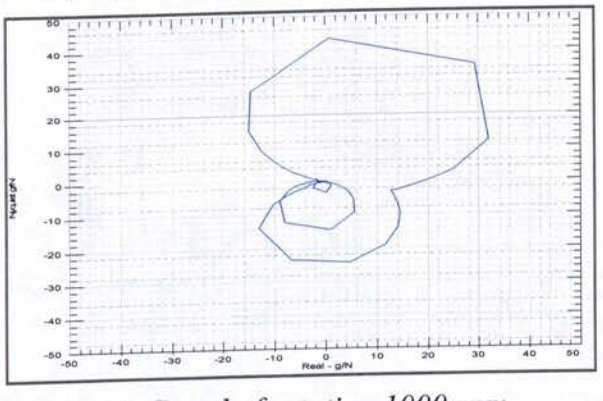

(c)- Speed of rotation 1000 rpm.

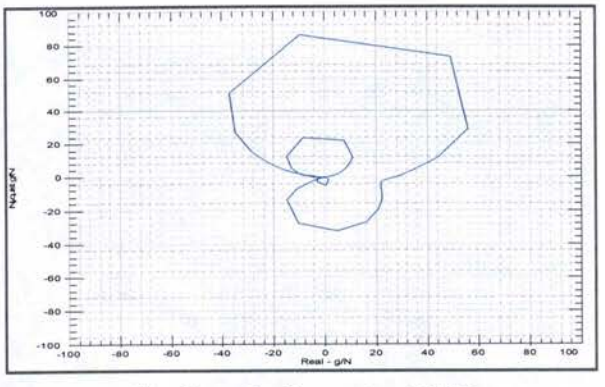

(d)- Speed of rotation 2000 rpm.

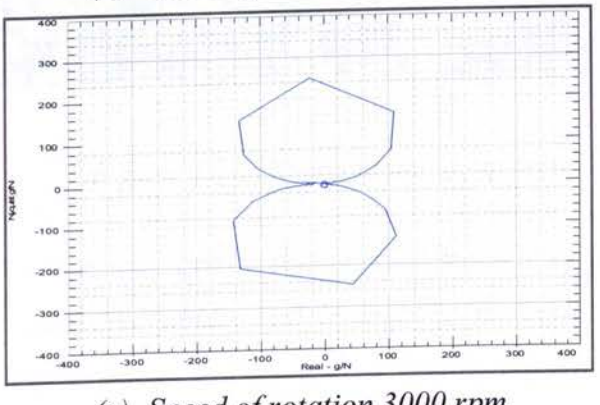

(e)- Speed of rotation 3000 rpm.

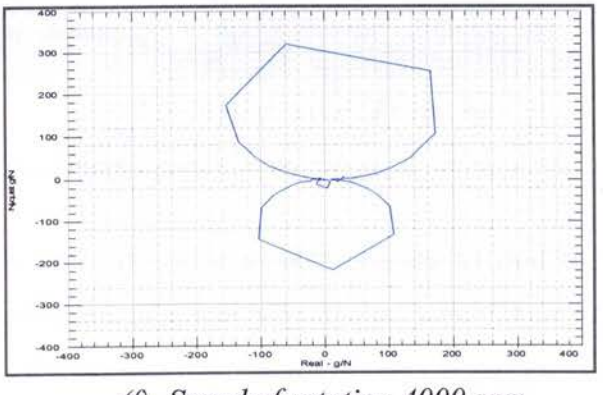

(f)- Speed of rotation 4000 rpm.

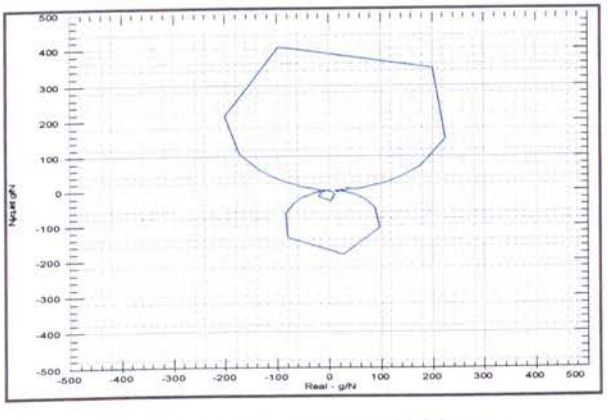

(g)- Speed of rotation 6000 rpm.

Figure 4.33 Experimental result show Nyquist plot (frequency response function curve) imaginary versus real for different speeds of rotation (overhung rotor).

The main benefit of using the Nyquist plot comes from its circularity property in the complex plane. The data point does not connect full circles because of frequency resolution, and that is clear in Figure 4.33g.

4.6 Shaker test

4.6.1 Experimental setup using shaker test with rig

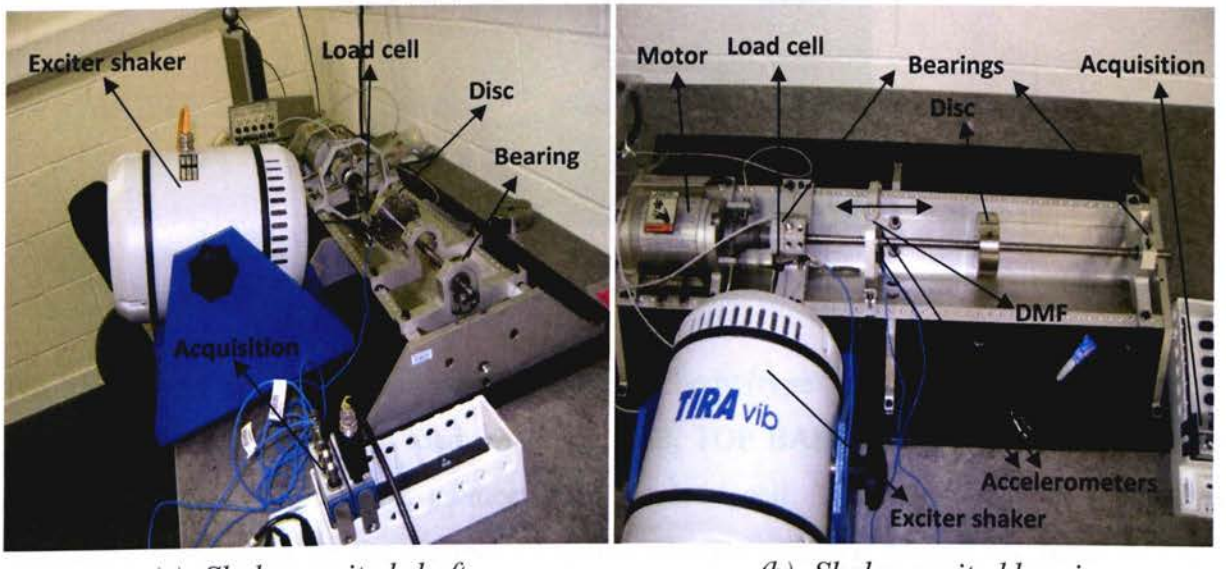

(a)- Shaker excited shaft. *(b)- Shaker excited bearing.*

Figure 4.34 Experimental setup shows attachment of the electromagnetic exciter.

An electromagnetic shaker, also known as an electro dynamic shaker is used to find the natural frequencies and extract the modes of vibration of a machine or structure. The test rotor is shown in Figure 4.34; mainly consist of a shaft and disc have mechanical properties are shown in Table 4.1, and two plain bearings. The shaft length is 610 mm, and the effective rotor length is 480 mm (the effective rotor length is the distance between the bearing blocks). The testing of the process was conducted on the rotating machine. Then, the experimental testing was carried out using the electromagnetic shaker, and two accelerometers were installed at Designed Movement Frame (DMF) in Y and Z directions see Figure 4.34b.

4.6.1.1 Electromagnetic shaker specifications

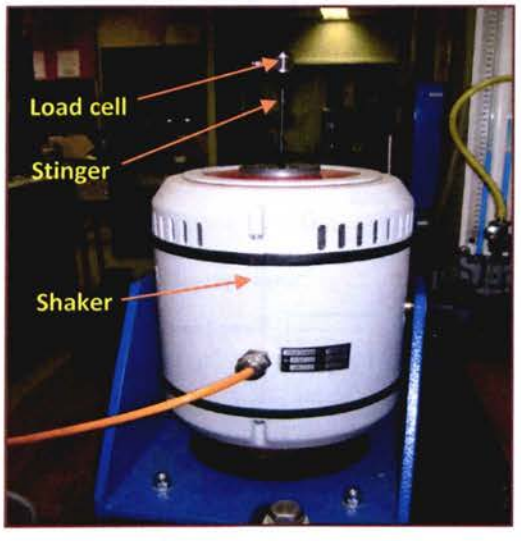

Figure 4.35 Electromagnetic shaker body.

The Figure 4.35 shows the electromagnetic shaker body (type TIRA vibration, TIRA GmbH, S521, V 22, Nr 142/07) with load cell (type PCB, TOP BASE, SN 25580, 208 CO_1). The acquisition system IDAQ was connected to the load cell. The other channels are set to 'Response' depending on the number of accelerometers available to use, the name of each channel was assigned to the 'Name' column within the software. The module (NI-9263) was connected to the IDAQ Chassis. This is an output module which generates signal. A (BNC) cable was connected from the (NI-9263) module to the amplifier 'input' slot at the back of the amplifier, then the signal type can be selected and the parameters adjusted according to the test requirements.

4.6.1.2 Data acquisition

The amplifier has been used to provide significant vibration levels to drive the shaker and excite the model with different excitation input signals. Accelerometers responses send the signals to the computer through an acquisition IDAQ channel. The data (signals) received from the input (load cell) and output (accelerometer) sensors are directed to the smart office software through an USB2 port, and hence, the frequency response function of the system can be calculated and displayed in graphical form, Figure 4.36 shows test setup–for the electromagnetic shaker test.

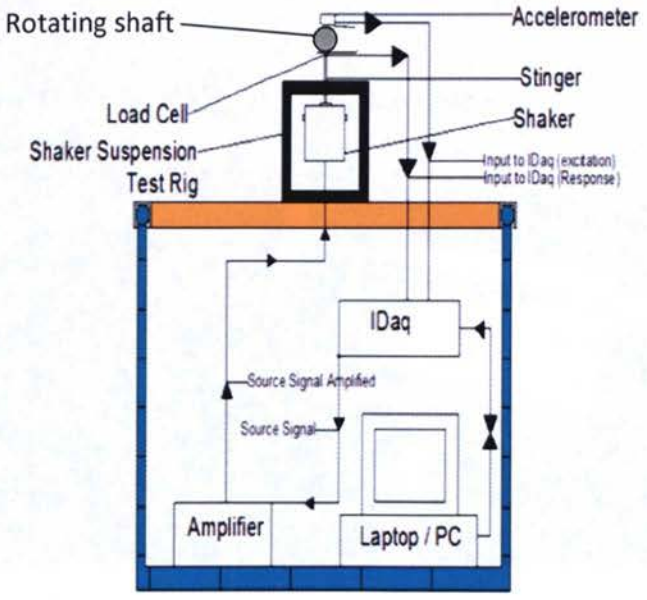

Figure 4.36 Test setup design.

4.6.1.3 Design movement frame of accelerometers to carry out vibration test

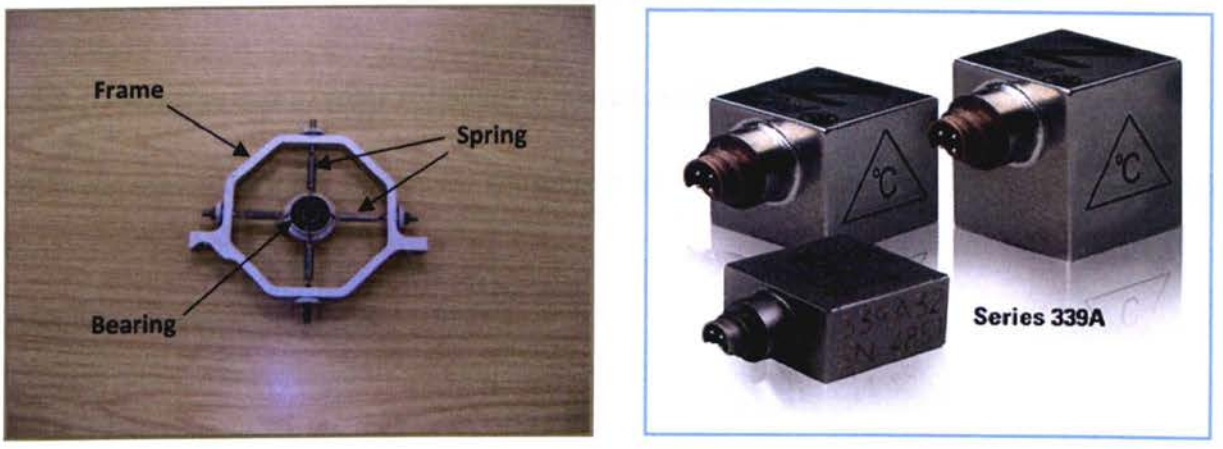

Figure 4.37 Designed movement frame base for the accelerometers.

The accelerometers were attached to the test structure in (Y and Z) direction perpendicular to the shaft longitudinal axis using either bees wax or a high-strength adhesive. The attachment points were on the outer surface of the bearing mounted in the DMF which was mounted on the supporting structure of the rotor system as shown in Figures 4.37 and 4.38.

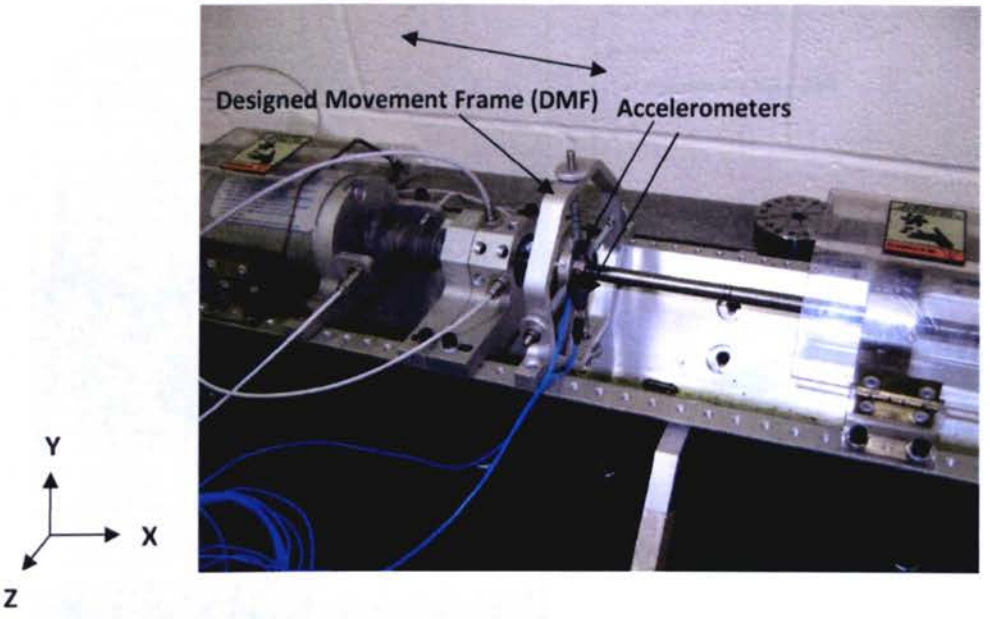

Figure 4.38 Designed Movement Frame (DMF) mounted on the supporting structure of the rotor system.

4.6.2 Experimental results with electromagnetic shaker

4.6.2.1 Vibration test of rotor rig using different excitation input signals

Different excitation input signals for shaker test have been used to find natural frequency and to extract mode shape:-

a) Random wave signal Figure 4.39.

b) Burst random wave signal Figure 4.40.

c) Sine wave signal Figure 4.41.

In Figure 4.39 Random wave signal has been used with stationary load (one disc) in the middle, FRF versus frequency (Hz) and the first mode shape with natural frequency of 31.25 Hz, the first mode shape of response simulates a first degree of freedom mode with maximum deflection in the middle.

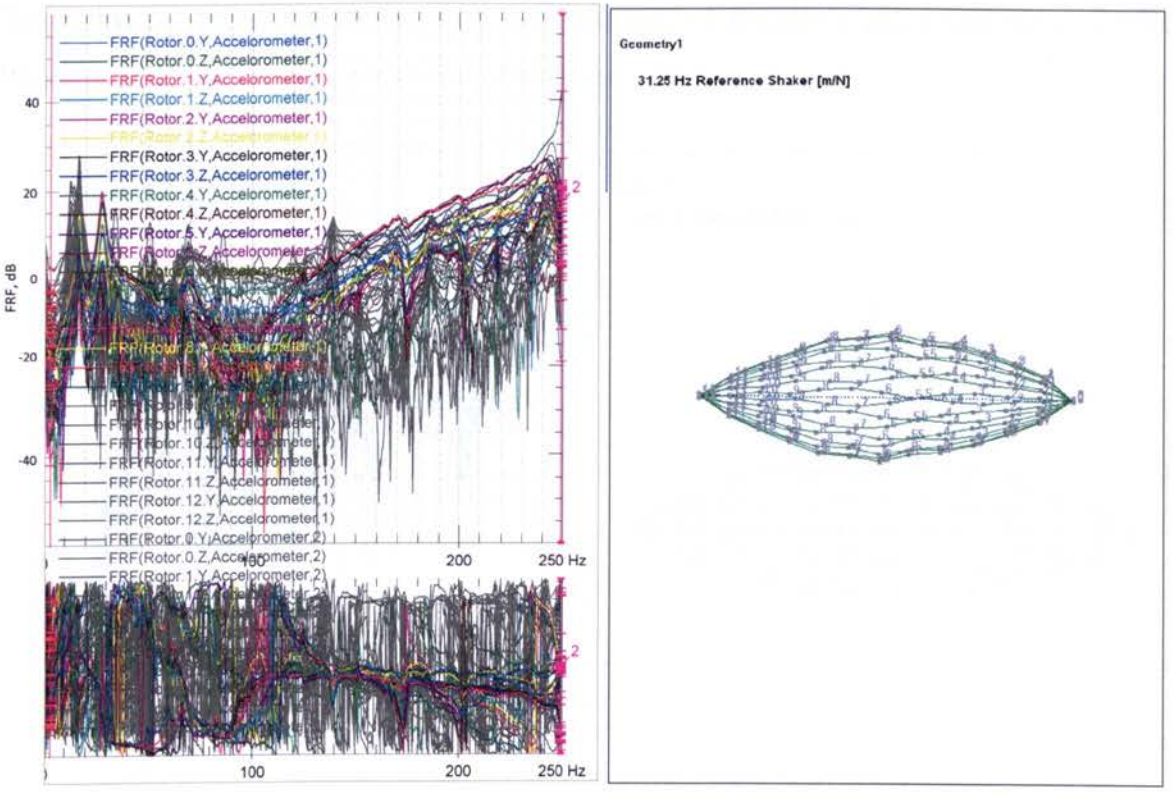

(a)- First mode shape. Natural frequency 31.25Hz.

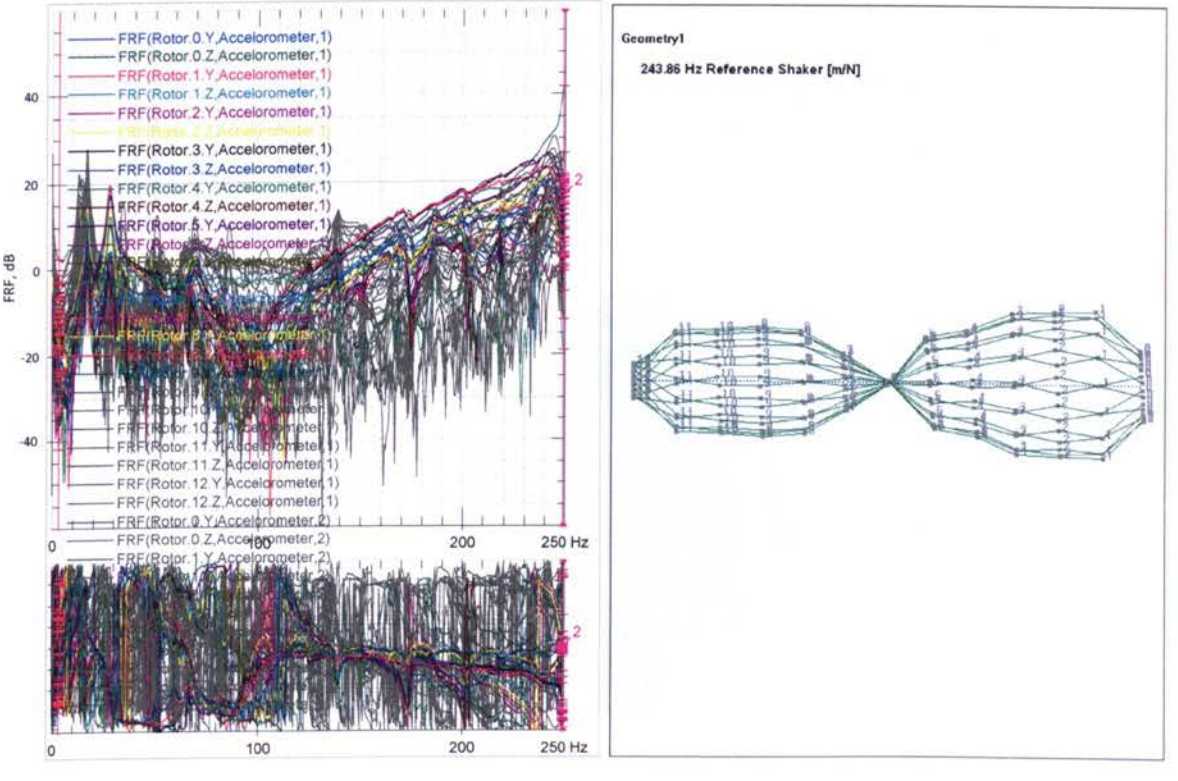

(b)- Second mode shape. Natural frequency 243.86Hz.

Figure 4.39 Mode shape of rotating system with one disc configuration shows FRF versus frequency (Hz), range (0-500) Hz. Random wave signal.

The following Figures 4.40 and 4.41 show the natural frequency and mode shape for Burst Random and Sine wave signals using shaker test.

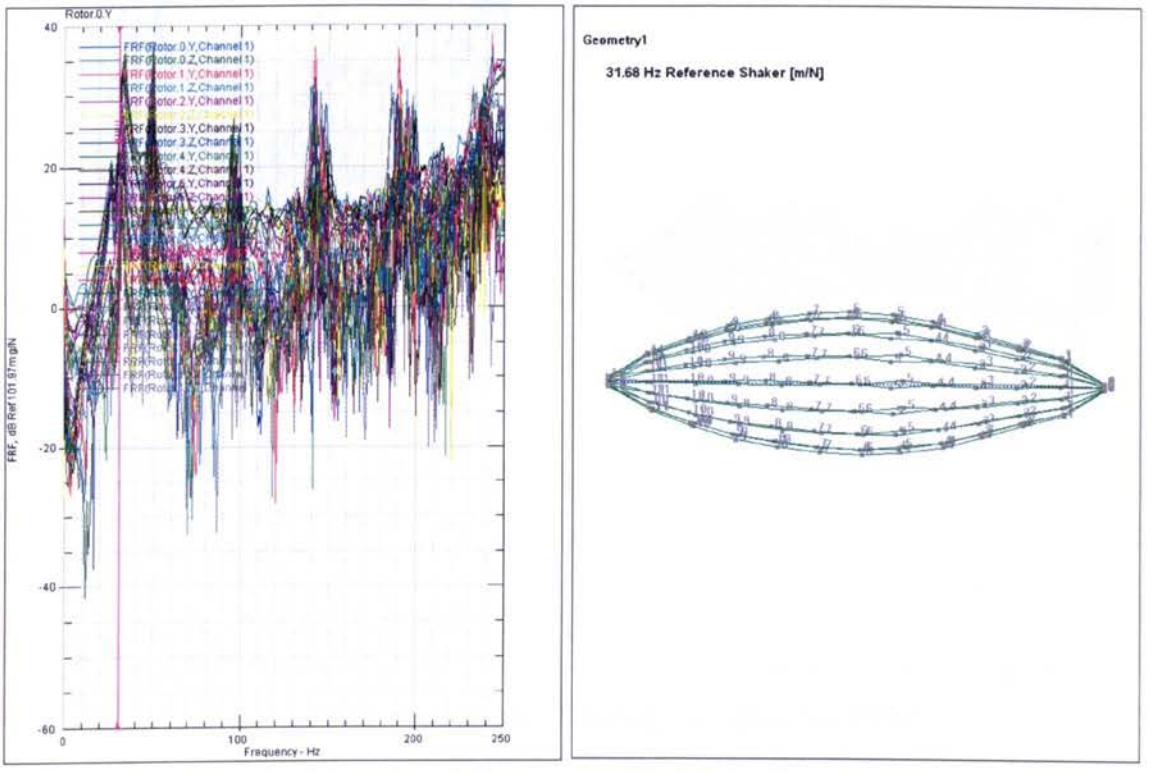

(a)- First mode shape. Natural frequency 31.68Hz.

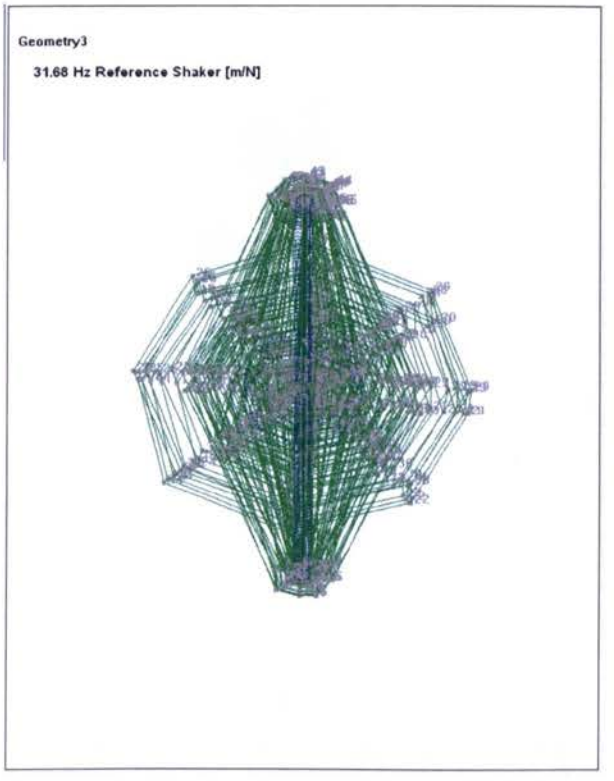

(b)

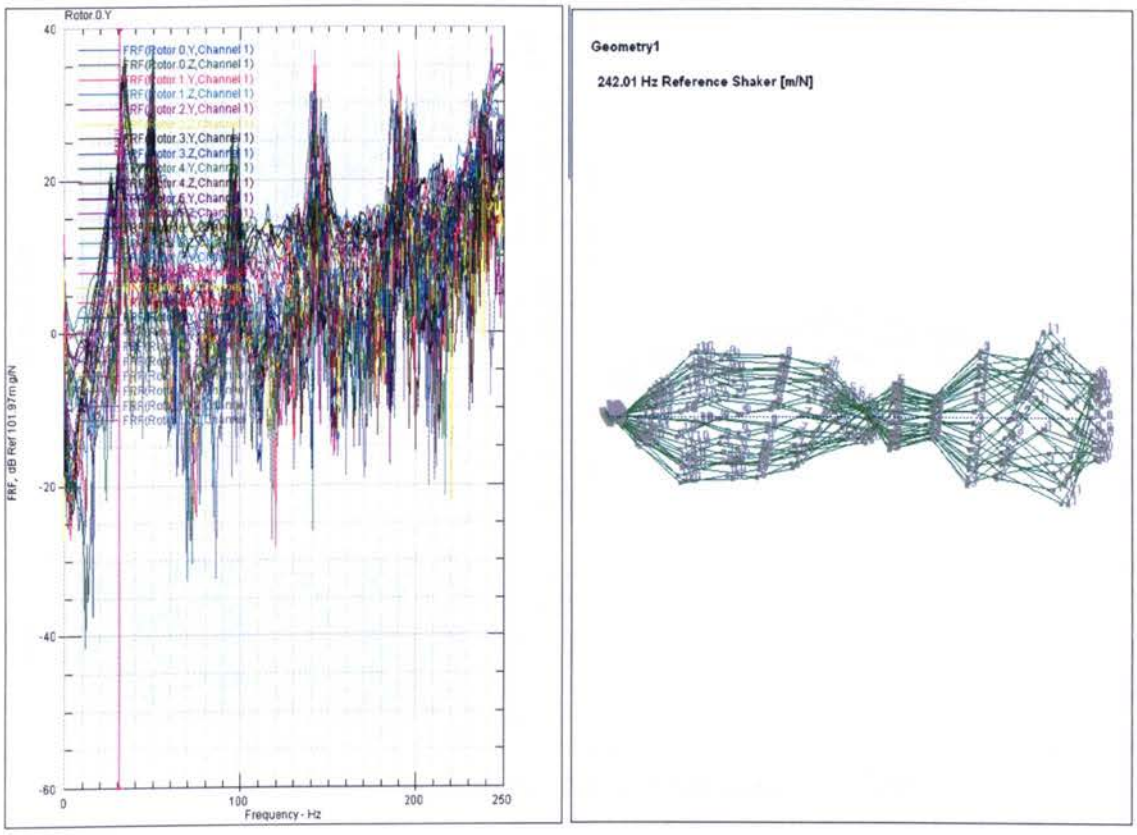

(c)- Second mode shape. Natural frequency 242.01Hz.

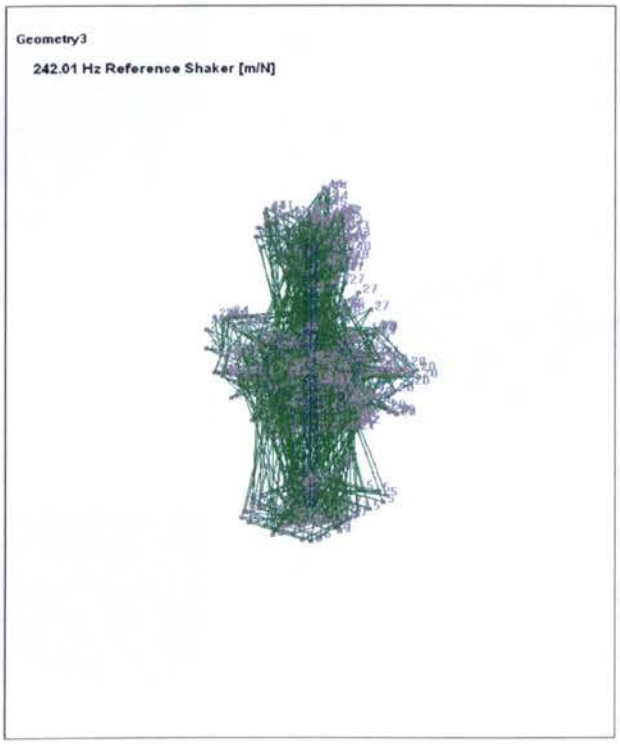

(d)

Figure 4.40 Mode shape of rotating system with one disc configuration shows FRF versus frequency (Hz), range (0-500) Hz. Burst Random wave signal.

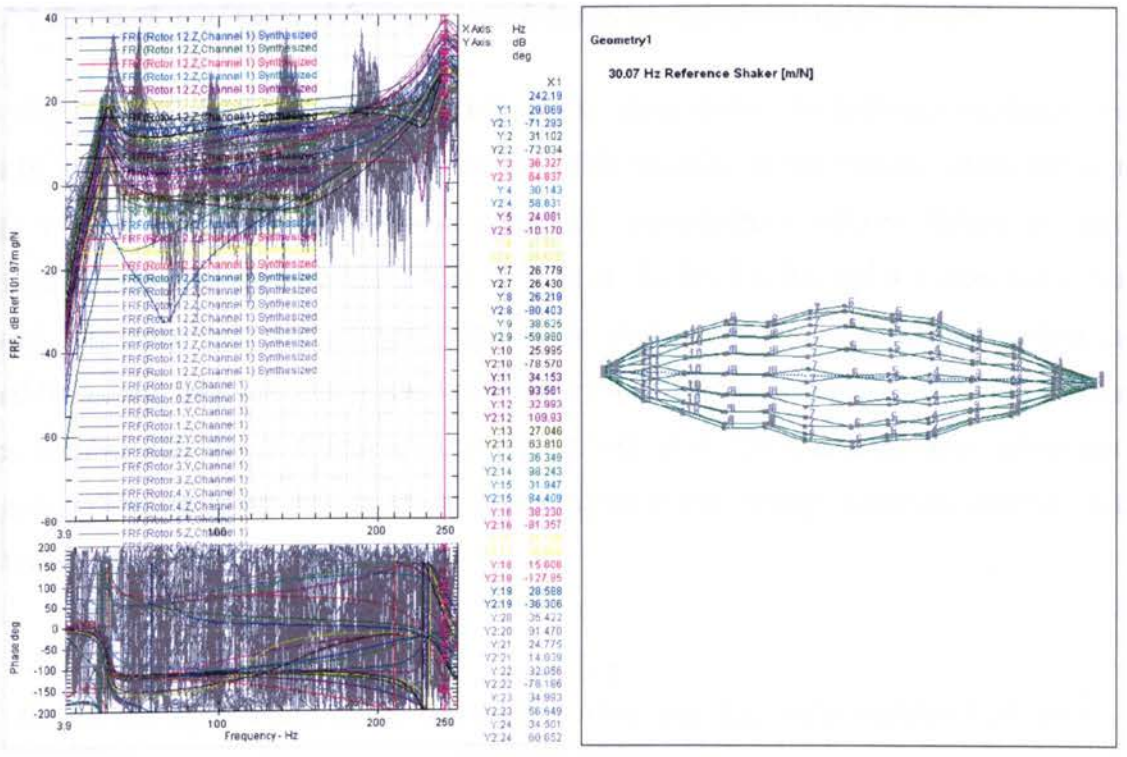

(a)- First mode shape. Natural frequency 30.07Hz.

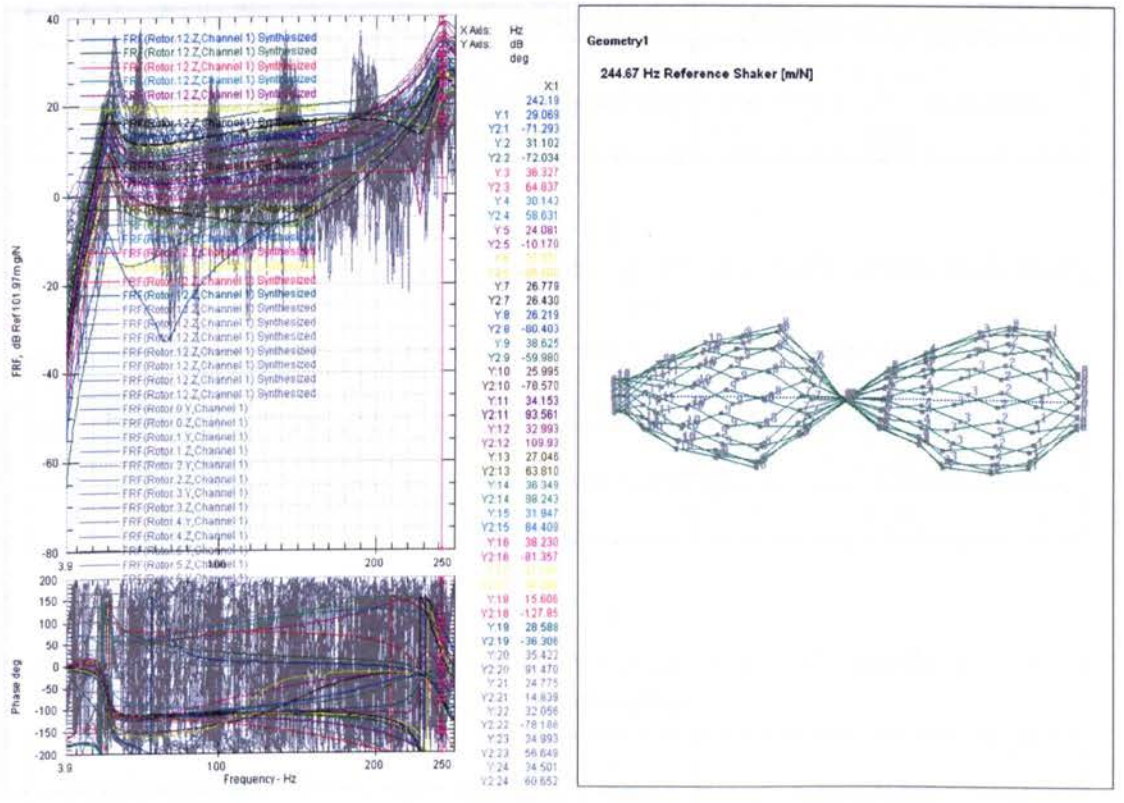

(b)- Second mode shape. Natural frequency 244.67Hz.

Figure 4.41 Mode shape of rotating system with one disc configuration shows FRF versus frequency (Hz), range (0-500) Hz. Sine wave signal.

4.6.2.2 Extraction of natural frequency and damping ratio from modal analysis

The Figures 4.39-4.41 show the response of the rotor system to different excitation input signals for the first and second mode shapes with one disc in the middle, in the frequency range of (0-500)Hz. Using different excitation waveforms produces values of natural frequencies which are in agreement with each other. Tables 4.5, 4.6 and 4.7 show the value of natural frequency (Hz) and damping ratio ξ for shaker test with different excitation input signal (Random, Sine and Burst Random). Figure 4.42 shows the relationship between mode shape number and natural frequency and Figure 4.43 shows the damping ratio versus natural frequency. The damping ratio is lower in the higher mode (lightly damped) and the system reach resonance when $\omega = \omega_n$.

Table 4.5
Shaker test is fixed and accelerometer is moving, one disc in the middle (0-500) Hz, Random signal.

Mode shape No.	Natural frequency (Hz)	Damping ratio (ζ) %
1	31.25	19.36
2	243.86	8.02

Table 4.6
Shaker test is fixed and accelerometer is moving, one disc in the middle (0-500) Hz, Sine wave signal.

Mode shape No.	Natural frequency (Hz)	Damping ratio (ζ) %
1	30.07	18.82
2	244.67	7.26

Table 4.7
Shaker test is fixed and accelerometer is moving, one disc in the middle (0-500) Hz, Burst Random signal.

Mode shape No.	Natural frequency (Hz)	Damping ratio (ζ) %
1	31.68	19.77
2	242.01	7.98

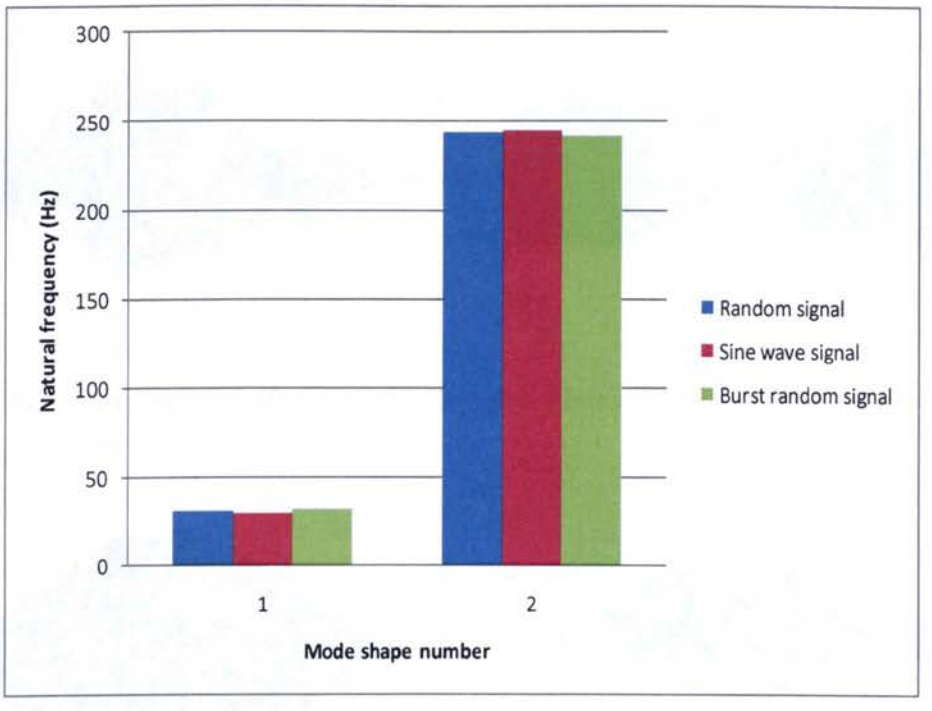

Figure 4.42 Relationship between mode shape numbers versus natural frequency (Hz), shaker test.

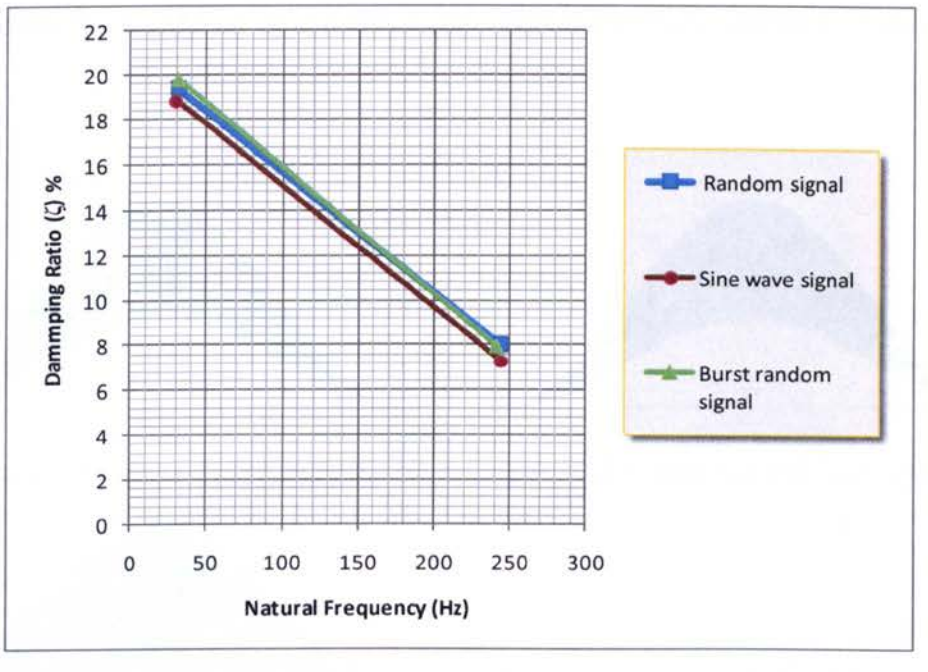

Figure 4.43 Damping ratio (ξ) versus natural frequency (Hz), shaker test.

4.6.2.3 Window time record for different excitation source using shaker test

Different window functions were used to reduce leakage for different excitation sources as shown in the Figure 4.44.

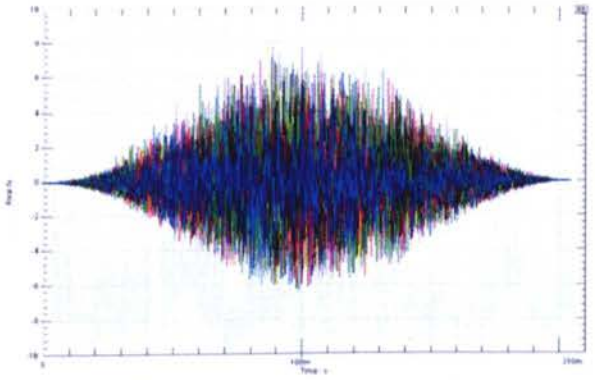

(a)- Window time record, shaker test, Random signal.

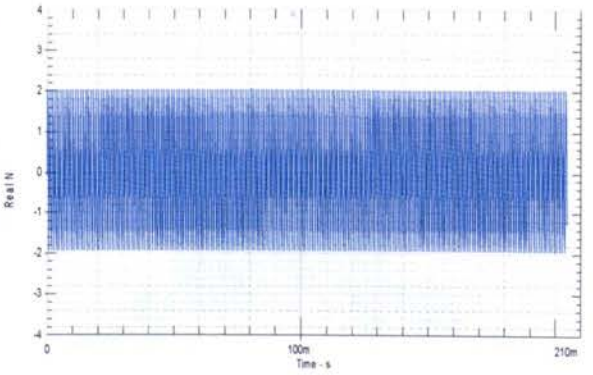

(b)- Time record Sine wave signal, 500 Hz.

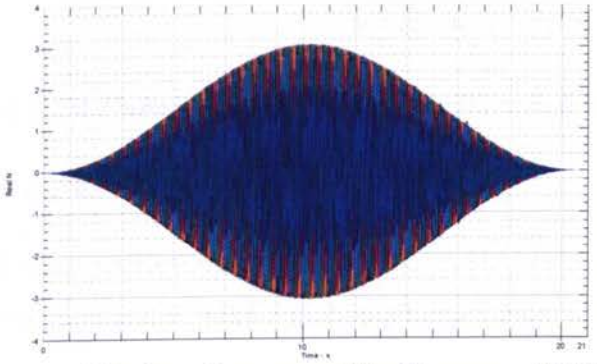

(c)- Window time record for Sine wave16 Hz.

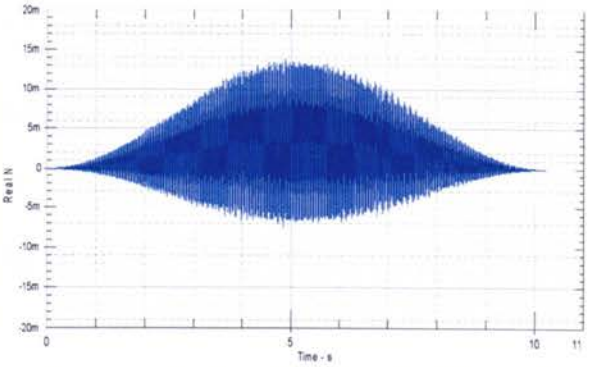

(d)- Widow time record Sine wave 32 Hz.

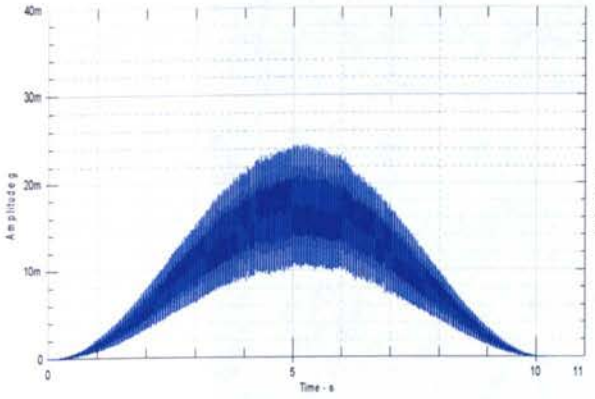

(e)- Widow time record Sine wave 32 Hz.

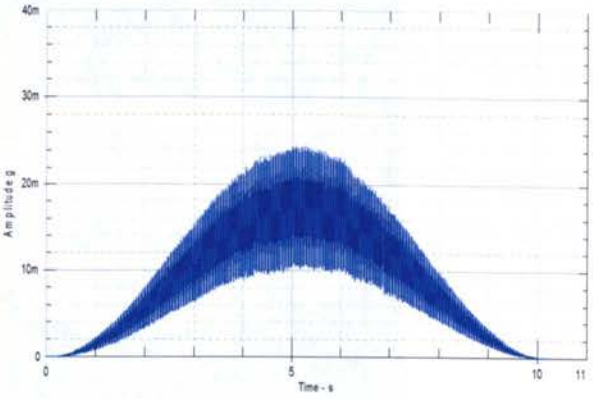

(f)- Widow time record Sine wave 50 Hz.

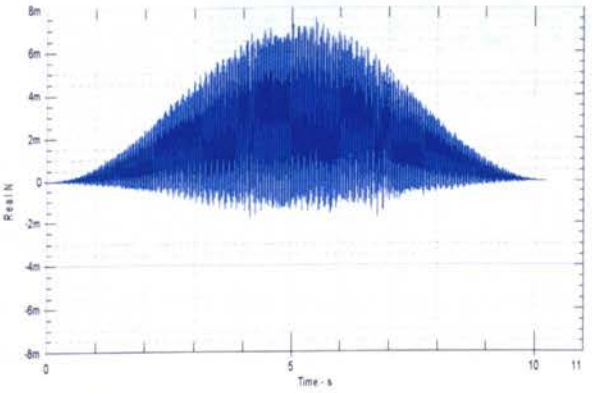

(g)- Window time record Sine wave 50 Hz.

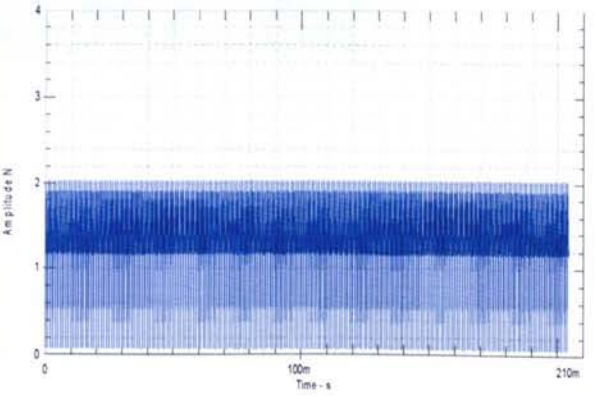

(h)- Time record Sine wave 500 Hz.

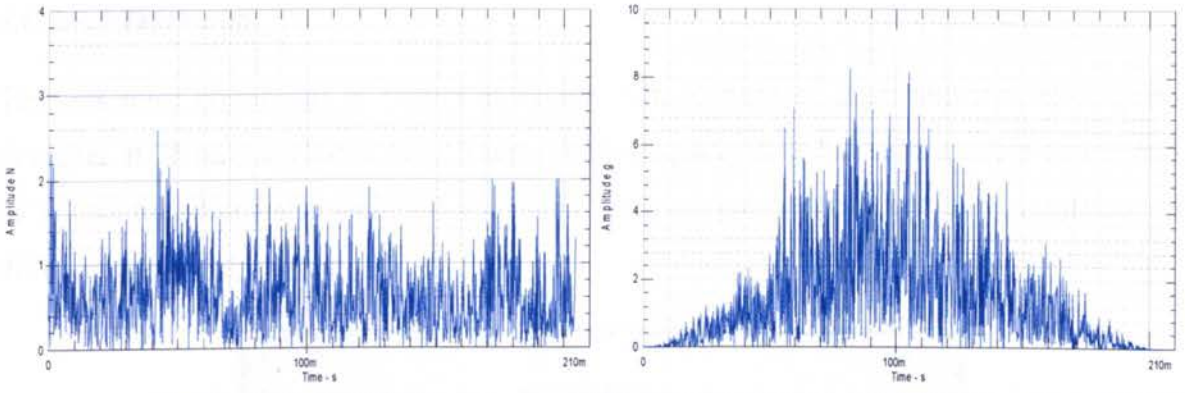

(i)- Random signal 500 Hz. *(k)- Window time record Random signal 500 Hz.*

Figure 4.44 Different shapes of window time record for different excitation source signal using shaker test with hanning window.

4.6.2.4 Unbalance effect using oscilloscopic technique

4.6.2.4.1 Specifications

Using oscilloscope type HM 205-3, HAMEG, 20 MHz,

Storage scope, HM 205-3, see Figure 4.45.

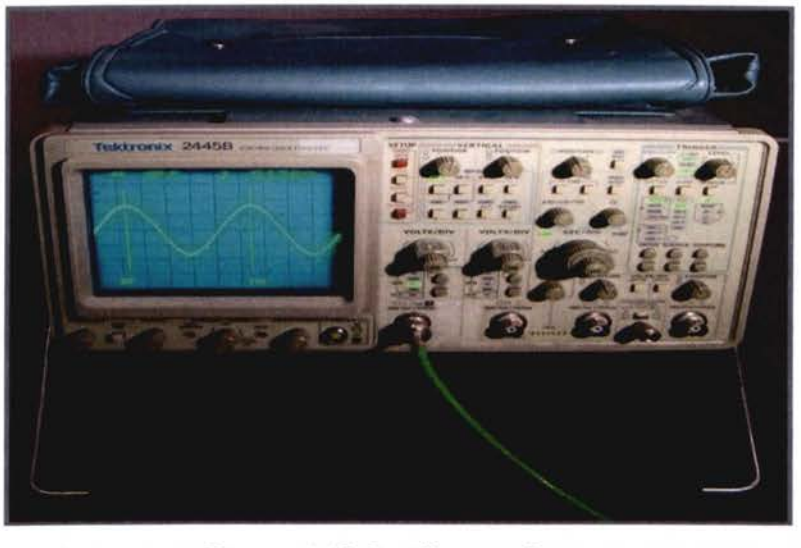

Figure 4.45 Oscillscope device.

4.6.2.4.2 Proximity sensor

Beside the accelerometers, one of the other devices which could be used to obtain the response of a system is proximity probes which are sensors able to detect the presence of nearby objects without any physical contact. Proximity sensor often emits an electromagnetic or electrostatic field, or a beam of electromagnetic radiation (infrared for instance) and looks for changes in the field [53].

4.6.2.4.3 Test setup

The test rotor (rotor rig) is shown in Figure 4.46; consist of shaft and two discs (with a diameter of 75 mm, each disc has 16 screw holes, equally distributed on a circle with a radius of 32 mm for adding trial weights), the output from the proximity sensor using oscillscope for different speeds of rotation.

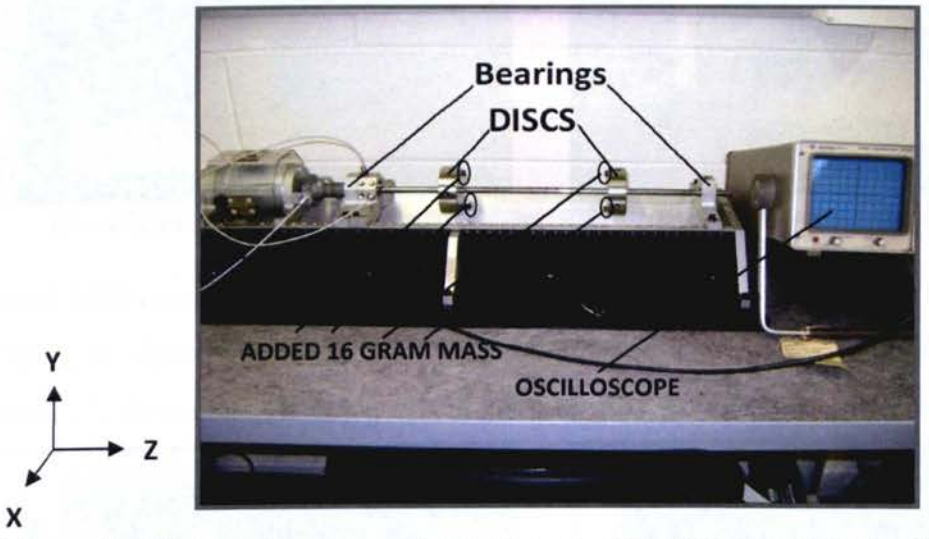

Figure 4.46 Setup of a rotor with two discs configuration connected with oscilloscope.

4.6.2.4.4 The outcome results

Oscilloscopic technique (Time domain) is used with shaker test. An excessive load (8 gram for each disc) is added to the loading of the system (in the 25% and 75% of the effective shaft length). The excessive loading is away from the centre of the shaft by 30 mm, the added masses in the disc 1 at angles (45°, 225°) and in disc 2 at angles (180°, 0°), with different speeds of rotation. As it can be seen from the experimental Figures 4.47-4.50, when adding 16 gram mass (8 gram per each disc) at the same conditions and dimensions for two discs configuration with hammer test can reduce the amplitude of vibration. This gives more reliability to modal testing method used in this thesis.

The reduction in the amplitude is due to the correcting balanced masses reduces the eccentricity and resulting in the reduction of the centrifugal force causing reduction in the radius of shaft orbit.

At speed 1000 rpm, without mass.

For disc 1, X-direction 2.3 cm.

For disc 2, Y-direction 1.8 cm.

At speed 1000 rpm, with mass.

8 gram, for disc 1, angle 45°, 225°, X-direction 2.1 cm.

8 gram for disc 2, angle 180°, 0° ,Y-direction 1.5 cm.

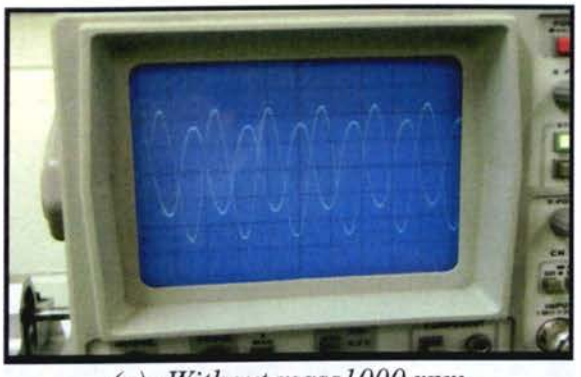

(a)- Without mass1000 rpm.

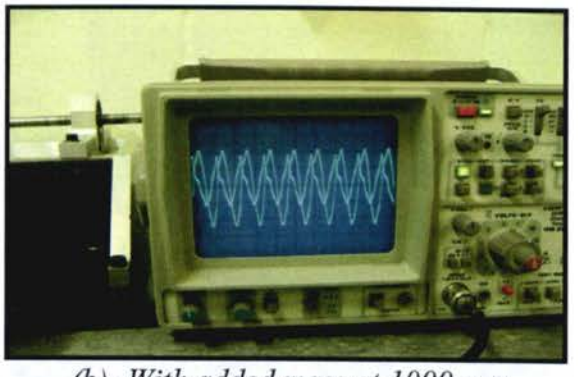

(b)- With added mass at 1000 rpm.

Figure 4.47 Amplitude in X, Y direction, 1000rpm.

At speed 1500 rpm, without mass.

For disc 1, X- direction 1.6 cm.

For disc 2, Y-direction 1.1 cm.

At speed 1500 rpm, with mass.

8 gram, for disc 1, angle 45°, 225°, X-direction1.5cm.

8 gram for disc 2, angle 180°, 0° ,Y-direction 1.0cm.

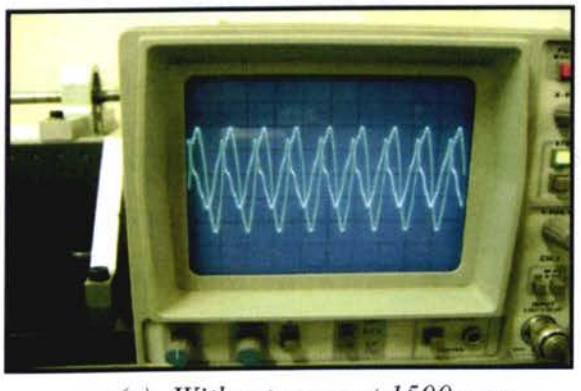

(a)- Without mass at 1500 rpm.

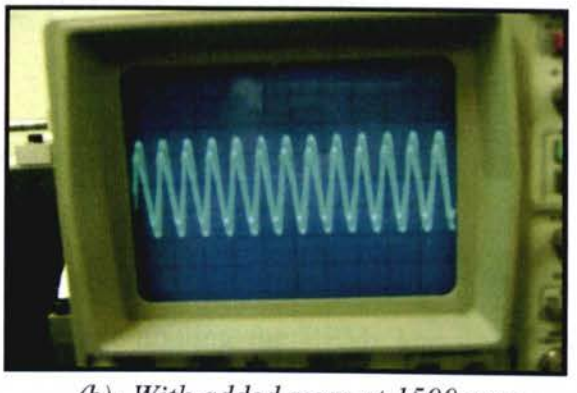

(b)- With added mass at 1500 rpm.

Figure 4.48 Amplitude in X, Y direction, 1500rpm.

At speed 2000 rpm, without mass.

For disc 1, X- direction 1.6 cm.

For disc 2, Y- direction 1.3 cm.

At speed 2000 rpm, with mass.

8 gram, for disc 1, X- direction 1.4 cm.

8 gram, for disc 2, Y- direction 1.1 cm.

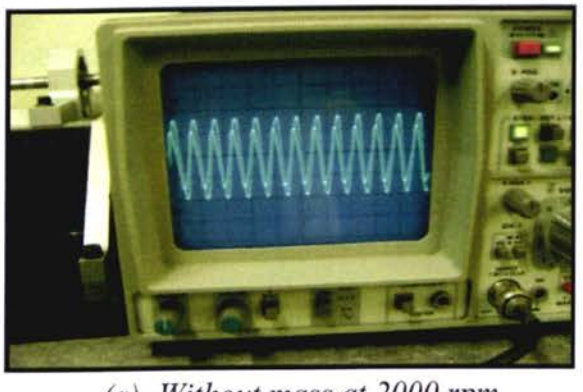

(a)- Without mass at 2000 rpm.

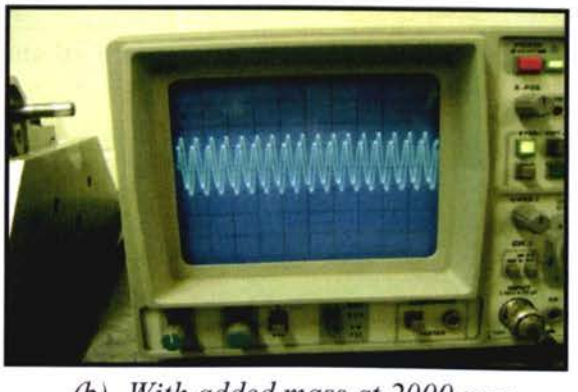

(b)- With added mass at 2000 rpm.

Figure 4.49 Amplitude in X, Y direction, 2000rpm.

At speed 3000 rpm, without mass.

For disc 1, X-direction 0.6 cm.

For disc 2, Y-direction 0.4 cm.

At speed 3000 rpm, with mass.

8 gram for disc 1, angle 45°, 225°, X-direction 0.5cm.

8 gram for disc 2, angle 180°, 0°, Y-direction 0.3cm.

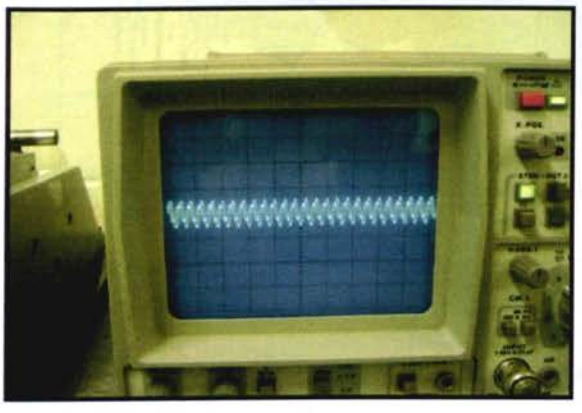

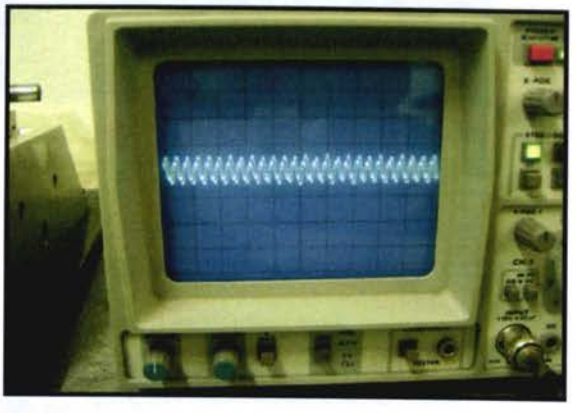

(a)- Without mass at 3000 rpm. *(b)- With added mass at 3000 rpm.*

Figure 4.50 Amplitude in X, Y direction, 3000rpm.

4.7 Vibration analysis software in experimental method

4.7.1 The Tacho Spline Fit Wizard

The Tacho Spline Fit Wizard was initially used in former Smart Office, but it is still available for certain applications.

The Tacho Spline Fit Wizard first estimates the machine RPM as a function of time by determining the time between the Tacho pulses and computing the RPM. The raw RPM estimate is not defined for every acquisition time point. It fits a cubic spline to the raw RPM estimate to get a clean estimate of the machine RPM as a function of time. The resulting RPM versus time function is defined for every acquisition time point.

In the Tacho Spline Fit Wizard, set parameter to remove the effects of noise and missing pulses, set the trigger level, slope, hold off percentage, and select the number of knots for the cubic spline fit. Handle rapidly changing RPM data by inserting break points in the spline fit, see Figure 4.51.

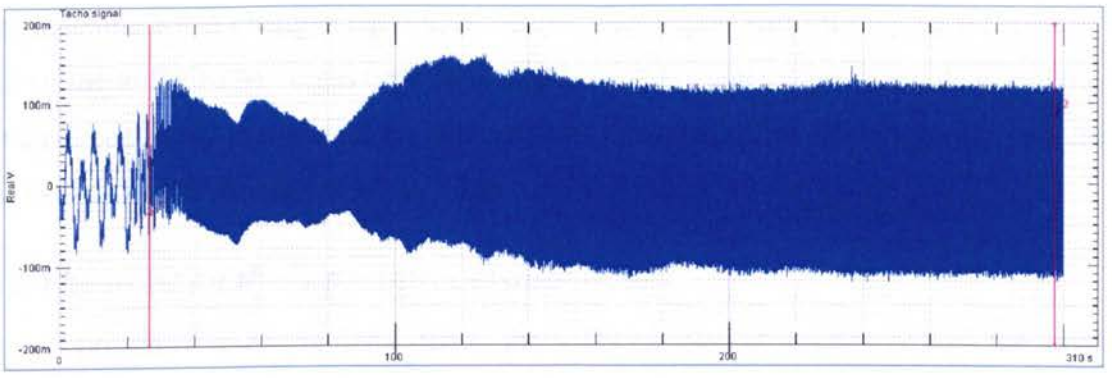

(a)

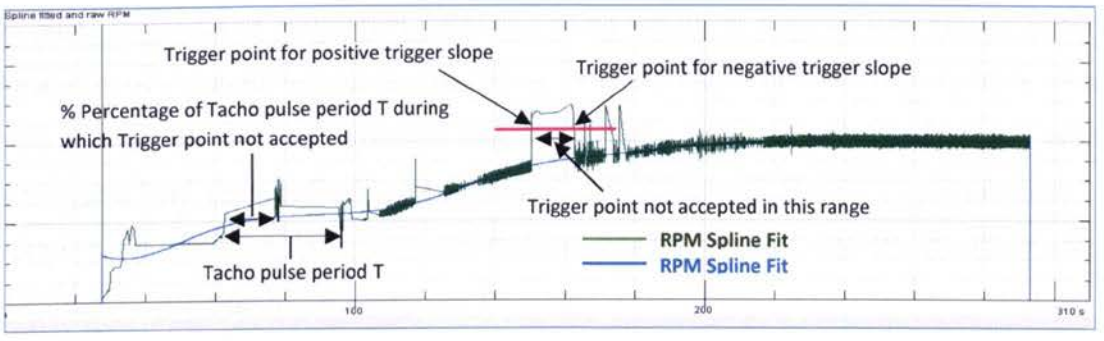

(b)

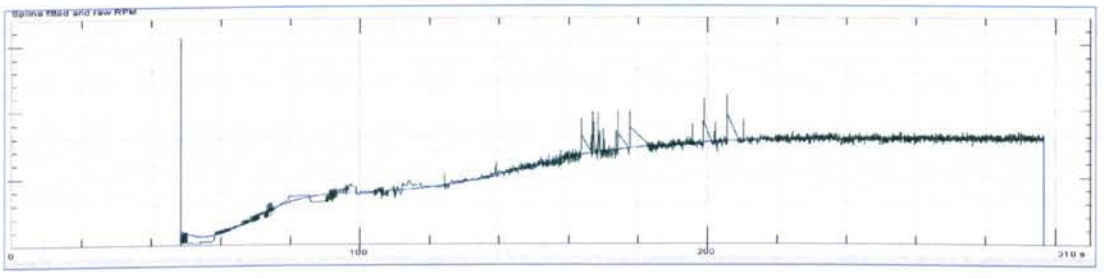

(c)

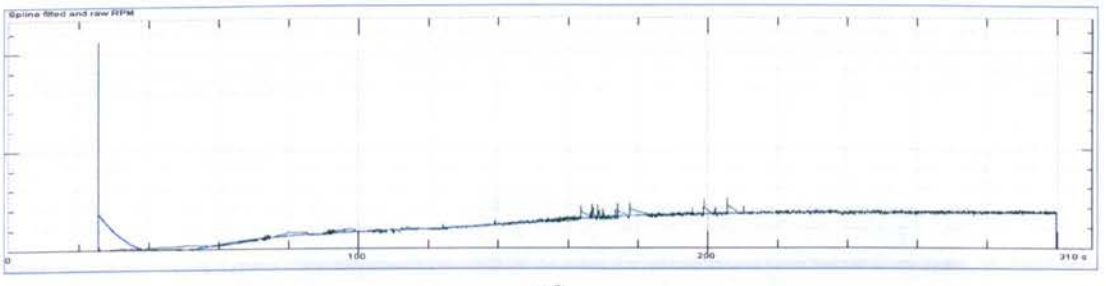

(d)

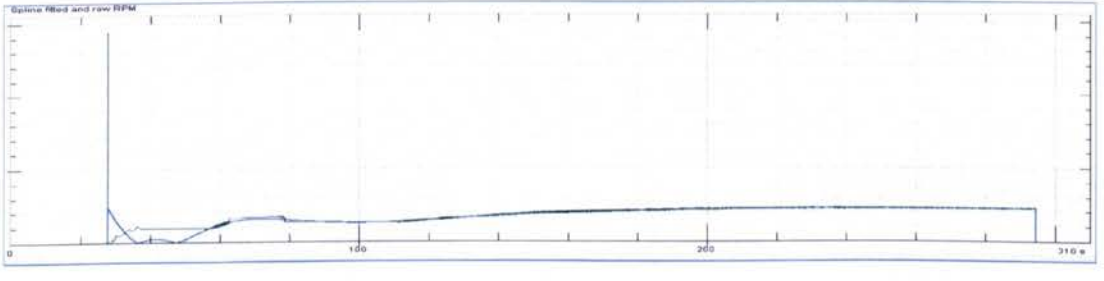

(e)

Figure 4.51 Removing outlying data points from Tacho measurement.

If the machine RPM changes rapidly, as occurs with a gear shift, it may be difficult to fit a cubic spline to the RPM versus time data. In this case, we can set break points where the first derivative continuity constraints are relaxed. The resulting spline fit will go through the raw RPM estimate at the break point time value.

4.7.2 The orbit analysis post-processing wizard

This part presented a test rig dedicated to the study of rotating machinery with the advent of computer-based data collectors and trending software.

In the past, diagnosis of equipment problems using vibration analysis was mostly dependent on the ability of the maintenance technician or the plant engineer. However, today's vibration analysis equipment utilizes software that has greatly enhanced the analysis of vibration measurements and the prediction of equipment performance. Before computer-based data collectors, most vibration programs consisted of recording overall velocity, displacement, and acceleration measurements on a clipboard.

The advent of computer-based data collectors and trending software made this whole trending process much more cost-effective. The first system only recorded overall measurements. Spectral data still had to be taken with a spectrum analyzer. Those programs based only on overall measurements were usually successful in identifying a machine developing a problem [136-141].

This orbit analysis tool has been designed for bearing and shaft analysis. It post-processes a time history file that must include a once-per-revolutions key phasor signal to provide a speed and reference for Top Dead Centre (TDC). Various filters are available to smooth the data over a number of revolutions.

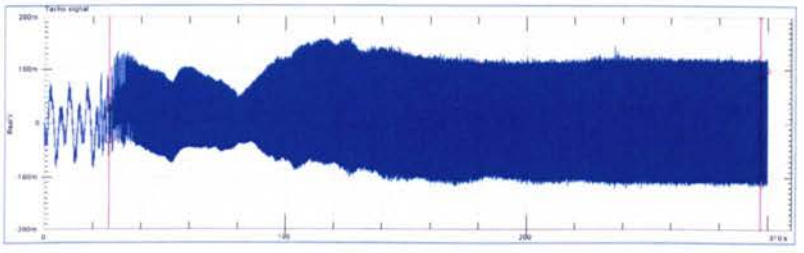

(a)- Real versus time (s).

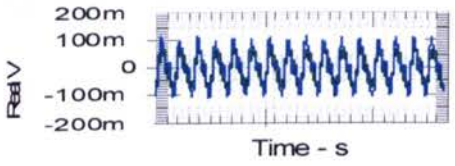

(b)- y, axis measurement.

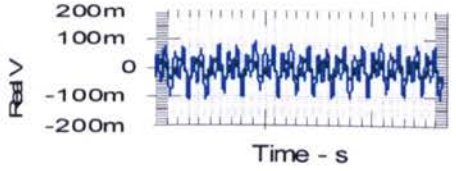

(c)- z, axis measurement.

Figure 4.52 Signal detection in y and z axis measurement direction.

From Figure 4.53, we notes orbit analysis direction lean to left and then to the right during rotation of the machine because it transfer the excitation harmonic force around each point in the orbit during the test, that is clear in Figure 4.54 demonstration accurate diagnosis of machine vibration conditions, including bearing vibration simplifies the task and increases the speed of collecting vibration monitoring data. Figures 4.55 and 4.56 show orbits analysis fundamentals behaviour of the rotor system at the different measured planes in first critical speed for channel one and two; for channel two Figure 4.56d without filter (HP filter) and Figure 4.56f without showing row data filter and Figure 4.56g shows change of performance for each point in the orbit, plot to trigger.

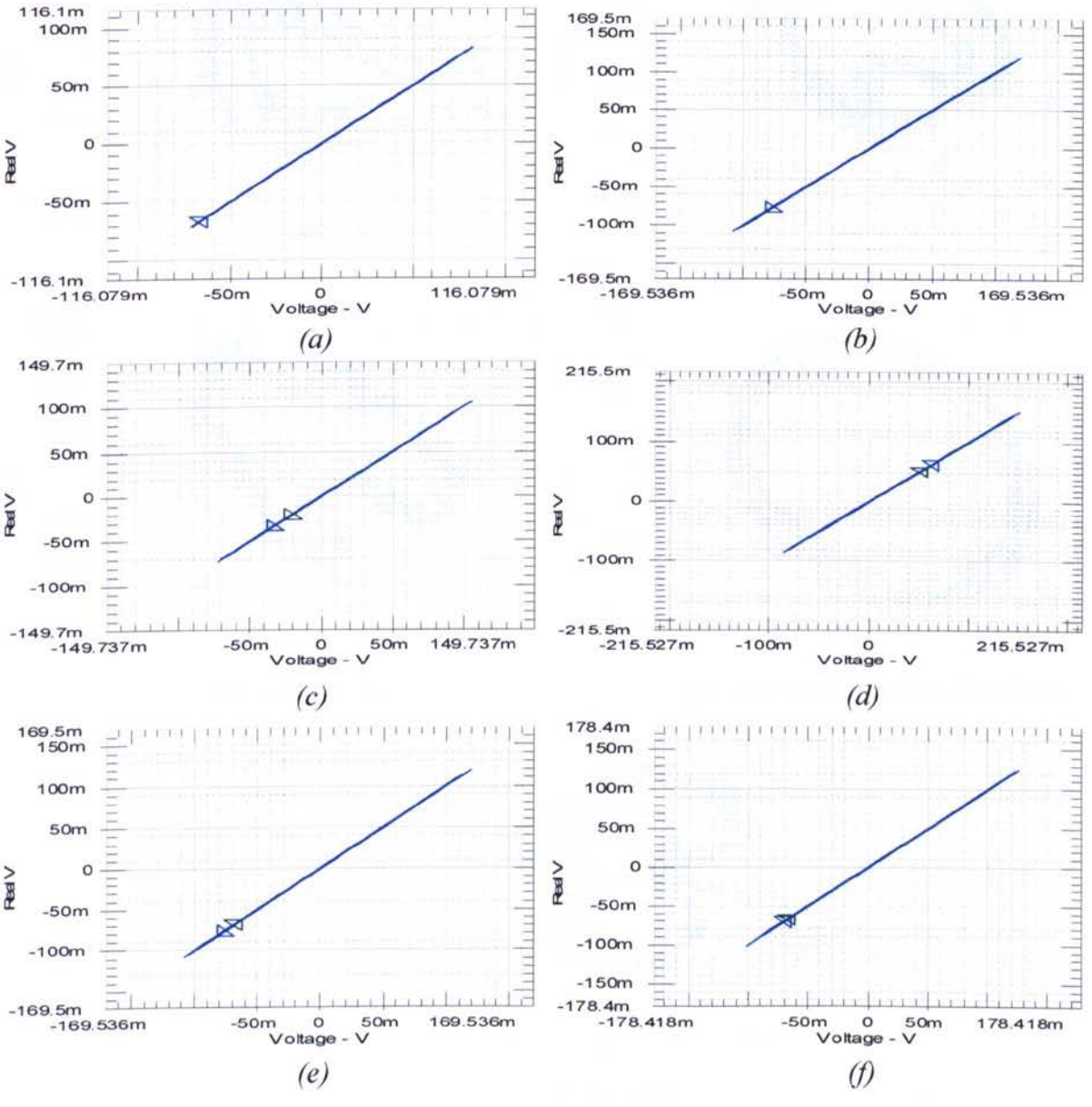

Figure 4.53 Experimental orbit analysis directions in rotor dynamics.

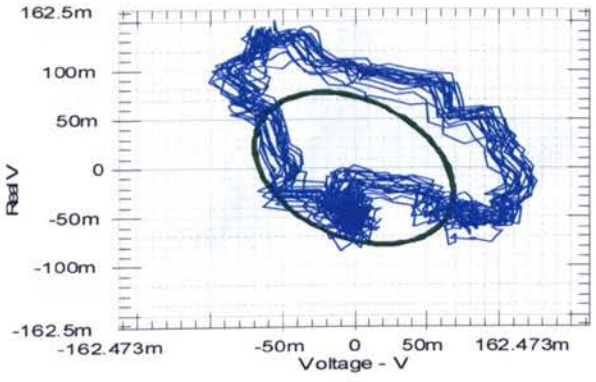

(a)

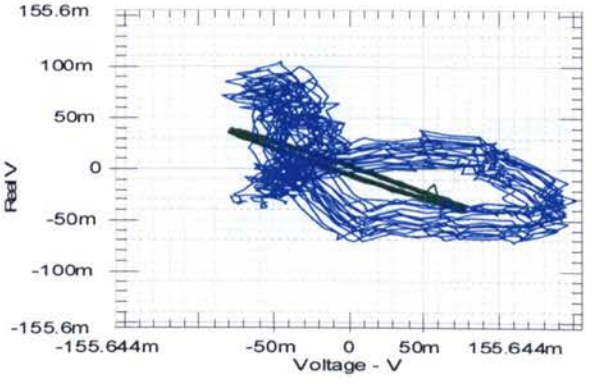

(b)

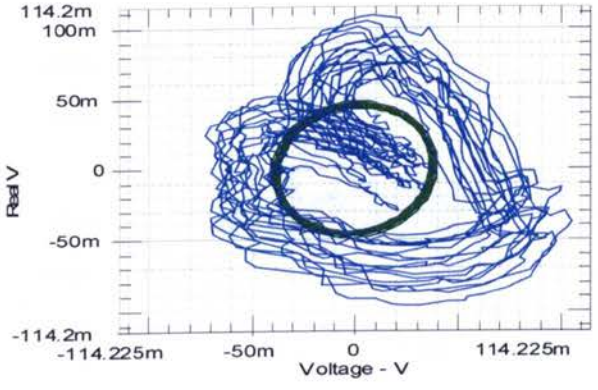

(c)

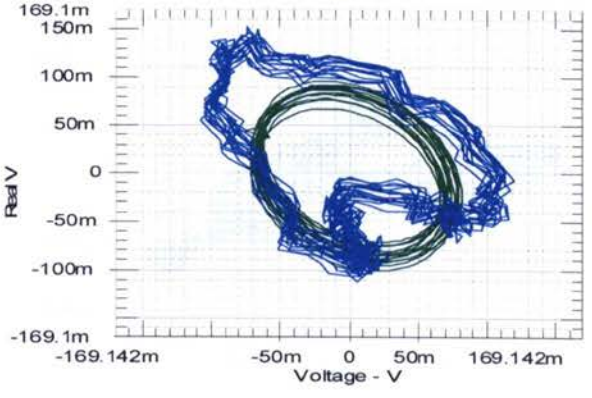

(d)- Without filter (HP filter).

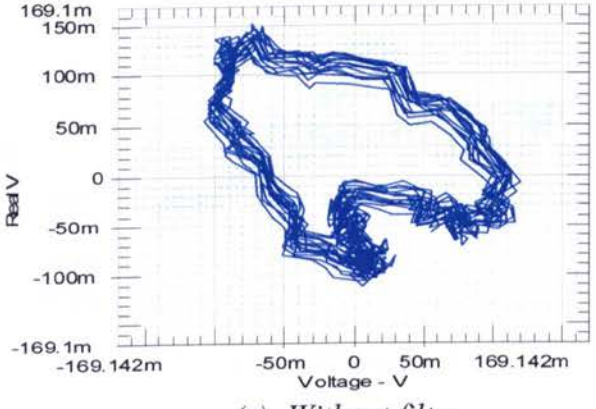

(e)- Without filter.

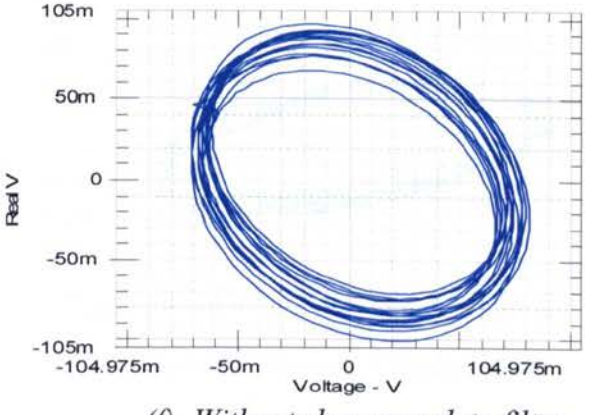

(f)- Without show row data filter.

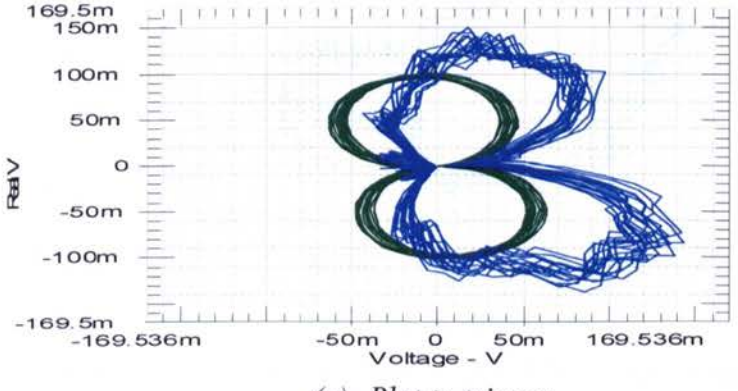

(g)- Plot to trigger.

Figure 4.54 Experimental orbit analysis fundamentals behaviour for keyphasor.

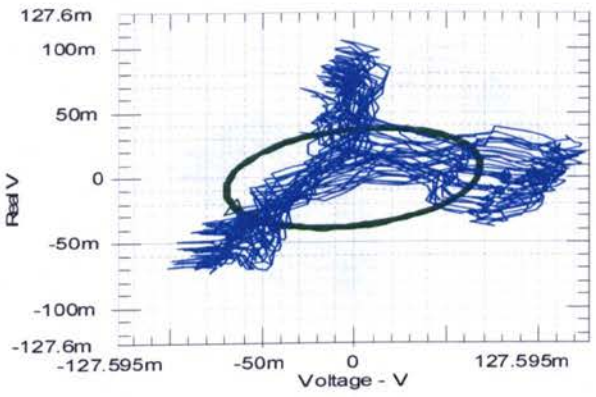

(a)

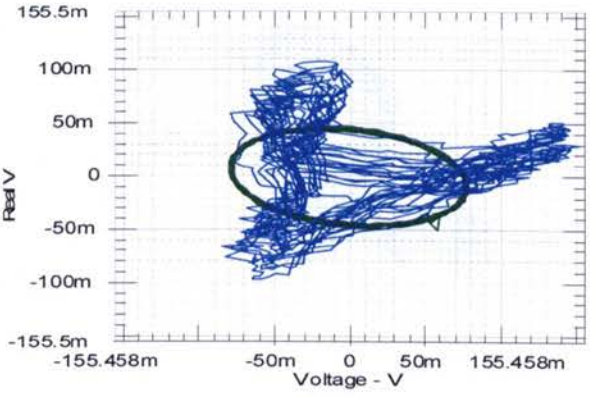

(b)

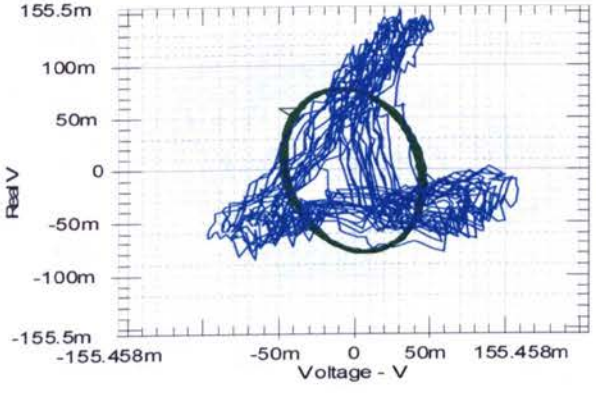

(c)

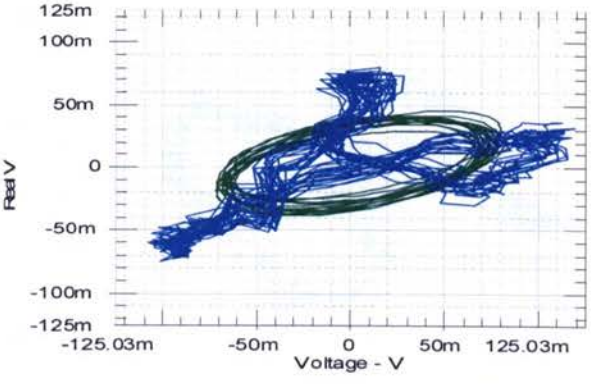

(d)- Without filter (HP filter).

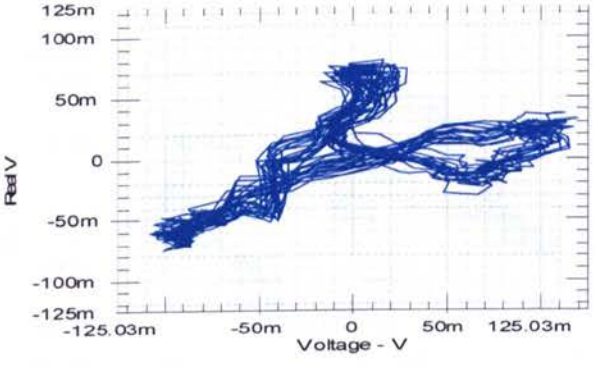

(e)- Without filter.

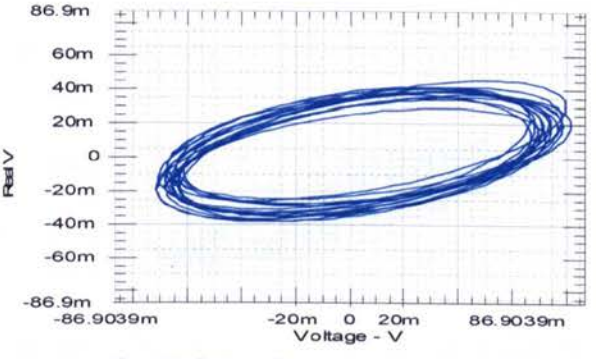

(f)- Without showing row data filter.

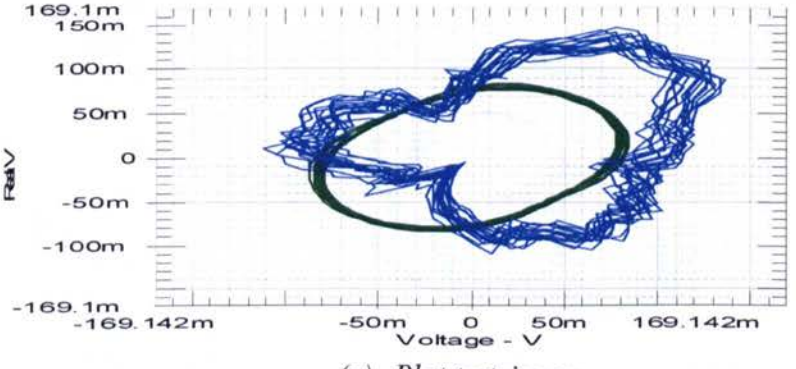

(g)- Plot to trigger.

Figure 4.55 Experimental orbits analysis fundamentals behaviour of the rotor at the different measured planes in first critical speed for channel one.

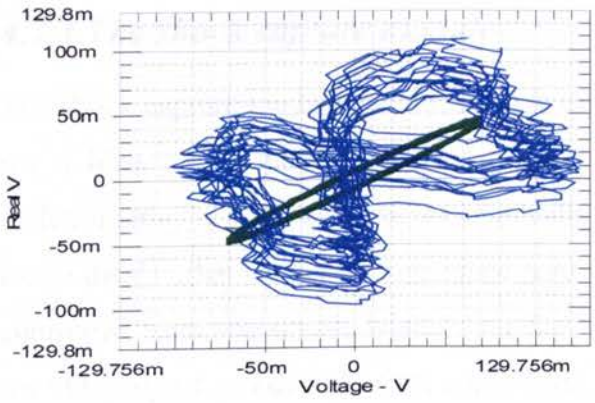

(a)

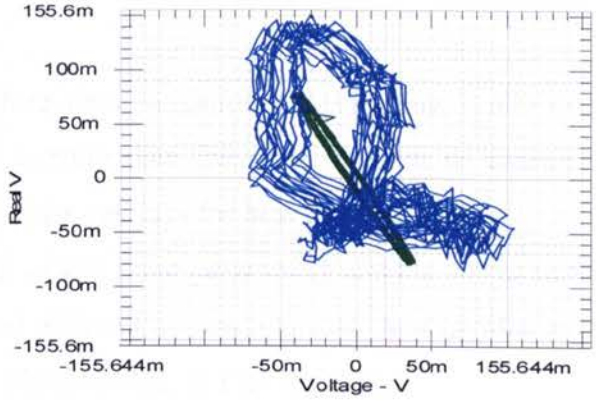

(b)

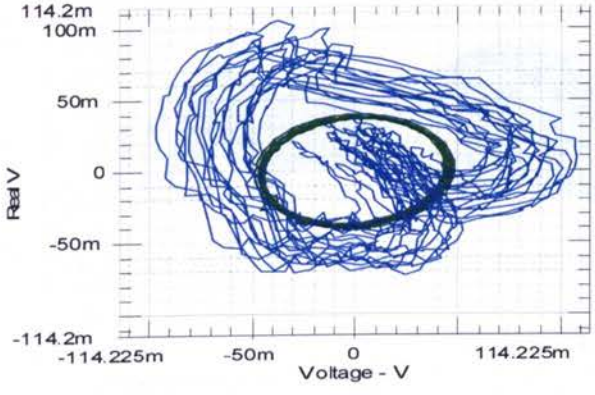

(c)

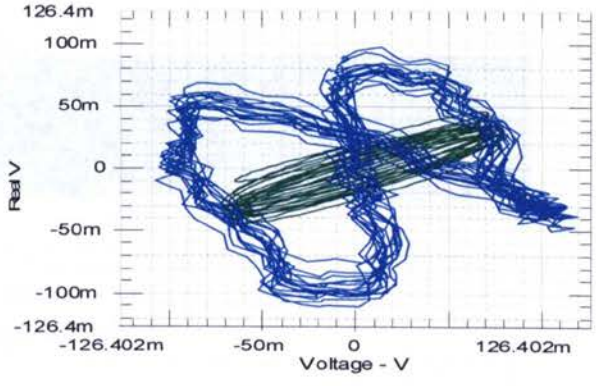

(d)- Without filter (HP filter).

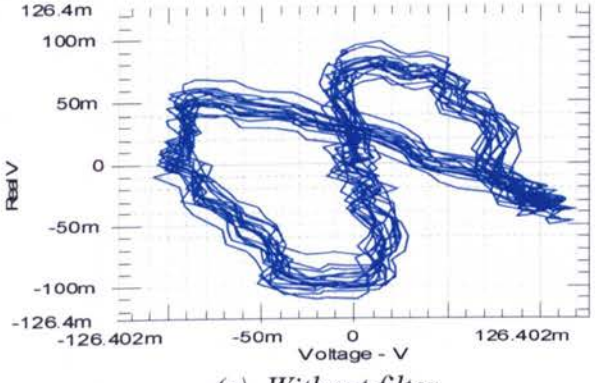

(e)- Without filter.

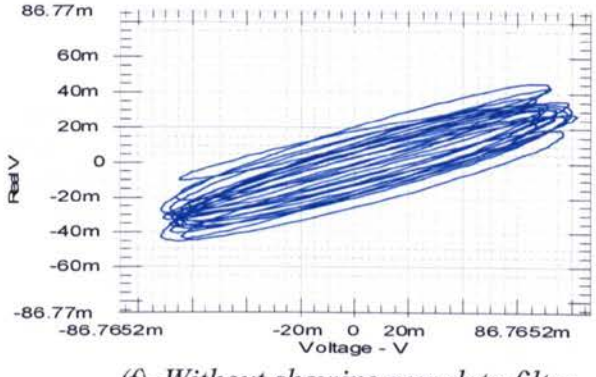

(f) -Without showing row data filter.

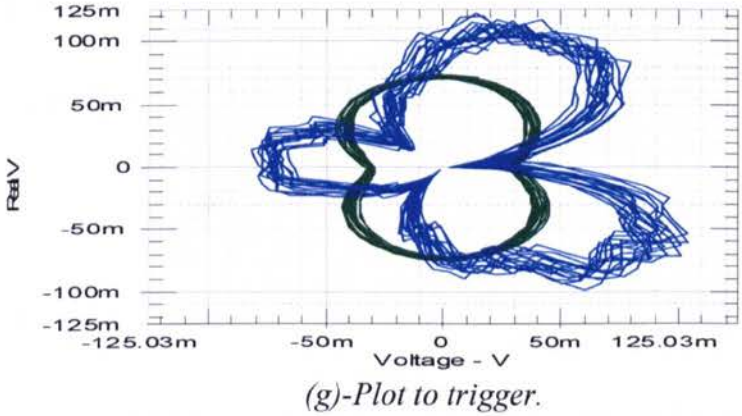

(g)-Plot to trigger.

Figure 4.56 Experimental orbits analysis fundamentals behaviour of the rotor at the different measured planes in first critical speed for channel two.

4.7.3 The shock capture module

The shock capture module provides shock capture, data validation and reporting. It allows to use a library of standard test limit overlays, capture data from any number of channels, including triax's, filter the data, automatically adjust overlays for best fit [44, 137].

In the display that we get an immediate readout of key pulse parameters and the whole test is controlled from one simple window for fast and efficient use even by user less familiar with the SO analyzer and details of the application, which is clear in Figure 4.57.

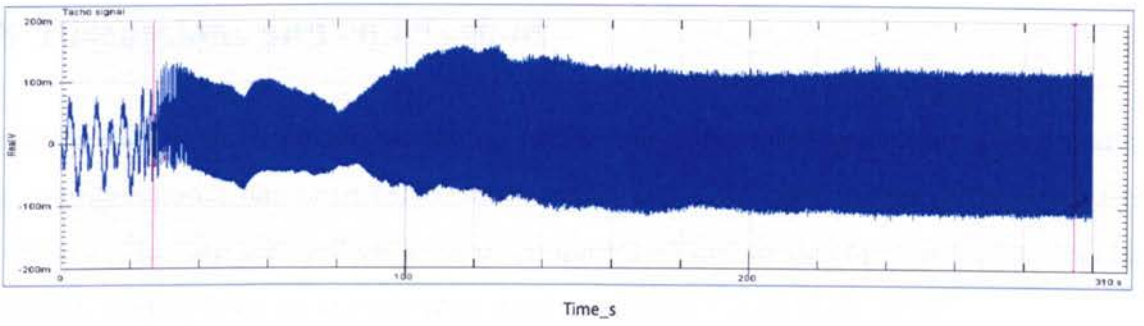

(a)- Tacho signal.

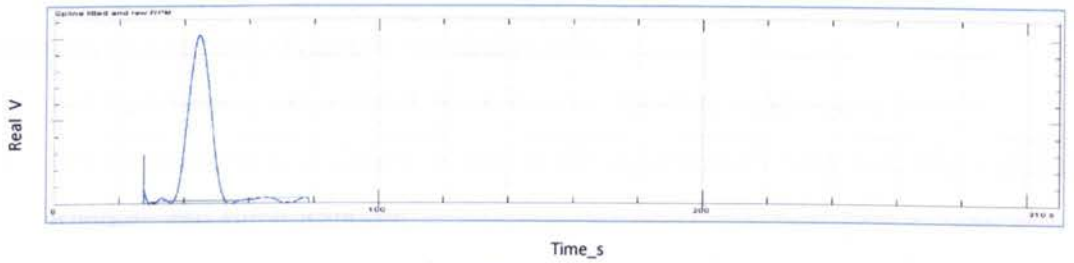

(b)- Before use filter.

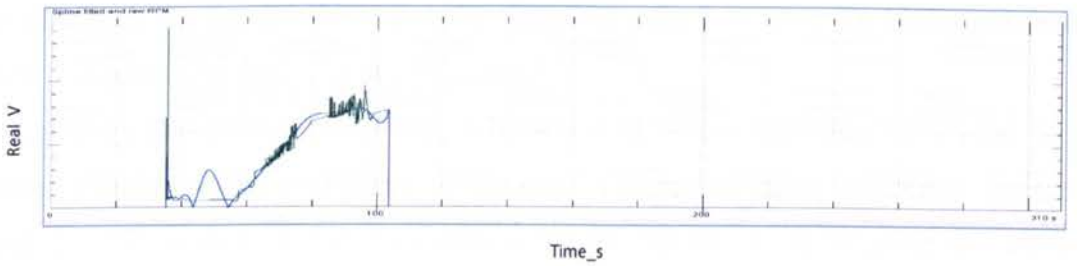

(c)- After used window filter with increasing the speed.

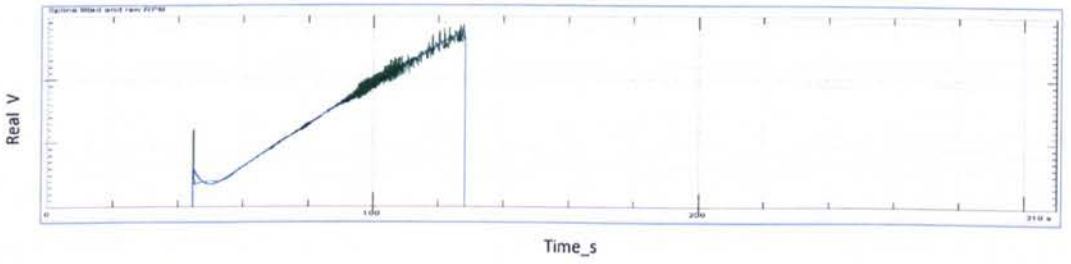

(d)- Improved or decayed shock capture after used window filter.

Figure 4.57 Shock capture module.

From this part we can conclude the smart office vibration analysis software is an essential tool for analyzing and evaluating the mechanical vibration that occurs in rotating machinery. Vibration condition monitoring involves transmitting large quantities of data from a transducer to a separate data collector for subsequent processing and analysis. The software is then used in analysis of multiple machine vibration parameters to assess operating performance. Maintenance personnel then use the data to determine if unscheduled maintenance is necessary or if shutdown is required [139, 142].

4.8 Discussions and conclusions

In this present work, a system modelling methodology for rotating structures (one and two disc configurations) has been established, which could be used in the design of rotating machinery. The step that underlies the development of this modelling process has also been presented, starting from an experimental work conducted as part of the study.

The behaviour of a rotor system under load was investigated using two different experimental techniques: experimental hammer and shaker tests:

- For the hammer test, a transient excitation vibration signal was used.
- For the shaker test, different excitation vibration signals were used which include Sine, Random and Burst Random.

For one disc configuration the modal parameters (natural frequency and damping ratio) have been obtained, the results show that the damping ratio ζ is lower in higher mode (lightly damped) as shown in Table 4.2 and Figure 4.7.

The results presented in Figures 4.9, 4.10 and 4.11, show the effect of Modal Balancing Method (MBM) for different speeds of rotation. The results show that MBM method could reduce the vibration near the first critical speed sharply while keeping the vibration at working speed at a proper level; resulting in reduction of the vibration more effectively.

The natural frequency and damping ration for two discs configuration shown in Table 4.3 and Figure 4.18, prove the same fact that the damping ratio is lower in higher mode.

The FRF and mode shapes for rotor setup before and after added mass for two discs configuration are shown in Figures 4.20, 4.21 and 4.22 for the first, second and third mode shape, respectively. As it can be seen from these figures, the FRF amplitude of the system is reduced by 19 db for first, 6 db for second and 5 db for third mode, due to applying a trial weight of 16 grams load to the system (8 gram per each disc) at the same speed, meaning the

amplitude of vibration is reduced in the shaft after added mass in the disc 1 at Ø (45°, 225°) and in disc 2 at Ø (180°, 0°), resulting in reduction in the noise due to reduction in excess vibration. This gives more reliability to the work done for one disc configuration.

Investigation of the behaviour of a rotor system with strong gyroscopic effect has been carried out, by increasing the rotational speed split of natural frequency occurs, the magnitude of split depends on the ratio of the polar mass moment of inertia (I_0) to the diameter mass moment of inertia (J). This is shown on the FRF measured for various speeds of rotation.

Extraction of damping ratio from experimental part for the first and second mode at speed 30 rpm shows that the damping ratio is lower in higher mode; as shown in Table 4.4 and Figure 4.27.

The modal testing results show the natural frequency and mode shapes for different speeds of rotation, see Figures 4.31 and 4.32, the natural frequency of the rotor splits up as the speed of rotation increases. From these figures we conclude, the rotor whirl is either in the same direction as rotation or against rotation, which results into both forward and backward whril mode. The frequencies are affected by both the mass (m) and diameteral mass moment of inertia (J).

The gyroscopic effect becomes more pronounced by reducing the length, the overhung load and the inward bearing, and by increasing the rotational speed, the gap between the forward and backward whirl increases.

The explanation for the above behaviour is due to the gyroscopic effect that occurs whenever the mode shape has an angular (conical/rocking) component. Considering the Forward Whirl as shaft speed increases, the gyroscopic effects essentially act like an increasingly stiff spring on the central disc for the rocking motion. Increasing stiffness acts to increase the natural frequency. While for Backward Whirl, the effect is reversed, increasing rotor spin speed acts to reduce the effective stiffness, thus reducing the natural frequency (the gyroscopic terms are generally written as a skew-symmetric matrix added to the damping matrix-the net result, though, is stiffening/softening effect).

In the case of the first modes of the machines (cylindrical modes), very little effect of the gyroscopic terms was noted, because the centre disc was whirling without any conical motion. So, it can be said that, if the mode shape of rotating structure is non-conical, the gyroscopic effects do not appear.

An electro-dynamic shaker can be used to produce a various types of excitation functions; i.e. Sine, Random, Burst Random, etc.

By connecting an electro-dynamic shaker to outer casing of shaft and plain bearing via a push rod, the shaker could be used for exciting the system.

Random and Burst Random signals give a better coherence and were quicker compared to the Sine signal in shaker tests.

- Sine signals (16, 32 and 50 Hz), gave really bad coherence in shaker tests.
- All the signals acquired the mode shapes at 16 and 49 Hz.

Using shaker test for one disc in the middle to find natural frequency and extract the mode shape shown in Figures 4.39-4.41, the values of experimental technique for different excitation signals are in agreement with each other as shown in Tables 4.5-4.7 and Figures 4.42 and 4.43.

Oscilloscopic technique (Time domain) has been used to validate the results obtained from shaker test for correcting the unbalance in the system.

When using oscilloscope with shaker test for two discs (multistage), the locations of the adding balance masses in suppressing the vibration amplitudes are decided to be at angles for disc 1, Ø (45°, 225°) and for disc 2, Ø (180°, 0°), respectively. This method gives more reliability to the unbalance using shaker test for more complicated model system.

Oscilloscopic results in Figures 4.47-4.50 show that when adding 16 gram mass (8 gram per each disc) at the same location and dimension for two discs can reduce the amplitude of vibration, and are in agreement with results obtained from Modelling Balancing Method (MBM) for two discs (multistage) configuration using hammer test (transient signal).

In addition, vibration analysis techniques in experimental Smart Office software have been used to gives insight about the behaviour of rotor dynamic system.

Orbit analysis software is used to demonstrate accurate diagnosis of machine vibration conditions, including bearing vibration simplifies the task and increases the speed of collecting vibration monitoring data, this shown in Figures 4.52-4.56.

From Figure 4.57 shock capture module is happened at beginning when the rotor turn on (initial rotation) this effect is very high at this region, and it has been improved or decayed by using windowing filter as shown in Figure 4.57d.

CHAPTER 5

Finite Element Analysis of Rotating Machinery

5.1 Introduction

Increased complexities of rotating machinery and demands for higher speeds and greater power have created complex vibration problems. Engineering judgments based on understanding of physical phenomena are needed to provide the diagnosis and methods for correcting the rotating machinery faults. A computer program can be used to calculate the dynamic behaviour of the system: critical speeds, stability charts, frequency response function due to unbalance and modal parameter (natural frequency, mode shape). There is a growing tendency today to extract information about the prognostic parameters based on system analysis through various diagnostic techniques, so as to assess the health of the plant or equipment [143-147]. In this chapter, we apply the finite element and other calculation methods developed in the previous chapters to the systems with multidisc of various mass and geometry configuration in order to identify the dynamic behaviour of the systems in real life situation.

Field balancing of flexible rotor system is a key technique to reduce vibration in power plants. In recent decades, the balancing theory has been thoroughly studied, and various balancing techniques have been developed. However, the existing balancing methods are still potential for improvements in accuracy and efficiency. Increased running speeds and there requirements for rotating machinery to operate within specified levels of vibration mean that the control of machinery vibration is essential in today's industry [148-151]. A thorough study that describes the dynamic behaviour of a rotating machine requires integrating not only the correct rotating shaft model but also the accurate boundary conditions such as the properties of the bearing supports and the external forces on the system. Fortunately, thanks to the sufficient computing power that is generally available and affordable nowadays, there are many programmed procedures and solution packages for analyzing the stability, steady-state and transient responses of individual rotor systems [152-154]. However, there is no adequate commercial software which is designed to solve the topics of interest in the rotor-dynamic system. This has motivated the current study to develop the finite element model for the investigation of the vibration behaviour of a rotor-dynamic. The conditions of stability for the rotor-dynamic system are explored thoroughly by varying some of the significant design

parameters, such as the bearing stiffness and damping, the eccentricity and the adding mass for the optimum balance effect etc [155-158]. The variations of the vibration amplitudes at certain major locations of the rotor system and its sensitivity to the relating design parameters are also examined completely. A finite element simulation was developed in this thesis for solving the dynamic properties of the rotor dynamic system. These dynamic properties include the natural frequencies, mode shapes and damping ratio for the rotor system with either the rigid modes or flexible modes. It is also capable of solving the transient analysis of the vibration and the orbits for the application (cutting tools) of the rotating machines as in simulation results.

5.1.1 Rotor-dynamics of a shaft assembly based on model of axisymmetric rotor

Rotor-dynamics plays a crucial role in identifying critical speeds, and to ultimately design rotating structures that tolerate extremely high vibrations. This example illustrates the application of rotor-dynamics analysis procedures using the Nelson-Mcvaugh [90] rotor model.

A 2-D axisymmetric representation of the 3-D solid model is used to perform a rotor-dynamic analysis. The results of the 2-D axisymmetric model analyses are compared to the full 3-D solid model results.

This problem demonstrates the following concepts and techniques:

- Axiharmonic meshing of a 3-D geometry
- Disc and bearing modelling
- Gyroscopic effects in rotating structures and modal analysis
- Campbell diagram analysis
- Determination of critical speeds
- Unbalance response analysis
- Orbit plot
- Performance benefits of 2-D axisymmetric models

5.1.2 The benefits of the finite element analysis method for modelling rotating structures

The Finite Element (FE) method used in ANSYS offers an attractive approach to modelling a rotor-dynamic system. While it may require more computational resources compared to standard analyses, it has the following advantages:

- Accurate modelling of the mass and inertia
- A wide range of elements supporting gyroscopic effects
- The use of the CAD geometry when meshing in solid elements
- The ability of solid element meshes to account for the flexibility of the disc as well as the possible coupling between disc and shaft vibrations.
- The ability to include stationary parts within the full model or as substructures.

5.2 Methodology in FE modelling

ANSYS mechanical APDL (ANSYS Parametric Design Language), Product Launcher

Simulation Environment: ANSYS 12

LICENSE: ANSYS Academic Teaching Advanced

5.2.1 FE anaylsis of a rotor dynamic system consist of one or multidisc in the effective length using ANSYS 12

A rotating structure generally consists of rotating parts, stationary parts, and bearings linking the rotating parts to the stationary parts or the ground. Understanding the relationships between these parts is important for modelling process.

The disc in Figure 5.1, was made of steel, Young's modulus = 225 GPa, Poisson's ratio = 0.28, density = 7800 kg/m^3 and shear modulus = 87.89 GPa. While the shaft was shown in Figure 5.2 made of Iron which has a Young's modulus = 147 GPa, Poisson's ratio = 0.287, density = 7870 kg/m^3 and shear modulus = 82 GPa, see Table 4.1 in chapter 4.

5.2.1.1 Defining material properties

Defining the material properties for a rotor-dynamic analysis is no different from defining them in any other analysis. Use the MP or TB commands to define linear and nonlinear material properties.

5.2.1.2 Defining element type

To define element types selected for the rotating parts that were modelled must support gyroscopic effects. The CORIOLIS command documentation lists the elements for which the gyroscopic matrix is available.

All rotating parts must be axisymmetric.

5.2.1.3 Modelling

The modelled disc drawn as a points in ANSYS program, see Figure 5.1.

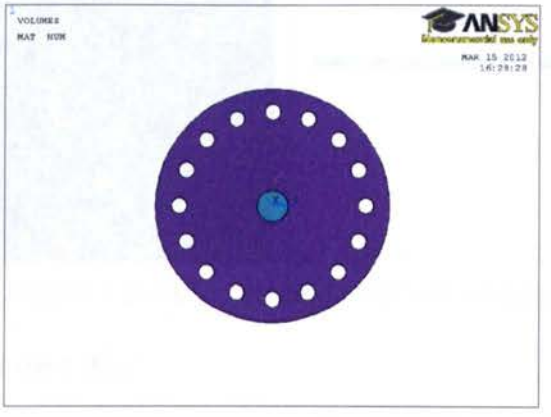

Figure 5.1 Modelled disc included holes.

Then the area extruded in x direction to produce the volume, see Figure 5.2.

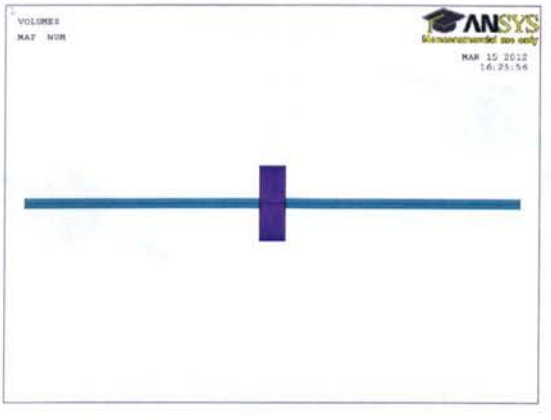

Figure 5.2 Show extrudes area in x direction.

5.2.2 Make the disc and shaft one volume using several methods

A- Method 1

Prior to meshing Glue option in ANSYS may be used which effectively delete areas of volumes selected and create a new area that will be shared by both of volumes.

Meshing can then be applied, after that there will be created only one set of nodes those are shared by both of volumes, volume 1 for shaft and volume 2 for disc, see Figure 5.3.

B- Method 2

Mesh both of the volumes with using the same mesh size and element shape at contact surface, and then use merge nodes at contact surface.

C- Method 3

Select nodes with mouse and then create component or assemble then select shaft and disc.

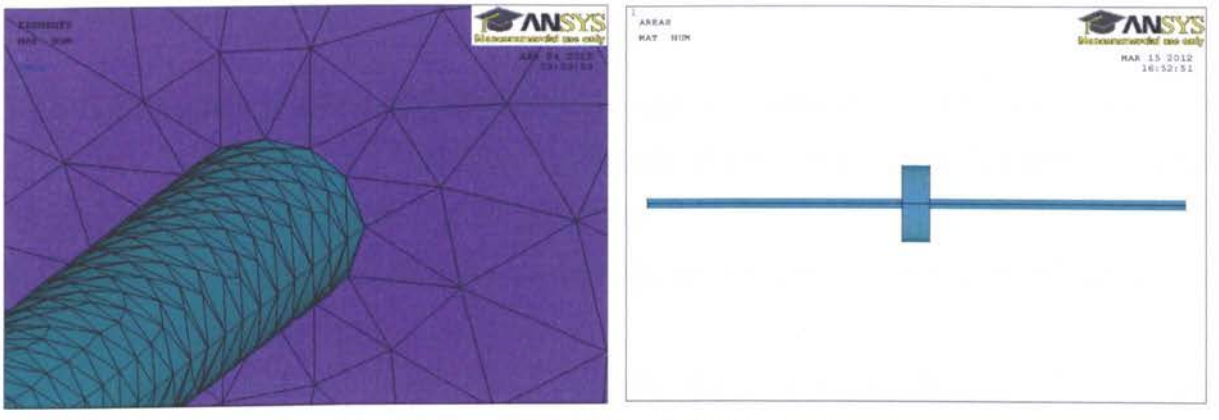

Figure 5.3 Make disc and shaft one volume.

5.2.3 Make more than one disc

Copy option can be used to create more than one disc copy the modelling using volume, the ANSYS ask about the direction of place needed to copy in, see Figure 5.4.

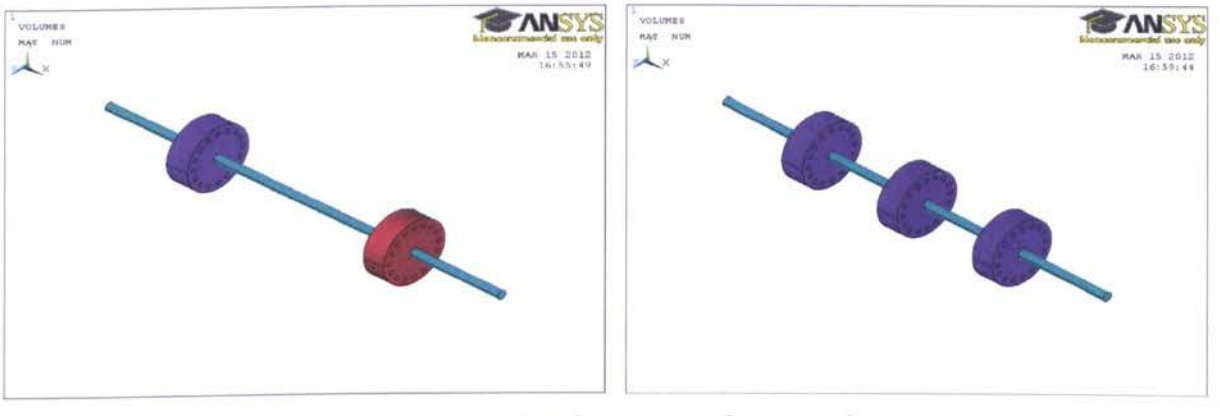

Figure 5.4 Copy more than one disc.

5.2.4 Mesh the model

Meshing

Creating a one volume model, then meshing could be applied by choosing meshed size in order to solve it, see Figure 5.5.

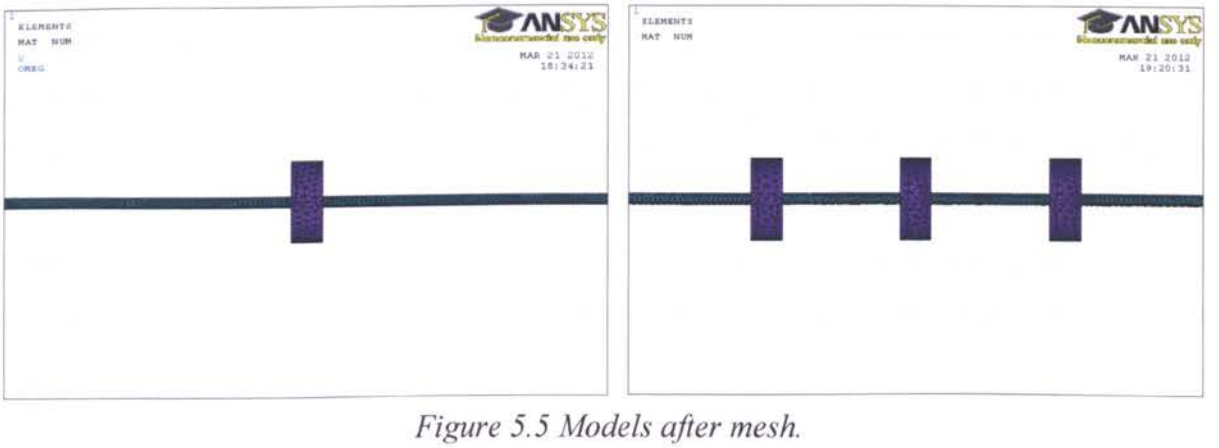

Figure 5.5 Models after mesh.

5.2.5 Solving the model

The solution phase of a rotor-dynamic analysis adheres to standard ANSYS conventions; the gyroscopic matrices as well as possibly the bearing matrices may not be symmetric. Modal, harmonic and transient analyses can be performed.

(i) Performing a modal analysis allows reviewing the stability and obtaining critical speeds from the Campbell diagrams.

(ii) A harmonic analysis allows to calculate the response to synchronous (for example, unbalance) or asynchronous excitations. Any sustained cyclic load will produce a sustained cyclic response (a harmonic response) in a structural system. Harmonic response analysis gives the ability to predict the sustained dynamic behaviour of the structures, thus enabling to verify whether or not the designs will successfully overcome resonance, fatigue, and other harmful effects of forced vibrations. Harmonic response analysis is a technique used to determine the steady-state response of a linear structure to loads that vary sinusoidally (harmonically) with time.

(iii) A transient analysis allows studying the response of the structure under transient loads (for example, a 1 G shock) or analyzing the start-up or stopping effects on a rotating spool and the related components.

Pre-stress can be an important factor in a typical rotor-dynamic analysis, which include pre-stress in the modal, transient or harmonic analysis.

5.2.5.1 Solving the model for shaft and disc

A- Model BEAM188, 3-D, 2-node beam for shaft

BEAM188 element description

BEAM188 is suitable for analyzing slender to moderately stubby/thick beam structures. The element is based on Timoshenko beam theory which includes shear-deformation effects. It provides options for unrestrained warping and restrained warping of cross-sections.

It is a linear, quadratic, or cubic two-node beam element in 3-D. BEAM188 has six or seven degrees of freedom at each node. These include translations in the x, y, and z directions and rotations about the x, y and z directions. A seventh degree of freedom (warping magnitude) is optional. This element is well-suited for linear, large rotation, and/or large strain nonlinear applications, see Figure 5.6.

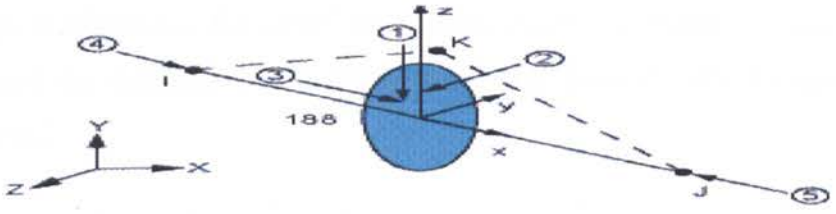

Figure 5.6 BEAM188 geometry.

The BEAM188 element has been used for this model because of (length/thickness) was small and the time can be saved and using BEAM188 element to get the bending stress, strain and reaction bearing for shaft but the limitation was final shape shown as a straight lines not real shape despite the accuracy of results.

B- Model SOLID187, 3-D, 10-node for shaft and disc

SOLID187 element description

SOLID187 element is a higher order 3-D, 10-node element. SOLID187 has a quadratic displacement behavior and is well suited to modelling irregular meshes such as those produced from various CAD/CAM systems.

The element is defined by 10 nodes having three degrees of freedom at each node: translations in the nodal x, y and z directions.

These models show the real shape (solid geometry). This model can be selected for disc and shaft with higher diameter.

The geometry, node locations, and the coordinate system for this element are shown in Figure 5.7.

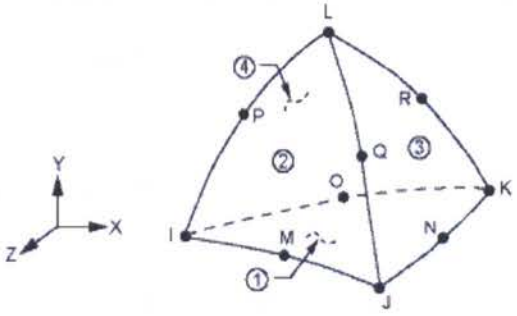

Figure 5.7 SOLID187 geometry [159].

Element loads are described in node and element loads. Pressures may be input as surface loads on the element faces as shown by the circled numbers, for this reason this element was

more suitable. Furthermore, the model used in this study has irregular surfaces and included curved surfaces, for this reason SOLID187 element is more suitable for modelling irregular surfaces meshes.

C- Model SOLID273 for disc and shaft

General axisymmetric solid with 8 base nodes

SOLID 273 element description

SOLID273 is suitable for modelling axisymmetric solid structures in 2-D only. The element has quadratic displacement behavior on the master plane and is well suited to modelling irregular meshes on the master plane such as those generated by various CAD/CAM systems. It is defined by eight nodes on the master plane, and nodes created automatically in the circumferential direction based on the eight master plane nodes, see Figure 5.8.

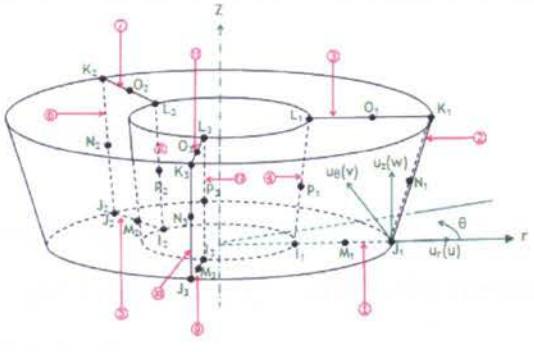

Figure 5.8 SOLID273 geometry.

The element does not support the expansion pass of a super element with large rotation. For this reason ANSYS plots the elements in 3-D and the results on both nodal planes and all integration planes in the circumferential direction; otherwise, ANSYS plots the elements in 2-D and the results on the master plane.

D- Model SOLID272

General axisymmetric solid with 4 base nodes

SOLID272 Element description

SOLID272 may be used to model axisymmetric solid structures. It is defined by four nodes on the master plane, and nodes created automatically in the circumferential direction based on the four master plane nodes. The total number of nodes depends on the number of nodal planes. Each node has three degrees of freedom: translations in the nodal x, y and z directions. The element allows a triangle as the degenerated shape on the base plane to

simulate irregular areas. The geometry, node locations, and the coordinate system for this element are shown in Figure 5.9.

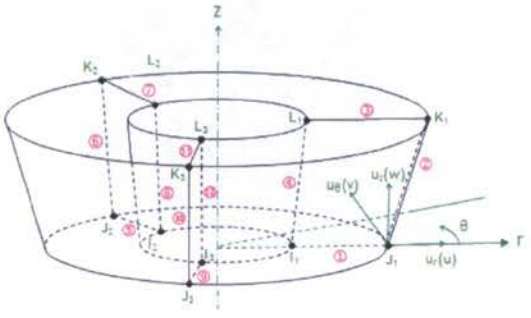

Figure 5.9 SOLID272 geometry, KEYOPT (2) = 3.

The area of the base element must be non zero. The base element must lie on one side of the axisymmetric axis and the axisymmetric axis must be on the same plane as the base element (master plane). ANSYS software has been drawing the elements in 2-D, and the results on the master plane.

5.2.5.2 Solving the model for bearings

Bearings are used to support the rotor in the lateral direction. Two identical un-damped and linear orthotropic bearings were modelled using COMBI214 elements as shown in the Figure 5.10, with a 2-D axisymmetric model.

The X, Y, and Z axes should be added to the Figure 5.11, 3-D geometry for directions.

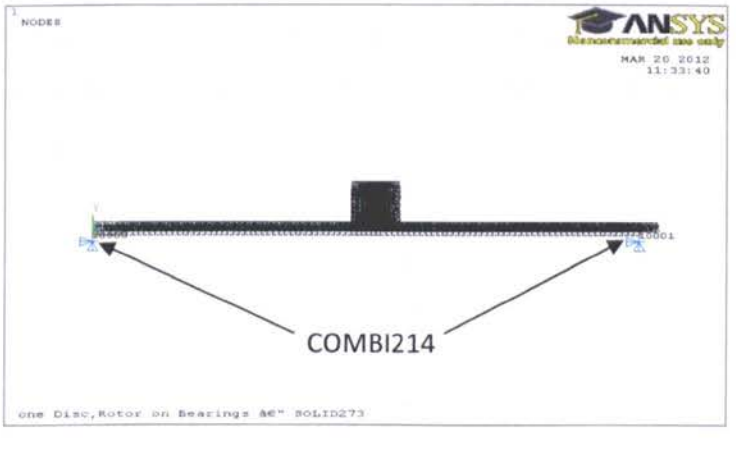

Figure 5.10 Bearings modelled with COMBI214 elements, 2-D solid model.

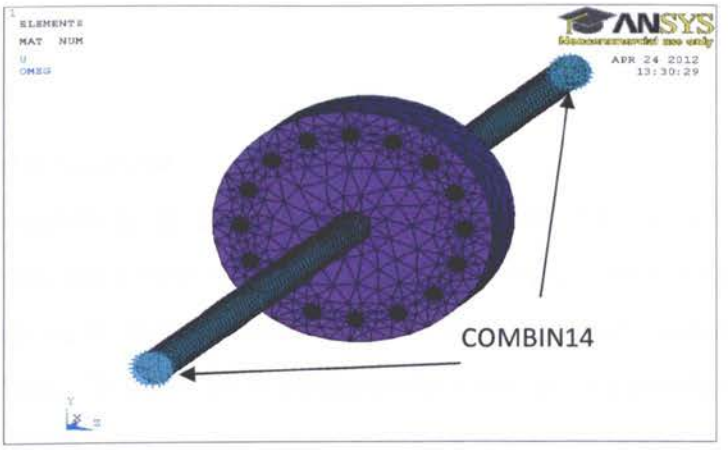

Figure 5.11 Bearings modelled with COMBIN14 elements, 3-D solid model.

The contact pairs shown in the Figures 5.10 and 5.11 must be created to model the bearings. The contact pairs are modelled in a similar fashion to the disc modelled in the previous section. To model an orthotropic bearing, an additional node is created at the centre of the cross section of the rotor at the bearing location. This node is then connected to pilot node using COMBI214 elements. To visualize this element, offset the node along the Y-direction without altering the results as shown in the Figure 5.10.

A- COMBI214

2-D spring-damper bearing

COMBI214 element description

COMBI214 has longitudinal as well as cross-coupling capability in 2-D applications. It is a tension-compression element with up to two degrees of freedom at each node: translations in any two nodal directions (x, y or z). COMBI214 has two nodes plus one optional orientation node. No bending or torsion is considered. Eventually, COMBI214 capability was used in 2-D applications, see Figure 5.12.

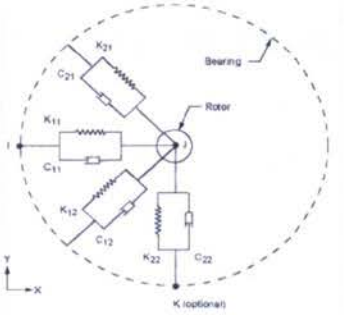

Figure 5.12 COMBI214 geometry.

For linear analyses, I and J can be coincident.

B- COMBIN14

Spring-damper

COMBIN14 element description

COMBIN14 has longitudinal or torsional capability in 1-D, 2-D or 3-D applications. The longitudinal spring-damper option is a uniaxial tension-compression element with up to three degrees of freedom at each node: translations in the nodal x, y and z directions. No bending or torsion is considered. The torsional spring-damper option is a purely rotational element with three degrees of freedom at each node: rotations about the nodal x, y, and z axes, see Figure 5.13.

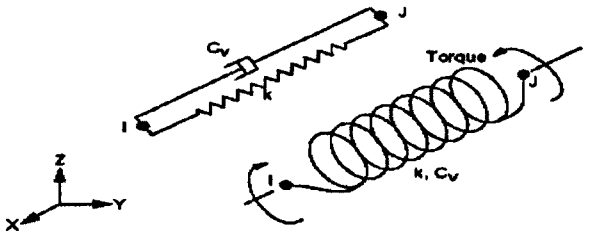

Figure 5.13 COMBIN14 geometry.

2-D elements must lie in a z = constant plane.

COMBIN14 assumptions and restrictions

The longitudinal spring element stiffness acts only along its length. The torsion spring element stiffness acts only about its length, as in a torsion bar.

The element allows only a uniform stress in the spring.

5.3 FE simulation of model

5.3.1 Finite element model of rotating machinery, one disc

A model of rotor system consisting of one disc and two bearings with multi degree of freedom (Y and Z directions) has been used to demonstrate the above capability, see Figure 5.14. The modelling technique has been applied in ANSYS 12, Post-processing commands /POST26. Applying of gyroscopic effect to rotating structure was carried by using CORIOLIS command. This command also applies the rotating damping effect. CMOMEGE specifies the rotational velocity of an element component about a user–defined rotational

axis. OMEGA specifies the rotational velocity of structure about global Cartesian axes. A spring/damper element, COMBIN14 has been used for model the bearings [159, 160].

(a)- 3-D ANSYS APDL. *(b)- 2-D ANSYS APDL.*

Figure 5.14 Finite element model of rotating machinery, one disc.

Generally, a 3-D model directly available from the CAD can be used for the analysis Figure 5.14a; however, 3-D models result in a large number of nodes and elements. This chapter demonstrates how to extract a plane 2-D model as shown in Figure 5.14b from the 3-D model shown in Figure 5.14a, which can be analyzed by using far fewer nodes and elements.

A 2-D axisymmetric representation of the 3-D solid model is used to perform a rotor dynamic analysis. The results of the 2-D axisymmetric model analyses agree with the full 3-D solid model results, and the results from experiments.

5.3.1.1 ANSYS results of natural frequency and mode shapes

ANSYS results of natural frequency and mode shape of one disc in the centre with two bearings have been shown in Figure 5.15.

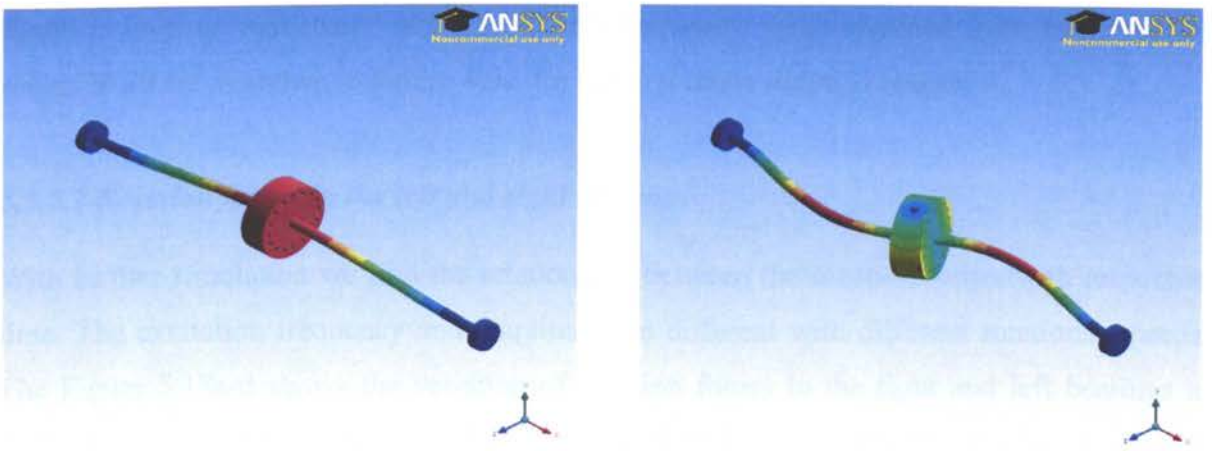

(a)-First mode shape. Natural frequency 29.95Hz. *(b)-Second mode shape. Natural frequency 243.68Hz.*

(c)-Third mode shape. Natural frequency 522.02Hz.

(d)-Fourth mode shape. Natural frequency 612.54Hz.

Figure 5.15 Different mode shapes of shaft with one disc and two bearings, 3-D.

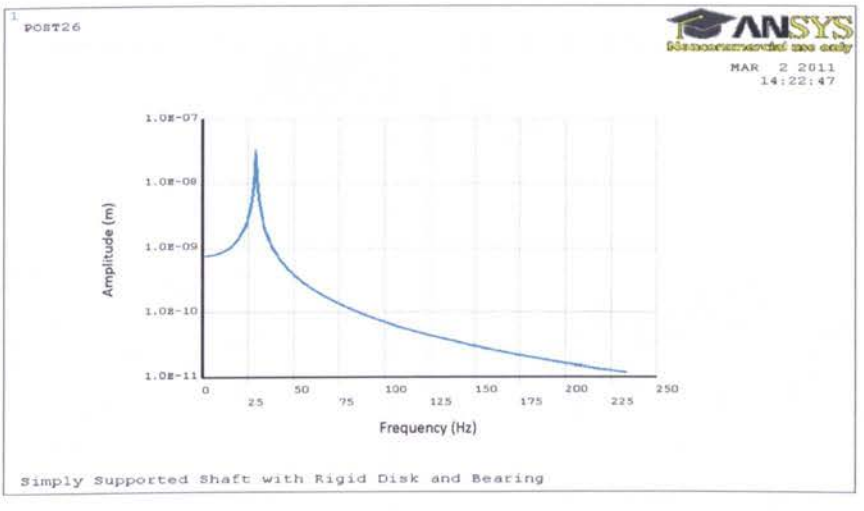

Figure 5.16 Frequency response function for the first mode shape.

From the Figure 5.16 the value of natural frequency is 29.93 Hz, obtained from ANSYS figure is in good agreement with the natural frequency value obtained from experimental setup, 29.79 Hz as shown in Figure 4.9a, for the first mode shape in chapter 4.

5.3.1.2 Reaction forces in the left and right bearings

With further simulation we find the relationship between the reaction forces with respect to time. The excitation frequency and amplitude are different with different rotational speeds. The Figure 5.17a-d shows the variation of reaction forces in the right and left bearings at different speeds of rotation, from the figure the right bearing carry the maximum reaction force.

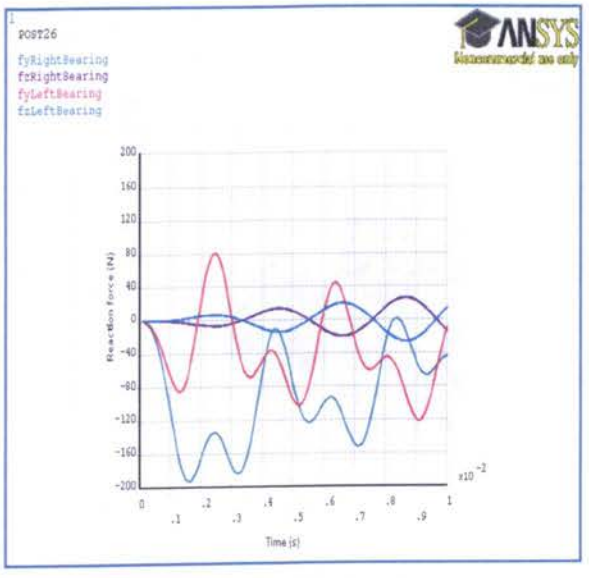

(a)-Reaction force (Fy and Fz) at 1000rpm.

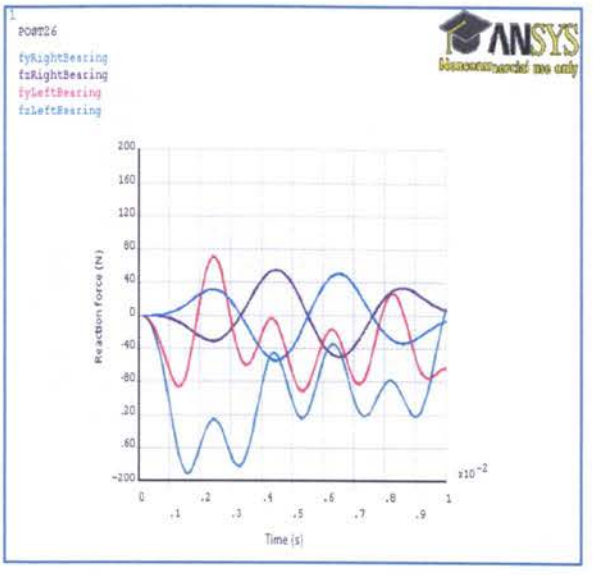

(b)-Reaction force (Fy and Fz) at 3000rpm.

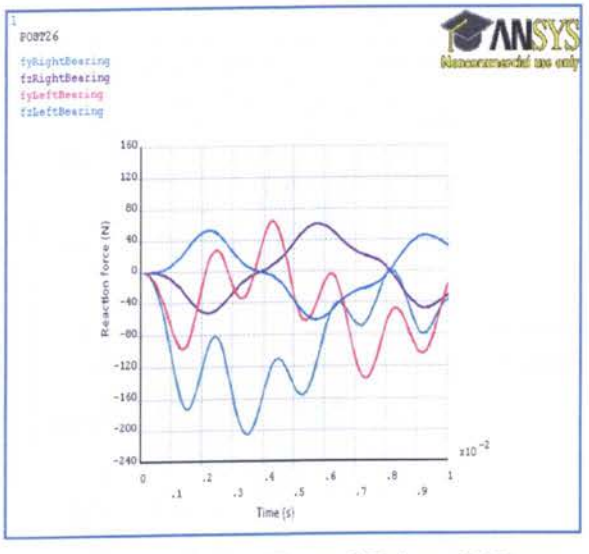

(c)-Reaction force (Fy and Fz) at 6000rpm.

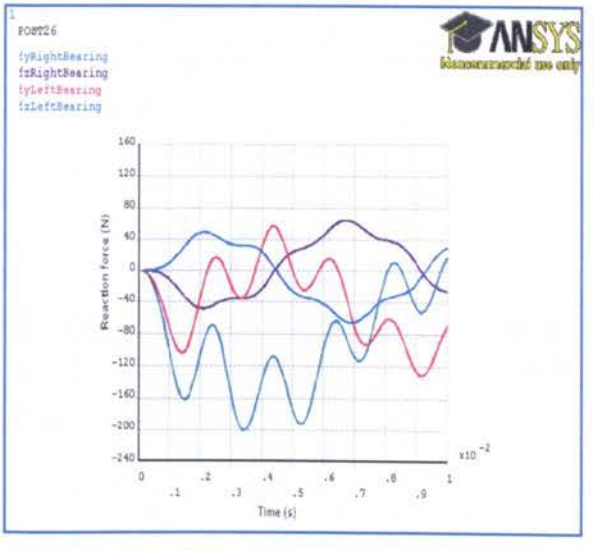

(d)-Reaction force (Fy and Fz) at 10000rpm.

Figure 5.17 Variation of bearings reaction force versus time at different speeds of rotation, one disc in the middle.

5.3.1.3 Effect of unbalance with added mass on bending stress

We find the relationship between the bending stress with time see Figure 5.18a and b, and detect the performance of bending stresses at one disc in the middle when added 8 gram mass on it.

The bending stress decreases in both directions of motion (Y and Z) resulting in reduction of the reaction force in the bearing and subsequent increase in the life of the bearing.

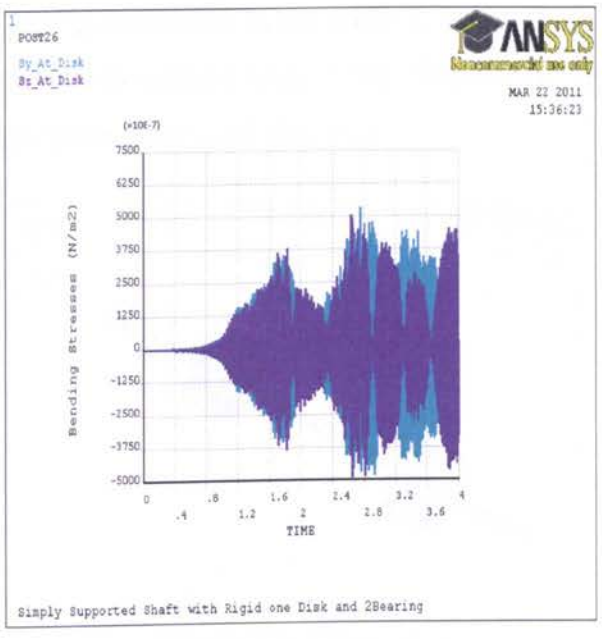

(a)-Before added mass.

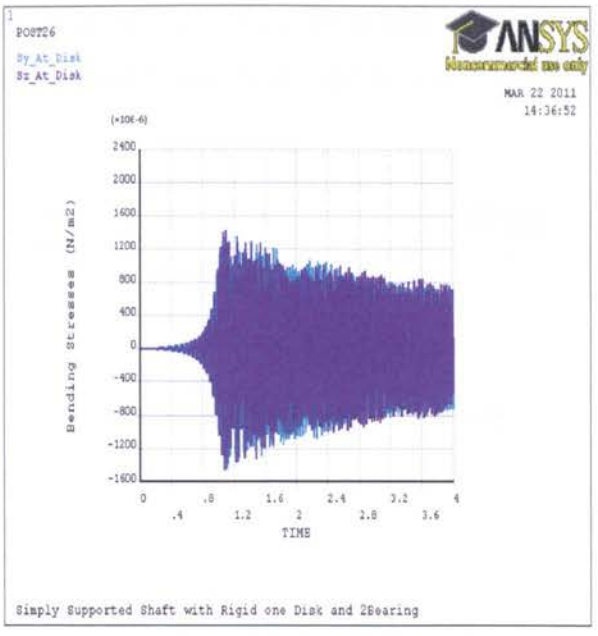

(b)-After added 8 gram mass.

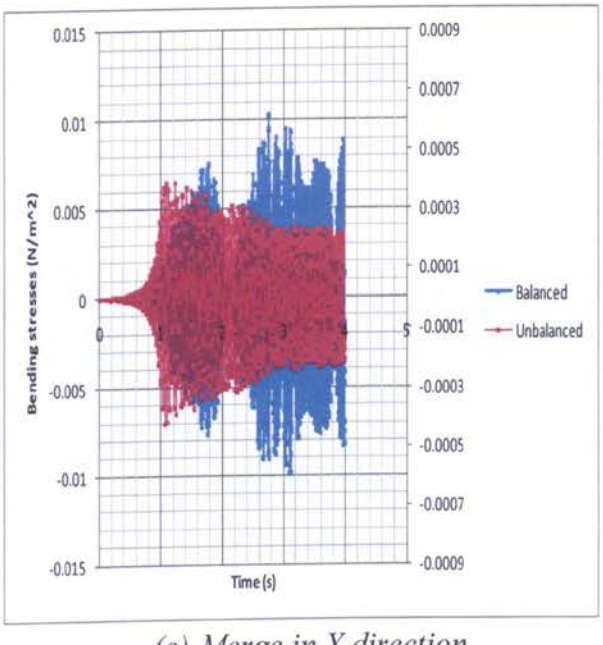

(c)-Merge in Y direction.

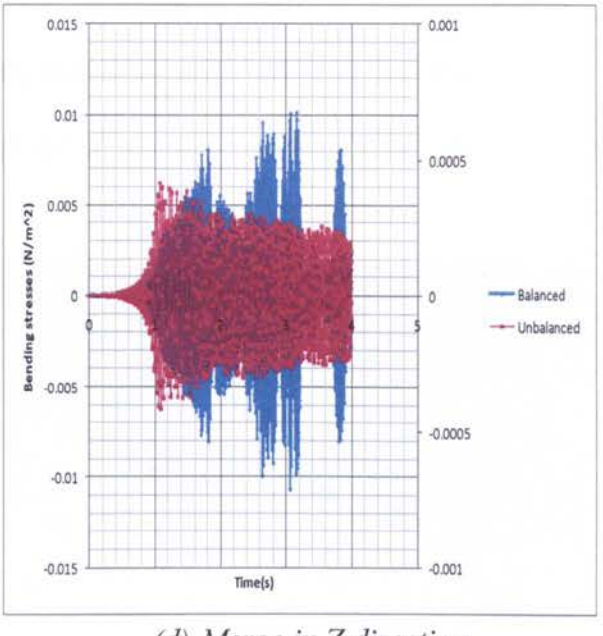

(d)-Merge in Z direction.

Figure 5.18 Relationship between the bending stress with respect to time, one disc.

5.3.2 Finite element model of rotating machinery, two discs

A model of rotor system with two discs and multi degree of freedom model has been used, see Figure 5.19a and b. The excitation frequency is synchronous or asynchronous with the rotational velocity of a structure [159, 161].

As a continuation to the work done for one disc, this section demonstrates how to extract a plane 2-D model Figure 5.19b from the 3-D model Figure 5.19a which can be analyzed using far fewer nodes and elements.

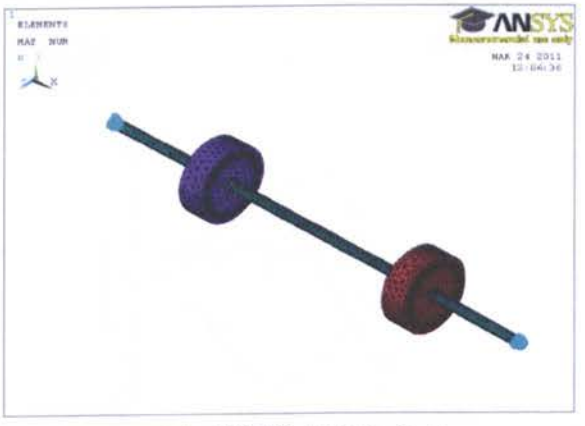

(a)-ANSYS APDL, 3-D.

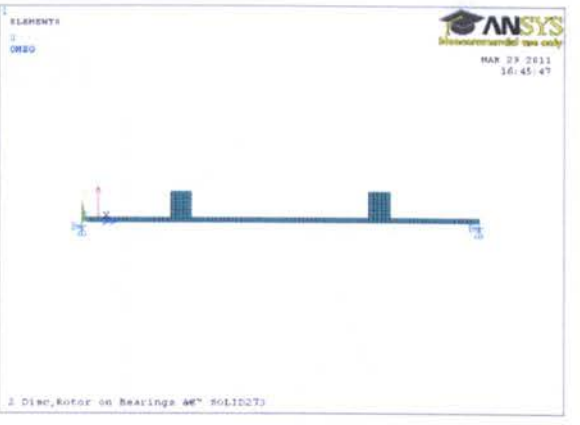

(b)- ANSYS APDL, 2-D.

Figure 5.19 Finite element model of rotating machinery, two discs.

5.3.2.1 ANSYS natural frequency and mode shapes for two discs with two bearings

ANSYS results of natural frequency and mode shape of two discs in the effective length with two bearings have been shown in Figure 5.20.

(a)- First mode shape natural frequency 37.03Hz, 3–D.

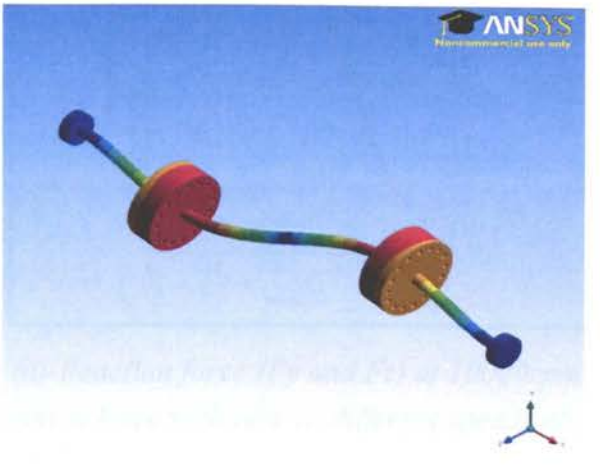

(b)-Second mode shape natural frequency 117.21Hz, 3–D.

Figure 5.20 Finite element simulations, different mode shapes.

5.3.2.2 Reaction forces in the left and right bearings, two discs

The bearings used for supporting rotating machinery are one of the crucial elements by which the safe operation of the machinery is ensured, so in this section we study the bearing behaviour for two discs configuration.

Figure 5.21a-d shows the performance of reaction forces in the right and left bearings at various speeds of rotation. From the figure, the right bearing carry the maximum reaction force.

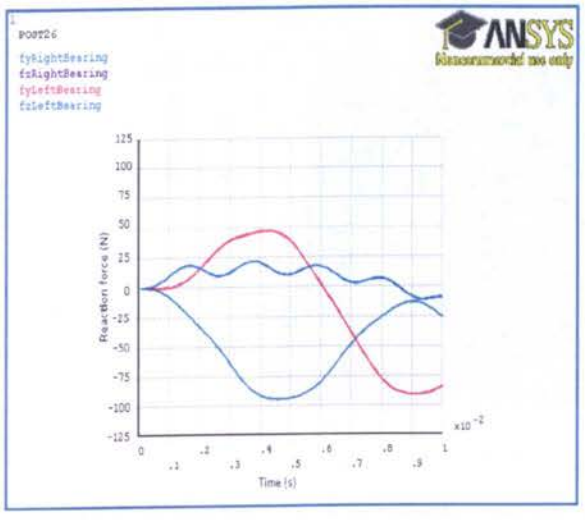

(a)-Reaction force (Fy and Fz) at 1000rpm.

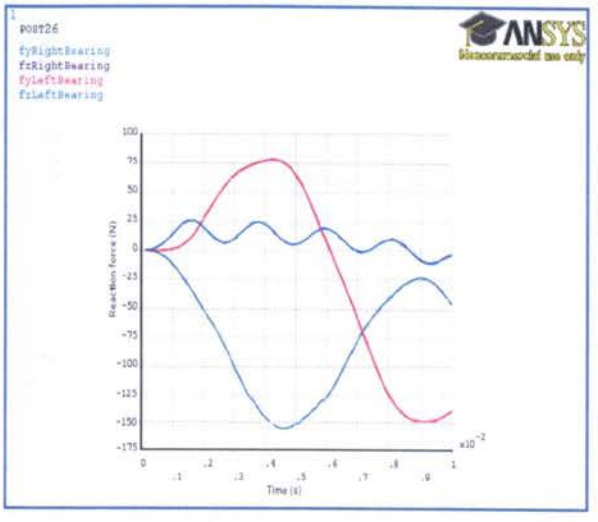

(b)-Reaction force (Fy and Fz) at 3000rpm.

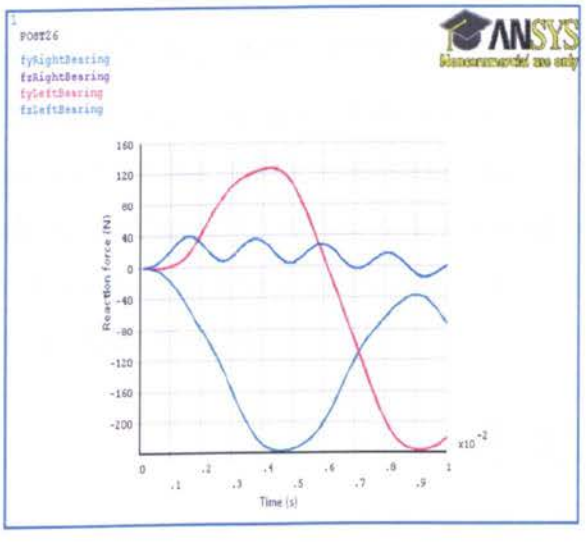

(c)-Reaction force (Fy and Fz) at 6000rpm.

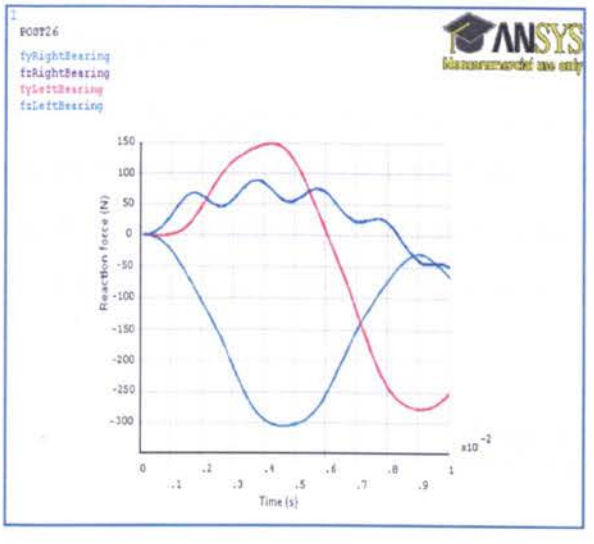

(d)-Reaction force (Fy and Fz) at 10000rpm.

Figure 5.21 Relationship between bearings reaction force with time at different speeds of rotation, two discs.

5.3.2.3 Effect of unbalance with added mass, two discs

ANSYS simulation in Figure 5.22 shows the added 16 gram mass at the same location and configuration performed in modal testing method can reduce the amplitude of vibration. The results and graphs are in agreement with each other in both experimental work and ANSYS simulation models to further verify the accuracy of the work done in chapter 4.

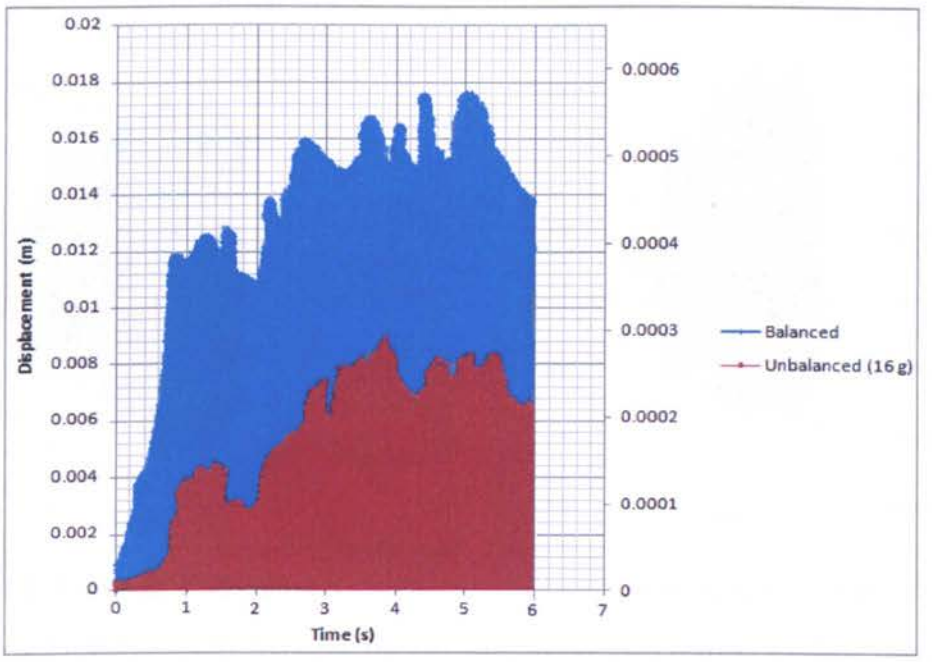

Figure 5.22 Comparison for displacement versus time, without added mass and after added 16 gram mass.

5.3.2.4 Effect of unbalance with added mass on bending stress

The cyclic bending stress is shown in Figure 5.23a and b, the variation of bending stress with time for the two discs configuration and addition of 8 gram at disc 1, and 8 gram at disc 2, are shown in Figure 5.23c and d, it is clearly shown that the bending stress decreases in both directions of motion (Y and Z), that mean reduce the reaction force in the bearing to increase in the life of bearing.

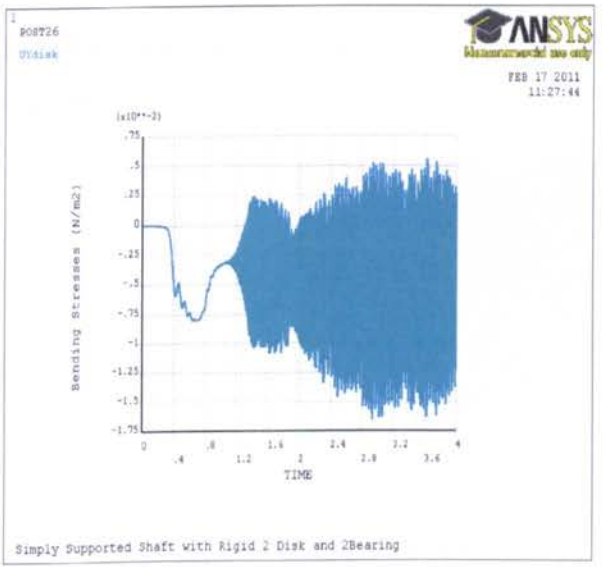

(a)-Before added mass.

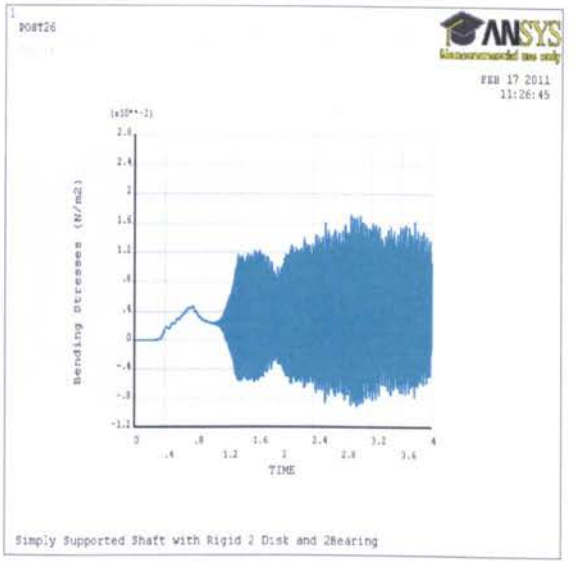

(b)-After added 16 gram mass.

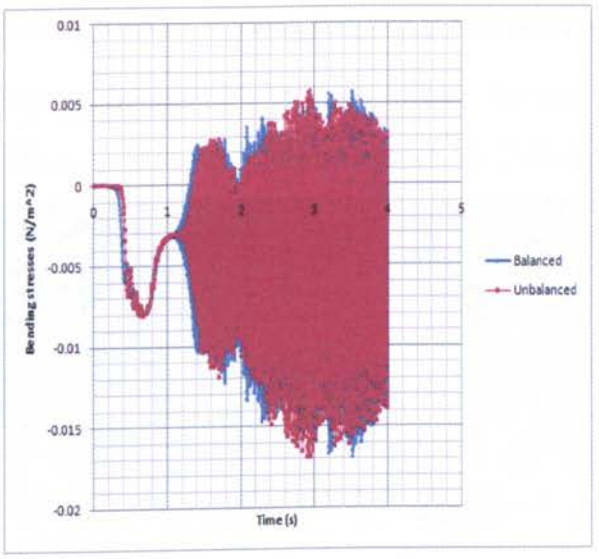

(c)-Merge in Y direction.

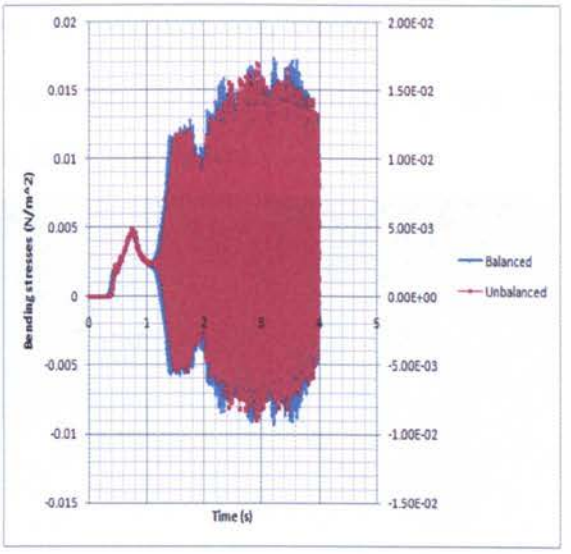

(d)-Merge in Z direction.

Figure 5.23 Relationship between the bending stress with respect to time, two discs.

5.3.3 Finite element model of rotating machinery, overhung disc rotor

A model of rotor system with an overhung disc with multi degree of freedom (Y and Z directions) has been used as shown in Figure 5.24. ANSYS is used to model the system. Campbell diagram is widely used in rotor-dynamics to plot eigen frequencies versus rotating speed RPM and we can find it in other applications such as vibro-acoustics tool, CAMPBELL command was used in input file. Applying the gyroscopic effect to rotating structure was carried out by using CORIOLIS command. This command also applies the rotating damping effect. Synchronous excitation was applied with the rotational velocity of a structure in a harmonic analysis; then Campbell diagram data has been plotted and printed [162-164].

Figure 5.24 Finite element model (overhung geometry).

5.3.3.1 ANSYS natural frequency and mode shapes for overhung configuration

Natural frequency and mode shapes for one disc in the end with two bearings (gyroscopic effect), 3-D in ANSYS workbench are shown in the following figure:

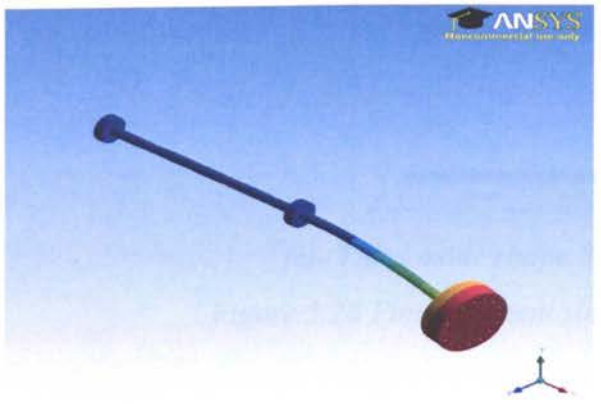

(a)- First mode shape. Natural frequency 15.47 Hz.

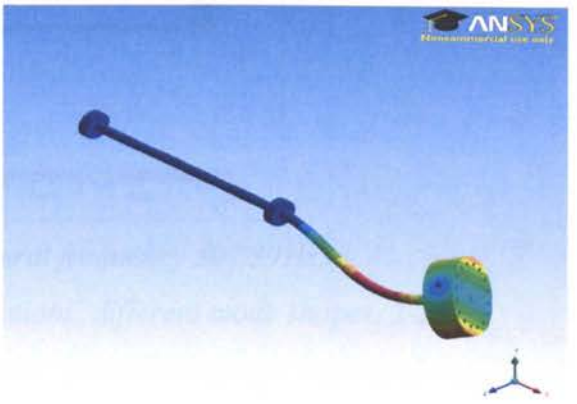

(b)- Second mode shape. Natural frequency 217.01Hz.

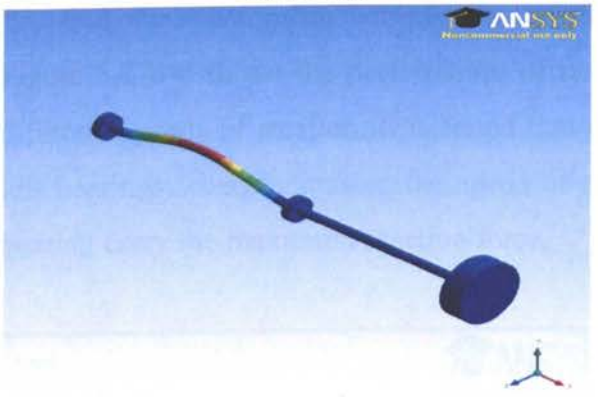

(c)- Third mode shape. Natural frequency. 508.06 Hz

(d)- Fourth. Natural frequency 626.85Hz.

Figure 5.25 Finite element simulations, different mode shapes, 3-D.

While the ANSYS APDL results for one disc in the end with two bearings (gyroscopic effect) in 2-D is shown in Figure 5.26.

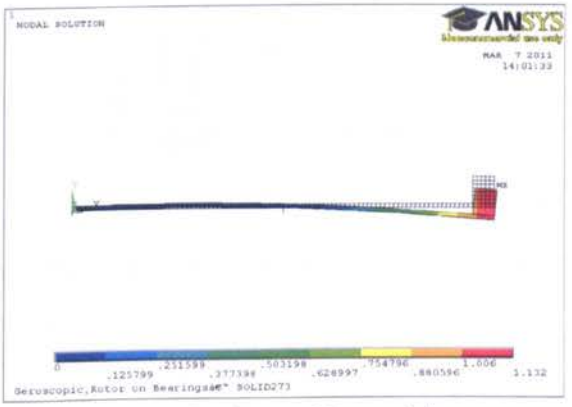

(a)- First mode shape. Natural frequency 15.703 Hz.

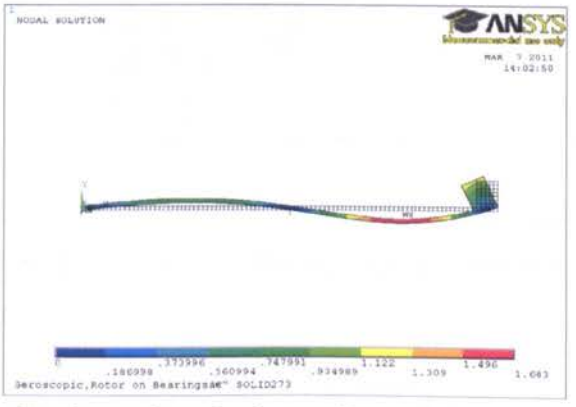

(b)- Second mode shape. Natural frequency 216.8 Hz.

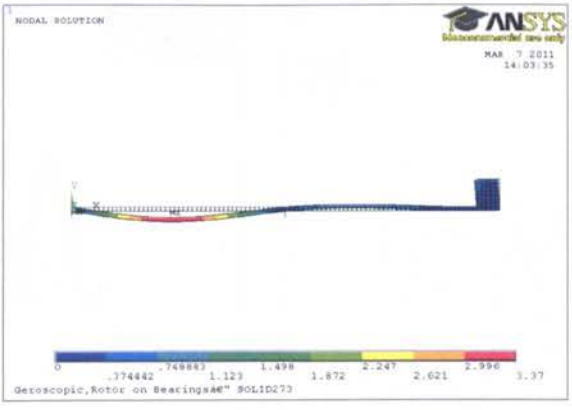

(c)- Third mode shape. Natural frequency 507.39Hz.

Figure 5.26 Finite element simulations, different mode shapes, 2-D.

5.3.3.2 Response forces in the left and right bearings (overhung rotor)

We find the relationship between the reaction forces with time by using FE simulation. Figure 5.27a-d shows the performance of reaction forces in the right and left bearings with different speeds of rotation. It is found that the reaction force increasing for both right and left bearings when increasing the speed of rotation. From the graphs we conclude the left bearing carry the maximum reaction force.

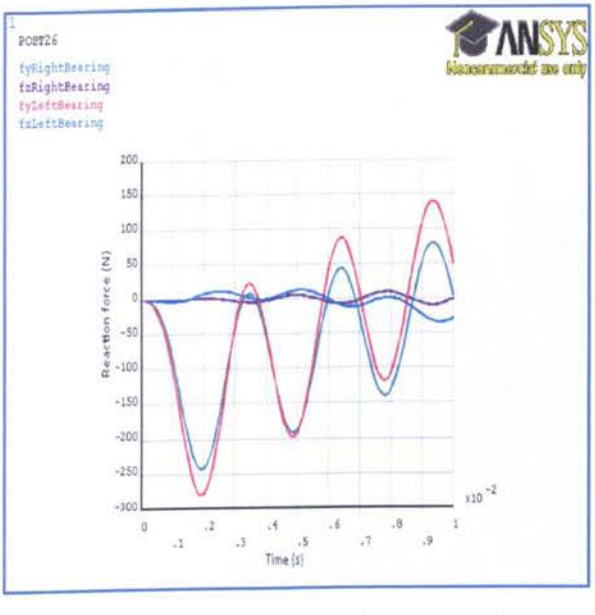

(a)- Reaction force (Fy and Fz) at 1000rpm.

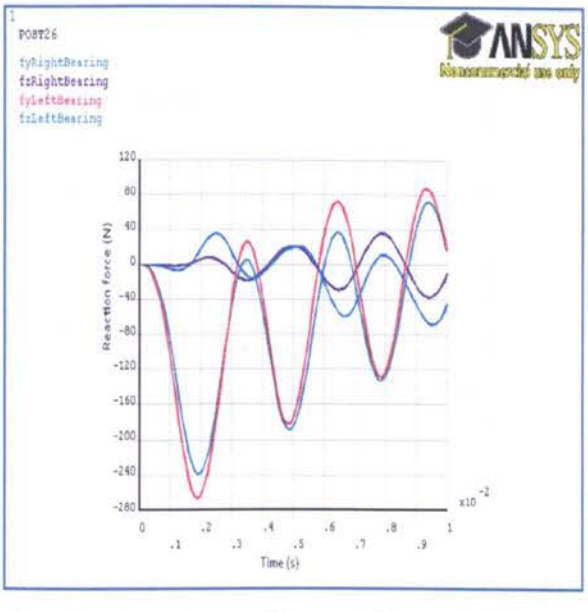

(b)- Reaction force (Fy and Fz) at 3000rpm.

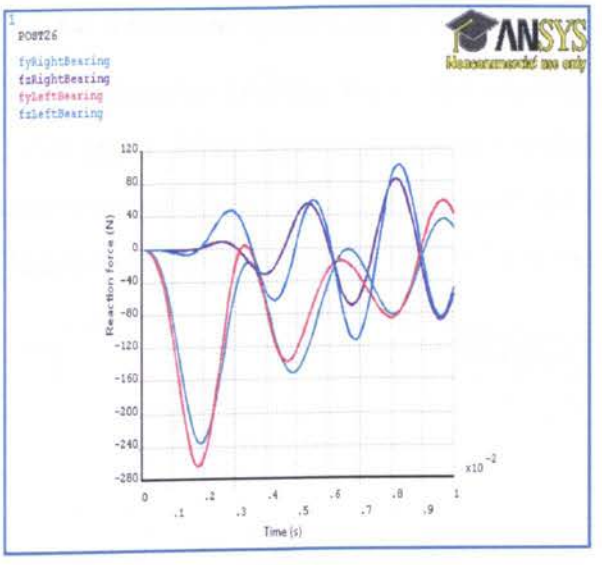

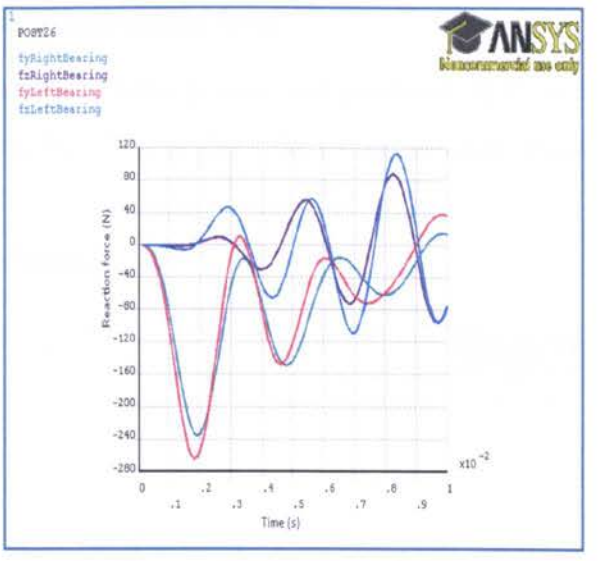

(c)- Reaction force (Fy and Fz) at 6000rpm. *(d)- Reaction force (Fy and Fz) at 10000rpm.*

Figure 5.27 Variation of bearings reaction force versus time at different speeds of rotation, overhung rotor.

5.3.3.3 Unbalance with added mass, simulation results

In this set simulation, unbalance loading of 8 gram mass is applied to the overhung rotor disc system, to prove that the vibration amplitude is reduced when adding unbalance mass. ANSYS simulation of this set is shown in Figure 5.28.

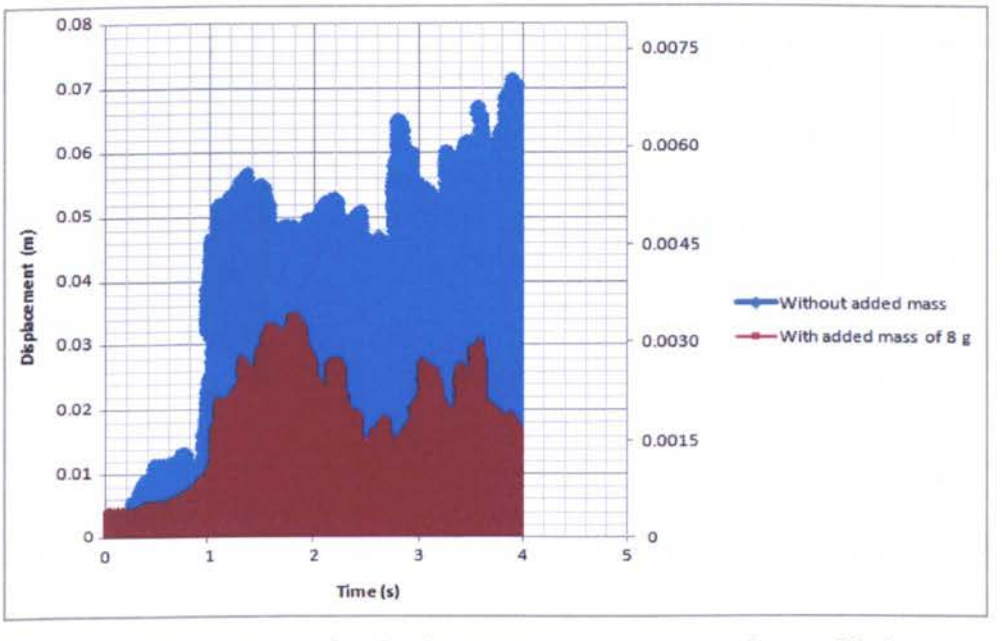

Figure 5.28 Comparison for displacement versus time, without added mass and after added 8 gram mass, overhung rotor.

5.3.3.4 Behaviour of bending stresses in unbalance with added mass

The relationship between the cyclic bending stress with time is obtained as shown in Figure 5.29a and b. When 8 gram mass added to the disc. The figures show the cyclic bending stress decreases in both direction of motion (Y and Z).

That means reduction in the reaction force in the bearing.

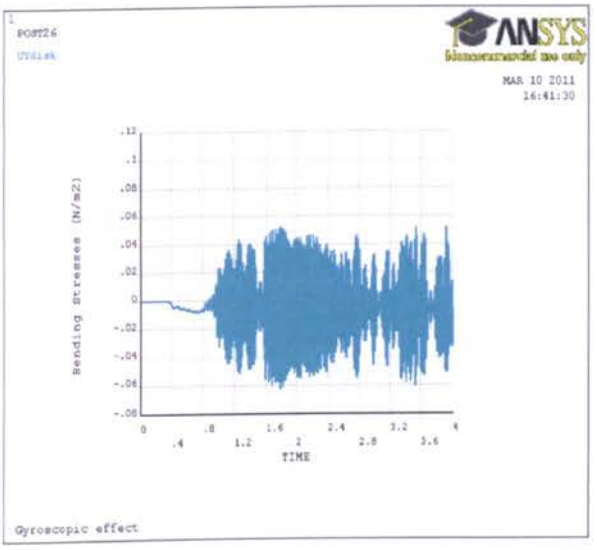

(a)-Bending stresses in Y direction before added mass.

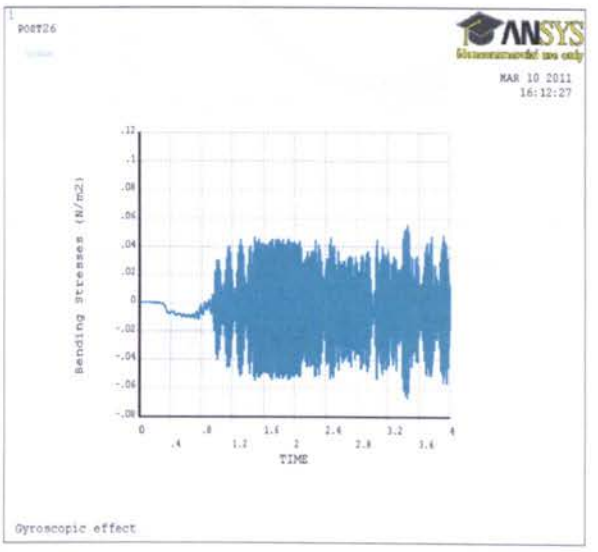

(b)- Bending stresses in Y direction after added 8 gram mass.

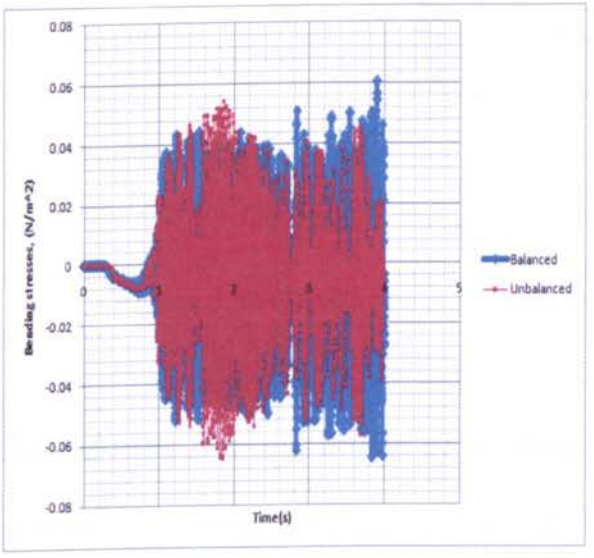

(c)- Merge in Y direction.

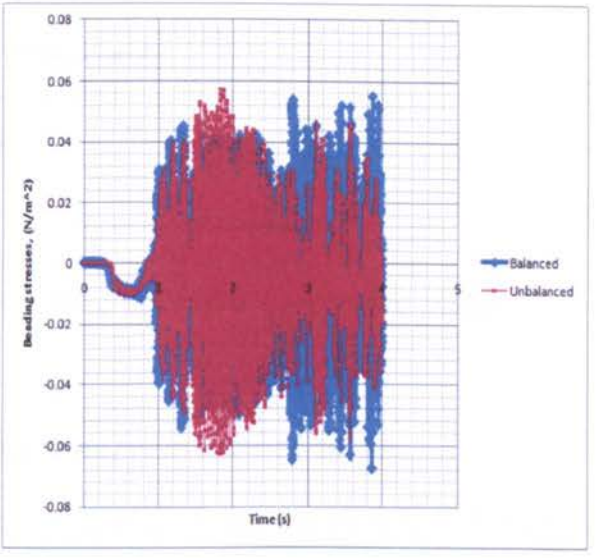

(d)- Merge in Z direction.

Figure 5.29 Relationship between the bending stresses versus time, overhung rotor.

The bending stress sample in Y and Z directions is shown in Figuer 5.30, before and after added 8 gram mass.

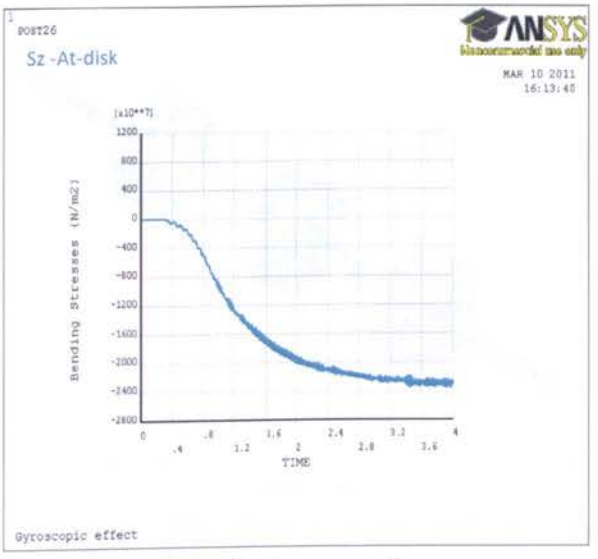

(a)- Sz before added mass.

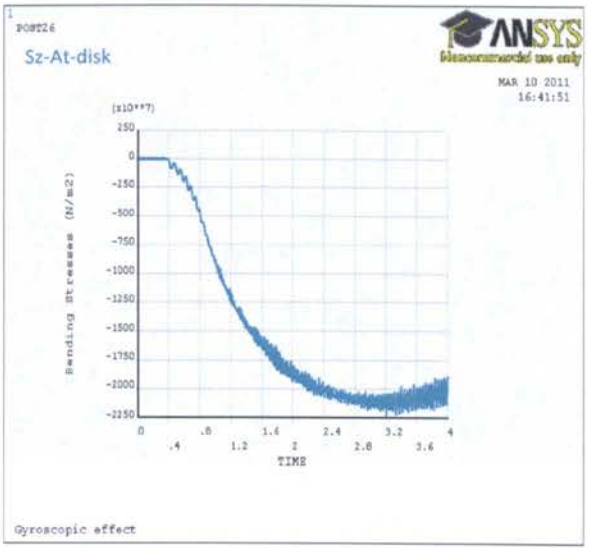

(b)- Sz after added 8 gram mass.

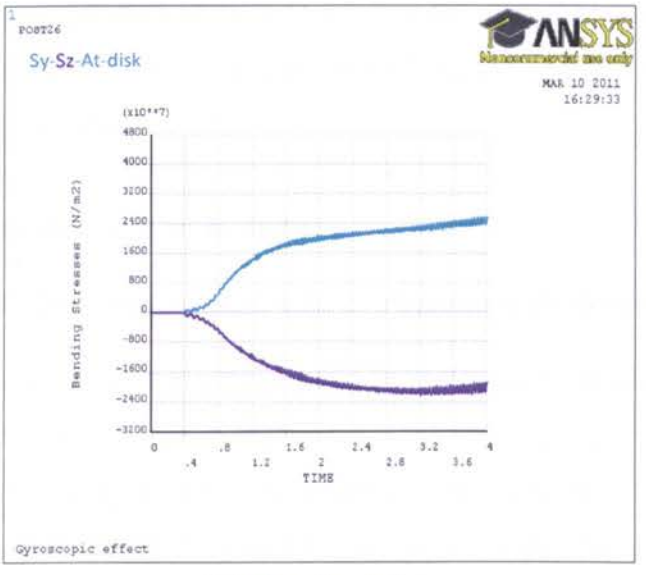

(c)- Sy –Sz at disc.

Figure 5.30 Bending stresses sample in Y and Z directions (gyroscopic effect).

5.3.4 Finite element model of rotating machinery, multidisc rotor

A model of rotor system for identical multidisc has been used, see Figure 5.31. ANSYS 12 has been used as in previous sections. The Finite Element (FE) method used in ANSYS offers an attractive approach to modelling a rotor dynamic system. While it may require more computational resources compared to standard analyses.

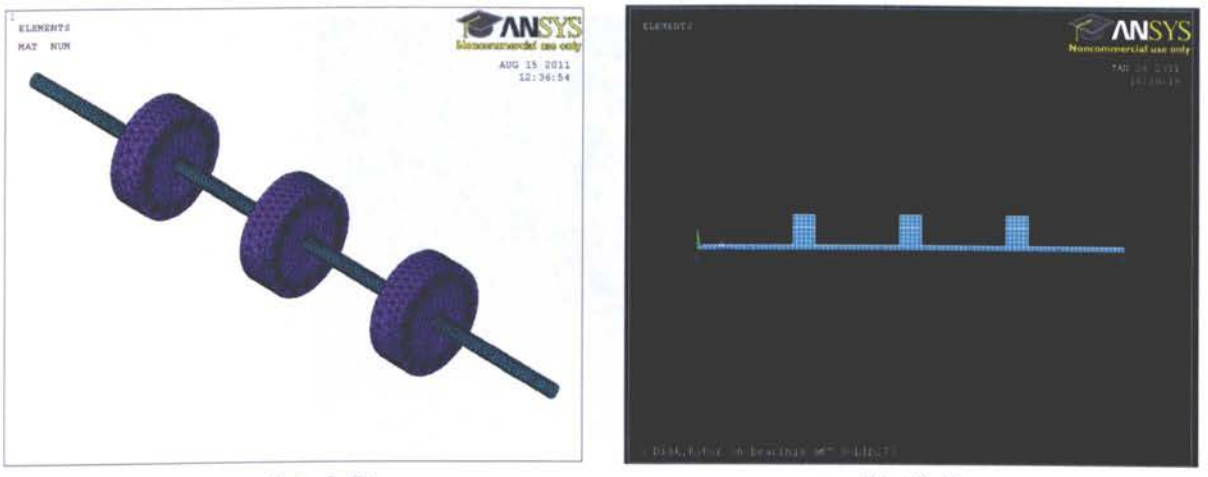

(a)- 3-D. *(b)- 2-D.*

Figure 5.31 Finite element model of rotating machinery (multidisc), ANSYS APDEL, d=75 mm.

A 2-D axisymmetric representation of the 3-D solid model is used to perform a rotor dynamic analysis. The results of the 2-D axisymmetric model analyses Figure 5.31b, agree with the full 3-D solid model results Figure 5.31a.

5.3.4.1 ANSYS analysis for identical multidisc

5.3.4.1.1 Identical multidisc configuration with two bearings, d=75 mm

FE simulation for identical multidisc rotor system have been performed in different cases by using identical three discs of 75 mm in diameter for the first case, and (100, 50) mm for the second and third one to investigate the effect of change mass on the natural frequency values and mode shapes. Several natural frequencies and mode shapes have been calculated; the results of 2-D model analysis are in a good agreement with 3-D model results.

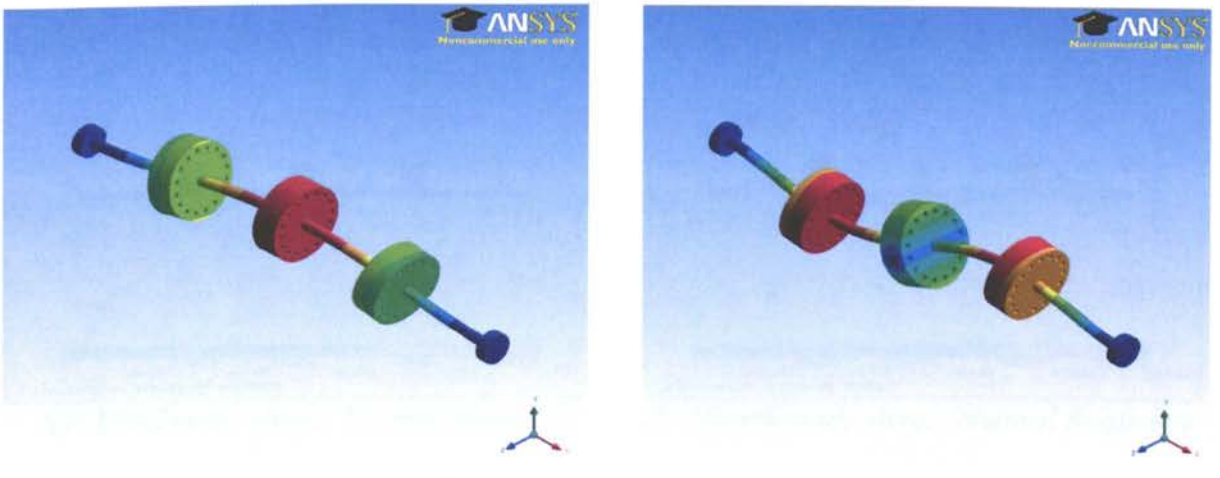

(a)- First mode shape. Natural frequency 28.77 Hz. *(b)- Second mode shape. Natural frequency 116.06 Hz.*

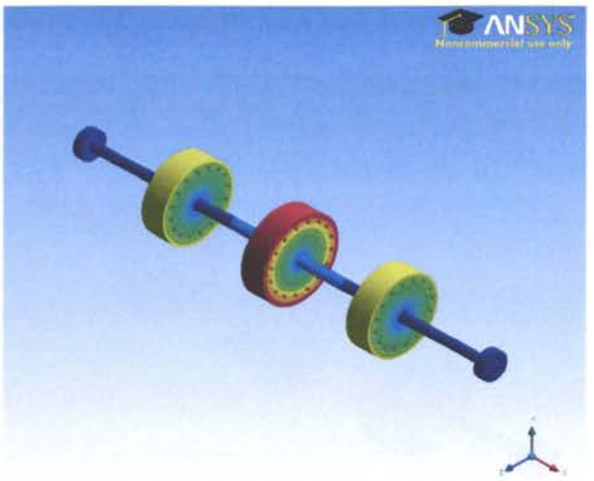

(c)- Third mode shape. Natural frequency 191.88 Hz.

Figure 5.32 Finite element simulations, identical multidisc with different mode shapes, ANSYS workbench, 3-D, d=75 mm.

(a)- First mode shape. Natural frequency 28.56 Hz.

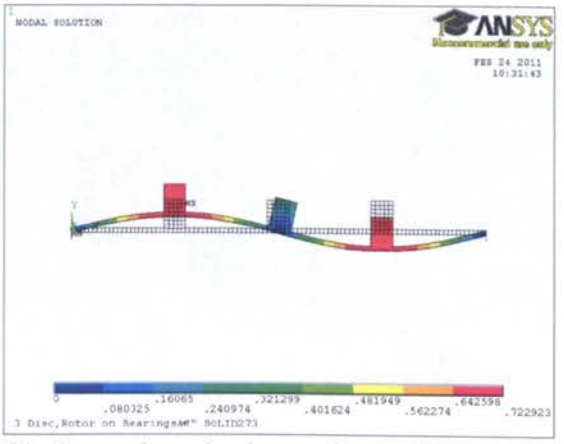

(b)- Second mode shape. Natural frequency 115.2 Hz.

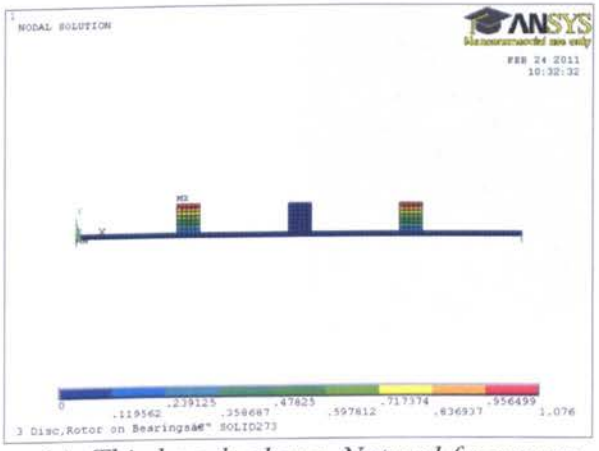

(c)- Third mode shape. Natural frequency 191.41Hz.

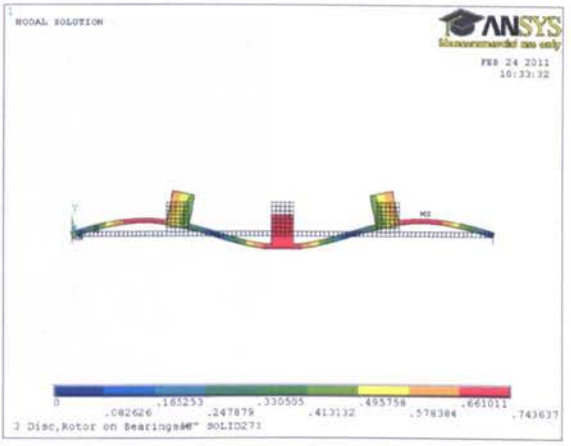

(d)- Fourth mode shape. Natural frequency 260.21Hz.

Figure 5.33 Finite element simulations, different mode shapes, ANSYS APDL, 2-D, d=75 mm.

5.3.4.1.2 Identical multidisc configuration with two bearings, d=100 mm

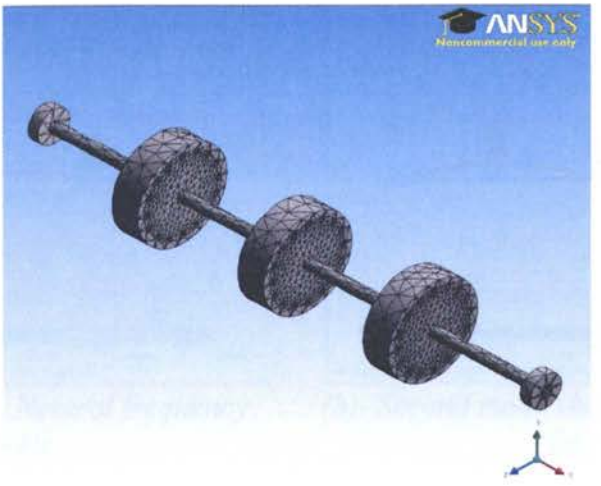

Figure 5.34 Finite element model of rotating machinery (multidisc), ANSYS workbench, 3-D, d=100 mm.

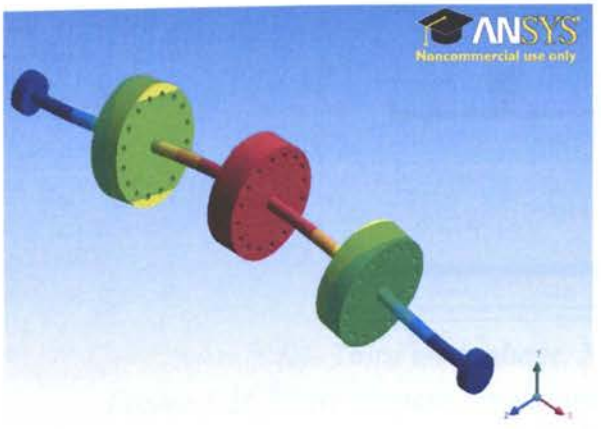

(a)- First mode shape. Natural frequency 21.03 Hz.

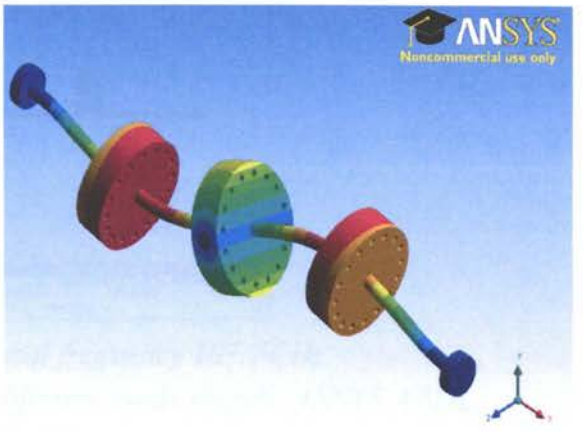

(b)- Second mode shape. Natural frequency 85.95 Hz.

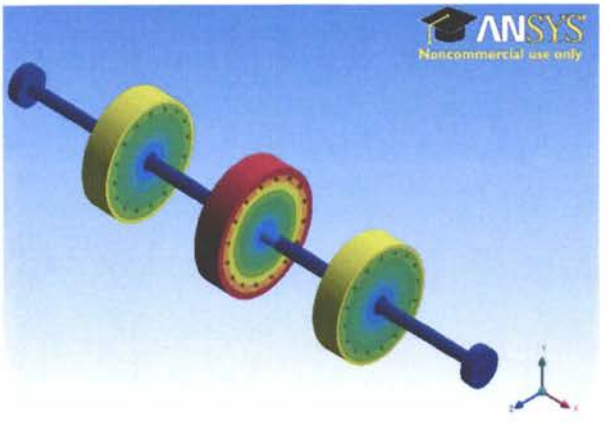

(c)- Third mode shape. Natural frequency 108.01 Hz.

Figure 5.35 Finite element simulations, identical multidisc with different mode shapes, ANSYS workbench, 3-D, d=100 mm.

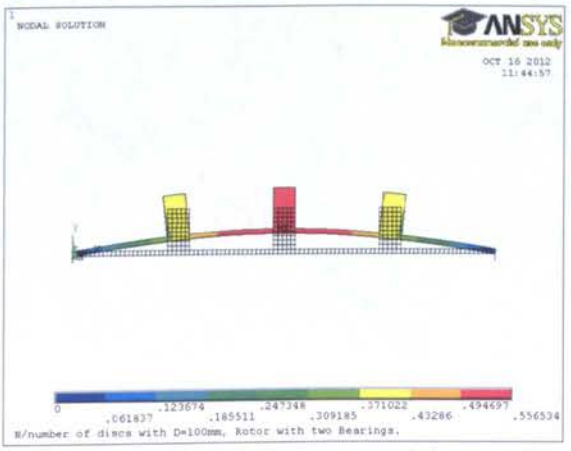

(a)- First mode shape. Natural frequency 21.66 Hz.

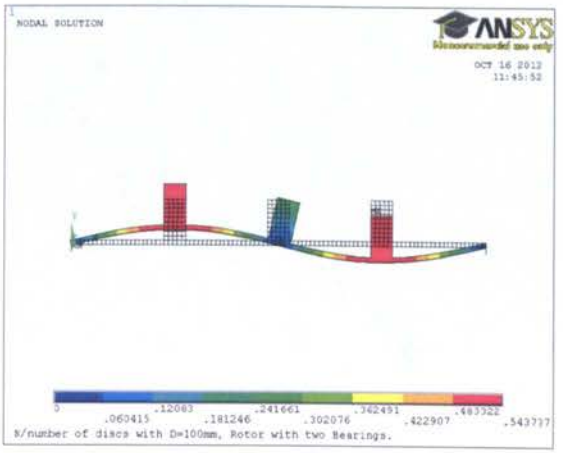

(b)- Second mode shape. Natural frequency 86.619 Hz.

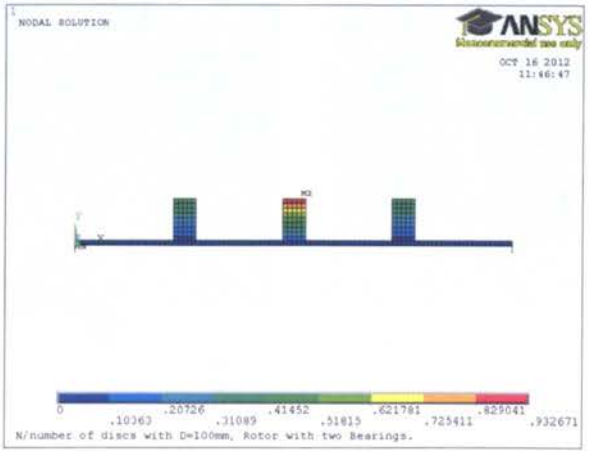

(c)- Third mode shape. Natural frequency 107.74 Hz.

Figure 5.36 Finite element simulations, different mode shapes, ANSYS APDL, 2-D, d=100 mm.

5.3.4.1.3 Identical multidisc configuration with two bearings, d=50 mm

Figure 5.37 Finite element model of rotating machinery (multidisc), ANSYS workbench, 3-D, d=50 mm.

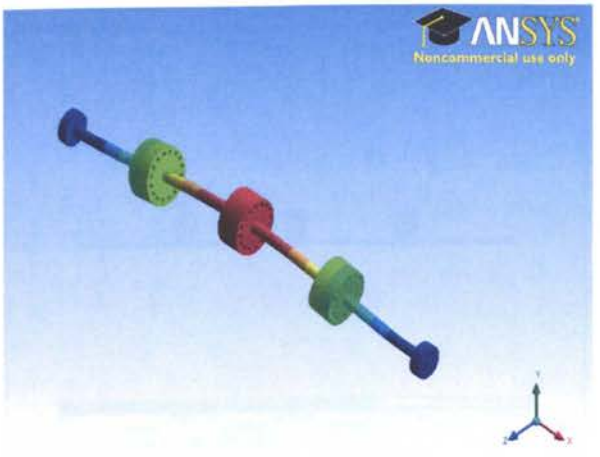

(a)- First mode shape. Natural frequency 40.83 Hz.

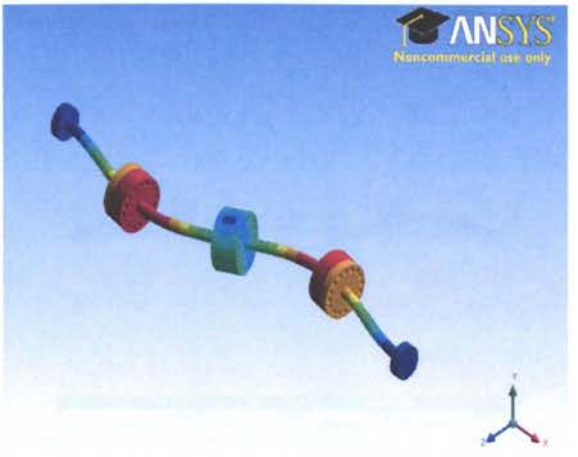

(b)- Second mode shape. Natural frequency 166.88 Hz.

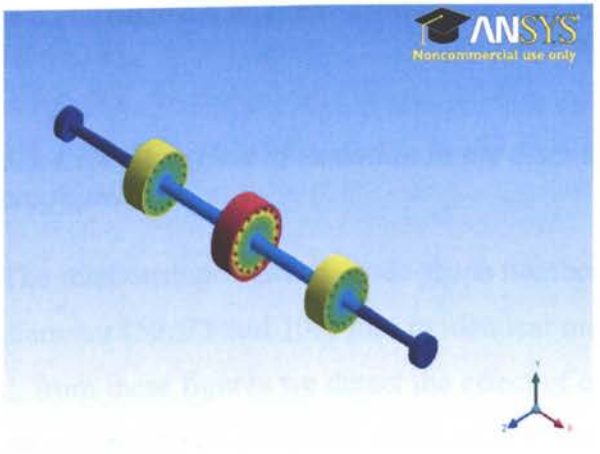

(c)- Third mode shape. Natural frequency 380.22 Hz.

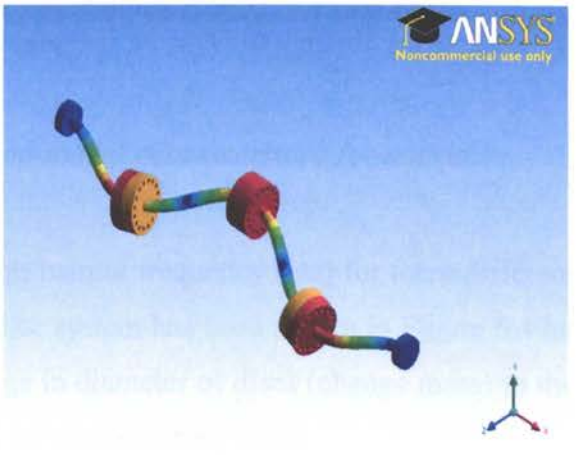

(d)- Fourth mode shape. Natural frequency 560.21Hz.

Figure 5.38 Finite element simulations, identical multidisc with different mode shapes, ANSYS workbench, 3-D, d=50 mm.

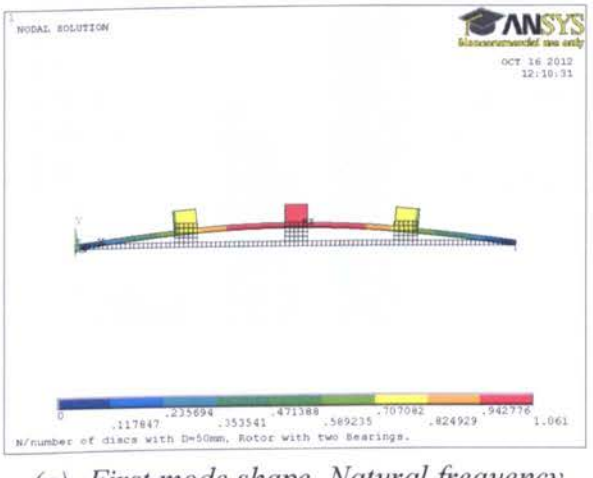

(a)- First mode shape. Natural frequency 41.302 Hz.

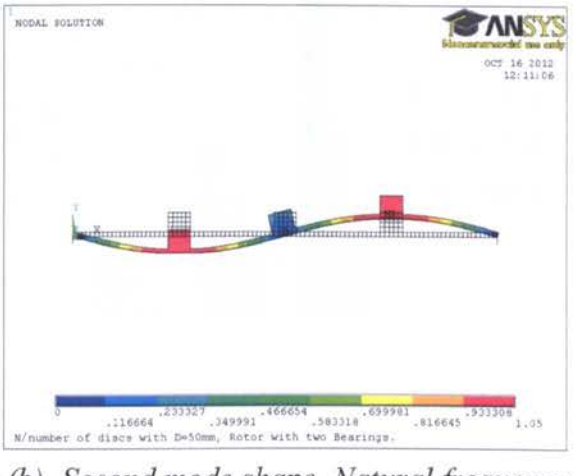

(b)- Second mode shape. Natural frequency 167.39 Hz.

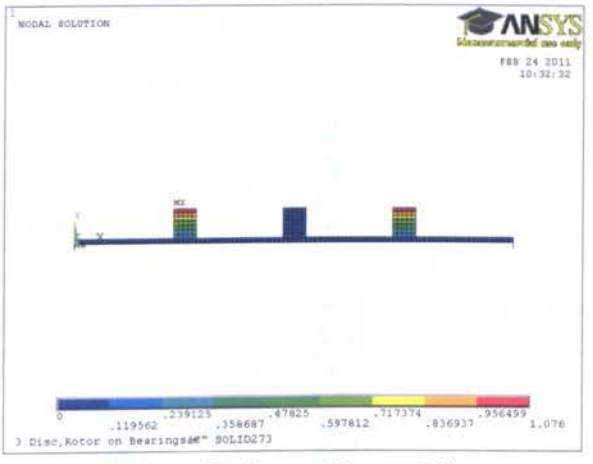

(c)- Third mode shape. Natural frequency 381.48 Hz.

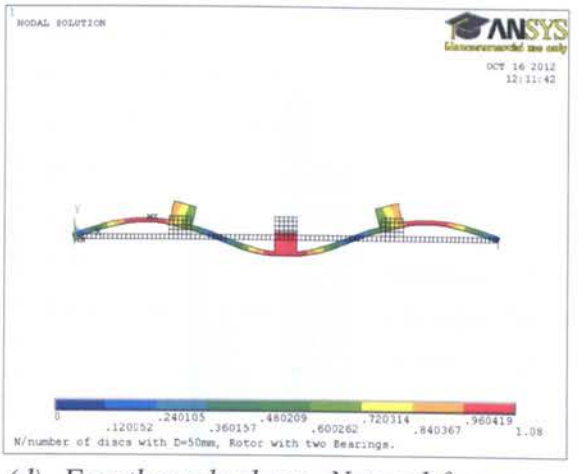

(d)- Fourth mode shape. Natural frequency 562.21Hz.

Figure 5.39 Finite element simulations, different mode shapes, ANSYS APDL, 2-D, d=50 mm.

5.3.4.1.4 The effect of variation in the discs size on modal characteristics for multidisc configuration

The relationship between mode shape number with natural frequency (Hz) for three different diameter (50, 75 and 100) mm in identical multidisc system has been shown in Figure 5.40a-d, from these figures we detect the effect of change in diameter of discs (change mass) to the natural frequency and mode shape on one, two, three and overhung discs.

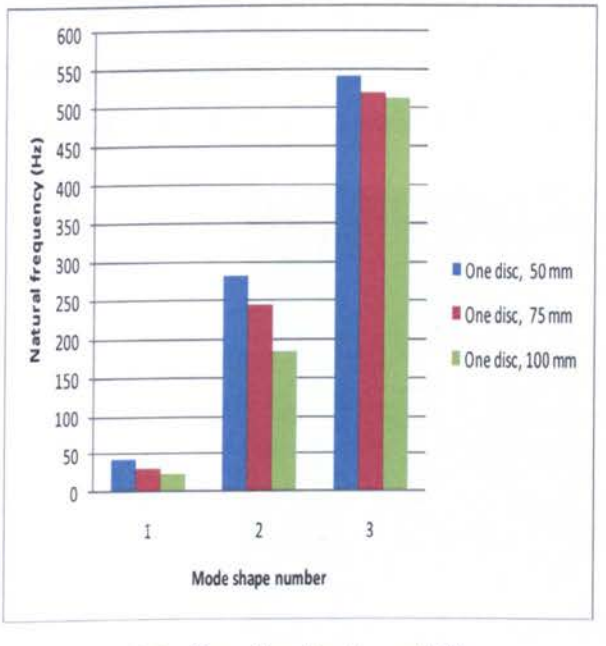

(a)- One disc in the middle.

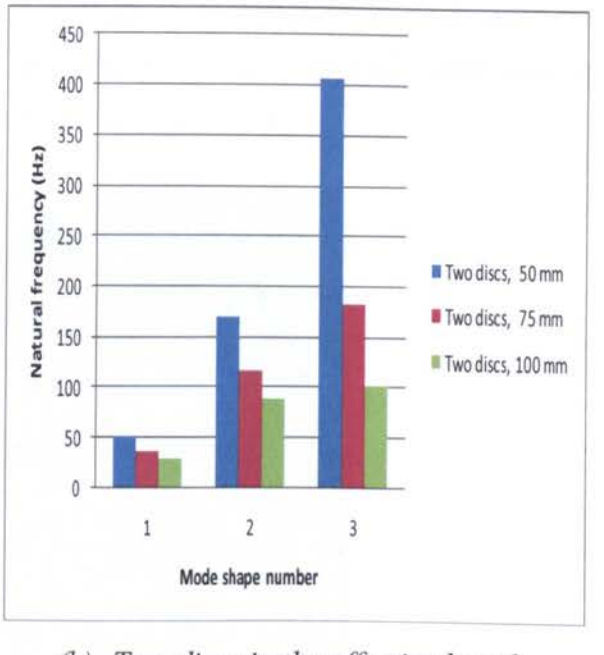

(b)- Two discs in the effective length.

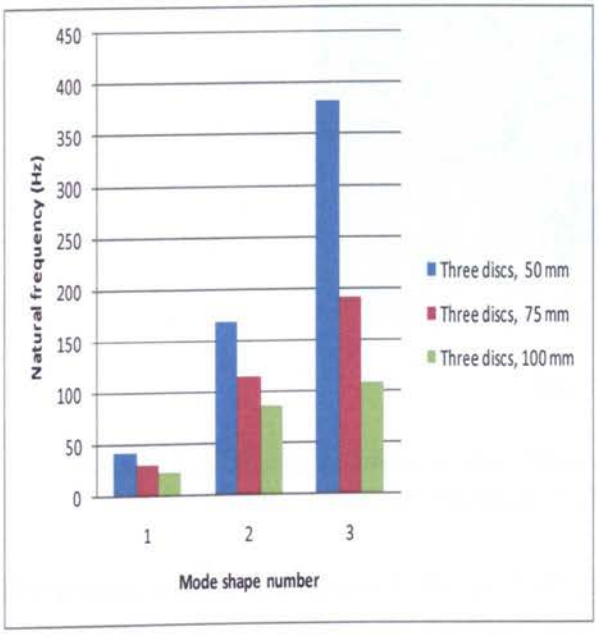

(c)- Three discs in effective length.

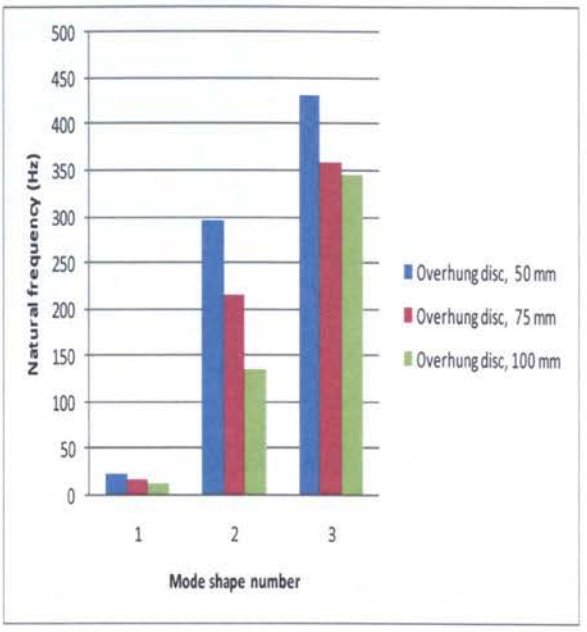

(d)- Overhung disc.

Figure 5.40 Relationship between mode shape number versus natural frequency with different discs masses.

5.3.4.2 ANSYS analysis for rotor system (multistage) with different dimensions and geometry definition

5.3.4.2.1 Identification of natural frequency and mode shape for multidisc with different dimensions and geometry definition

We can extend our study to detect the behaviour of more complicated systems used for various industrial applications, see Figure 5.41, by developing the model with multidisc of different dimensions and geometry definition as shown in Figure 5.42.

Figure 5.41 Turbine, one example of multidisc rotor systems [126, 165].

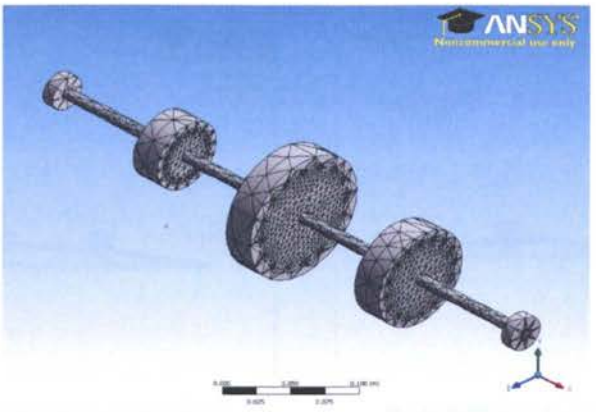

Figure 5.42 Finite element model, rotating machinery (multidisc) with different dimensions and geometry definition, ANSYS workbench, 3-D.

The results shown in Figures 5.43 and 5.44 are natural frequencies and mode shapes of 2-D models which are in agreement with the results of 3-D models giving further insights into the work carried out in this thesis for using FE simulation method for validation.

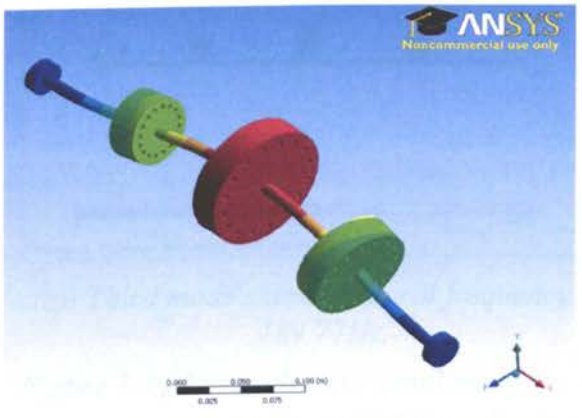

(a)- First mode shape. Natural frequency 27.33 Hz.

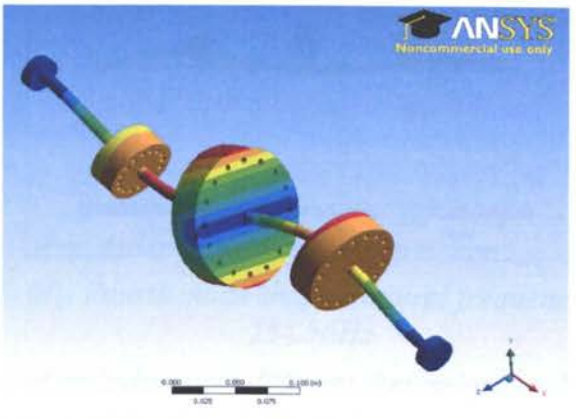

(b)- Second mode shape. Natural frequency 116.88 Hz.

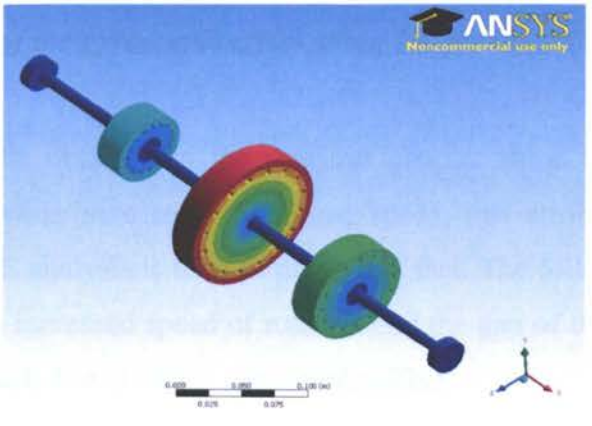

(c)- Third mode shape. Natural frequency 190.51 Hz.

Figure 5.43 Finite element simulations for rotor of multidisc with different dimensions and geometry definition, different mode shapes, ANSYS workbench, 3-D.

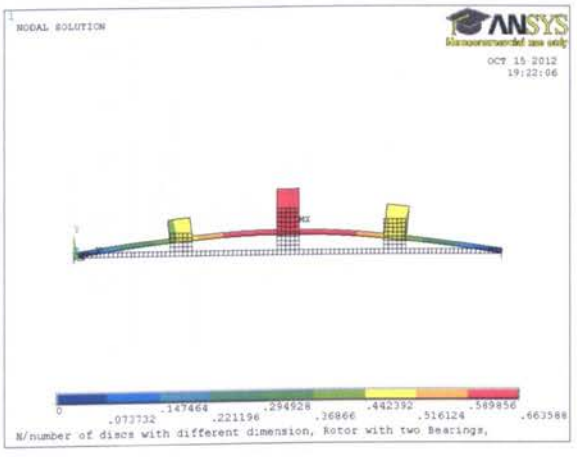

(a)- First mode shape. Natural frequency 27.72 Hz.

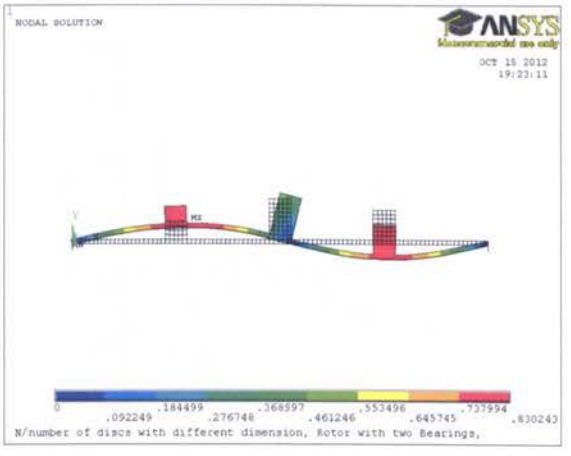

(b)- Second mode shape. Natural frequency 117.55 Hz.

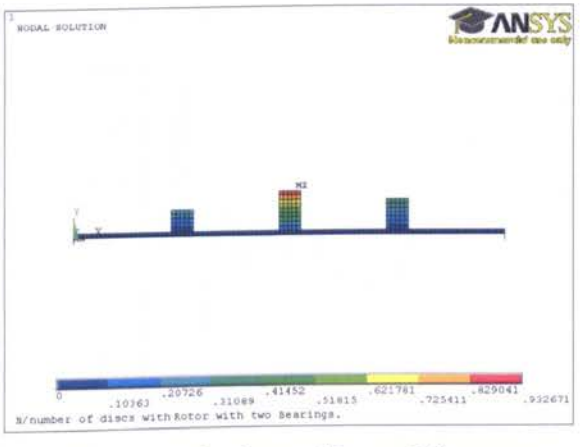

(c)- Third mode shape. Natural frequency 189.77Hz.

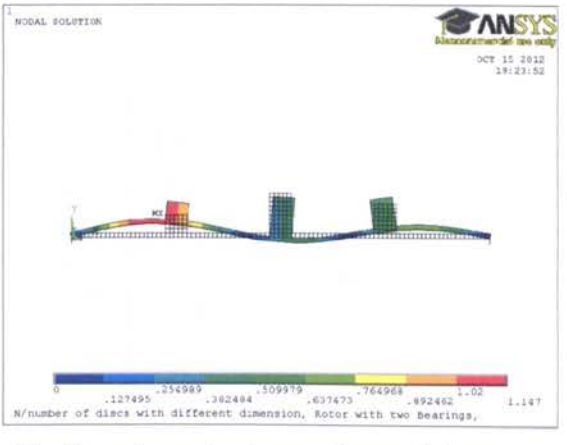

(d)- Fourth mode shape. Natural frequency 254.56Hz.

Figure 5.44 Finite element simulations for rotor of multidisc with different dimensions and geometry definition, different mode shapes, ANSYS APDL, 2-D.

5.3.4.2.2 Identification of the gyroscopic effect using FE for multidisc with different dimensions

The modal testing results obtained in the previous chapter show that the split of natural frequencies widens up with increase in rotational speed, this attributed to the gyroscopic effect. In this chapter, FE analysis is used to prove this fact. The following figures show that the FRF curve split with increased speed of rotation and the gap of this split increased as the speed of rotation increased, due to strong gyroscopic effect.

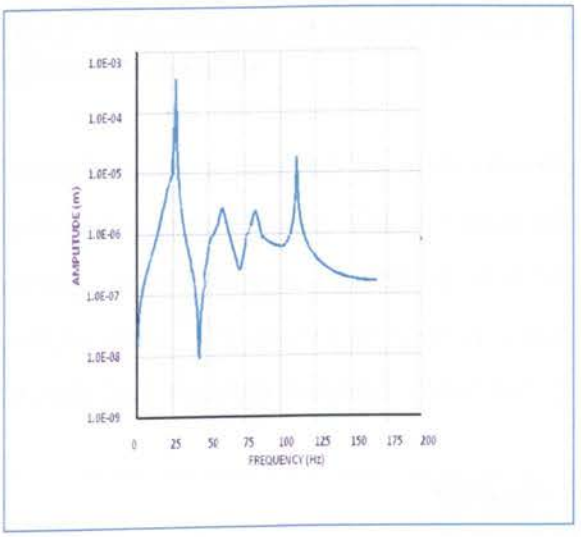

(a)- At speed 30 rpm.

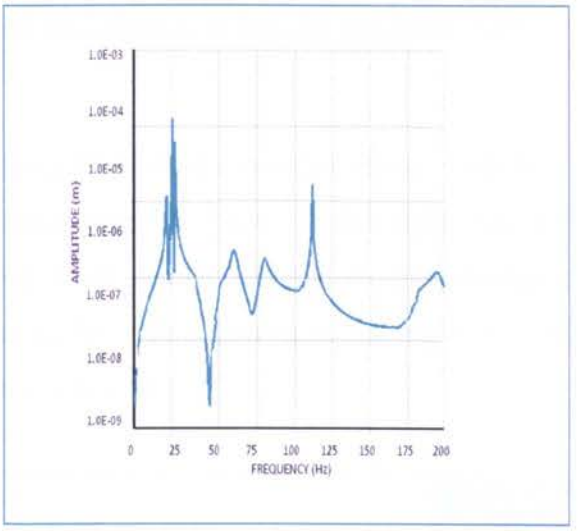

(b)- At speed 1000 rpm.

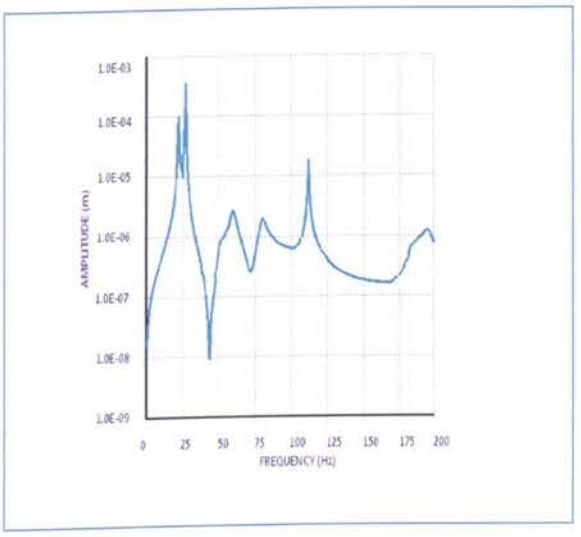

(c)- At speed 2000 rpm.

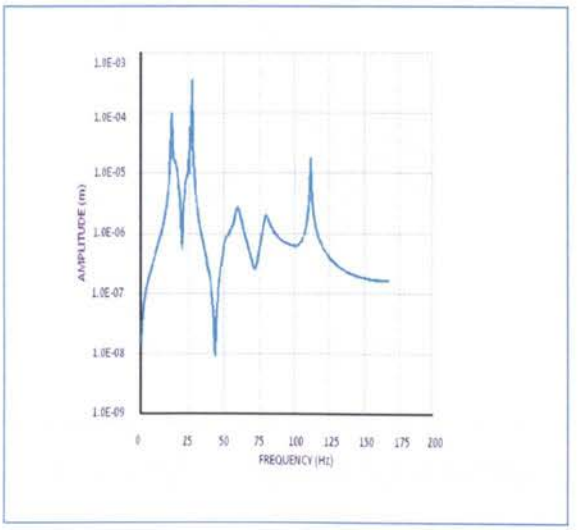

(d)- At speed 4000 rpm.

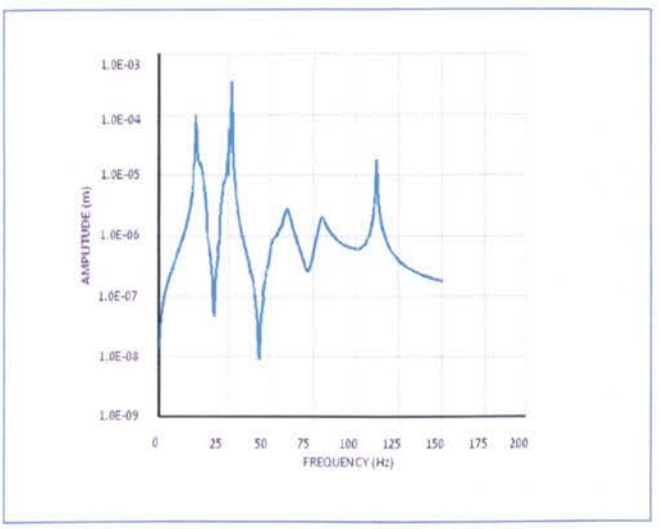

(e)- At speed 6000 rpm.

Figure 5.45 FE simulation results show frequency response function curve, FRF versus natural frequency (Hz), for different speeds of rotation.

5.3.4.2.3 Performance of reaction forces in the left and right bearings for multidisc with different dimensions

Through further simulation we obtain the relationship between the reaction forces with time. From the Figure 5.46a-d, the behavior of dynamic reaction forces in the right and left bearings with different speeds of rotation have been shown in this model (multidisc configuration). The maximum reaction force value in the Y direction right bearing that mean the right bearing carry maximum load during the rotor run up.

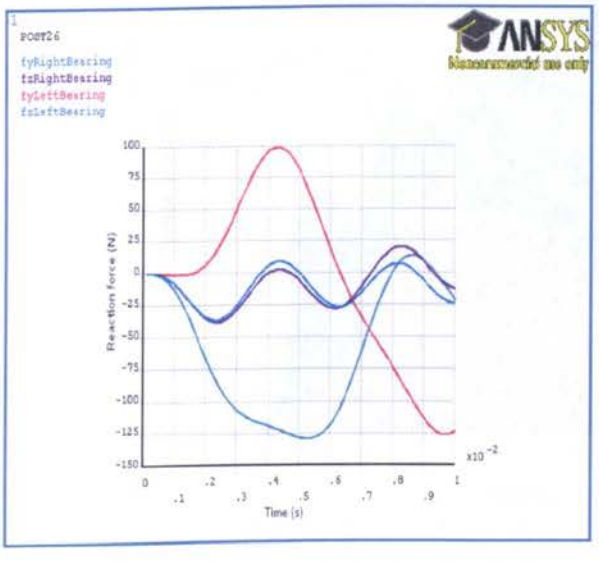

(a)- Reaction force (Fy and Fz) at 1000rpm.

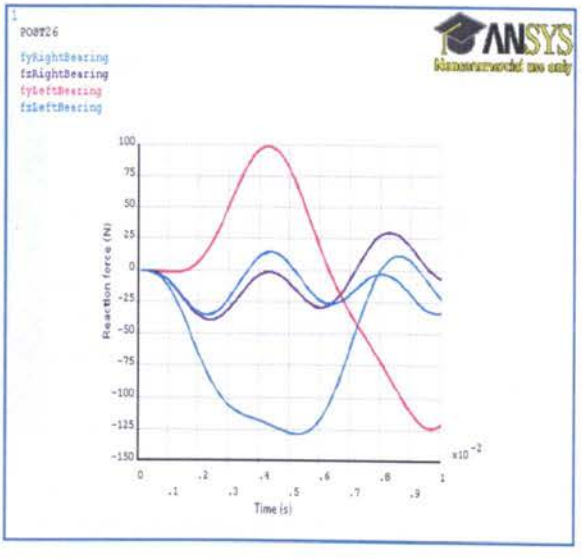

(b)- Reaction force (Fy and Fz) at 3000rpm.

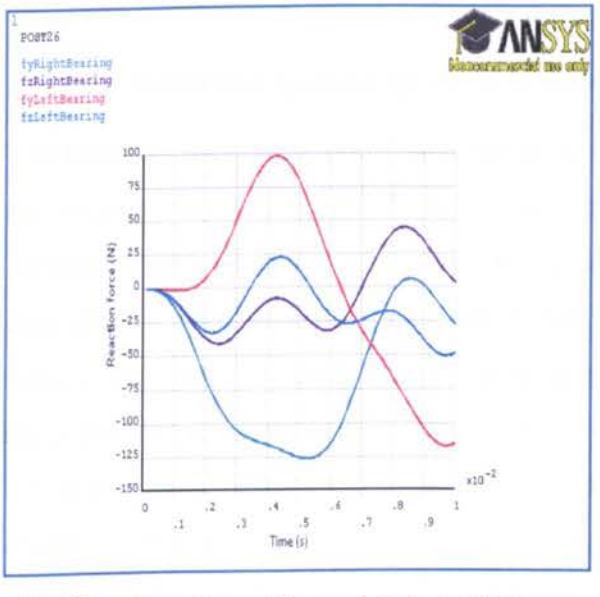

(c)- Reaction force (Fy and Fz) at 6000rpm.

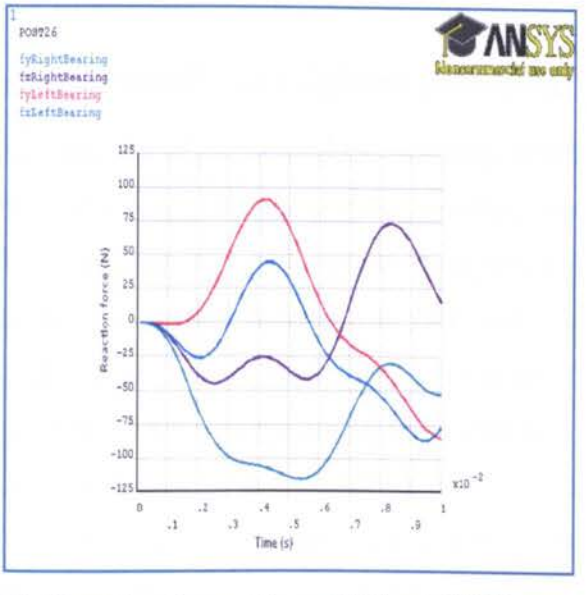

(d)- Reaction force (Fy and Fz) at 10000rpm.

Figure 5.46 Relationship between bearings reaction force versus time at different speeds of rotation, multidisc configuration.

5.3.4.2.4 Unbalance on multistage model with different dimensions and geometry definition

ANSYS simulations in Figure 5.47 show that when added 24 gram mass to the system (8 gram per each disc), the displacement of vibration is reducing by 0.9×10^{-2} m at the same speed of rotation.

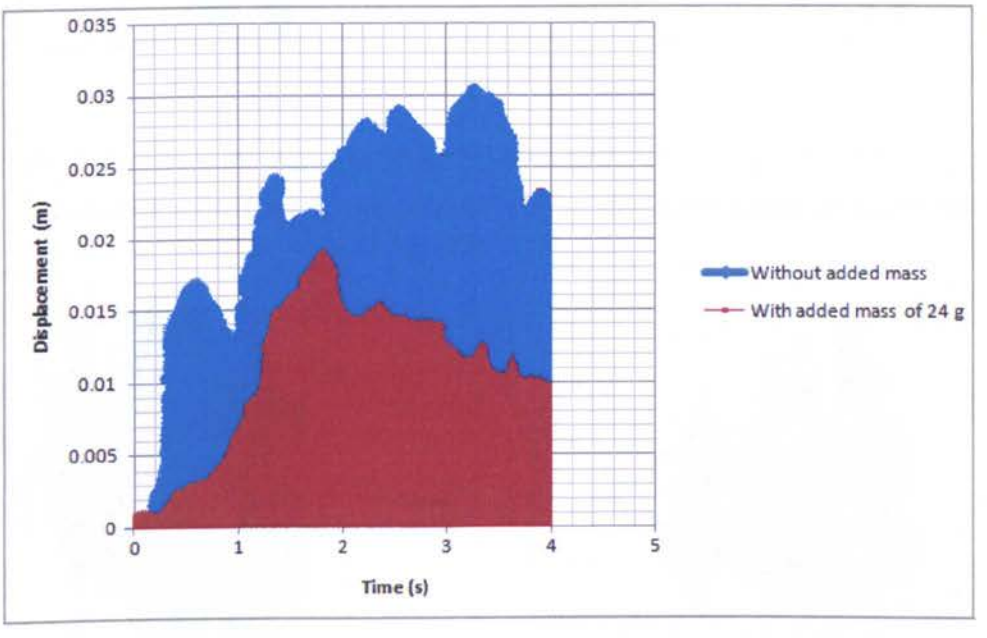

Figure 5.47 Comparison for displacement versus time, without added mass and after added 24 gram mass, multidisc.

5.3.4.2.5 Behaviour of bending stress in unbalance for multidisc with different dimensions

The bearings used for supporting rotating machinery are one of the crucial elements by which the safe operation of the machinery is ensured. In recent years, with continuing demands for increased performance, many rotating industrial machines are now being designed for operation at high speed, a trend which has resulted in increased mechanical vibration and noise problems [153, 166]. So, the cyclic bending stress has been studied. Figure 5.48a and b show the variation of bending stress with time for the multidisc configuration and addition of 24 gram mass on discs (8 gram in disc 1, 8 gram in middle disc 2, and 8 gram in disc 3). It is clearly shown that decreases in both direction of motion (Y and Z), that mean reduction in the reaction force in the bearing to increase the life of bearing and also support the results obtained from FE simulations at Figures 5.18, 5.23 and 5.29.

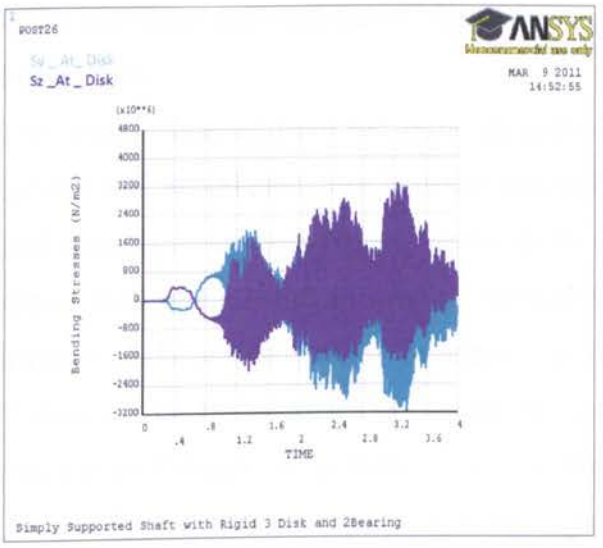

(a)- Before added mass.

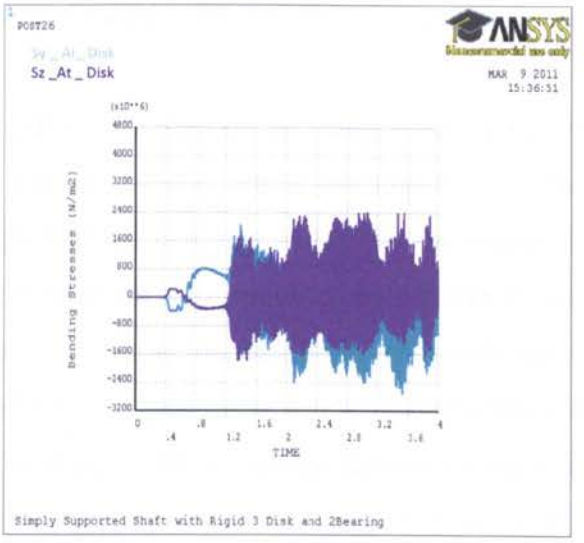

(b)- After added 24 gram mass.

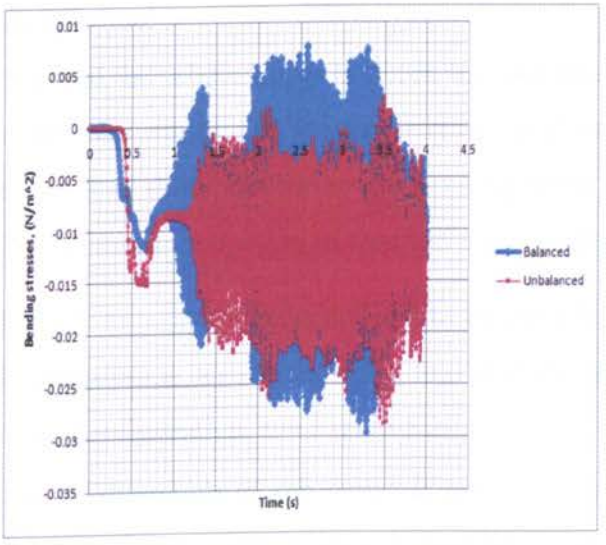

(c)- Merge in Y direction.

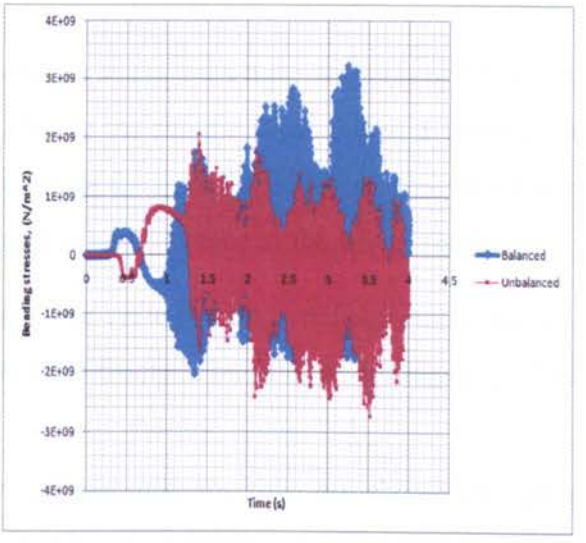

(d)- Merge in Z direction.

Figure 5.48 Variation of the bending stress with time, multidisc configuration.

5.4 Discussions and conclusions

FE analysis has been performed in this chapter to give further insight into the work performed in chapter 4. It is envisaged that a database could be created consisting of complete mathematical model of the machine which includes both the supporting structures as well as the moving parts and is based on the structural dynamics characteristics of the system. FE simulations are used to prove the reliability of the modal testing technique and to obtain the natural dynamic characteristics of the rotor system as well as obtaining the parameters for correcting the unbalance in the system.

FE results show different natural frequencies and mode shapes for one disc configuration, see Figure 5.15.

The results obtained from the experimental and numerical analysis by using ANSYS 12 are used to find the relationships between the cyclic reaction bearing forces, see Figure 5.17. The performance of reaction bearing forces in the right and left bearings with different speeds is shown in Figure 5.17a-d, it is found that with increase in speed of rotation, the reaction forces increase for both right and left bearings. The figure also show the maximum reaction force in Y direction for the bearings, the rotor transient effect disappears after a few second while the reaction in Z direction increases slowly in both bearings until it reaches maximum value as the speed increases, the results show the right bearing carry maximum reaction force in the beginning, which is a good indication of lubrication level for a particular bearing to increase its life time.

We find the relationships between the dynamic bending stress with time, see Figure 5.18a and b, the performance of bending stresses with one disc in the middle when added 8 gram mass to the disc show that the cyclic bending stress decreases for both directions of motion (Y and Z) that means reduction in reaction force in the bearing and increase in the life of the bearing.

Further simulation is carried out to investigate the rotor system with two discs configuration. FE simulation results show the first and second natural frequencies and mode shapes for two discs configuration, see Figure 5.20.

The relationships of the dynamic reaction bearing forces with the time are shown in Figure 5.21a-d, the reaction force in Y direction increases when increasing the speed of rotation for left and right bearings, while in Z direction the reaction force increases slightly at first when the rotor run up and then decreases slowly. There is maximum reaction force value in the Y direction for the right bearing, this mean the right bearing carry maximum load. In order to investigate the effects of design parameters on the noise of rotor-bearing systems, the effects of radial clearance and width of bearing, lubricant viscosity for various rotational speeds have been investigated. It is found that, as a general rule, the noise of the bearing decreases when the lubricant viscosity increases, the width of the bearing increases, and the radial clearance of the bearing decreases.

ANSYS simulation in Figure 5.22 shows the added 16 gram mass can reduce the amplitude of vibration, which is the same fact obtained by using modal testing for the same configuration.

The variation of bending stress with time is shown in Figure 5.23a and b and the performance of bending stresses for two discs configuration are obtained before and after adding 16 gram mass.

Plain bearings reduce friction in machinery by presenting a minimal surface area. This is because only very small areas of each bearing are in contact with the surface. Therefore, the bearing is indeed a very useful thing for machinery to work.

FE simulations show the natural frequency and mode shape at speed 30 rpm for overhung rotor configuration in Figure 5.25 (3-D) and 5.26 (2-D) are in agreement with experimental results shown in Figure 4.28 and 4.29 in chapter 4.

The relationship between the reaction bearing forces with time is shown in Figure 5.27a-d. It is found that the reaction force increases for both right and left bearings when increasing the speed of rotation, the maximum reaction force in Y direction in left and right bearings when the rotor is started, which decreases after a few seconds. While the reaction forces in Z direction began increasing slowly in the left and right bearings until reached maximum value as the speed is increased from rest. The left bearing carries maximum reaction force initially as shown in Figure 5.27a.

The simulation values obtained from the ANSYS in Figure 5.28, show when adding 8 gram mass to the overhung rotor disc, the vibration amplitude is reduced.

The effect of balancing on cyclic bending stress at overhung rotor disc system is shown in Figure 5.29, when adding 8 gram mass in the disc, the bending stress decreases in both directions of motion (Y and Z) resulting in improvement in the bearing life time.

The performance of multistage rotor systems with load in the effective length (multidisc) has been investigated in this chapter. FE analysis of the rotor is used to develop a multistage rotor system model, using ANSYS 12 in vibration analysis.

Figures 5.32-5.39 show different natural frequencies and mode shapes of identical multidisc rotor system using ANSYS 12 for 2-D and 3-D model analysis which are in agreement with each other.

The relationship between natural frequencies and variation in mass of the disc (disc dimensions) has been obtained and the effect of this change on the natural frequency of the rotor system is investigated, the results show that the increase in the disc mass and dimensions resulting in decrease in the natural frequency and vice versa, see Figure 5.40. This validates the theoretical vibration law of free undamped natural frequency $\omega_n = (K/M)^{1/2}$.

A multistage rotor system with different dimensions and geometry definition has been studied, see Figures 5.42-5.44.

Another modal parameter which is the FRF has been obtained using FE simulation shown in Figure 5.45 for multdisc rotor system with different dimensions and at different speeds of rotation, the results show that the gap of split increased when the speed of rotation increased because of strong gyroscopic effect, which prove the FRFs results obtained by using modal testing method discussed in chapter 4.

Dynamic reaction bearing force (*N*) has been obtained, see Figure 5.46. The behaviour of reaction forces in Figure 5.46a-d show reaction force in Y direction at left and right bearings, first constant after a few second increases when the rotor run up, then decreases slightly with further increase in the speed, while the reaction force in Z direction increases slightly at first when the rotor run up in right and left bearings then increases highly with increasing speed of rotation. The maximum reaction force value is in the Y direction right bearing that mean the right bearing carry maximum load during the rotor run up.

The simulation in Figure 5.47 for multidisc configuration, prove when added 24 gram mass to the system (8 gram per each disc) at the same speed, can reduce the displacement of vibration and that support the results of FE simulation obtained for one and two discs.

Further simulation is carried out to investigate the variation of bending stress with time, see Figure 5.48a-d. It shows the performance of bending stresses at multidisc configuration before and after added 24 gram mass to the model.

In this chapter, we use FE to identify natural dynamic characteristics of multistage rotor system and obtaining the parameters for correcting the unbalance in the rotor system. FE analysis can be used to achieve the most accurate computational simulation of all dynamic parameters in rotor systems to validate the results obtained from the modal testing method discussed in this thesis.

Present chapter is to investigate the effects of design parameters on the noise produced by rotor-bearing systems, and study the reaction force acting to the right and left bearing, with the effect of change in disc mass and geometry of the natural frequency.

This chapter demonstrates finite element models using the eigen analysis capability used to simulate the vibration and the results were compared with modal testing data. The results show that two-dimensional model and using symmetry during the modelling process can produce analysis results with acceptable accuracy and performance.

We can use the above procedure to model systems with any number of discs of variable mass and geometry.

Also from this chapter, a rotor-dynamic analysis involves most of the general steps found in any ANSYS analysis, as follows:

Build the model.	A rotating structure generally consists of rotating parts, stationary parts, and bearings linking the rotating parts to the stationary parts and/or the ground. Understanding the relationships between these parts is often easier when the model is constructed to separate and define them.
Define element types.	The elements selected for the rotating parts of the model must support gyroscopic effects. The CORIOLIS command documentation lists the elements for which the gyroscopic matrix is available. All rotating parts must be axisymmetric. Model the stationary parts with any of the 3-D solid, shell, or beam elements available in the ANSYS element library. We can also add a stationary part as a substructure. Model the bearings using either a spring/damper element COMBIN14 or a bearing element COMBI214.
Define materials.	Defining the material properties for a rotor-dynamic analysis is no different to defining them in any other analysis. Use the MP or TB commands to define linear and nonlinear material properties.
Define the rotational velocity	Define the rotational velocity using either the OMEGA or CMOMEGA command. Use OMEGA if the whole model is rotating. Use CMOMEGA if there are stationary parts and/ or several rotating parts having different rotational velocities. CMOMEGA is based on the use of components.
Account for gyroscopic effect	Use the CORIOLIS command to take into account the gyroscopic effect in all rotating parts as well as the rotating damping effect.
Mesh the model.	Use the ANSYS meshing commands to mesh the parts. Certain areas may require more detailed meshing and/or specialized considerations.
Solve the model.	The solution phase of a rotor-dynamic analysis adheres to standard ANSYS conventions, keeping in mind that the gyroscopic matrices (as well as

	possibly the bearing matrices) may not be symmetric. Modal, harmonic and transient analyses can be performed. Performing several modal analyses allows reviewing the stability and obtaining critical speeds from the Campbell diagrams. A harmonic analysis allows to calculate the response to synchronous (for example, unbalance) or asynchronous excitations. A transient analysis allows studying the response of the structure under transient loads (for example, a 1 G shock) or analyzing the start-up or stopping effects on a rotating spool and the related components. Pre-stress can be an important factor in a typical rotor-dynamic analysis. We can include pre-stress in the modal, transient or harmonic analysis.
Review the results.	Use POST1 (the general postprocessor) and POST26 (the time-history postprocessor) to review results. Specific commands are available in POST1 for Campbell diagram analysis (PLCAMP, PRCAMP), animation of the response (ANHARM) and orbits visualization and printout (PLORB, PRORB).

CHAPTER 6

Validation of Modal Data in Rotating Machinery Using Finite Element Analysis

6.1 Validation of one disc configuration results

The first stage of the project was to assemble and set up the rig (RK4 rotor kit) by placing the bearing to obtain the desired boundary condition for the system as shown in Figure 4.5 in chapter 4. In order to calculate the stiffness of the structure, one set of load was placed at the centre of the shaft.

By applying an impact excitation to the system and using the SO software, we find the first natural frequency response function of the system to be 29.79 Hz, see Figure 6.1. In this figure the FRF of the system is shown in the left hand side, and on the right hand side the first associated mode shape is presented. As it was expected, the first mode shape of the response with maximum deflection in the middle. This result was validated using ANSYS12 (Mechanical APDL and Workbench) simulation, see Figure 6.2a and b. The result of natural frequency and mode shape agree with each other. Similarly for the second mode, see Figures 6.3 and 6.4 for the range 0-500 Hz.

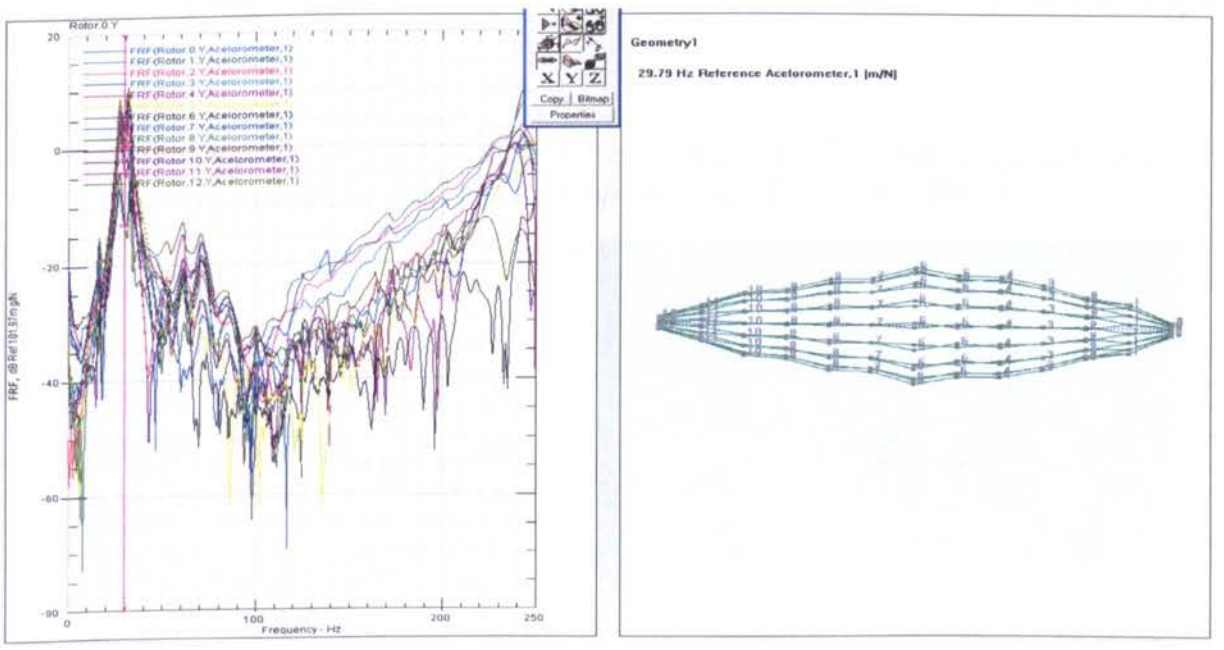

Figure 6.1 Load in the middle for one disc configuration, FRF versus frequency (Hz), first mode shape, natural frequency 29.79Hz, range 0-500 Hz.

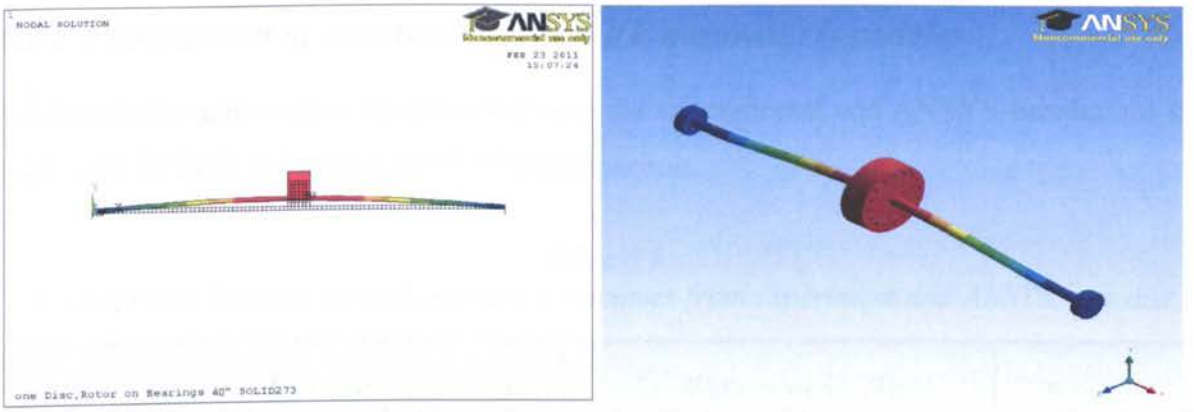

(a)-Natural frequency 29.93Hz, 2-D. *(b)-Natural frequency 29.95Hz, 3-D.*

Figure 6.2 Finite element simulations, first mode shape, one disc with two bearings.

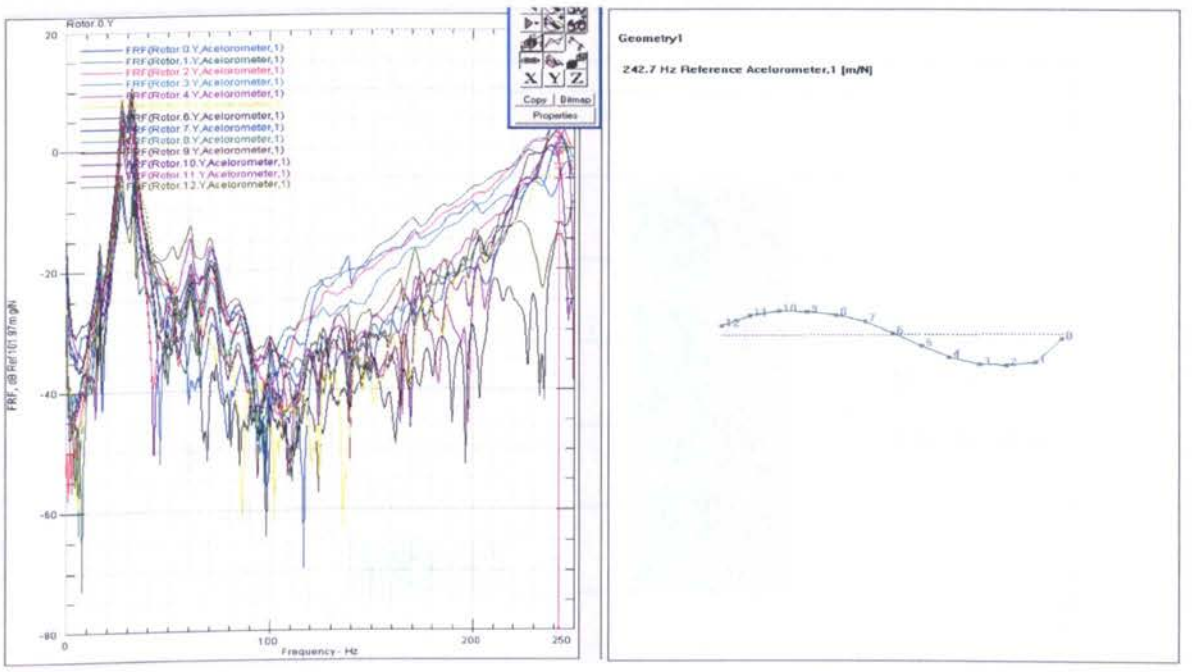

Figure 6.3 Load in the middle for one disc configuration, FRF versus frequency (Hz), second mode shape, natural frequency 242.7Hz, range 0-500 Hz.

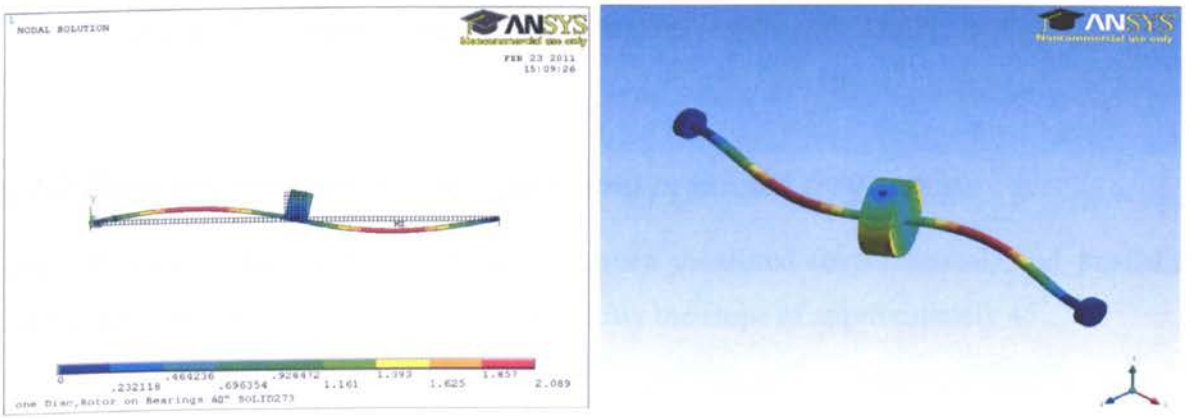

(a)-Second mode shape, natural frequency 243.71Hz, 2-D. *(b)-Second mode shape, natural frequency 243.68Hz, 3-D.*

Figure 6.4 Finite element simulations, second mode shape, one disc with two bearings.

6.1.1 Comparison of experimental and FE natural frequencies

All the results agree with each other between the experimental and ANSYS simulations see the results in Table 6.1 and Figure 6.5 for comparison.

Table 6.1
Comparison between natural frequency outcomes from experiment and ANSYS, one disc.

Mode shape	f_n (ANSYS), (Hz)	f_n Experiment, (Hz)	Error %
1	29.94	29.79	0.498
2	243.71	242.74	0.399

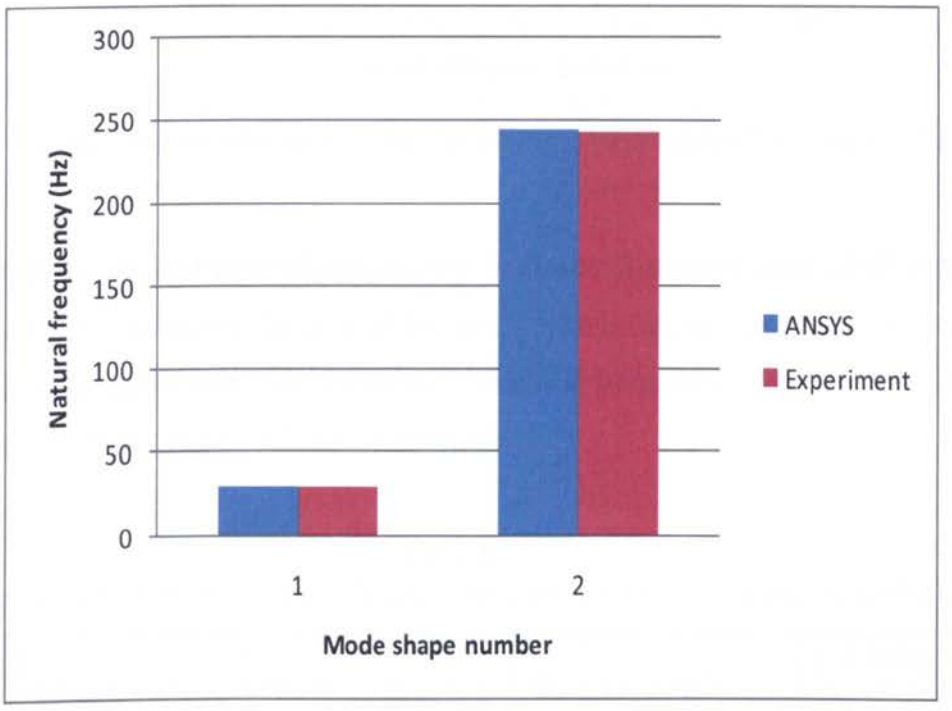

Figure 6.5 Natural frequency experimental results with ANSYS, one disc.

6.1.2 Relationship between measured and predicted frequency

The following graphs show comparison between measured (experimental) and prediected natural frequency (ANSYS), see Figure 6.6 shows the slope of approximately 45°.

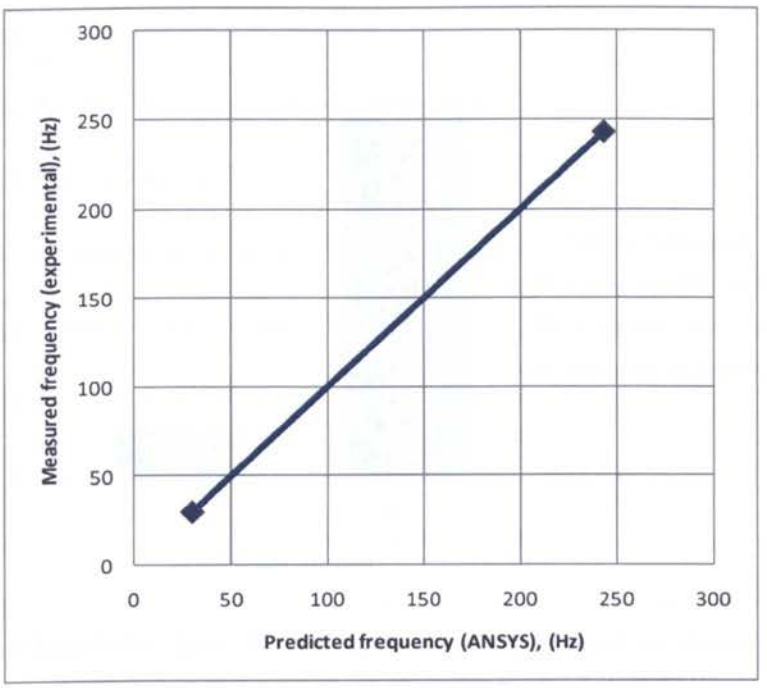

Figure 6.6 Comparison between measured and predicted frequency (Hz).

6.1.3 Comparison of natural frequency between hammer and shaker test

From Table 6.2 the values of the natural frequency with different excitation waveforms using shaker test are in agreement with the values of natural frequency using hammer test for one disc configuration, see Figure 6.7 for comparison.

Table 6.2
Comparison experimental value of natural frequency between hammer and shaker test.

Mode shape	Hammer test, fn (Hz)	Shaker, Random test, fn (Hz)	Shaker, Sine wave test, fn (Hz)	Shaker, Burst Random test, fn (Hz)
1	29.79	31.25	30.07	31.68
2	242.74	243.86	244.67	242.01

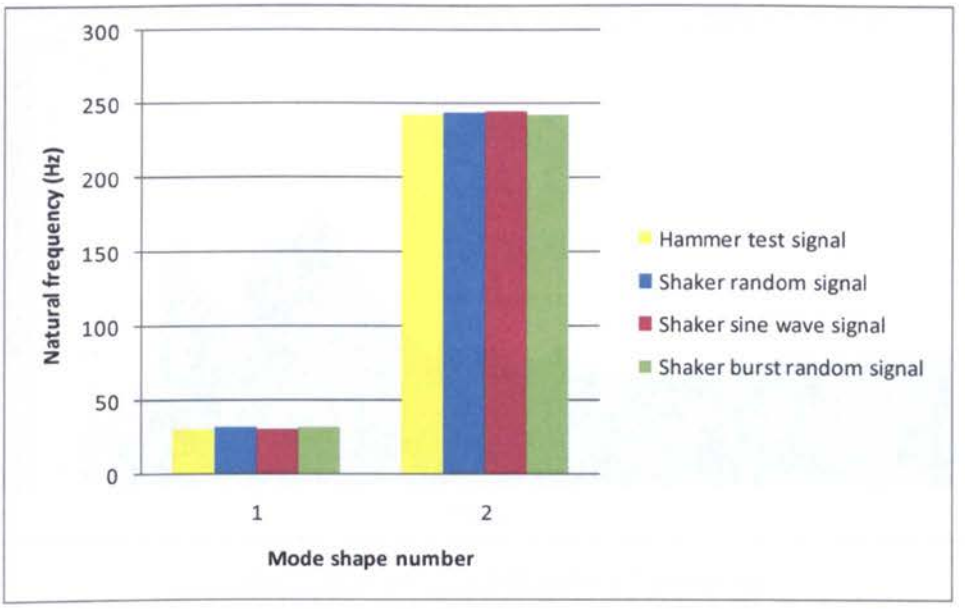

Figure 6.7 Comparison experimental value of natural frequency between hammer and shaker test (different excitation input signals).

6.1.4 Results of unbalance with added mass using shaker test and FE for one disc configuration

Figure 6.8 shows the displacement versus time before (a) and after (b) adding the unbalance mass at speed of rotation 1000 rpm. It can be seen from the figure, the amplitude of the system has been reduced by 0.007 m. That means when adding 8 gram mass in one disc in the middle with angles 135° and 315° using experimental shaker test, the amplitude would be reducing. This result was validated using FE simulation shown in Figure 6.9.

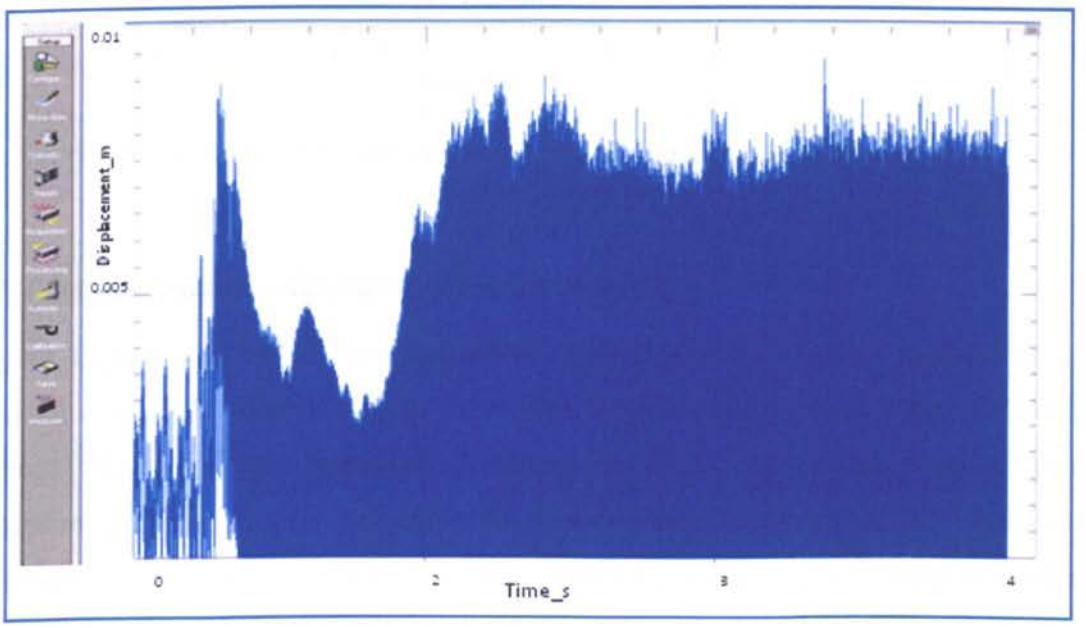

(a)- Balanced, before added mass.

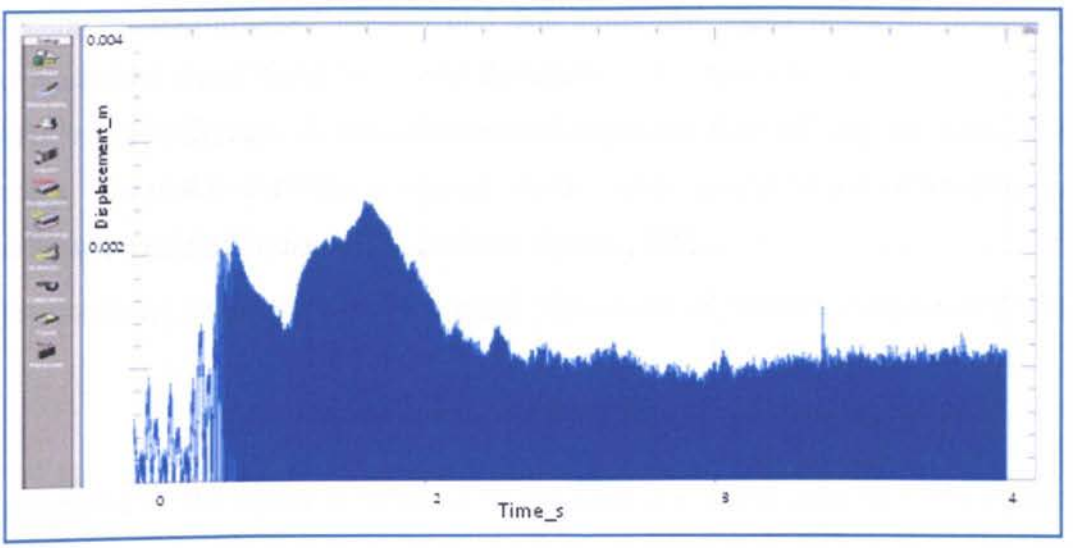

(b)- Unbalanced, after added 8 gram mass.
Figure 6.8 Displacement versus time using shaker test, Time domain.

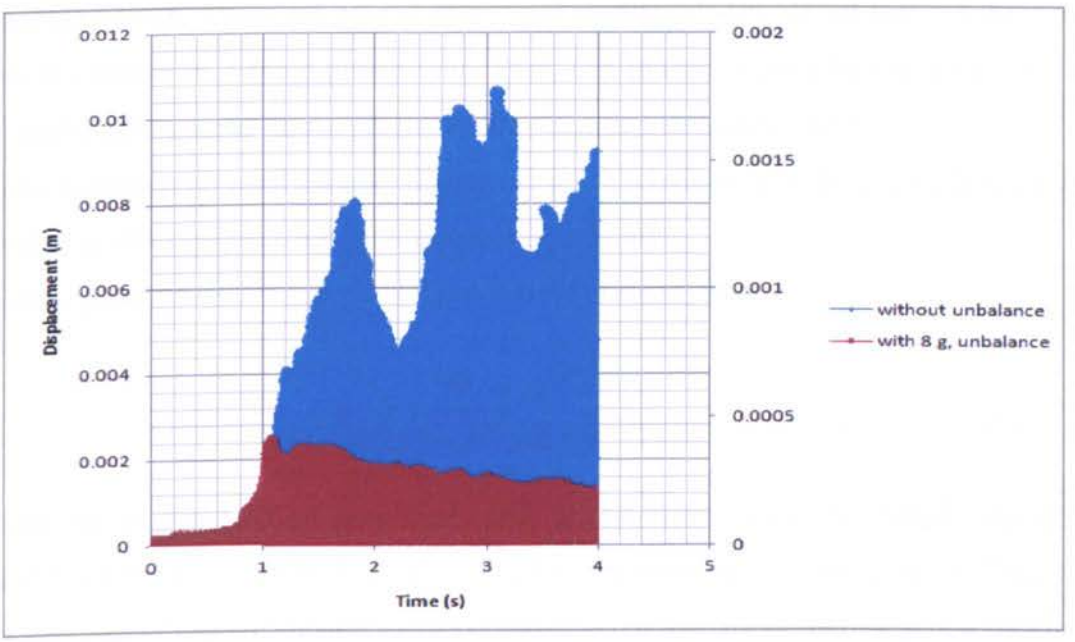

Figure 6.9 FE simulations, displacement versus time, without added mass and after added 8 gram mass.

6.1.5 Lissajous figure diagnosis in rotor systems

Lissajous figures also called Bowditch curve, pattern produced by the intersection of two sinusoidal curves the axes of which are at right angles to each other. First studied by the American Mathematician Nathaniel Bowditch in 1815, the curves were investigated independently by the French mathematician Jules-Antoine Lissajous in 1857–58. Lissajous used a narrow stream of sand pouring from the base of a compound pendulum to produce the curves [167].

When using an oscilloscope, we can plot one sinusoidal signal along the x-axis against another sinusoidal signal along the y-axis; the result is a Lissajous figure.

The oscilloscope displays a two dimensional representation of one or more potential differences. The plot is normally of voltage on the y-axis against time on the x-axis, making the oscilloscope useful for displaying periodic signals [168].

In mathematics, a Lissajous curve is the graph of a system of parametric equations [169],

$$x = A \sin(at + \delta), \quad y = B \sin(bt) \qquad 6.1$$

The appearance of the figure is sensitive to the ratio a/b. For a ratio of 1, the figure is an ellipse, with special cases including circles ($A = B$, $\delta = \pi/2$ radians) and lines ($\delta = 0$). Another simple Lissajous figure is the parabola ($a/b = 2$, $\delta = \pi/2$). Other ratios produce more complicated curves, which are closed only if a/b is rational. The visual form of these curves is often suggestive of a three-dimensional knot, and indeed many kinds of knots, including those known as Lissajous knots, project to the plane as Lissajous figures.

Lissajous figure on an oscilloscope, displaying a 3:1 relationship between the frequencies of the vertical and horizontal sinusoidal inputs, respectively.

Lissajous figures when $a = 1$, $b = N$ (N is a natural number) then

$$\delta = \frac{N-1}{N}\frac{\pi}{2} \qquad 6.2$$

Lissajous curves can also be generated using an oscilloscope (as illustrated). An octopus circuit can be used to demonstrate the waveform images on an oscilloscope. Two phase-shifted sinusoid inputs are applied to the oscilloscope in X-Y mode and the phase relationship between the signals is presented as a Lissajous figure.

On an oscilloscope, we suppose x is channel 1 and y is channel 2, A is amplitude of channel 1 and B is amplitude of channel 2, a is frequency of channel 1 and b is frequency of channel 2, so a/b is a ratio of frequency of two channels, finally, δ is the phase shift of channel 1. In order to find a resonant frequency we need to search for a Lissajous figure. This looks like an ellipse and should be clearly noticeable on the oscilloscope. However it is important to be consistent, see Figure 6.10.

A purely mechanical application of a Lissajous curve with a =1, b =2 is in the driving mechanism of the Mars light type of oscillating beam lamps popular with railroads in the

mid-1900s. The beam in some versions traces out a lopsided Figure 6.11, pattern with the "8" lying on its side.

When the input to an LTI (Linear, Time-Invariant) system is sinusoidal, the output is sinusoidal with the same frequency, but it may have different amplitude and some phase shift. Using an oscilloscope that can plot one signal against another (as opposed to one signal against time) to plot the output of an LTI system against the input to the LTI system produces an ellipse that is a Lissajous figure for the special case of $a = b$. The aspect ratio of the resulting ellipse is a function of the phase shift between the input and output, with an aspect ratio of 1 (perfect circle) corresponding to a phase shift of $\pm 90^{\circ}$ and an aspect ratio of ∞ (a line) corresponding to a phase shift of 0° or 180° degrees. The Figure 6.10 summarizes how the Lissajous figure changes over different phase shifts. The phase shifts are all negative so that delay semantics can be used with a causal LTI system (note that - 270° degrees is equivalent to + 90° degrees). The arrows show the direction of rotation of the Lissajous figure see Figure 6.11a [168-170].

The experimental technique uses oscilloscope with rotor rig (two discs) in effective length; the display is usually a CRT (Cathode Ray Tube) or LCD (Liquid Crystal Display) panel which is laid out with both horizontal and vertical reference lines we can demonstrate the waveform images on an oscilloscope.

The objective of this part is to provide the reader with an insight into developments in the field of Lissajous curve, with particular regard to rotating machines. The subject of it in rotating machinery is vast, including the diagnosis of items such as rotating shafts, gears and pumps.

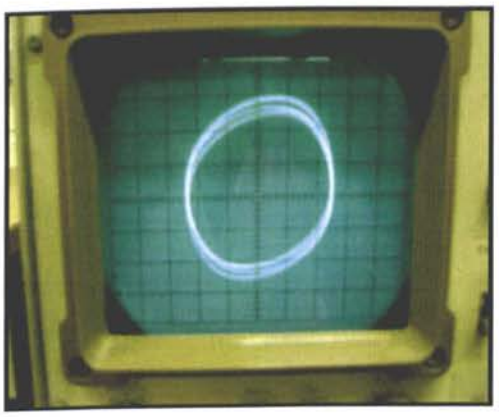

(a)

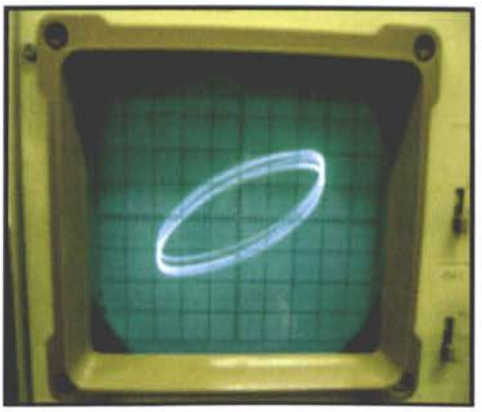

(b)

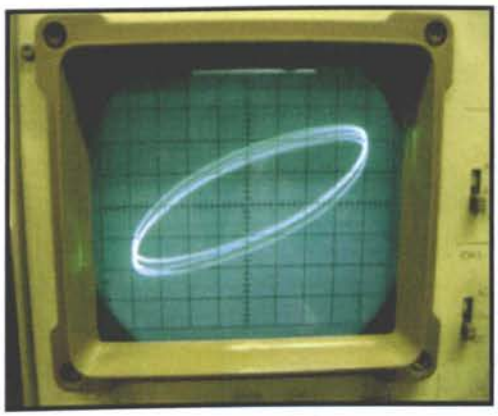

(c)

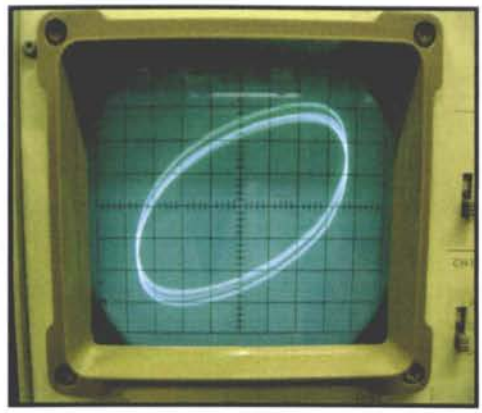

(d)

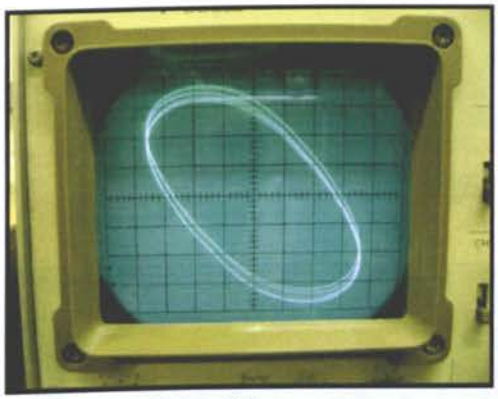

(e)

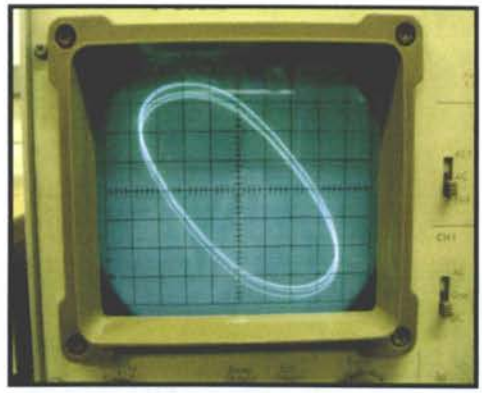

(f)

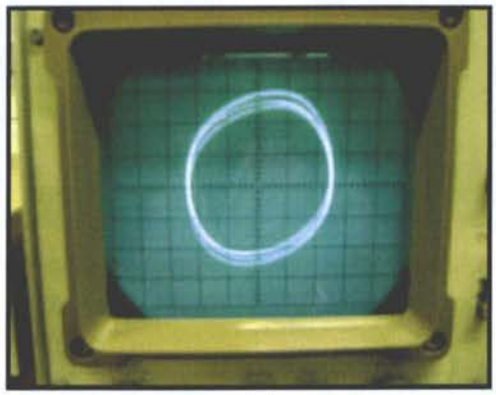

(g)

Figure 6.10 Input frequencies are identical, but the phase variance between them creates the shape of an ellipse.

A Lissajous figure is produced by taking two sine waves. This is easily done on an oscilloscope in XY mode.

In the following examples the two sine waves have equal amplitudes.

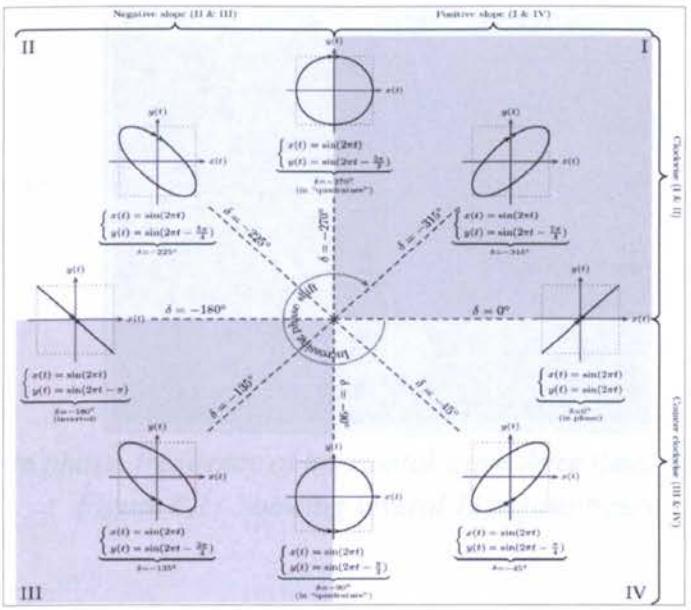

(a)- For different phase delays [168].

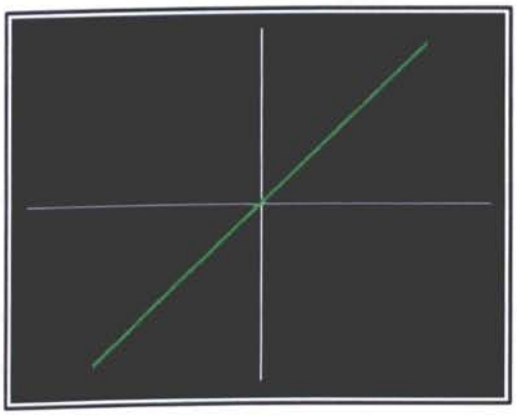

(b)- When the two sine waves are of equal frequency and in-phase we get a diagonal line to the right.

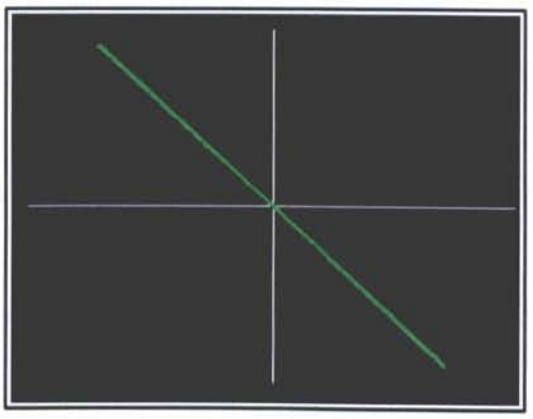

(c)- When the two sine waves are of equal frequency and 180° degrees out-of-phase we get a diagonal line to the left.

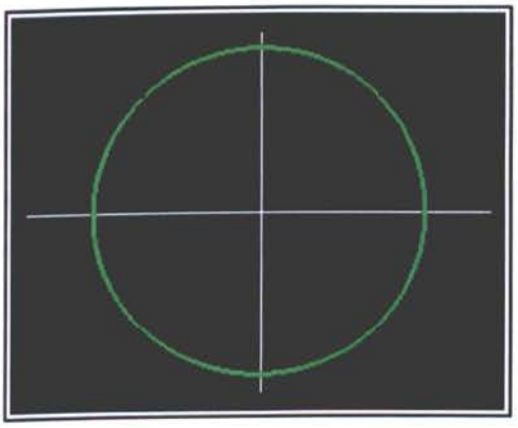

(d)- When the two sine waves are of equal frequency and 90° degrees out-of-phase we get a circle.

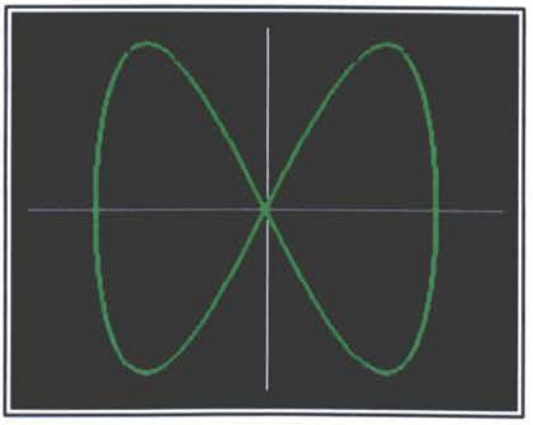

(e)- Two sine waves in phase, frequency of horizontal wave twice frequency of vertical wave.

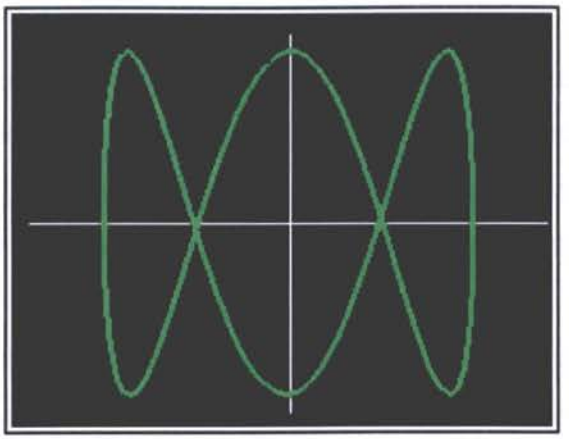

(f)- Two sine waves in phase, frequency of horizontal wave three times frequency of vertical.
Figure 6.11 Showing several Lissajous figures.

This should not be a big surprise, because when

$$X = \sin(a) \quad and \quad Y = \sin(a + 90) = \cos(a) \ldots\ldots\ldots\ldots\ldots\ldots\ldots\ldots 6.3$$

$$X \times X + Y \times Y = \sin(a) \times \sin(a) + \cos(a) \times \cos(a) = 1 \ldots\ldots\ldots\ldots\ldots 6.4$$

This is the parametric equation for a circle having a radius of 1.

A Lissajous figure displayed on an oscilloscope can be used to give a quick estimate of the relative phase of two signals at the same frequency. The plots presented here represent [168].

$$X = \cos(\omega t), \qquad Y = \cos(\omega t + \varnothing) \ldots\ldots\ldots\ldots\ldots\ldots\ldots\ldots\ldots\ldots 6.5$$

Where the phase angle $\varnothing$ is indicated in degrees by the number the top right of each plot. To use this catalogue, adjust the oscilloscope so that the X and Y signals have exactly the same amplitude (8 division's peak-to-peak) the pattern is accurately centred on the screen.
An oscilloscope is easily the most useful instrument available for testing circuits because it allows we see the signals at different points in the circuit. The best way of investigating an electronic system is to monitor signals at the input and output of each system block.

6.1.6 RPM Spectral Map Wizard

There are two types of vibration analysis investigations that are commonly done today. The first involves analyzing the mechanical vibration of new products that are tested. The second

involves analyzing the vibration that exists in rotating machinery such as compressors, turbines, and motors. Advances in computing power and software have greatly enhanced the vibration analysis process for both new and existing products. The most common software package for analyzing new products is finite element analysis software. Vibration in existing machinery is analyzed with integrated software that enhances the vibration analysis equipment.

Analyzing rotating data requires a tachometer measurement to estimate the machine RPM as a function of time. The accuracy of the RPM versus time function is important for analyzing rotating data [171-174].

Vibration measurements can be expressed in terms of displacement, velocity, acceleration, and high frequency content (for bearing condition detection). Most data collectors use FFT (Fast Fourier Transform) to convert the data from the time domain to the frequency domain. Vibration data collectors have a built-in PC interface that allows transfer of the measurements to a PC for data management. Analysis software displays spectrum, trend, waterfall plots, and waveform for advanced analysis. To assess a machine, the vibration data is compared with historical profiles from the same machine.

The Smart Office (SO) Analyzer Rotate Solutions contain several wizards for analyzing rotating data which can be accessed via the analysis menu [175, 176].

Spline Fit a tachometer measurement to estimate the RPM as a function of time with the Tacho Spline Fit Wizard which used to:-

- Create frequency versus amplitude versus time plots with the RPM Spectral Map Wizard.
- Compute selected orders as a function of RPM with the Computed Order Tracking Wizard.
- Create an Orbit Plotting analysis using time history RPM data (e.g. for bearing and shaft analysis). Alternatively, use the SO analyzer configuration page and select the rotate and the Postprocessing options.

An RPM spectral map plots frequency along the x-axis, amplitude along the y axis, and shaft speed in revolutions per minute RPM along the z-axis. View an RPM spectral map to determine:

- How vibration changes with machine speed, and
- Which components are related to rotational speed.

Structural resonances can cause increases in vibration level with RPM. Resonances are fixed in frequency and are straight lines in the map. Orders are multiples of the fundamental

running speed of the machine. Order related components move across the map, to the right as RPM increases [56, 133].

The RPM Spectral Map Wizard computes the frequency spectra for each RPM value by:

1) Locating the time point of the given RPM value from the RPM versus time spline fit.

2) Selecting the time samples around the determined RPM time, and

3) Applying a window to the resulting measurement time block and performing a Fourier transform. In the RPM Spectral Map Wizard, select the window type for the Fourier transforms the time block-size and the RPM range and resolution for the RPM spectral map. Structural resonances occur at constant frequency lines in the map, while order related components vary frequency with RPM. View the order, frequency, and RPM values with a single cursor or harmonic cursors.

6.1.6.1 Waterfall display

A waterfall plot is a three-dimensional plot which shows grid lines for only one of the axes. The result is a series of "mountain" shapes that appear to be side by side, resembling a waterfall, see Figure 6.12. The waterfall plot is often used to show how two-dimensional information changes over time or some other variable. The term "waterfall plot" is sometimes used interchangeably with "spectrogram" or "Cumulative Spectral Decay" CSD plot.

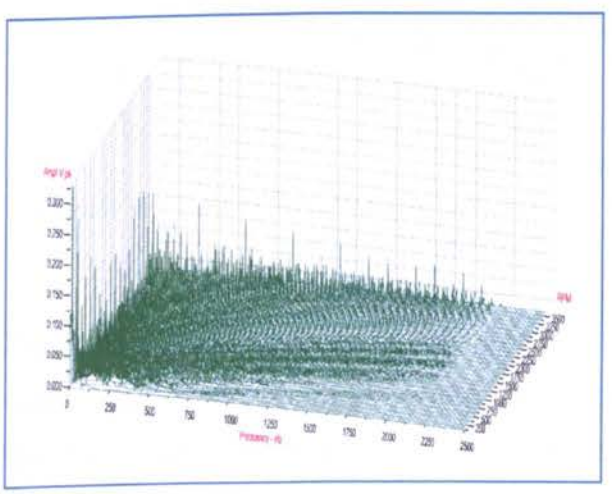

(a)- At speed 1000 rpm.

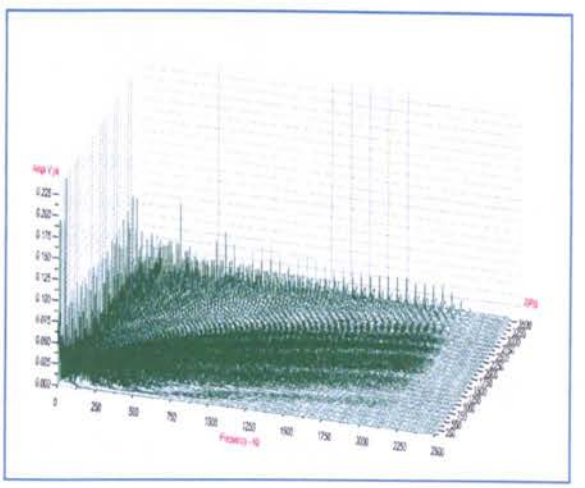

(b)- At speed 2000 rpm.

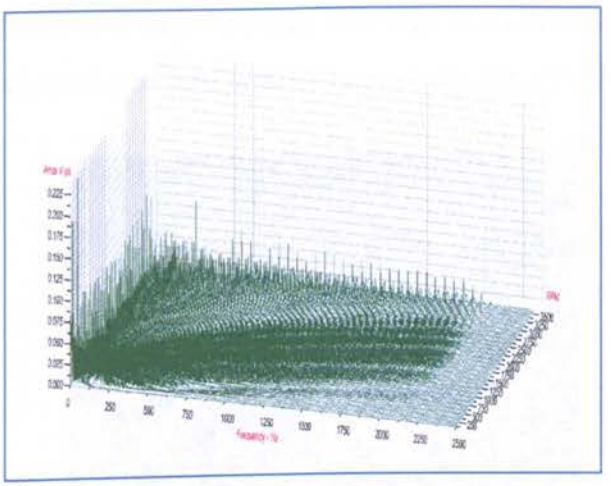

(c)- At speed 3000 rpm.

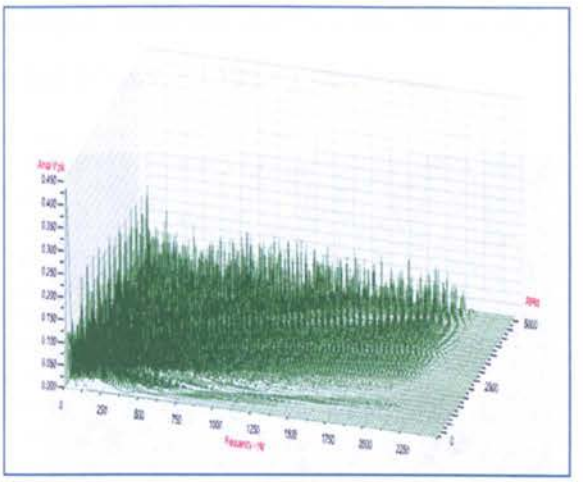

(d)- At speed 4000 rpm.

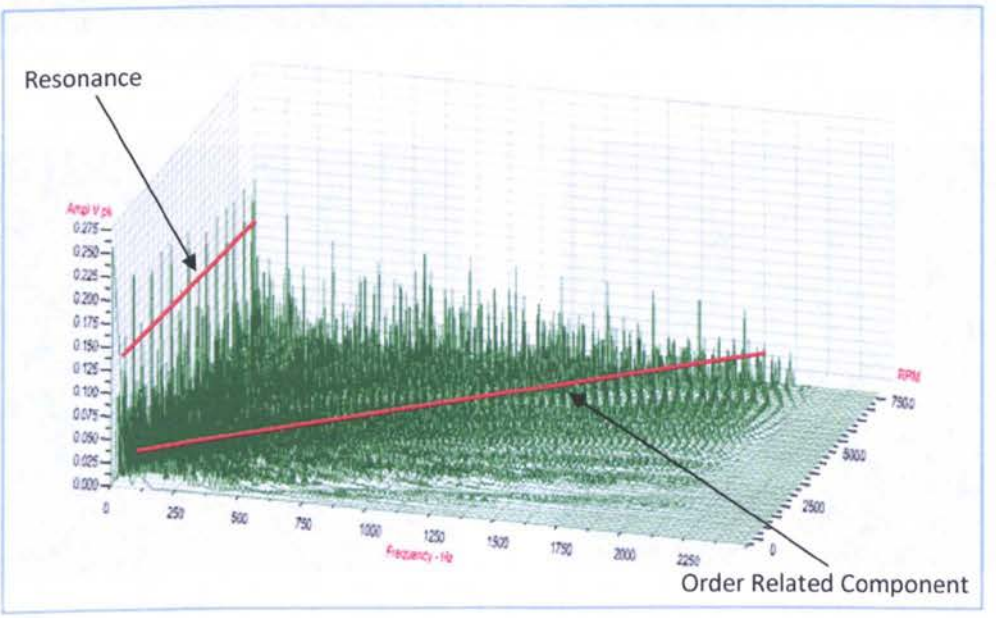

(e)- At speed 6000rpm.

Figure 6.12 RPM Spectral map wizard with resonances and order related components at different speeds of rotation (Waterfall display).

From Figure 6.12 we can see that when the speed of rotor increases, the amplitude at the same value of the natural frequency rises accordingly. And we can conclude the rotational speed (angular velocity) of the rotor does affect on amplitude of the response.

6.1.6.2 Modifying the properties of the Waterfall display by Colormap displays

We can switch between a waterfall plot and colormap displays. Figure 6.13 shows the order related components move across the map, to the right as RPM increases and this results agreed with the results obtained from waterfall display in Figure 6.12.

From this study we can conclude the vibration analysis software can be used effectively to analyze new products, or to evaluate the vibration that occurs in rotating machinery.

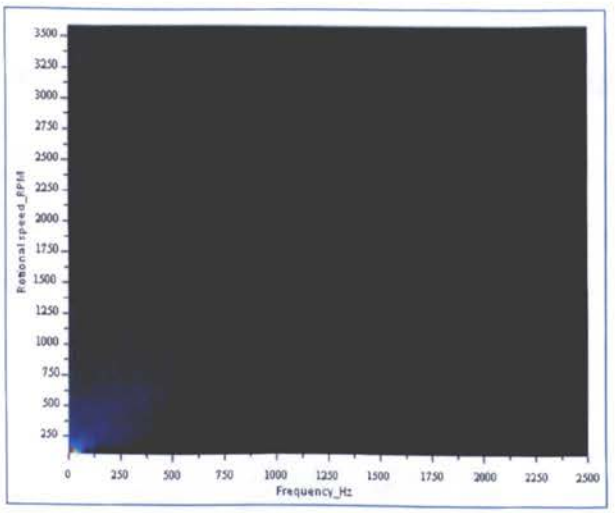

(a)- At speed 1000 rpm.

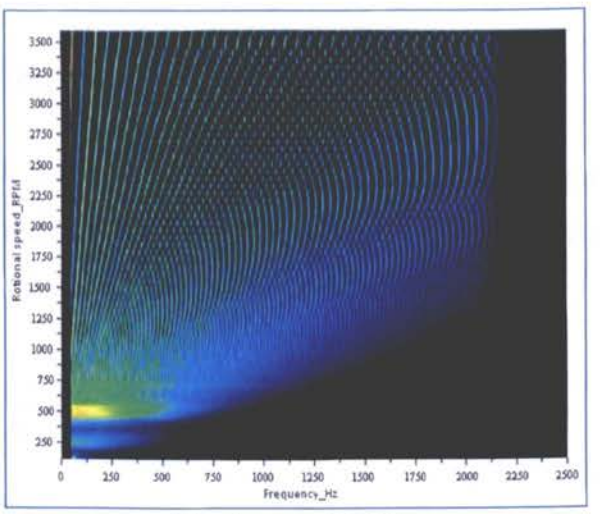

(b)- At speed 2000 rpm.

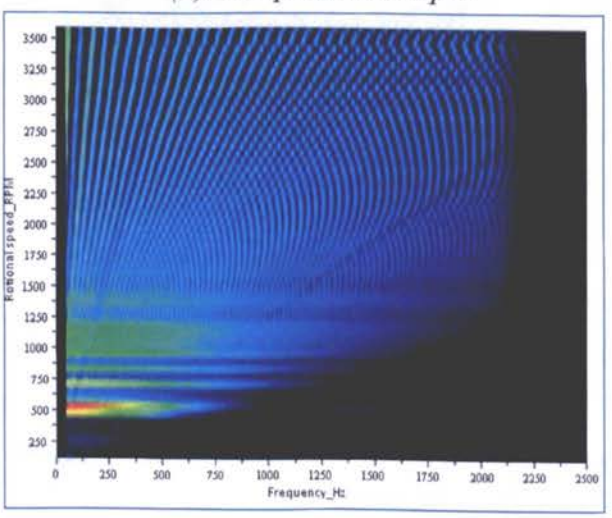

(c)- At speed 3000 rpm.

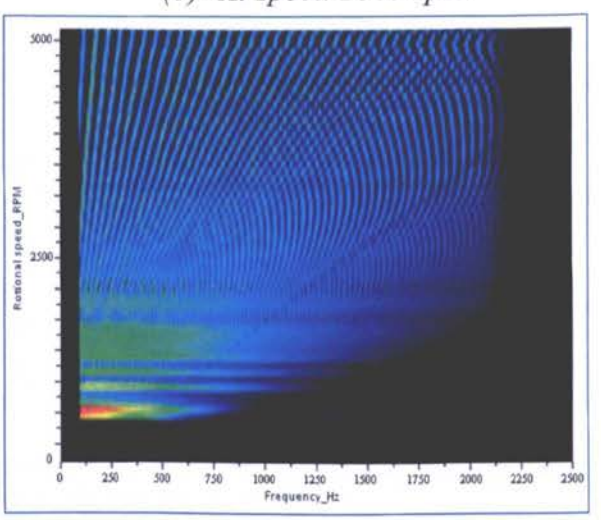

(d)- At speed 4000 rpm.

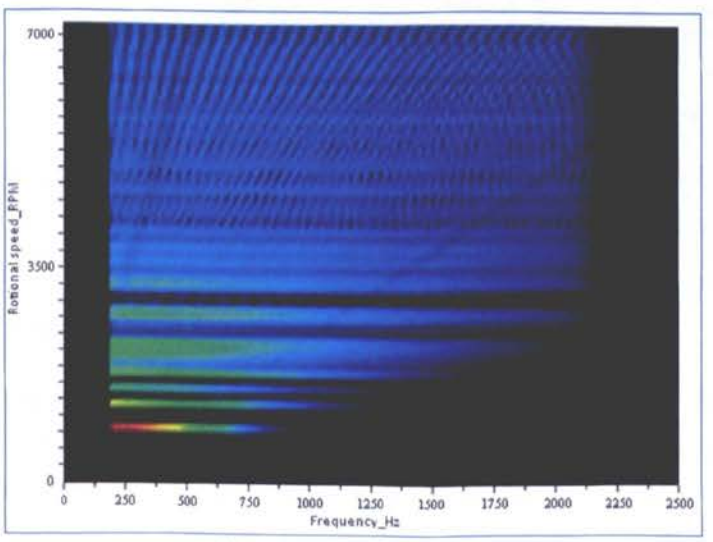

(e)- At speed 6000 rpm.

Figure 6.13 RPM Spectral map wizard, Colormap displays at different speeds of rotation.

Finally, by using vibration analysis software for assessing machinery vibration is a cost-effective method to minimize down time and maximize equipment utilization.

6.2 Validation of two discs configuration results

The modal testing results that shown in Figures 6.14, 6.16 and 6.18 for two discs to obtain natural frequencies and extract mode shapes are in agreement with values obtained from the simulation values outcome from ANSYS, shown in Figures 6.15, 6.17 and 6.19.

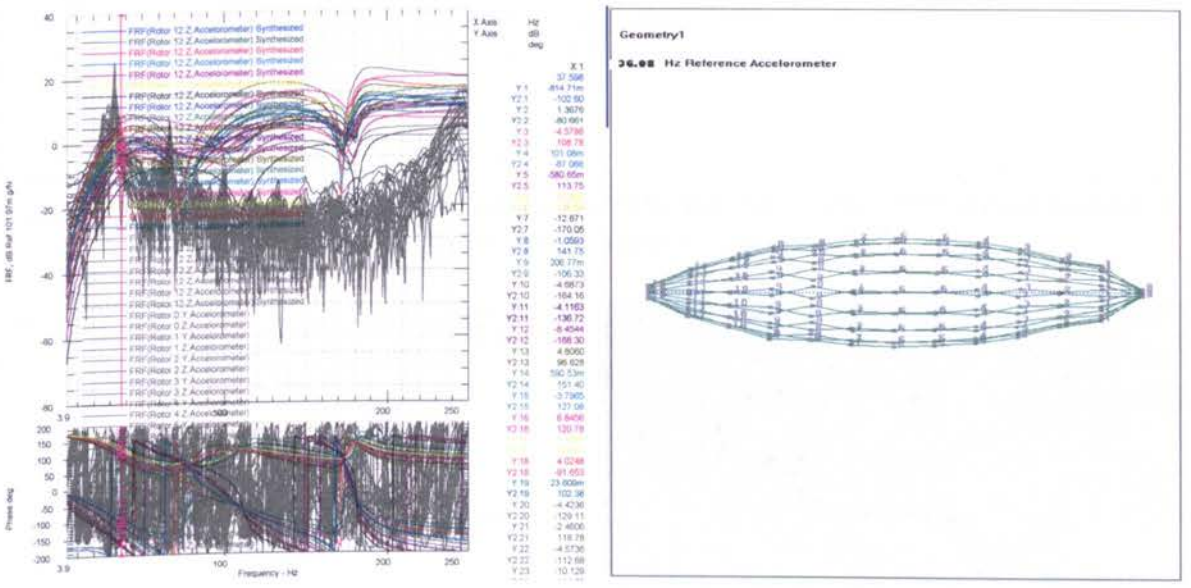

Figure 6.14 Mode shape of the rotating system with two discs shows FRF versus frequency (Hz), first mode shape. Natural frequency 36.08Hz.

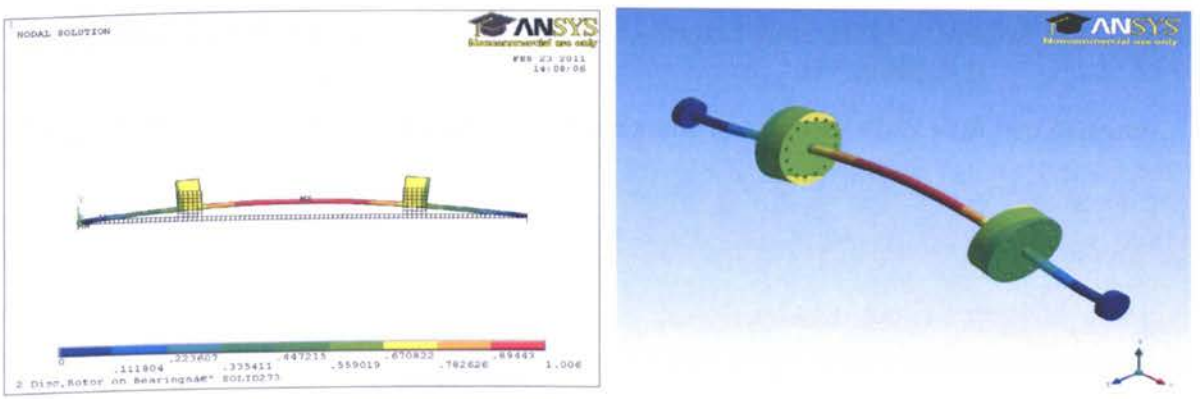

(a)- First mode shape. Natural frequency 37.015Hz, 2-D.

(b)- First mode shape. Natural frequency 37.03Hz, 3-D.

Figure 6.15 Finite element simulations, first mode shape, two discs with two bearings.

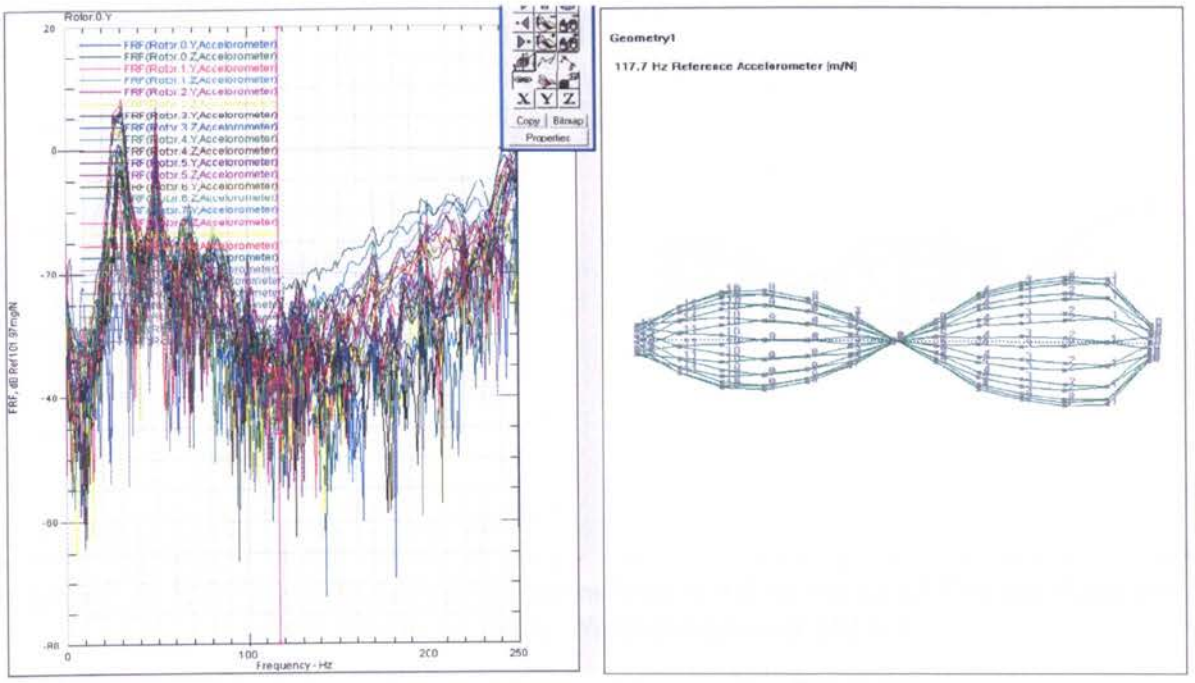

Figure 6.16 Mode shape of the rotating system with two discs shows FRF versus frequency (Hz), second mode shape. Natural frequency 117.7Hz.

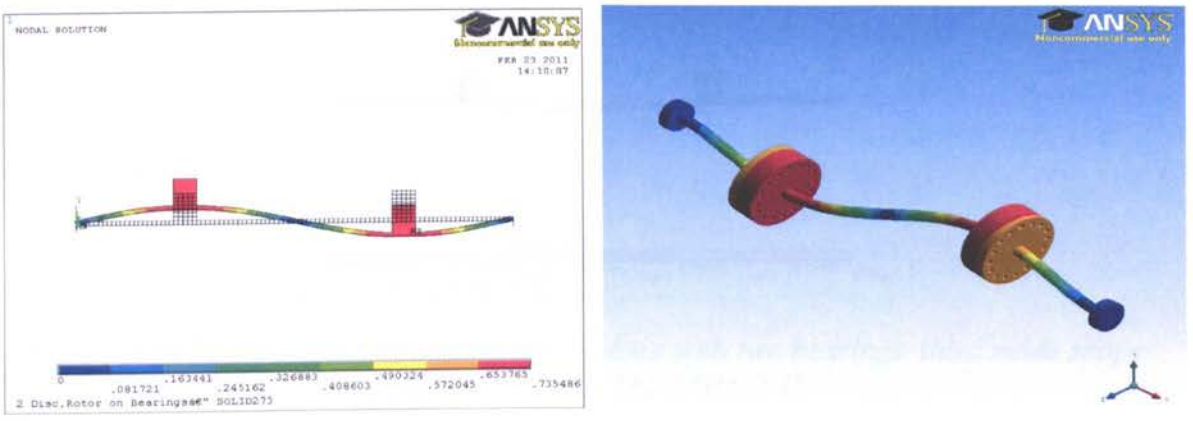

(a)-Second mode shapes. Natural frequency 117.17Hz, 2-D.

(b)-Second mode shapes. Natural frequency 117.21Hz, 3-D.

Figure 6.17 Finite element simulations, second mode shape, two discs with two bearings.

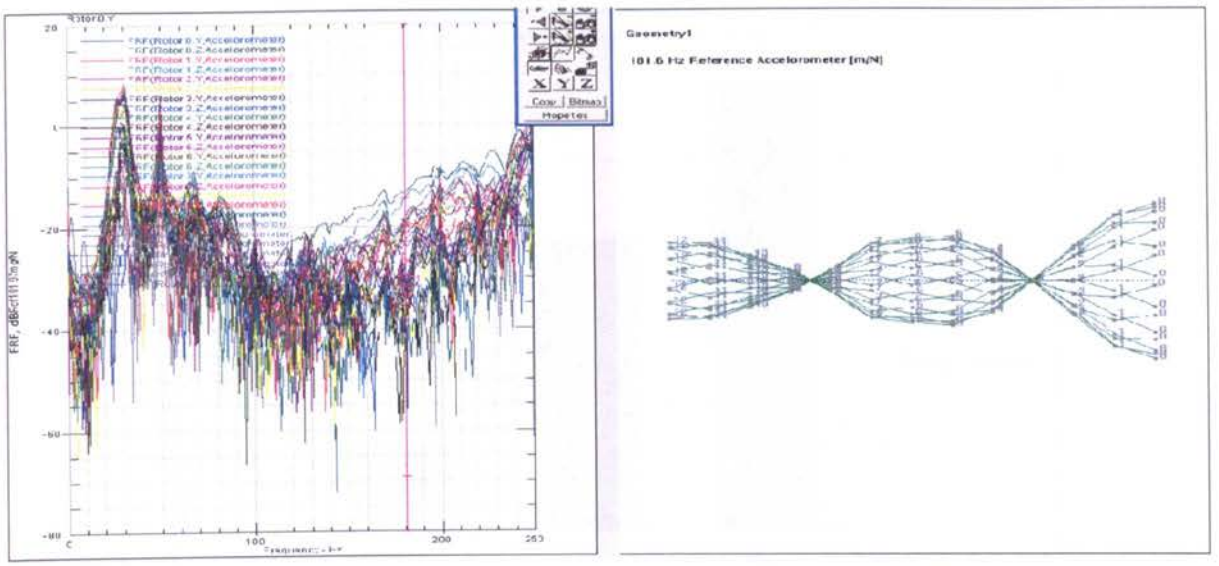

Figure 6.18 Mode shape of the rotating system with two discs shows FRF versus frequency (Hz), third mode shape. Natural frequency 181.6Hz.

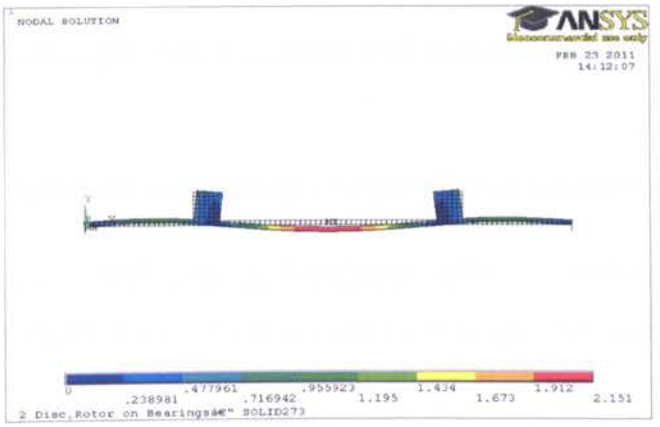

Figure 6.19 Finite element simulations, two discs with two bearings, third mode shape. Natural frequency 181.34Hz, 2-D.

6.2.1 Comparison of experimental and FE natural frequencies for two discs

The results for experimental and analytical method using FE are shown in Table 6.3 and Figure 6.20 as can be seen the natural frequencies from two methods show agreement.

Table 6.3
Comparison between natural frequency outcomes from experiment and ANSYS, two discs.

Mode shape	ANSYS (Hz)	Experiment (Hz)	Error %
1	37.06	36.1	2.525
2	117.17	117.7	-0.452
3	181.34	181.6	-0.143

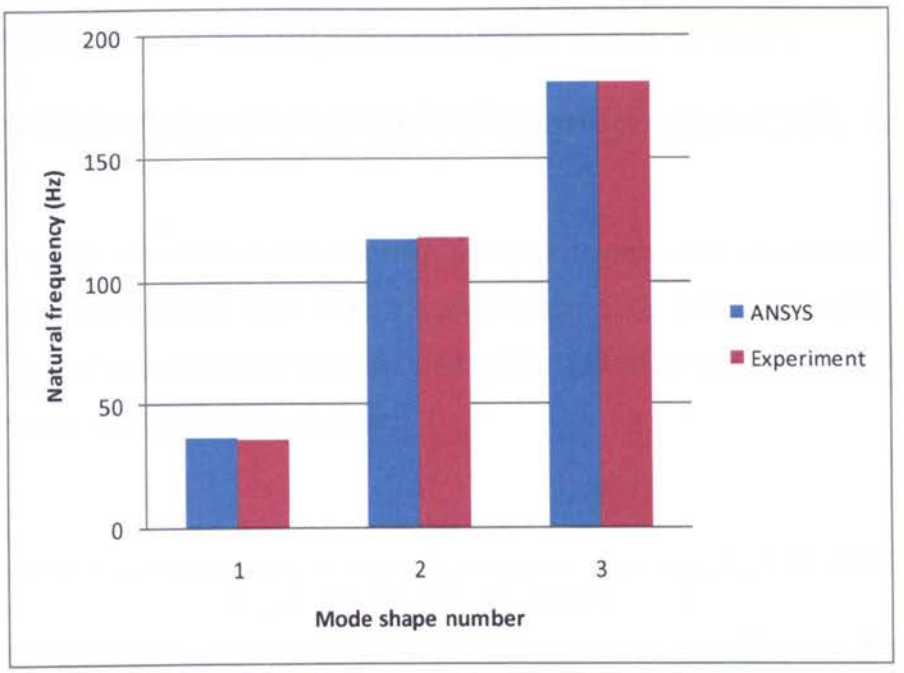

Figure 6.20 Natural frequency experimental results with ANSYS, two discs.

6.2.2 Relationship between measured and predicted frequencies for two discs

The comparison between experimental and predicted ANSYS simulation, natural frequency is shown by a graph in Figure 6.21, we can see the slope is approximately 45°.

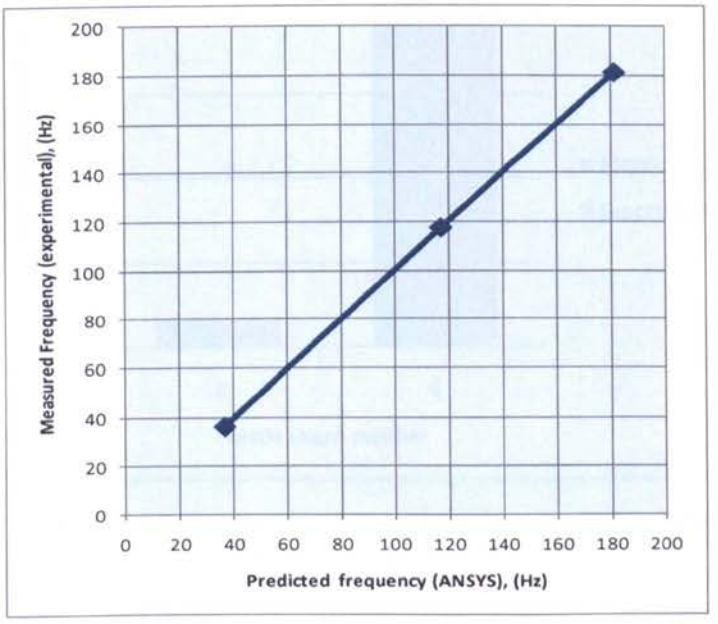

Figure 6.21 Comparison between measured and predicted frequency (Hz).

6.3 Validation of overhung disc configuration results

6.3.1 Comparison of experimental and FE natural frequencies for overhung rotor system

All the results agree with each other between the experimental and simulation ANSYS for overhung rotor at speed 30 rpm (see Table 6.4 and Figures 6.22, 6.23 for comparison). Figure 6.23 suggest that no experimental error because all the points lie on the 45° straight line of slope as mentioned in Figure 1.4 in chapter 1.

Table 6.4
Comparison between natural frequency outcomes from experiment and ANSYS at speed 30 rpm, overhung rotor configuration.

Mode Shape	fn in FE (Hz)	fn in Experimental (Hz)	Error %
1	15.703	15.137	1.158
2	216.8	216.51	-0.134

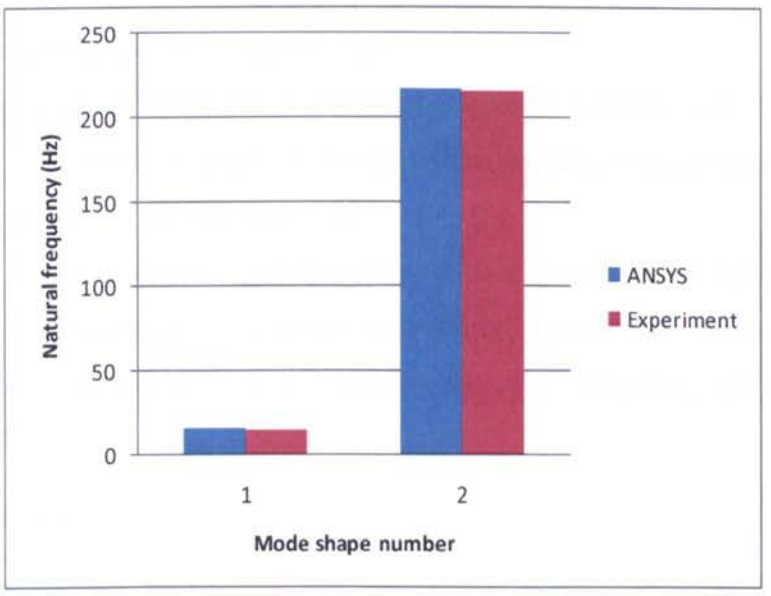

Figure 6.22 Mode shape number versus natural frequency (experiment and ANSYS), overhung rotor configuration.

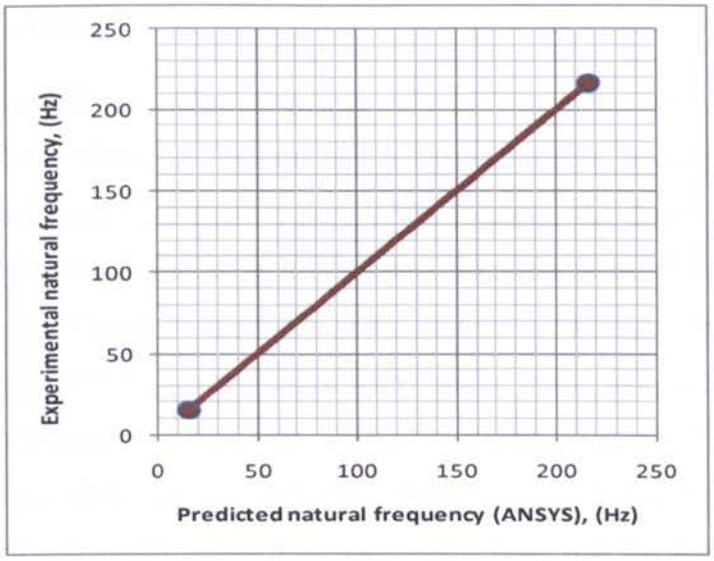

Figure 6.23 Experimental results of natural frequency versus ANSYS results, overhung rotor configuration.

6.3.2 Campbell diagram

A Campbell diagram is named for Wilfred Campbell, who has introduced this concept.

In rotor-dynamical systems, the eigen frequencies often depend on the rotation speed due to the induced gyroscopic effects. Campbell diagram might represent the following cases:

1) Analytically computed values of eigen frequencies as a function of the shaft's rotation speed, this case is also called "whirl speed map".

2) Experimentally measured vibration response spectrum as a function of the shaft's rotation speed (waterfall), the peak locations for each slice usually corresponding to the eigen frequencies as mentioned in previous section.

The plot showing the variation of eigen frequency with respect to rotational speed may not be readily obtained. For example, if the gyroscopic effect is significant on an eigen mode, its frequency tends to split so much that it crosses the other frequency curves as the speed increases [162, 177].

6.3.2.1 Critical speeds

The PRCAMP command, also prints out the critical speeds for a rotating synchronous (unbalanced) or asynchronous force. The critical speeds correspond to the intersection points between frequency curves and the added line $F=s.\omega$ (where s represents $SLOPE > 0$) as specified via PRCAMP. Because the critical speeds are determined graphically, their accuracy depends upon the quality of the Campbell diagram [159, 178]. To retrieve and store critical speeds as parameters, GET command could be used.

6.3.2.2 Whirls and stability

As eigen frequencies split with increasing spin velocity which can be due to backward and forward whirl, ANSYS identifies forward and backward whirls, and unstable frequencies. Because of the orbit shape the shaft makes when rotating, the first mode is sometimes referred to as a "Cylindrical" mode. If it is viewed from the front, the shaft appears to be bouncing up and down. Therefore this mode is also known as "bounce" or "translator" mode. The whirling motion of the rotor (orbit shape path) can be in the same direction as the shafts rotation or can be in the opposite direction. This gives rise to the labels "Forward Whirl" FW and "Backward Whirl" BW, shows rotor cross sections over the course of time for both synchronous forward and synchronous backward whirl. Note that for forward whirl, a point on the surface of the rotor moves in the same direction as the whirl. Thus, for synchronous forward whirl (i.e. unbalance excitation) a point at the outside of the rotor remains to the outside of the whirl orbit [179, 180].

With backward whirl, on the other hand, a point at the surface of the rotor moves in the opposite direction as the whirl to the inside of the whirl orbit during the whirl.

6.3.3 Validation of Backward and Forward natural frequencies

According to the Equation 3.130 in chapter 3, the critical speed of the rotating system splits into two critical speeds as rotational speed increases as shown in Table 6.5, this behaviour can be seen in the Figures 4.31 in chapter 4, Figure 5.47 in chapter 5 and Figure 6.24, the gap widens up as the speed increases.

Like it was discussed, this phenomenon is known as gyroscopic effect and occurs because of the BW and FW of the rotor. The eigenvectors would show these phenomena.

Figure 6.25a shows the experimental and calculated values and the relationship between the natural frequencies with increases in speed of rotation for the first mode. When the speed increases the gap between the two lines expands due to strong gyroscopic effect and validation with FE result shown in the Figure 6.25b.

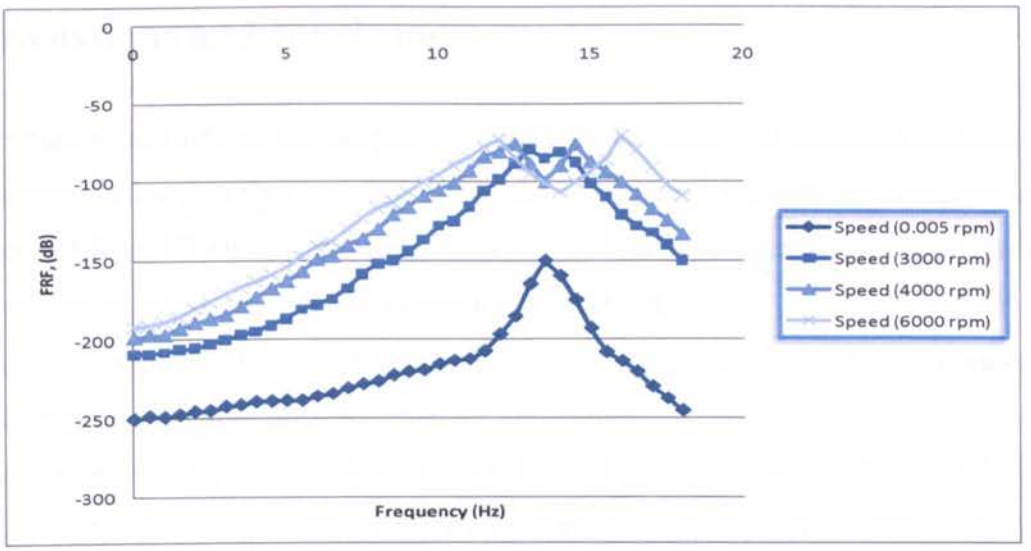

Figure 6.24 Frequency Response Functions (FRFs) versus natural frequency (Hz), theoretical calculations.

Table 6.5
Backward and Forward natural frequencies in experimental and theoretical calculations of overhung rotor for first mode shape.

Speed of rotation(rpm)	***Experimental Results(Hz),BW***	***Experimental Results(Hz),FW***	***Theoretical values, f_1(Hz),BW***	***Theoretical values, f_2(Hz),FW***
30	*15.137*	*15.137*	*14.3*	*14.3*
2000	*13.184*	*15.137*	*13.5*	*15.2*
3000	*13.184*	*15.625*	*13.136*	*15.616*
4000	*12.695*	*15.625*	*12.765*	*16.071*
6000	*12.695*	*16.113*	*12.056*	*17.016*

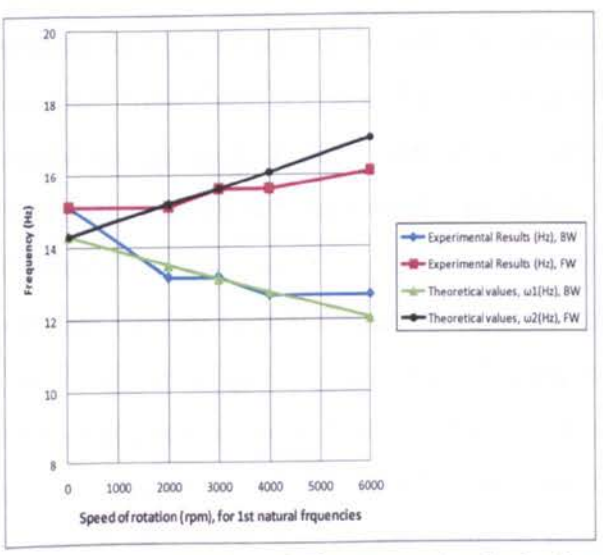

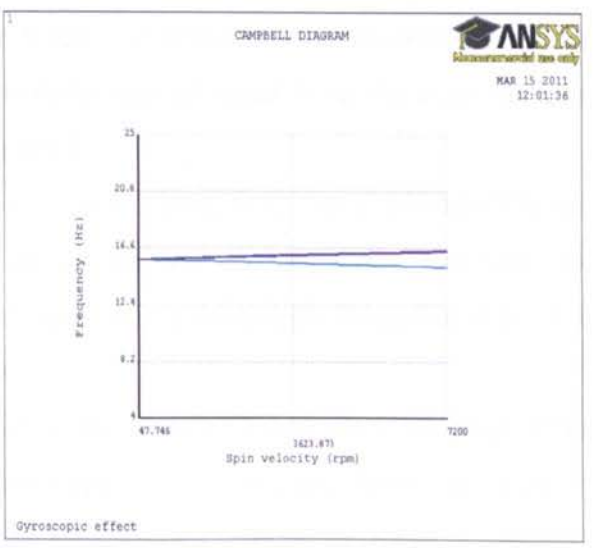

(a)- Experimental and Theoretical calculations. *(b)- ANSYS simulation.*

Figure 6.25 Natural frequencies versus speeds of rotation, first mode shape for overhung rotor (Campbell diagram).

6.4 Discussions and conclusions

The purpose of the study in this chapter was using modal testing in vibration analysis, which would involve subsequently obtaining the modal parameters and making comparisons with data obtained from FE simulation using ANSYS 12. The experimental technique on rotating structures was investigated by Finite Element (FE) method.

The modal testing method is used to obtain the natural frequency and extract the mode shape is in agreement with values obtained from FE simulation.

The simulation values obtained from ANSYS (see Figures 6.2 and 6.4) show the natural frequency and mode shape which are in agreement with the values obtained from the experimental method shown in Figure 6.1 for first mode and Figure 6.3 for second mode shape, the comparison values with ANSYS data are tabulated in Table 6.1 and shown in Figure 6.5.

Comparison of natural frequency obtained from experimental technique is often done by a simple tabulation of the two sets of results but a more useful format is by plotting the experimental value against the predicted one for each of the modes included in the comparison (see Figure 6.6).

The values of natural frequency and mode shape obtained by using shaker test are in agreement with the values obtained from hammer test, see Table 6.2 and Figure 6.7 for comparison. The parameters for correcting the unbalance in the system using shaker test with their validation using FE simulation are shown in Figures 6.8 and 6.9, the amplitude of the system has been reduced by adding unbalance mass. Furthermore, the simulation values obtained from the ANSYS in Figure 6.9 give the same fact obtained from the experimental modal testing method see Figures 4.9-4.11 in chapter 4.

Vibration analysis software results are shown in Figures 6.12 and 6.13. Spectral Map Wizard (Waterfall display and Colormap display) with shaker test are used as a new technique to validate the first natural frequency value obtained from the impact test performed in chapter 4. The results show good agreement with each other.

Waterfall plug-in Spectral Map Wizard adds a new dimension to the results view point. This specific plug-in is able to collect and to synchronize all data coming from the plug-in analyzers in a stack. Results are arranged regarding the different references (RPM, Time, and Levels) and represented in 3-D or profiles views. The structural resonances occur at constant frequency lines in the map, while order related components vary frequency with RPM.

Structural resonances can cause increases in vibration level with RPM. Resonances are fixed in frequency and are straight lines in the map, see Figure 6.12. Orders are multiples of the fundamental running speed of machine. Order related components move across the map to the right as RPM increases. We validate the result with Colormap displays shown in Figure 6.13 to prove the same fact.

The modal testing results (natural frequency and mode shape) that shown in Figures 6.14, 6.16 and 6.18 for two discs (multistage) system are in agreement with values obtained from FE simulation shown in Figures 6.15, 6.17 and 6.19. Comparison of these results is presented in Table 6.3 and Figure 6.20.

Comparison of natural frequencies obtained from experimental technique and FE simulation, is often performed by a simple tabulation of the two sets of results as shown in Figure 6.21. In this way it is possible to see not only the degree of correlation between the two sets of results, but also the nature and (possible case) any discrepancies which may exist. The points plotted should lie on or close to straight line of slope Figure 1.4 [11].

For overhung disc configuration plotting the experimental value against the predicted one for each of the modes included in the comparison is shown in Table 6.4 and Figures 6.22, 6.23.

Whirl motion has been studied using experimental modal analysis and validation of the results is performed by FE simulation together with the theoretical calculations.

The calculated values obtained from Equation 3.130 are in agreement with the values obtained from the experimental data that shown in Table 6.5. During the research work, the Frequency Response Function (FRF) of the rotor is found and displayed in graphical form, see Figure 6.24. In this figure, the FRF value is in agreement with experimental and ANSYS simulation, the gap widens up as the speed increases due to BW and FW whirl.

Campbell diagram is used to show the split of natural frequencies for overhung rotor disc system due to gyroscopic effect, see Figure 6.25, this split results in forward and backward whirling speeds. Campbell digram is obtained by using all three methods namely modal testing, theoretical calculations and FE simulation.

In this chapter mathematical model has been used, however more elaborate models based on a much large degree of freedom may be used based on compliance or stiffness influence coefficients. The final conclusions from this chapter demonstrate the validation of modal testing results with FE simulations and theoretical calculations for the values of natural frequency, mode shape and balance, unbalance parameters. The results show good agreement to each other.

CHAPTER 7

Conclusions with Recommendations for Future Work

7.1 Conclusions

Application of modal testing in rotating machinery and modal parameters identification has been investigated for the purpose of updating the mathematical model and predicting the response and providing basis for fault diagnosis. Balancing effect and bearing behaviour are two of issues investigated in this thesis.

In **chapter one** the backgrounds and motivation for the research work are discussed, the use of modal testing method in rotor dynamic system, subject of the research work, definition of problem, aim and objectives as well as an overview of thesis are outlined. In addition applications of modal testing model of rotating structure have been reviewed, and the issues arising from the use of modal testing method in the area of vibration analysis of rotor dynamic system have been discussed.

In **chapter two** the description of the modal analysis theory of single and multi degrees of freedom dynamic systems, and theoretical background for the measurement of the Frequency Response Function (FRF) is discussed. The importance of using the above methods in reducing vibration and noise in all rotating machines are demonstrated. Furthermore, reviews of the relevant literature on existing techniques for the balancing, auto balancing and modelling of rotating structures are presented.

In **chapter three** theoretical background of rotor dynamics prediction with a brief description of the basic elements of any rotor system including disc, shaft, bearings and seals with the determination of the model, mass unbalance, forces (synchronous and asynchronous) are reviewed, a description of the fundamental equations of motions together with the gyroscopic effect and its association with the rotating machinery are presented. The mathematical model of FRF for stationary and rotating structures are derived and described. From the equations the FRF for rotating structures with asymmetric system matrices show that denominator is identical to the ones for stationary structures with symmetric system matrices but the

difference is in numerator which is attributed to the behaviour of the rotor with strong gyroscopic effect.

In **chapter four** the various excitation methods and the mechanisms for successful implementation are tried and reported. Hammer and shaker tests are used to impact transient, Sinusoidal, Random and Burst Random excitations on the rotating elements of the system and the response measurements are also carried out on the rotating and stationary elements. A description of the experimental technique methodology used in this research work is presented. The experimental set up and measurement of the modal testing data are discussed. The natural dynamic characteristics of the rotor system with one, two and overhung discs configurations as well as the parameters for correcting the unbalance in the system are obtained.

The aim of increasing number of disc is to extend the study of rotor behaviour in multidisc systems and further investigate the reliability of the modal testing method to more elaborate rotor systems.

The description of using shaker test with rotor system is outlined in this chapter and the comparison between hammer and shaker test shows good correlation.

In shaker test, a special frame was designed and used around a plain bearing and the accelerometers were attached to the outer surface of the bearing to measure the response of the lateral motion on several points of the shaft. The excitation force with help of push rod was generated and applied to the shaft. This method can help to solve the problem in the attachment of shaker and force transducers to the rotor system.

Signal analysis in time domain (oscilloscope) has been used in this chapter to improve the amplitude unbalance in the system using Modal Balancing Method (MBM).

In addition vibration analysis software (Tacho Spline Fit Wizard, orbit analysis post processing wizard and shock capture module) has been carried out to assess the vibration monitoring in rotor systems and help in reducing the machine down time and to provide valuable information for the diagnosis of symptoms that helps in maintenance planning.

In **chapter five**, a description of the FE modelling methodology used in this research work is presented. The modelling techniques used in FE for a rotor system consisting of shaft, disc, bearings and their assembly are described.

In modelling process BEAM188 element has been used since the (length/thickness) is small, and the processing time efficiency is high. Results such as bending stress, strain and reaction force bearing was obtained final shape shown as a straight lines not real shape despite the accuracy of results. So, SOLID187 model has also been used to show the effect in more detail. This model can be used for disc and shaft with higher diameter. The model used in this study has irregular surfaces and included curved surfaces, so SOLID187 element was found to be more suitable for modelling irregular surfaces meshes.

This chapter delivered a description of FE method carried out to model the performance of a one, two and multistage rotor disc, more simulation using ANSYS software for the rotor-dynamic system with more loads in the effective length (three discs). The gyroscopic effect on the measured Frequency Response Functions (FRFs) was verified using Finite Element Analysis (FEA) for multdisc rotor system with different dimensions and at different speeds of rotation, the results show that the gap of split increased when the speed of rotation increased because of strong gyroscopic effect, which prove the FRFs results obtained by using modal testing method discussed in chapter 4.

We can use the procedure in this chapter to model systems with any number of discs of variable mass and geometry. It is also shown how a plane 2-D model can be extracted from 3-D model in FE, investigation of various aspects of the vibration and bearings behaviour are given. It is found that the bearings play a major role in the restraint of the vibration amplitudes of the rotor.

In **chapter six,** the dynamic behaviour of one, two and multistage disc configurations was investigated by two methods, the modal testing method results are in good agreement with results obtained from FE method, then several intermediate objectives achieved during the work including vibration suppression with different eccentricities of the unbalanced masses by different techniques.

The FE results are in good agreement with modal testing results which prove the reliability of the modal testing technique used in this thesis.

Vibration analysis software (spectral map wizard, waterfall and colormap displays) has been carried out, to interpret the signal analysis methods used to understand the performance of the rotor dynamic system and compare to the modal testing method.

Gyroscopic phenomena and its relationship with increasing rotational speed experimentally by modal testing method and computationally by FE (Campbell diagram) are further

investigated. The results show good agreement between the two methods and the theoretical method has been used for validation. The results shown that having an overhung load will make the gyroscopic effect occur in both, first and second mode of vibration that means it occurs at the lower frequencies. The Whirl motion has been detected and it either a Forward Whirl (FW) if it is in the same direction as the rotational velocity or Backward Whirl (BW) if it is in the opposite direction.

Chapter seven contains a discussion of the outcomes of the research and highlights the original aspects and important conclusions of the work. Areas for further study are also proposed.

We conclude that FE method results are in good agreement with results obtained from the modal testing method which demonstrate the reliability and accuracy of modal testing method for dynamic characterisation in design stage of rotor dynamic systems which is the main objective of the research work done in this thesis.

Modal testing data can be used to update the FE model at regular intervals and then calculate the new bearing reactions and bending stress values. So, if any balanced mass added and which result in reduction in vibration amplitude.

7.2 Recommendations for future work

The work that has been presented in this thesis covers the experimental and theoretical formulation and validation of a modal testing and analysis data for rotating machinery structures.

Further improvements to the method may result from research work regarding the following issues:

(a) Develop the model and experimental techniques further for more complex systems containing more unknown and partly interrelated parameters.

(b) Increasing disc numbers and more industrially orientated applications.

(c) Addressed and interpreted appropriately centrifugal force in rotating machine.

These issues will be described with more detail in the future work.

References

[1] James, M. L, Smith, G. M., Wolford, J. C. and Whaley, P. W., "Vibration of mechanical and structural systems: with microcomputer applications", Publisher: Harpercollins College Div, January 1994.

[2] Jenkins, L. S., "Vibration performance of a wasting house RCP during continuous change in mass unbalance at the pump coupling", in EPRI 8th International Workshop on Main Coolant Pump, Pitts burgh, 1996.

[3] Lawrence, N. Virgin, "Vibration of axially loaded structures", published by: Cambridge University Press, 2007.

[4] Swanson, E., Powell, D. and Weissman, S., "A practical review of rotating machinery critical speeds and modes", Journal Sound and Vibration, vol. 39, no. 5, pp. 10-17, May 2005.

[5] Animesh, Chakraborty, "Dynamic balancing in NMR double rotor system", Journal of Spectrochimica Acta, part A: Molecular and Biomolecular Spectroscopy, vol. 56, no. 14, pp. 2725-2727, 11 may 2000.

[6] Wowk, V., "Machinery vibration balancing", 1st ed., McGraw-Hill, New York, 1998.

[7] Yao, G. Z., Qiu ,Y., Meng, G., Fang, T. and Fan, Y. B., "Vibration control of rotor system by disc type electro-hierological damper", Journal of Sound and Vibration, vol. 219, no. 1, pp. 175-188, 1999.

[8] Benaroya, Haym., "Mechanical vibration, analysis, uncertainties, and control", 2nd ed., Published by: CRC Press, USA, 2004.

[9] Haiwei, Lu., Jianguo, Zhu., Zhiwei, Lin. and Yauguang, Guo., "An inchworm mobile robot using electromagnetic linear actuator", Journal of Mechatronics, vol. 19, no. 7, pp. 1116-1125, October 2009.

[10] Basermann, A., Clinckemaillie, J., Coupez, T., Fingberg, J., Digonnet, H., Ducloux, R., Gratien, J. M., Hartmann, U., Lonsdale, G., Maerten, B., Roose, D. and Wilshaw, C., "Dynamic load–balancing of finite element application with the drama Library", Journal of Applied Mathematical Modelling, vol. 25, no. 2000, pp. 83-98, 2000.

[11] Ewins, D. J., "Modal testing: theory and practice", John Wily, Exeter, England, 1995.

[12] Bendat, S. and Piersol, A., "Random data: analysis and measurement procedures", 3rd ed., Wily–Interscience, 2000.

[13] Karimulla, Shaik, Gupta, R. K. and Gouthaman, G., "Design and development of high speed spin test facility", Advances in Vibration Engineering, vol. 8, no. 2, pp. 183-191, 2009.

[14] Fred, W. Beaufait, "Basic concepts of structural analysis", Prentice-Hall, 1977.

[15] Allemang, R. J., "Experimental modal analysis bibliography", Proceeding of the 2nd International Modal Analysis Conference and Exhibit, pp. 1085-1097, Orland, Florida, 6-9 February 1984.

[16] Jimin, He and Zhi-Fang, Fu, "Modal analysis", Oxford, Active Butterworth-Heinemann, 2001.

[17] Bracewell, R. N., "The Fourier transform and its applications", 3rd ed., McGraw-Hill Science/Engineering/Mathematics, 1999.

[18] Kenedy, C. C. and Pan Cu, C. D. P., "Use of vectors in vibration measurement and analysis", Journal of Aeronautical Sciences, vol. 14, no. 11, 1947.

[19] Simon, M. and Tomlinson, G. R., "Application of Hilbert transforms in the modal analysis of non linear systems", Journal of Sound and Vibration, vol. 96, no. 4, pp. 421-436, 1984.

[20] Zaveri, M. P. K., "Modal analysis of large structure multiple exciter systems", Brule and Kjaer Publications, 1989.

[21] Steven, K. K., "Modal analysis–an old procedure with a new look", Mechanical Engineering, 1985.

[22] Cooley, J. W. and Tukey, J. W., "An algorithm for the machine calculation of complex Fourier series", Mathematics of Computation, vol. 19, no. 90, pp. 297-301, 1965.

[23] Ewins, D. J. and Gleeson, P. T., "A method of modal identification of lightly damped structures", Journal of Sound and Vibration, vol. 84, no. 1, pp. 57-79, 1982.

[24] Goyder, H. G. D., "Methods and application of structural modelling from measured structural frequency response data", Journal of Sound and Vibration, vol. 68, no. 2, pp. 209-230, 1980.

[25] Dossing, O., "Going beyond modal analysis or IMAC in new key", keynote address, Proceedings of the 13th International Modal Analysis Conference, Nashville, vol. 2460, USA, 1995.

[26] Allemang, R. J., "Modal analysis–where do we go from here", Proceeding of the 11th International Modal Analysis Conference, Florida, USA, 1-4 February 1993.

[27] Mottershead, J. E., "On the natural frequencies and anti-resonances of modified structures", Proceedings of the 17th International Modal Analysis Conference, Kissimmee, vol. 3727, pp. 648, Florida, USA, 1999.

[28] Qu, L. S. and Qiu, H. Xu., "Rotor balancing based holospectrum analysis: principle and practice", China Mechanical Engineering, vol. 9, no. 1, pp. 60-63, China, 1998.

[29] Ewins, D. J. and Sidhu, J., "Correlation of finite element and modal test studies of practical structure", Proceeding of the 2nd International Modal Analysis Conference and Exhibit, vol. 4, pp. 756-762, Orlando, Florida, USA, 6-9 February 1984.

[30] Salter, J. P., "Steady state vibration", published by: Kenneth Mason Press, 1969.

[31] Keyu, Qi., Zhengjia, He., Zhen, Li., Yanyang, Zi. and Xuefeng, Chen., "Vibration based operational modal analysis of rotor systems", Journal of Measurement, vol. 41, no. 7, pp. 810-816, 2008.

[32] Halvorsen, W. G., Anatrol, C. and Brown, D. L., "Impulse technique for structural frequency response testing", Journal of Sound and Vibration, vol. 11, no.11, pp. 8-19, 1977.

[33] Silva, J. M. M. and Maia, N. M. M., "Modal analysis and testing", Kluwer Academic Publishers, 1999.

[34] Darlow, M. S., "Balancing of high speed machinery", Springer-Verlag Publication, New York, 1989.

[35] Chiang, L. H., Russell, E. L. and Braatz, R. D., "Fault detection and diagnosis in industrial systems", Springer-Verlag Publisher, Berlin, 2001.

[36] Lalanne, Michel and Ferraris, Guy., "Rotor dynamics prediction in engineering", 2nd ed., Publishing by John Wiley and Sons Ltd, England, 1998.

[37] Dobson, B. J., "Modification of finite element models using experimental modal analysis", Proceeding of the 2nd International Modal Analysis Conference and Exhibit, vol. 2, pp. 593-601, Orlando, Florida, USA, 6-9 February 1984.

[38] Peterson, E. L. and Mouch, T. A., "Modal excitation: force drop off at resonances", Proceeding of the 8th International Modal Analysis Conference, Kissimmee, pp. 1226-1231, Florida, 1990.

[39] Walter, P. L., "Accelerometer selection for and application to modal analysis", Proceedings of the IMAC XVII:17th International Modal Analysis Conference, Kissimmee, vol. 3727, no. 2, pp. 566-572, Florida, USA, 8-11 February, 1999.

[40] Landgraf, M. W., "Vibration testing of heavy machinery structure", Journal of Sound and Vibration, vol. 31, pp. 16-18, 1997.

[41] Reynolds, P. and Pavice, A., "Impulse hammer versus shaker excitation for the modal testing of building floors", Experimental Techniques, vol. 24, no. 3, pp. 39-44, 2000.

[42] Brown, D. L., "Structural dynamics / modal analysis–from here to", Journal of Sound and Vibration, vol. 34, no. 1, pp. 6-9.

[43] Rocklin, G. and Crowley, Vold J., "A comparison of H_1, H_2 and Hv frequency response functions", In Proceedings of the 3rd International Modal Analysis Conference, pp. 272-278, Florida, USA, January 1985.

[44] Allemang, R. J. and Brown, D. L., "Experimental modal analysis shock and vibration" Hand Book, Editor Cyril, M. Harris; Chapter 21, 4th ed., McGrew Hill, 1995.

[45] Brown, D. L., Zimmermann, R. D., Allemang, R. J. and Mergeay, M., "Parameter estimation techniques for modal analysis", SAE Technical Paper 790221, SAE Transactions, vol. 88, pp. 828-846, 1979.

[46] Hunt, D. and Peterson, L., "Multishaker broadband excitation for experimental model analysis", SAE Technical Paper 831435, October, 1983.

[47] Berman, A. and Wei, F. S., "Automated dynamic analytical modal improvement", NASA Contract Report, published by: National Aeronautics and Space Administration, Scientific and Technical Information, Branch, 1981.

[48] Formenti, D., "Excitation direction in modal testing–is it important", Journal of Sound and Vibration, vol. 34, no. 3, pp. 14-16, 2000.

[49] Comstock, T. R., "Improving exciter performance in modal testing", Proceedings of the 17th International Modal Analysis Conference, Kissimmee, vol. 3727, pp. 1770-1775, Florida, USA, 1999.

[50] Palazzolo, A. B., Kascak, A. F., Montague, G. T. and Lin, R. R., "Piezoelectric pushers for active vibration control of rotating machinery", ASME Transactions, Journal of Vibration, Acoustics, Stress and Reliability in Design, vol. 111, pp. 298-305, July 1989.

[51] Nielka, P. G., "Modal balancing of flexible rotors without test an experimental investigation", Journal of Sound and Vibration, vol. 90, no. 2, pp. 157-172, 1983.

[52] McConnell, K. G. and Paulo, S., "Vibration testing; theory and practices", John Wiley, Canada, 2008.

[53] Revision, J. "Rotor Kit", Part Number 126376-01, Bently Nevada LLC, USA, 2002.

[54] Bently, D. E., "What happened to the damping orbit", BNC, 1631 Bently Parkway South, Minden, Nevada, vol. 5, no. 2, pp. 782-3611, USA, 1984.

[55] http:/en.wikipedia.org/wiki/ Bentley Nevada, accessed: 5/7/2010

[56] M +P International, SO Analyser Operating Manual.

[57] Hillary, B. and Ewins, D. J., "The use of strain gauge in forces determination and frequency response function measurements", Proceeding of the 2nd International Modal Analysis Conference and Exhibit, vol. 3, pp. 627-634, Orlando, Florida, USA, 6-9 February 1984.

[58] He, J. and Lin, R. M., "Location of stiffness modelling errors using measured frequency response functions", Shock and Vibration Technology Review, vol. 3, no. 4, pp. 9-16, 1993.

[59] "The fundamentals of modal testing/application" Note 243-3, Agilent Technologies' Test and Measurement Support, Services and Assistance, Printed in USA, 5/100, 5954-7957E, 1997.

[60] Ghlaim, K. H. and Martin, K. F., "Reduced component modes in a damped system", Proceeding of the 2nd International Modal Analysis Conference and Exhibit, vol. 3, pp. 683-689, Florida, USA, 6-9 February 1984.

[61] Schwarz, B. J. and Richardson, M. H. "Experimental modal analysis", Vibrant Technology, Inc., CSI Reliability week, pp. 1-12, Florida, USA, October 1999.

[62] Singiresu, S. Rao, "Mechanical vibrations", 6th ed., Prentice-Hall, Inc., Singapore, 2005.

[63] Almeida, P. A. O. and Rodrigues, J. E. S., "Modal analysis of structure of cocker stadium", Proceeding of the 17th International Modal Analysis Conferences, Kissimmee, vol. 3727, pp. 1417-1422, Florida, USA, 1999.

[64] Dos Santos, J. V. A. and Reddy, J. N. "Vibration of Timoshenko beams using non-classical elasticity theories", Journal Shock and Vibration, vol. 19, no. 3, pp. 251-256, 2012.

[65] Daniel, B., Andreas, S., Hans, G. and Johannes, P., "An efficient multiple shooting based reduced SQP strategy for large scale dynamic process optimization: part II: software aspects and application", Journal of Computers and Chemical Engineering, vol. 27, no. 2, pp. 167-174, 2003.

[66] Xu, B., Qu, L. and Sun, R., "The optimization technique–based balancing of flexible rotors without test runs", Journal of Sound and Vibration, vol. 238, no. 5, pp. 877-892, December 2000.

[67] Goodman, T. P., "A least-squares method for computing balance corrections", ASME Transaction, Journal of Engineering Industry, vol. 86, no. 9, pp. 273-279, 1964.

[68] Shi, Liu., "A modified low–speed balancing method for flexible rotors based on holospectrum", Journal of Mechanical System and Signal Processing, vol. 21, no. 1, pp. 348-364, Xi an Jiao Tong University, 9 September 2005.

[69] Shi, liu. and Liangsheng, Qu., "A new field balancing method of rotor systems based on holospectrum and genetic algorithm", Journal of Applied Soft Computing, vol. 8, no. 1, pp. 446-455, January 2008.

[70] Liangsheng, Qu. and GH, Xu., "One decade of holospectral technique: review and prospect", Proceeding of ASME Design Engineering Technical Conference DET C99/VIB-8264, pp. 212-215, 1999.

[71] Liangsheng, Qu., Xiong, Liu., Gerard, P. and Yaodong, C., "The holospectrum: A new method for rotor surveillance and diagnosis", Mechanical Systems and Signal Processing, vol. 3, no. 3, pp. 255-267, 1989.

[72] Goldberg, D. E., "Genetic algorithms in search, optimization and machine learning", 1st ed., Addison–Wesley, reading MA, 1989.

[73] Tseng, Chyuan–Yow, Shih, Ting–Wei and Lin, Jun-Tsun, "Dynamic balancing scheme for motor armatures", Journal of Sound and Vibration, vol. 304, no. 1-2, pp. 110-123, 2007.

[74] Lund, J. W. and Tonneson, J., "Analysis and experimental in multi–plane balancing of flexible rotor", Transactions of The American Society of Mechanical Engineers, Journal of Engineering and Industry, vol. 94, no. 1, pp. 233-242, 1972.

[75] Edney, S. L., Fox, C. H. J. and Williams, E. J., "Tapered Timoshenko finite elements for rotor dynamics analysis", Journal of Sound and Vibration, vol. 137, no. 3, pp. 463-481, 1990.

[76] Wang, W. and Kirkhope, J., "New eigensolutions and modal analysis for gyroscopic/rotor systems, part 1: un-damped systems", Journal of Sound and Vibration, vol. 175, no. 2, pp. 159-170, August 1994.

[77] Dyka, C. T., Ingel, R. P. and Flippen, L. D., "A new approach to dynamic condensation for FEM", Journal of Computers and Structures, Published by Elsevier, vol. 61, no. 4, pp. 763-773, USA, November 1996.

[78] Rieger, N. F., "Balancing of rigid and flexible rotors", The Shock and Vibration Information Centre, Department of Defence, USA, 1986.

[79] Gyunghyun, Choi., "A goal programming mixed module line balancing for processing time and physical work load", Journal of Computers and Industrial Engineering, vol. 57, no. 1, pp. 395-400, 8 January 2009.

[80] Matanachai, S. and Yano, C. A., "Balancing mixed–model assembly lines to reduce work overload", IIE Transactions, vol. 33, no. 1, pp. 29-42, 2001.

[81] Gokcen, H. and Erel, E., "A goal programming an approach to mixed-model assembly line balancing problem", International Journal of Production Economics, vol. 48, no. 2, pp. 177-185, 1997.

[82] Michal, Manka and Tadeuz, Uhl., "Mechatronic design of fault detection isolation and restoration systems for rotating machineries", Journal of Mechanism and Machine Theory, vol. 44, no. 7, pp. 1439-1449, July 2009.

[83] Kyung, K. and Sundar, Mo. K., "A dominance–based design metric in multi-attributer robust design", Research in Engineering Design, vol. 12, no. 4, pp. 235-248, 2000.

[84] Mahfoud, J., Hagopain, J. Der., Levecque, N. and Steffen, V., "Experimental model to control and monitor rotating machines", Journal of Mechanism and Machine Theory, vol. 44, no. 2009, pp. 761-771, Accepted 19 April 2008.

[85] Lum, K. Y., Copple, V. T. and Bernster, D., "Adaptive autocertering control for an active magnetic bearing supporting rotor with unknown mass imbalance", IEEE Transaction on Control System Technology, vol. 4, pp. 587-597, 1996.

[86] Fuller, C. R., Elliott, S. J. and Nelson, P. A., "Active control of vibration", Published by Academic press, Virginia University, 1996.

[87] Tsai, Mi-Ching, Jia-sheng, Hu. and Feng-Rung, Hu., "Actuator fault and abnormal operation diagnosis for auto–balancing two-wheeled cart control", Journal of Mechatronics, vol. 19, no. 2009, pp. 647-655, 2009.

[88] Tang, Liang and Chen, Yiging, "Model development and adaptive imbalance vibration control of magnetic suspended system", Chinese Journal of Aeronautics, vol. 20, no. 5, pp. 434-442, 2007.

[89] Tiwari, R. and Chakravarthy, V., "Simultaneous identification of residual unbalances and bearing dynamic parameters from impulse responses of rotor bearing systems", Mechanical System and Signal Processing, vol. 20, no. 7, pp. 1590-1614, 2006.

[90] Nelson, H. D. and Mcvaugh, J. M., "The dynamics of rotor bearing systems using finite elements", ASME Journal of Engineering Industry, vol. 98, pp. 593-600, 1976.

[91] Zorzi, E. S. and Nelson, H. D., "Finite element simulation of rotor-bearing system with internal damping", ASME Journal of Engineering for Gas Turbines and Power, vol. 99, no. 1, pp. 71-76, 1977.

[92] Lin, Y. H. and Lin, S. C., "Optimal weight design of rotor systems with oil-film bearings subjected to frequency constraints", Finite Element in Analysis Design, vol. 37, no. 10, pp. 777-798, September 2001.

[93] Aleyaasin, M., Ebrahimi, M. and Whalley, R., "Vibration analysis of distributed - lumped rotor systems", Computer Methods in Applied Mechanics and Engineering, vol. 189, no. 2, pp. 545-558, 2000.

[94] Firoozian, R. and Zhu, H., "A Hybrid method for the vibration analysis of rotor-bearing systems", Journal of Mechanical Engineering Science, vol. 205, no. 2, pp. 131-137, 1991.

[95] Wu, J. S. and Yang, I. H., "Computer method for torsion-and- flexure-coupled forced vibration of shafting system with damping", Journal of Sound and Vibration, vol. 180, no. 3, pp. 417-435, 1995.

[96] Wu, Jia-Jang., "Prediction of lateral vibration characteristics of a full-size rotor-bearing system by using those of its scaled models", vol. 43, no. 10, pp. 803-816, 2007.

[97] Wu, T. X. and Thompson, D. J., "The vibration behaviour of railway track at high frequencies under multiple preloads and wheel interactions", The Journal of the Acoustical Society of America, vol. 108, no. 3, pp. 1046-1053, USA, 2000.

[98] Irretier, H., "History and development of frequency domain methods in experimental modal analysis", Journal de Physique, vol. 12, no. 11, pp. 91–100, 2002.

[99] Bucher, I. and Ewins, D. J., "Modal analysis and testing of rotating structures", Philosophical Transactions of The Royal Society of London Series A-Mathematical, Physical and Engineering Sciences, vol. 359, no. 1778, pp. 61–96, 2001.

[100] Irretier, H., "Mathematical foundations of experimental modal analysis in rotor dynamics", Mechanical Systems and Signal Processing, vol. 13, no. 2, pp. 183–191, 1999.

[101] Pennacchi, P., Bachschmid, N., Vania, A., et al., "Use of modal representation for the supporting structure in model-based fault identification of large rotating machinery Part 1-Theoretical Remarks", Mechanical Systems and Signal Processing, vol. 20, no. 3, pp. 662–681, 2006.

[102] Chaudhry, J., Wagner, M., He, F., et al., "A complete rotor-dynamic analysis of a rotor-disc system using finite element method", In Proceedings of the 8th IFToMM

International Conference on Rotor-dynamics, Held in Korean Institute of Science and Technology KIST, Seoul, Korea, 12-15 September 2010.

[103] Lees, A. W., "The least squares method applied to identify rotor foundation parameters", In Institution of Mechanical Engineers Conference on Vibrations in Rotating Machinery, pp. 209-216, Edinburgh, 1988.

[104] Leuridan, J. M., Brown, D. L. and Allemang, R. J., "Time domain parameter identification methods for linear model analysis: A unifying Approach", ASME Paper Number 85-DET-90, ASME Transaction, Journal of Vibration, Acoustics, Stress and Reliability in Design, 8 pages, 1985.

[105] Breathier, P., Ferraris, G. and Lalanne, M., "Prediction of critical speeds unbalance and non-synchronous forced response of rotor", Proceeding of the 53th Conference Shock and Vibration, 1983.

[106] Dimarogonas, D. Andrew and Paipetis, S. A., "Analytical methods in rotor dynamics", Applied Sciences Publishers, USA, 1983.

[107] Kronast, M. and Hildebrandt, M., "Vibro–acoustic modal analysis of automobile body cavity noise", Journal of Sound and Vibration, vol. 36, no. 6, pp. 20-23, 2000.

[108] Muszynska, A., "Fundamental response of rotor", BNC/ BRDRC Report, vol. 1, no. 86, pp. 1-22, 1986.

[109] Shigley, J. E., "Mechanical engineering design", 7th ed., Exclusive Rights by McGraw Hill Book Co., USA, 2003.

[110] Willems, N. and Holzer, S. M., "Critical speeds of rotating shaft subjected to axial loading and tangential torsion", ASME Journal of Engineering Industry, vol. 87, 6 pages, May 1967.

[111] Tran, D. M., "Comportment dynamiqe des rotors flexible", Thesis D. I., Lyon, France 1981.

[112] Edwards, S., Lees, A. W. and Friswell, M. I., "Experimental identification of excitation and support parameters of flexible rotor-bearings-foundation system from a single run-down", Journal of Sound and Vibration, vol. 232, no. 5, pp. 963-992, Wales, UK, 2000.

[113] Bently, D. E. and Muszynska, A., "Identification of bearing and seal dynamic stiffness parameters by steady-state load and squeeze film tests", Proceedings of the Symposium on Instability in Rotating Machinery, Carson City, Nevada, June 1985; NASA Conference Publication, vol. 2409, pp. 301-316, 1985.

[114] Delbez, A., Charlot, G., Ferraris, G. and Lalanne, M., "Dynamic behaviour of a counter –rotating air turbine starter", ASME Paper 93 GT 55, 1993.

[115] Ferraris, G., Maisonneuve, V. and Lalanne, M., "Prediction of the dynamic behavior of non-symmetrical coaxial co or counter–rotating rotors", Journal Sound and Vibration, vol. 195, no. 4, pp. 649-666, 1996.

[116] Guilen, P. M., Berthiet, P., Ferraris, G. and Lalanne, M., "Instability and unbalance response of dissymmetric rotor bearing systems", ASME Journal Sound Vibration, ACSTR Rel., vol. 110, July 1988.

[117] Ewins, D. J., "Modal testing: theory, practice and application", Mechanical Engineering Research Studies: Engineering Dynamics Series, Bal-dock, Hertfordshire, England, 2011.

[118] Fu, Z., "Vibration modal analysis and parameters identification", China, 1999.

[119] Inman, D. J., "Vibration: with control, measurement and stability", Chapter 2: Lumped parameter models, Prentice-Hall, Inc., New Jersey, 1989.

[120] Wilkinson, J. H., "The algebraic eigenvalue problem", 1st ed., Oxford University Press, USA, 21 April 1988.

[121] Dimarogonas, D. Andrew, "Vibration for engineering", 2nd ed., Prentice–Hall, USA, 1996.

[122] Eisenmann, R. C., "Machinery malfunction diagnosis and correction: vibration analysis and troubleshooting for process industries", Prentice Hall PTR, USA, 1998.

[123] Thompson, J. M. T. and Stewart, H. B., "Nonlinear dynamics and chaos", 2nd ed., Wily, 2002.

[124] Piersol, A. G., "Chapter 15: Measurement techniques", From "Shock and vibration hand book", by: Harris, C. M., 4th ed., McGraw-Hill Higher Education, 1995.

[125] Hutin, C., "Modal analysis is using appropriated excitation techniques", Journal of Sound and Vibration, vol. 34, no. 10, pp. 18-25, 2000.

[126] Vance, J. M., "Rotordynamics of turbomachinery", John Wiley and Sons, New York, USA, 1988.

[127] Muszynska, A., "Shaft vibration versus shaft stress, orbit", BNC, vol. 10, no. 3, pp. 775 -779, USA, December 1989.

[128] Samantaray, A. K., "Steady-state dynamics of a non-ideal rotor with internal damping and gyroscopic effects", Nonlinear Dynamics, vol. 56, no. 4, pp. 443–451, 2009.

[129] http://www.gepower.com/prod_serv/products/oc/en/downloads/rk4_rotor_kit.pd, accessed: 6/2/2012

[130] Bently, D. E., "Five basic parameters for rotating machinery monitoring and diagnostics", 1631 Bently Parkway South, Minden, Nevada, USA, December 1991.

[131] Electrical Steel Sheets, Nippon Steel Corporation, Tianjin Jianghailong Steel, Co, Ltd, 1998.

[132] Braun, S., "Application of computer–algebra simulation CALS in industry", Journal of Mathematics and Computer in Simulation, vol. 53, no. 4-6, pp. 249-257, Munchen, Germany, 28 July 2000.

[133] http://www.mpihome.com/, accessed: 9/4/2011

[134] Formenti, D. and Richardson, M. H., "Global curve fitting of frequency response measurements using the rational fraction polynomial method", IMAC, In Proceedings of the 3rd International Modal Analysis Conference, pp. 390–397, Florida, USA, 1985.

[135] Nikolai, N., Verichev, S. and Erofeyev, V., "Damping lateral vibration in rotary machinery using motor speed modulation", Journal of Sound and Vibration, vol. 329, no. 1, pp. 13-20, 16 September 2009.

[136] Völcker, C. and Cass, A., "Guidelines for space software process improvement", PASCON/ WO6-CCN5/TN8, Technical Note 8, no. 1, 19 December 2001.

[137] Ehrich, F. F., "Handbook of rotor-dynamics", 3rd ed., Krieger Publishing Company, Florida, USA, 2004.

[138] John, C. and Johnson, "Spike energy spectrum–where's the spike energy", Enter-act, Cincinnati, Ohio, USA, 1997.

[139] "Vibrations: analytical and experimental modal analysis", Course Number UC-SDRL-CN-20-263-662, Revision: February 1999.

[140] Change, J. B., Li, Tf. and Li, Pf., "The selection of time domain characteristic parameters of rotating machinery fault diagnosis", IEEE Xplore, International Conference in Logistics Systems and Intelligent Management, vol. 1, pp. 619-623, Harbin, China, 9-10 January 2010.

[141] Karpenko, E. V., Wiercigroch, M., Pavlovskaia, E. E. and Neilson, R. D., "Experimental verification of Jeffcott rotor model with preloaded snubber ring", Journal of Sound and Vibration, vol. 298, no. 4-5, pp. 907–917, 2006.

[142] Bridgman, P. W., "Dimensional analysis", New Haven-Connecticut, Yale University Press, 1963.

[143] Chen, W. J., "A note on computational rotor dynamics", ASME Journal Vibration and Acoustic, vol. 120, pp. 228–233, 1998.

[144] Nandi, A., Neogy, S. and Das, A. S., "Application of the harmonic balance technique to finite element models of asymmetric rotors via sparse kronecker products", Journal of Strain Analysis for Engineering Design, vol. 40, no. 6, pp. 549–557, 2005.

[145] Kalkat, M., Yildirim, S. and Uzmay, I., "Rotor dynamics analysis of rotating machine systems using artificial neural networks", International Journal of Rotating Machinery, vol. 9, no. 4, pp. 255-262, 2003.

[146] Emmanouilidis, C., MacIntyre, J., Cox, C., Macintyre, C. and Prof. C., "Neurofuzzy computing aided machine fault diagnosis", Proceeding of JCIS The 4th Joint Conference on Information Sciences, Research Triangle Park, North Carolina, vol. 1, pp 207-210, USA, 1998.

[147] Gmur, T. C. and Rodrigues, J. D., "Shaft finite elements for rotor dynamics analysis", ASME Journal of Vibration and Acoustics, vol. 113, pp. 482–493, 1993.

[148] Thearle, E. L. and Schenectady, N. Y., "Dynamics balancing of rotating machinery in field", ASME Transaction, Journal of Applied Mechanics, vol. 56, Paper AMP 56-19, pp. 745-753, 1934.

[149] Kumar, A. vanish, "A modified method for solving the unbalanced assignment problems", Applied Mathematics and Computation, vol. 176, no. 1, pp. 76-82, 2006.

[150] Ginsberg, J. H., "Mechanical and structural vibration, theory and applications", Georgia Institute of Technology, John Wily and Sons, Inc., USA, 2001.

[151] Alauze, C. A., Der Hagopain, J., Gaudiller, L. and Voinis, Ph., "Active balancing of turbo machinery; application to large shaft lines", Journal of Vibration and Control, vol. 7, no. 2, pp. 249-260, 2001.

[152] Tondl, A., "Some problems of rotor dynamics", Chapter 1: The effect internal damping on the stability of rotor motion and the rise of self-excited vibrations, Chapman and Hall Limited, London, 1965.

[153] Bash, T. J., "Active magnetic bearings used as an actuator for rotor health monitoring in conjunction with conventional support bearings", Thesis in Master of Science in Mechanical Engineering, Virginia Polytechnic Institute and State University, USA, 2005.

[154] Ozguven, H. N. and Levent Ozkan, Z., "Whirl speeds and unbalance response of multi bearing rotors using finite elements", Journal of Vibration, Acoustics Stress and Reliability in Design, vol. 106, no. 1, pp. 72–79, 1984.

[155] Rieger, N. F., "A comprehensive guide to computer programs for analysis rotor systems", Machine Design, vol. 22, pp. 89–95, 1976.

[156] Chen, X. F., Yang, S. J., Ma, J. X. and He, Z. J., "The construction of wavelet finite element and its application", Finite Elements in Analysis and Design, vol. 40, no. 5-6, pp. 541–554, 2004.

[157] Vyas, N. S. and Satishkumar, D., "Artificial neural network design for the fault identification in a rotor bearing system", Mechanism and Machine Theory, vol. 36, no. 2, pp. 157-175, 2001.

[158] Beatty, R. F., "Differentiating rotor response due to radial rubbing", Published by: California State University, Northridge, USA, 1982.

[159] ANSYS 12 Help Menu (can be found with ANSYS 12).

[160] Beley, A., Rajakumar, C. and Thieffry, P., "Computational methods for rotor-dynamics simulation", NAFEMS World Congress, Crete-Greece, 16-19 June 2009.

[161] Bathe, K. J., "Finite element procedures", 1st ed., Prentice-Hall, New Jersey, 1976.

[162] http://en.wikipedia.org/wiki/Rotordynamics#Campbell_diagram, accessed: 10/5/1012

[163] Khulief, Y. A. and Mohiuddin, M. A., "On the dynamic analysis of rotors using modal reduction", Finite Elements in Analysis and Design, vol. 26, no. 1, pp. 41–55, 1997.

[164] Rouch, K. E. and Kao, J. S., "Dynamic reduction in rotor dynamics by the finite element method", Journal of Mechanical Design, Transactions of the ASME, vol. 102, no. 2, pp. 360–368, 1980.

[165] Firoozian, R. and Stanway, R., "Design and application of a finite element package for modelling turbomachinery vibrations", Journal of Sound and Vibration, vol. 134, no. 1, pp. 115–137, 1989.

[166] Bachschmid, N. and Pennacchi, P., "Model based malfunction identification from bearing measurements", IMechE-7th International Conference on Vibrations in Rotating Machinery, University of Nottingham, UK, pp. 571–580, 12–14 September 2000.

[167] Cundy, H. and Rollett, A., "Lissajous's figures in mathematical models", 3rd ed., Stradbroke, England: Tarquin Publication, UK, 1989.

[168] Lawrence, J. D., "A Cataloge of special plane curves", Dover Publications, New York, USA, 1972.

[169] Wu, M. S. and Tsai, W. H., "Corrections for Lissajous figures in books", American Journal of Physics, vol. 52, no. 7, pp. 657-658, 1984.

[170] Guang, H. and Yiyang, "Demonstrating Lissajous figures with MATLAB and their applications", Journal of China Science and Technology Information, Electronic and Industrial College, Yiyang Hunan 413054, China, 2008.

[171] Strader, Joe, "Critical evaluation of IRD spike energy signatures", Annual Vibration Institute Meeting, St., Louis, Missouri, USA, 1993.

[172] Genta, G., "Dynamics of rotating systems", Springer, New York, USA, 2005.

[173] Okamoto, S., Sakata, M., Kimura, K. and Ohnabe, H., "Vibration analysis of a high speed and light weight rotor system subjected to a pitching or turning motion. II: A flexible rotor system on flexible suspensions", Journal of Sound and Vibration, vol. 184, no. 5, pp. 887–906, 1995.

[174] Pennacchi, P. and Vania, A., "Measures of accuracy of model based identifications of faults in rotor-machinery", 15th AIMETA Congress of Theoretical and Applied Mechanics, 2001a, SP ME 48, Taormina, Italy, 12-15 September 2001.

[175] Pennacchi, P. and Vania, A., "Measures of accuracy of model based diagnosis of faults in rotor-machinery", Proceeding of the 14th International Congress of Condition Monitoring and Diagnostic Engineering Management COMADEM 2001b, pp. 873–880, Manchester, UK, 2001.

[176] Bachschmid, N., Pennacchi, P., Tanzi, E. and Vania, A., "Accuracy of modelling and identification of malfunctions in rotor systems: experimental results", Journal of the Brazilian Society of Mechanical Sciences XXII, vol. 22, no. 3, pp. 423–442, 2000.

[177] Mahadevan, P., Jog, C. S. and Chatterjee, A., "Modal projections for synchronous rotor whirl", Proceedings of the Royal Society A, vol. 464, no. 2095, pp. 1739–1760, 2008.

[178] Barzdaitis, V., Bogdevicius, M., Didziokas, R. and Vasylius, M., "Modelling and diagnostics of gyroscopic rotor", Journal of Vibration Engineering, vol. 11, no. 4, pp. 627–635, 2009.

[179] Friswell, M. I., Penny, J. E. T., Garvey, S. D. and Lees, A. W., "Dynamics of rotating machines", Cambridge University Press, UK, 2010.

[180] Vance, J. M., Zeidan, F. Y. and Murphy, B., "Machinery vibration and rotor-dynamics", John Wiley and Sons, Inc. Hoboken, New Jersey, 2010.